Imperial College London
Department of Physics

Properties of Moduli Spaces of Supersymmetric Quiver Gauge Theories with 8 Supercharges

Author: Chunhao Li

Supervisor: Amihay Hanany

September 24, 2025

Submitted in part fulfilment of the requirements for the degree of Doctor of Philosophy in Physics of Imperial College London and the Diploma of Imperial College London.

lichunhaomax@gmail.com

Declaration of Originality

I, Chunhao Li, declare that the research work presented in this thesis is my own work, together with my collaborators Amihay Hanany, Marcus Sperling, Deshuo Liu, Guhesh Kumaran, and Sam Bennet. The work in the thesis has been published in the following two papers:

A. Hanany, G. Kumaran, C. Li, D. Liu and M. Sperling, *Actions on the quiver: discrete quotients on the Coulomb branch*, *JHEP* **05** (2024) 318, [2311.02773]

S. Bennett, A. Hanany, G. Kumaran, C. Li, D. Liu and M. Sperling, *Quiver subtraction on the Higgs branch*, *Nucl. Phys. B* **1016** (2025) 116917, [2409.16356]

Throughout this thesis, the work of other researchers has been appropriately cited and acknowledged to the best of the author's knowledge. A list of references is given in the bibliography.

Abstract

The thesis focuses on the study of moduli spaces of 3d $\mathcal{N} = 4$ supersymmetric field theories. Two aspects are emphasized. Firstly, discrete quotients of the Coulomb branch are studied. Secondly, the Hasse diagram for Higgs branches are studied. Both aspects are given by diagrammatic operations on the quiver diagrams.

In the Introduction and Background part, the framework of supersymmetry and the necessary mathematics underlying the following two chapters are introduced at a pedagogical level.

In the second part, it is shown that two families of quivers, the quivers with complete graphs and the quivers with multiple adjoint loops, have Coulomb branches related by a quotient of a permutation symmetry. Quotient of cyclic groups is also studied. The two operations can be combined to generate a quotient by a semi-direct product group of permutation and cyclic groups. The quotient relations are demonstrated by the Molien sum and Abelionization process. Examples are included to demonstrate the operations.

In the third part, a bottom to up quiver subtraction algorithm is introduced. The algorithm can generate the whole Hasse diagram for the Higgs branch of a single-laced unitary quiver. The interesting feature of the algorithm is that it gives the monodromy of slices around the leaves. It also calculates the Namikawa Weyl group.

Acknowledgements

My trip towards theoretical physics was initiated by my supervisor, Amihay Hanany. His enthusiasm towards discussion (and tea) has shaped me over the past four years and will still influence me in the many years to come. He was always open to discussion in his office and patient with any questions. His magic of Hilbert series, quivers, and branes is a great treasure for me. My gratitude to him is more than language can express, not only in academics, but also in life. It's such a pleasure for me to be his student.

I would also like to acknowledge Travis Schedler and his student, Tiziano Gaibisso, for all the discussions we had in the seminars. They are always willing to answer questions and open to discussions. Many interesting ideas originated from those discussions.

Special thanks to my examiners Stefano Cremonesi and Jerome Gauntlett. I'm so lucky to have them as my examiners.

A great thanks to my parents and grandparents who supported me throughout my whole past life. It's such a pride to grow up in this family.

I would also like to extend my sincere gratitude to Marcus Sperling and Antoine Bourget. It's always inspiring to talk with them. They rescued me many times when I was depressed.

Special gratitude is given to my friend since USTC, Ziwen Kong, who is always so kind to help. Without her, I cannot even survive during my first year of PhD.

I want to thank my academic pioneers Zhenghao Zhong, Julius Grimmingger, and Kirsty Gledhill. They taught me a lot of basic knowledge on quivers with great patience.

I've also benefited a lot from my academic brothers, Deshuo Liu, Guhesh Kumaran, Sam Bennet, and Elias van den Driessche. Great thanks for their accompaniment during my PhD life. Thanks go to Lorenzo Mansi as well.

Thanks Yang-hui He and Nadav Drukker, for organizing the LonTI lecture series, where I learned a lot of things in mathematics and physics.

Special thanks to Daniel Waldram and Shai Chester, who helped me with all the assessments in my PhD milestones.

Special thanks to my colleague Theo Keseman, who shares his passion for music with me. Special thanks are also given to my colleague Pulkit Ghoderao. I will always remember the times we spent in 503 watching movies together. My gratitude also goes towards all the other PhD and postdoc fellows for all the moments spent together, afternoon tea and board games, h-bar parties, toffees, Friday flashbacks, wall-climbing and running, Jazz night, and all the other shining moments in and outside Imperial.

Thanks to Deliang Zhong, Hongliang Jiang, Zhihao Duan, and Zihan Wang for all the suggestions not only in academics, but also in life.

Special thanks to Deshuo Liu, Yusheng Jiao, and Yiwei Liu, who are my first Chinese friends when I arrived in London.

Thanks to Yuanfan Cao for his beautiful singing. Thanks to my roommate Jieming Lin, Steven Hsia, Yuan Zhe, and Huidong Zhang, who helped with the bills for electricity and gas, and all the accompaniment.

I would also like to thank Ruoyun Huang and Junyue Lian, who share their passion for motorsport with me. Thanks for the time we spent together as the team ASUn.

Thank you all for the great memories we made during the years!

Dedication

This thesis is dedicated to Grandpa, the greatest pilot in the world. I love you very much!

Contents

List of Figures

List of Tables

Chapter 1

Introduction

This work focuses on the study of properties of moduli spaces of 3d $\mathcal{N}=4$ supersymmetric quiver gauge theories. Firstly, a discrete quotient on the Coulomb branch is studied, and the quotient operation can be realized by a diagrammatic operation on the quiver [11]. Secondly, the stratification structure of the Higgs branch is studied and summarized as a subtraction algorithm [2].

Before going into the details of the research works, a brief background introduction should be made on the basic concepts of the topics in this thesis. Supersymmetry, moduli spaces, and quiver gauge theories are explained in the following. In particular, the study of 3d $\mathcal{N}=4$ supersymmetric quantum field theories is motivated.

Quantum field theory has been a great success to explain elementary particle physics. In particular it describes all known particles and interactions between them. It has been a principal of quantum field theory that if the theory has more symmetry, then the theory can be simpler to solve. A typical quantum field theory can have spacetime symmetry, global symmetry, and gauge symmetry. So a natural question is what the most general symmetry a theory can have. The answer is given by *Coleman-Mandula theorem* that a theory can only have Poincaré symmetry and internal symmetries [12]. An exception is that if superalgebras are allowed, then the theory could have supersymmetry [13]. Supersymmetry is an extension of Lie algebras with $\mathbb{Z}_2$ grading. As a result, supersymmetry predicts that any particle state has a super partner: bosons have a fermionic partner and fermions have a bosonic partner. They have the same mass but differ in spin by one half. Theories with supersymmetry have many good properties. Super Poincaré algebra indicates bosonic and fermionic excited states always appear in pairs, and only ground states can have different numbers of bosonic states and fermionic states. Witten first studied the difference and postulated that it can be used as a characteristic of the theory [14]. There are also functions called Hilbert series counting chiral operators in the theory. With the help of supersymmetry, a lot of such indices, Hilbert series, and partition functions are exactly solvable, without the need for loop-by-loop perturbative calculations. This is the famous supersymmetric localization program [15], initiated by mathematicians and field theorists, and later developed to the supergravity community. Supersymmetry also guarantees certain quantities are protected under *renormalization group* flow [16]. Moreover, it is 'required' by a consistent string theory, and a lot of supersymmetric gauge theories can be engineered by brane constructions. As a result, despite the failure in searching supersymmetry at particle physics accelerators, supersymmetric theories are still a beautiful and fruitful thing to study and help us to understand their non-supersymmetric partners.

The moduli space of vacua for a quantum field theory is defined to be the set of all possible vacuum states. The moduli spaces can be either discrete or continuous, and they can have interesting geometric structures to study. There are both physics and mathematics motivations to study them. For the physicists, it is always the lowest energy states that are most interesting. Because they are simple to solve compared to other states, and laboratory experiments on accelerators can only detect low energy states in string theory. Low-energy effective theories are good tools for doing calculations around those lowest-energy states. The idea of moduli spaces actually originates from mathematics, such as moduli spaces of curves, and moduli spaces of different structures on a manifold. For the mathematicians, the moduli spaces of vacua always have rich structures, the metric on them, the singularities, and so on. Those structures always have a deep connection with physics. A typical study on the moduli space is Seiberg and Witten's work in 1994 to study the moduli spaces of 4d $\mathcal{N} = 2$ theories [17, 18].

Classically, one can solve the equation of lowest energy to get all vacuum solutions. But a lot of the solutions are lifted by quantum effects, making the study difficult at the quantum level. However, supersymmetry makes things simple in two ways. Firstly, for theories with supersymmetry, the moduli spaces are generically continuous, as compared to discrete points. Secondly, with supersymmetry, the lifting of vacuum states doesn't happen in general. The structures remain under quantum corrections. To describe the moduli spaces, only scalars can have non-zero expectation values in vacuum states because of Lorentz symmetry, so it is natural to use scalar vevs to parametrize the moduli space of vacua. So the moduli spaces have different branches depending on what scalars have non-vanishing vevs on them. As a result of the lowest energy equations, the moduli spaces of vacua have a rich algebraic geometry structure as varieties. It is also interesting to study particular field configurations, such as instanton solutions. The solutions have many parameters in them, and they all have physical significance. Most importantly they can be identified as the vacuum state solutions in some field theory.

As algebraic geometric objects, the moduli spaces of vacua have coordinate rings, the *chiral ring*. A polynomial can be calculated for the chiral ring, the *Hilbert series*. Physically, the series is counting chiral operators in the theory. As a tool to study the theory, they can reveal many interesting properties of the theory, such as the global symmetry, the dimension of the moduli space, and so on [19]. As compared to an index, the Hilbert series can change in different strong coupling regime, while an index is usually insensitive to continuous deformation.

A large family of Lagrangian theories is represented by a quiver [20]. In brief, a quiver diagram provides information about the gauge group and the representation of matter in the theory, so the Lagrangian is completely and compactly encoded in a single quiver diagram. The motivation to study quiver gauge theories comes from string theory. A great number of quiver gauge theories can be engineered by brane systems. For example, 3d $\mathcal{N}=4$ theories are engineered in Type IIB string theories by D3-D5-NS5 brane systems. The world volume theory living on the D3 branes suspended between the intervals between the five branes is represented by a quiver diagram read out directly from the brane configurations [21]. Then tools from string theory can be used to study quiver gauge theories. The relevant example in this thesis is that 3d mirror symmetry is a result of S-duality in string theory [22]. Then the lessons learned from this family of quivers coming from string theory can be generalized to all other quivers.

Many complicated operations in field theories can be represented by simple diagrammatic operations on the quivers. For example, the Higgsing procedure can be represented by a simple quiver subtraction algorithm [2, 23], or a decay and fission algorithm [24, 25]. Gauging of a global symmetry can also be represented by a subtraction or a polymerization algorithm on the quiver [26, 27].

The motivation for the study of 3d $\mathcal{N}=4$ theories has many aspects [21, 28–41]. During the past few years, there has been enormous development in the geometry for Higgs branch of SCFT's with 8 supercharges [42–50], due to the techniques of magnetic quivers (see [45, 46, 51–58] and subsequent works), and 3d mirror symmetry. From representation theoretic arguments, there's no interacting SCFTs in dimensions higher than 6 [59, 60]. Construction of SCFTs in d=3,4,5,6 involves different methods such as brane systems and compactifications [61–65], but lots of those theories are non-Lagrangian and arise from the strong coupling limit, raising many difficulties to study them. One example is the moduli space of vacua in the strong coupling regime.

Since Higgs branches for SCFTs with 8 supercharges are hyper-Kähler [66], many of those spaces can be constructed as the Coulomb branch of a 3d $\mathcal{N}=4$ gauge theory represented by a quiver diagram, and the quivers are called *magnetic quivers*, corresponding to co-dim 3 magnetic BPS objects. The manetic quivers can be used to study the moduli spaces of many theories in the strong coupling regime.

3d $\mathcal{N}=4$ supersymmetric quantum field theories is a remarkable laboratory for the interplay between physics and mathematics. They have a moduli space of vacua with rich structures to study. Most surprisingly, those moduli spaces come in pairs, *3d mirror dual pairs* [28]. From a mathematics point of view, as symplectic singularities [67], many tools can be utilized to characterize their moduli spaces. Their coordinate ring, with a Poisson bracket on it, can be extracted from an Abelianization procedure [33], practically captured by a Hilbert series calculation [32]. They are also stratified spaces whose containing relations and local singularities are summarized by Hasse diagrams [68]. Much progress has been made in the symplectic duality program [69, 70]. From a physics perspective, the Hilbert series is counting half BPS chiral operators, graded by R-charges [71]. The singularities in the geometry reveal the breakdown of the low-energy effective description, and the possible appearance of new sets of massless states.

When Coulomb branch of a quiver has a symmetry, it is natural to ask what if the symmetry is gauged and whether the gauged theory is still given by a quiver. Our work in [1] focused on discrete automorphism symmetries acting on quiver diagrams, which turn out to be discrete symmetries on the Coulomb branch. In particular, when a quiver has an Abelian part, with a permutation symmetry exchanging U(1) gauge factors, then the permutation group can be gauged and the procedure gives an S_n orbifold of the original Coulomb branch. The resulting quiver has a non-Abelian node with multiple adjoint loops. This generalizes the previous work on discrete gauging in the sense that it applies to quivers with a shape of complete graph, which arise naturally as magnetic quivers for class $\mathcal{S}$ theories with irregular punctures. Besides, when there are Abelian gauge groups, the charge can be changed and a $\mathbb{Z}_n$ group can also be gauged, which generate a 1-form symmetry. This also gives an orbifold of the original Coulomb branch. Two technical tools are utilized to verify the quotient relation. One is the Molien sum on the Hilbert series. The other is the Abelianization procedure. The Molien sum formalism generalizes immediately to the O/Sp quivers, while the Abelianization doesn't obviously apply. Since the complete graph quiver and multiple loop quiver have a Class $\mathcal{S}$ origin, it is interesting to explore our result from a Hitchin system analysis. It is also meaningful to work out what local singularities the multiple loop quivers have in the Coulomb branch. Examples include non-normal isolated singularities μ_p.

From the point of 3d mirror symmetry, it's also meaningful to study the Higgs branch stratification and local singularities. Our work in [2] gives a complete solution to this problem for simply laced unitary quivers. By studying the Higgsing patterns, a quiver subtraction algorithm is worked out to give quivers for the slices. A complete list of local isolated singularities is worked out. The interesting thing is a monodromy acting on the slice along the base leaf, which can only happen in codimension 2. This gives the slice an additional symmetry. Although locally the slice doesn't change, this affects the Coulomb branch, i.e. the symplectic dual of the slice. The Namikawa Weyl group is also folded by the monodromy group. This is an analog as in F theory when the elliptic fibre is not split, a monodromy acting on the elliptic fibre around the discriminant locus can fold the gauge algebra. In a future work, analytic structures in the refined Hilbert series related with different Higgsing patterns is also analyzed. It is previously understood that when the flavor symmetry is broken by vev, the Hilbert series is given by a residue calculation. But it is also possible that after Higgsing the flavor symmetry doesn't change, and in this case there is a pole in Hilbert series of order higher than 1. This happens when a vev is assigned to a GIO with R charge higher than 2. This structure also sheds light on a recipe for calculating Hilbert series for decorated quivers. It is also expected that whenever non-flavor Higgsing is happening, different leaves in the Coulomb are dual to the same slice in the Higgs branch, and vice versa. There're also other interesting future directions to work on. For example, a quiver subtraction algorithm for O/Sp quivers can be worked out in a similar way by analyzing the Higgsing patterns. Stratification for theories with 4 supercharges is also expected. The difficulty is F-flat spaces are not always a complete intersection, i.e. F-term equations can have syzygies and not necessarily transform in the adjoint representation, which is different from the case of 8 supercharges.

In the next chapter, some basic background knowledge is introduced, including the calculation of Coulomb branch and Higgs branch Hilbert series, 3d mirror symmetry, magnetic quivers, and stratification of the moduli space.

1.1 Plan of the thesis

This thesis is organized as following:

- In the second chapter, a pedagogical explanation of all the objects studied and all tools used in the following chapters is briefly introduced
- In the third chapter, gauging of a discrete symmetry is presented, either a permutation symmetry or a cyclic symmetry.
- In the fourth chapter, stratification of Higgs branches are studied and summarized by a quiver subtraction algorithm. Different from previous quiver subtraction, the subtraction algorithm in this chapter features a bottom to up procedure, where the quivers for the slices are results of the subtraction, instead of the leaves.

Chapter 2

Background

In this chapter, a pedagogical introduction to the background materials is given. Topics including 3d $\mathcal{N} = 4$ supersymmetry, moduli spaces, chiral operators, monopole formula, and stratified spaces are introduced. All the introduction is organized toward the 3d mirror symmetry. The discussion is for completeness and relevance of following chapters. Some details are omitted and references are given when necessary.

2.1 3d $\mathcal{N}$=4 supersymmetry

The standard reference for supersymmetric field theories is [72–74]. Particularly for 3d, reference is [75, 76].

We start from the supersymmetry algebra. We focus on the SUSY algebra in flat spacetime $\mathbb{R}^{2,1}$ or $\mathbb{R}^3$. The spin group is SU(2) and the spinors transform in the fundamental representation which is pseudo-real. The R-symmetry of extended supersymmetry is SO(N). We mainly focus on the 3d $\mathcal{N} = 4$ superconformal field theories, and the superconformal symmetry is OSp(4|4).

Apart from the ordinary Poincaré algebra, which includes the commutation relations between the momentum P^μ and angular momentum $M^{\mu\nu}$, supersymmetry introduces the fermionic generators which are Majorana spinors and anti-commutation relations between them:

$$\{Q^I_\alpha, Q^J_\beta\} = \delta^{IJ}(\gamma^\mu)_{\alpha\beta}P^\mu \tag{2.1}$$

The indices α, β are spinor indices. The super charges transform in the vector representation of the R-symmetry SO(N) and I, J from 1 to N are the corresponding indices. In the case of $N = 4$, the R-symmetry is $\mathrm{SO}(4) = \mathrm{SU}(2)_H \times \mathrm{SU}(2)_C$. The conformal symmetry of flat 3-dimensional spacetime and the R-symmetry together constitute the bosonic part of the superconformal symmetry OSp(4|4).

Next we introduce the massless supermultiplets of 3d $\mathcal{N}=4$ theories. The vector multiplets and hyper multiplets can all be decomposed into 3d $\mathcal{N}=2$ vector multiplets and chiral multiplets. The 3d $\mathcal{N}=2$ chiral multiplets have 1 Weyl fermion ψ and 1 complex scalar ϕ. We can write it as $\Phi=(\phi,\psi)$. The 3d $\mathcal{N}=2$ vector multiplets have 1 vector A, 2 gauginos χ, and 1 real scalar σ. We can write it as $V=(\sigma,\chi,A)$. The vector A corresponds to the dual photon. Then the 3d $\mathcal{N}=4$ supermultiplets can be constructed as sums. The hypermultiplet is composed of 2 chiral multiplets. We write it as $H=(\Phi_1,\Phi_2)$. The vector multiplet is composed of 1 chiral multiplet and 1 vector multiplet. We write it as $Z=(\Phi,V)$. Those can also be obtained by firstly studying 4d $\mathcal{N}=2$ theories and then compactify to 3d $\mathcal{N}=4$ theories as in [77]. For the purpose of moduli spaces later, we are mainly interested in the scalars in the supermultiplets. Under the R-symmetry $\mathrm{SU}(2)_H\times\mathrm{SU}(2)_C$, the 2 complex scalars in the hypermultiplet transform as $[1;0]$ and the 4 real scalars in the vector multiplet transform as the adjoint of $\mathrm{SU}(2)_C$ and a singlet. There are also mass parameters and FI parameters. The mass transforms in adjoints of $\mathrm{SU}(2)_C$ and the FI parameter transforms in adjoints of $\mathrm{SU}(2)_H$.

An interesting feature of 3d $\mathcal{N}=4$ theories is the dual photon [78]. Since in 3d, the vector field has only 1 polarization, it's natural to think of it as a scalar. The equation of motion for a vector field reads $\mathrm{d}*F=0$. This immediately implies the 1-form $J=*F$ is closed. Thus J can be written as the exact form $J=d\gamma$. The 0-form γ is often referred to as the dual photon. Its equation of motion writes as $\mathrm{d}*\mathrm{d}\gamma=0$. The conservation of the current J reveals there is a hidden symmetry, often called topological symmetry, because the topological property of spacetime is explicitly used here.

3d $\mathcal{N}=4$ theories have global symmetries with the form of $G_H\times G_C$. The G_H is the flavor symmetry rotating hypermultiplets and the G_C is the topological symmetry from the dual photon. In the UV, there's only the Abelian topological symmetry and it can be enhanced to a non-Abelian symmetry in the IR.

2.2 Quiver gauge theories

To specify a 3d $\mathcal{N}=4$ theory, firstly a gauge group G should be specified. Then a matter representation R in which the hypermultiplets transform should be specified. Plenty of interesting theories (G,R) are given by a quiver diagram where G is a product of groups $G=G_1\times G_2\times\ldots G_n$ and the representation R is a direct sum of bifundamental representations of the factor groups [20].

Firstly 3d $\mathcal{N}=2$ quivers are introduced. A 3d $\mathcal{N}=2$ quiver diagram is composed of a set of nodes and a set of oriented arrows between the nodes. Note the similarity between a quiver diagram and a category and formally a quiver diagram can be thought of as a functor. To specify a 3d $\mathcal{N}=2$ gauge theory, we associated a factor of gauge group G_i to each node. For each arrow pointing from node j to node i, we associated a $\mathcal{N}=2$ chiral multiplet transforming in the fundamental representation of G_i and anti-fundamental representation of G_j. In addition, the superpotential is also needed to specify explicitly. The Lagrangian is then completely fixed by all those data if the mass parameters and FI parameters are taken to be 0, and the Kähler potential is canonical.

Then 3d $\mathcal{N} = 4$ quivers can be doubled from a 3d $\mathcal{N} = 2$ quiver. By a doubled quiver, we mean for each oriented arrow, there is another oriented arrow with the orientation reversed. A single unoriented line is drawn for this pair of arrows. The unoriented line represents a $\mathcal{N} = 4$ hypermultiplet with the pair of oriented arrows representing the two $\mathcal{N} = 2$ chiral multiplets of the hypermultiplet. The superpotential is fixed by the $\mathcal{N} = 4$ supersymmetry.

In summary, a quiver is a compact way of specifying a theory. The essence of quivers comes from string theory, because the bifundamental representations come naturally from string states stretching between two different sets of branes.

2.3 Moduli spaces of vacua

As the name indicates, the moduli space of vacua is the parameter space for the set of all gauge inequivalent vacua given by the theory. Each point in the space is a vacuum state of the theory, or a solution of the vacuum equations. The moduli space is usually parametrized by the vacuum expectation values of scalars in the theory. The moduli space can be studied in many aspects, either in geometry such as the metric on it, or in algebra such as the coordinate ring and symplectic structure. Physically, it is interesting to study the singularity structure of the moduli space because the low-energy effective description of the theory is often a sigma model towards the moduli space, and singularities are where the low-energy description breaks down, usually due to degrees of freedom that were integrated out becoming relevant.

Supersymmetry puts constraints on the geometry of the moduli space [66]. For theories with 4 supercharges the moduli space is Kähler and for theories with 8 supercharges the moduli space is hyper Kähler. Pedagogically one can think of a sigma model with some target space parametrized by the fields in the theory. Then the existence of SUSY transformation puts constraints on the target space geometry. The R-symmetry of the theory plays the role of structure group of the special geometry.

The moduli space of vacua has many different interesting subspaces termed as branches [17, 18]. Physically one can think that scalars in different species of supermultiplets parametrize different branches. A particular branch is defined by requiring some scalars to have zero vacuum expectation values and then this branch is parametrized by the other scalars. Note the similarity as subvarieties. For the example of a 3d $\mathcal{N} = 4$ theory, the moduli space has two interesting branches to study: the Higgs branch and the Coulomb branch. The Higgs branch is parametrized by the scalars in the hypermultiplets while the scalars in the vector multiplets have zero vevs. The R-symmetry factor $\mathrm{SU}(2)_H$ serves as the structure group for the hyper Kähler geometry. The flavor symmetry G_H is the isometry group preserving the hyper Kähler structure. There are non-renormalization theorems that the Higgs branch doesn't receive quantum corrections although this is not the case for Coulomb branch. Classically the Coulomb is parametrized by the scalars in the vector multiplets, but it gets quantum corrections. The R-symmetry factor $\mathrm{SU}(2)_C$ serves as the structure group for the hyper Kähler geometry. The topological symmetry G_C is the isometry group preserving the hyper Kähler structure.

To solve for the Higgs branch, one needs to solve for the F and D term equations, which are the real and complex moment map equations. Then the Higgs branch is obtained by taking the quotient by the gauge group. This procedure is termed as hyper Kähler quotient, or GIT quotient, or categorical quotient in mathematics. As for the Coulomb branch, classically the scalars in the vector multiplet take values in the maximal torus of the gauge group. Then the Coulomb branch is the space of all the scalars (3 real scalars + 1 periodic dual photon for each Abelian factor) quotient by the Weyl group of the gauge group. But the Coulomb branch receives quantum corrections both perturbative and non-perturbative [77, 79]. To illustrate this, the gauge invariant combinations of vector multiplet scalars are local operators and only take into account smooth configurations, but they don't take the contribution from the monopole operators which are charged under the topological symmetry. So the monopole operators constitutes an important part in the study of Coulomb branch.

A monopole operator is characterized by the failure of describing the gauge vector field in a single coordinate chart and the singularity of the gauge vector fields at the insertion point [78]. Around the insertion point of the monopole operator, one needs two hemi-spheres as coordinate patches to specify the gauge vector fields. By requiring the transition function between the two patches to be smooth and single-valued, the Dirac quantisation condition is found which states the magnetic charges should live as a co-character of the gauge group $\mathrm{Hom}(\mathrm{U}(1), G)$, the weight lattice of the Langlands dual group of the gauge symmetry.

2.4 3d mirror symmetry

There is an exciting duality among 3d $\mathcal{N} = 4$ theories due to the involution of SO(4) R-symmetry. Two different theories turn out to be the same at the IR point [28]. The Coulomb branches and the Higgs branches of the two theories swap in the duality. Thus there are two geometric equalities: the Coulomb branch of one theory equals the Higgs branch of the other theory, and vice versa. But in fact, there are more equalities in the duality. The mass parameters turn out to become the FI parameters of the dual theory. The vortex line and the Wilson lines are swapped in the duality.

Physicists are interested in the duality between the two theories. Given a theory, physicists ask what is the dual theory. Mathematicians are more interested in the duality between the two spaces, and ask what the dual space of a given space is [69, 70].

2.5 Counting chiral operators

The chiral operators are defined as gauge invariant operators annihilated by chiral derivatives. They have the important property that the correlation function of any time ordered product of chiral operators is independent of the spacetime location. The set of all chiral operators has the algebraic structure of a ring, called chiral ring [72, 80, 81].

It is important to notice the relation with complex algebraic geometry in mathematics. The chiral derivative is an analog of the complex holomorphic derivative. So chirality is a similar property as holomorphicity. One of the key ideas of complex algebraic geometry is that a geometric space can be studied from the ring of holomorphic functions defined on it. So a branch of the moduli space can be studied from the chiral operators that admit non-zero vevs on it. Thus chiral operators corresponds to holomorphic functions on the moduli space. If one assumes the chiral ring is the same as the coordinate ring, then the moduli space where a set of chiral operators can take non-zero vevs is thus the spectrum of the chiral ring. There are two typical sets of chiral operators. One can have non-zero vevs on the Coulomb branch and is called Coulomb branch chiral ring. Its spectrum is the Coulomb branch. The other can have non-zero vevs on the Higgs branch and is called Higgs branch chiral ring. Its spectrum is the Higgs branch.

The chiral ring is a graded ring. The grading is given by the weights of an SU(2) R-symmetry group, depending on whether it is Coulomb branch chiral ring or Higgs branch chiral ring. Selecting a Cartan subalgebra of the SU(2) is equivalent to picking up a complex structure from the hyper Kähler structure of the geometry. For the graded ring, the Hilbert series counting operators at each grading can provide lots of information about the ring.

For the Higgs branch, the chiral ring composed of gauge invariant combinations of the hyper multiplet scalars subjecting to the F and D term equations. So the Hilbert series is calculated by a Molien-Weyl integral over the complexified gauge group. The integrand is composed of the PE of the generators and the relations of the F-flat space. For the Coulomb branch, the Hilbert series is calculated by the monopole formula.

Here a brief review of the monopole formula is given. The Coulomb branch chiral ring operators are monopole operators dressed by complex scalars in the vector multiplet. The Hilbert series counts those dressed monopole operators, graded by their conformal dimension. A bare monopole operator is labelled by its magnetic charge $m \in \mathrm{Hom}(\mathrm{U}(1), G) = \Lambda_{\omega}^{G^{\vee}}$, which is the coweight lattice of the gauge group G. For gauge group G and hypermultiplet representation $\mathcal{R}$, the conformal dimension is given by [22, 82–84]

$$\Delta(m) = -\sum_{\alpha\in\Phi^{+}} |\langle\alpha, m\rangle| + \frac{1}{4}\sum_{\omega_i\in\mathcal{R}} |\langle\omega_i, m\rangle|. \tag{2.2}$$

The set of positive roots α of the algebra $\mathfrak{g}$ are denoted by Φ^{+}, and the ω_i are the weights for the matter representation $\mathcal{R}$ for the hypermultiplets. If the representation $\mathcal{R}$ is polarizable,

$\mathcal{R} = \mathcal{N} \oplus \bar{\mathcal{N}}$, then the conformal dimension simplifies to

$$\Delta(m) = -\sum_{\alpha \in \Phi^+} |\langle \alpha, m \rangle| + \frac{1}{2} \sum_{\omega_i \in \mathcal{N}} |\langle \omega_i, m \rangle|. \tag{2.3}$$

Then the refined Hilbert series is given by:

$$\mathrm{HS}(z,t) = \sum_{m \in \Lambda_\omega^{G^\vee}/\mathcal{W}_G} z^{J(m)} t^{2\Delta(m)} P_G[G_m](t)\,. \tag{2.4}$$

Here t is a fugacity for R-charge, and z is a fugacity for counting topological quantum numbers $J(m)$. There is a dressing factor, $P_G[G_m](t)$, accounting for the dressing of the monopole operators by the complex scalar in the vector multiplet, and it depends on the residual gauge group G_m that is unbroken by the magnetic charges. The dressing factor is counting Casimir invariants of the unbroken gauge group G_m.

The practical difficulty for the calculation of monopole formula comes from the infinite summation over the magnetic lattice, because the absolute values in the monopole formula divides the cone into many subregions. But usually one can compute the first few terms of the Hilbert series and this can already reveal lots of useful information.

The Hilbert series can be used to check 3d mirror pairs. Since the Higgs branch and Coulomb branch of a mirror pair swaps with each other, the Hilbert series of the Higgs branch of one theory should equal to the Hilbers series of the Coulomb branch of the mirror theory, and vice versa. Note that there are 4 Hilbert seies needed to be calculated and 2 equalities needed to be checked.

Another useful tool is Plethystic exponential, and its inverse, Plethystic logarithm [71, 85]. The Plethystic exponential of a multi-variable function is defined as:

$$\mathrm{PE}[f(t_1, t_2, \dots, t_n)] = \exp\left(\sum_{k=1}^{\infty} \frac{f(t_1^k, t_2^k, \dots, t_n^k)}{k} \right) \tag{2.5}$$

and the inverse transform is given by:

$$\mathrm{PL}[g(t_1, t_2, \dots, t_n)] = \sum_{k=1}^{\infty} \frac{\mu(k)}{k} \log(g(t_1^k, t_2^k, \dots, t_n^k)) \tag{2.6}$$

where $\mu(k)$ is the Möbius function.

Since the elements of the chiral ring can be constructed as symmetric products of certain generators, it often more useful to study a generating set of generators and relations. The Plethystic logarithm of Hilbert series is used to count the generators and relations generating the whole ring. Reversely, the Plethystic exponential is counting symmetric products of a given set of generators and relations. There is another version of Plethystic exponential and logarithm related with anti-symmetric products, but for the purpose of this thesis, only the symmetric version introduced here is relevant.

2.6 Stratification and Hasse diagram

In previous sections on moduli spaces, the importance of singularity structure is pointed out. So it is helpful to have a notion of how singular a singularity is, and then study the singular levels at different singular loci. One can imagine that different singular levels hint different phases of the theory. This is because at different singular loci, different sets of scalars acquire vevs and break the symmetry. The effective description is also different. Thus a diagram encoding the singular loci can be regarded as a phase diagram of the physical theory [8].

In mathematics, this notion coincides with the idea of stratification. Since the moduli spaces of our interests are symplectic singularities, a brief review of stratification of a symplectic singularity is reviewed, from both algebraic and geometric point of view.

From geometry, one can think of the stratification of a space as decomposing the space into a disjoint union of a sequence of subspaces. For a variety, one can look at the singular loci of the space. The singular loci itself is again a variety, either reducible or irreducible, of a smaller dimension. Then one can do the same procedure again. In this procedure, the variety is decomposed into a series of open subspaces which have different levels of singularity. Those spaces are called leaves. This series of subspaces have a partial ordering defined. One leaf is smaller than another if the first is contained in the closure of the second. Examples include [86, 87].

From algebra [88], a variety has its coordinate ring. For our interest, the symplectic singularity has a Poisson bracket defined on its coordinate ring. Then one can study the Poisson ideals of the coordinate ring. Note that there are always two trivial Poisson ideals, the whole ring itself and the identity element, as long as the singularity is not trivial (a point). The set of all Poisson ideals also has a partial ordering on it defined by containing relations. Interestingly, it can be shown for a symplectic singularity that the two notions of partial ordering coincide with each other. Physically, this matches the structure produced by partial Higgsing.

The partial ordering becomes more clear if one draws a Hasse diagram for it. A Hasse diagram can be drawn for any partially ordered sets. In the diagram, each point represents an element in the set. An oriented arrow is drawn connecting two points if there is a partial ordering between the two elements represented by the two corresponding points. For symplectic singularities, one more thing should be added, the *transverse slice*. The transverse slice itself is a symplectic singularity, and its dimension equals to the codimension of the smaller singularity inside the bigger singularity. The dimension of the singularity is always written by the point conventionally.

A phyisical comment follows from the discussion above. If one starts from the most singular point on the moduli space, i.e. the origin of the space, the point has the biggest global symmetry. It is invariant under the full $G_H \times G_C$ global symmetry. Then if one moves on the Higgs branch, the flavor symmetry G_H is broken while the topological symmetry G_C is preserved. As one moves to the less and less singular loci of the Higgs branch, the flavor symmetry is broken further and further. The same thing happens on the Coulomb branch but the broken symmetry is G_C.

Chapter 3

Discrete quotients on the Coulomb branch

This chapter introduces two operations in quiver gauge theories. The first operation, *collapse*, takes a quiver with a permutation symmetry S_n and gives a quiver with adjoint loops. The corresponding 3d $\mathcal{N} = 4$ Coulomb branches are related by an orbifold of S_n. The second operation, *multi-lacing*, takes a quiver with n nodes connected by edges of multiplicity k and replaces them by n nodes of multiplicity qk. The corresponding Coulomb branch moduli spaces are related by an orbifold of type $\mathbb{Z}_q^{n-1}$. Collapse generalises known cases that appeared in the literature [89–91]. These two operations can be combined to generate new relations between moduli spaces that are constructed using the magnetic construction.

3.1 Introduction

In recent years diagrammatic techniques on 3d $\mathcal{N} = 4$ quiver gauge theories have been developed and provide insight and simple tools to study their moduli spaces of vacua. Examples of diagrammatic techniques on 3d $\mathcal{N} = 4$ quiver gauge theories include *quiver subtraction* [23] which can be used to study the stratification of the Coulomb branch into a finite number of symplectic leaves [92–94] or to study hyper-Kähler quotients of Coulomb branches [26]. The former also has a realisation in string theory [95, 96].

More pertinent to this work is the study of discrete actions on the Coulomb branch via diagrammatic techniques. Examples include *folding* [97, 98] and *discrete gauging* [89–91, 98]. These realise discrete actions on the Coulomb branch.

One result of this work is a generalisation of the discrete gauging of a bouquet of U(1) in 3d $\mathcal{N} = 4$ unitary quiver gauge theories introduced in [89–91]. The discrete gauging of such a bouquet has a realisation in M-theory as a stack of M5 branes probing an A_k singularity and making these M5 branes coincident. There is a natural S_n action permuting the n M5. The reduction of the M-theory set-up to Type IIA corresponds to the same S_n action on

NS5 branes. The magnetic quiver [54] for the theory on the worldvolume of the D6 branes has a bouquet of the U(1) gauge nodes when the NS5 are not coincident and becomes a U(n) gauge node with an adjoint hypermultiplet when the NS5 are coincident. This is illustrated below with the U(1) in the bouquet shown in orange:

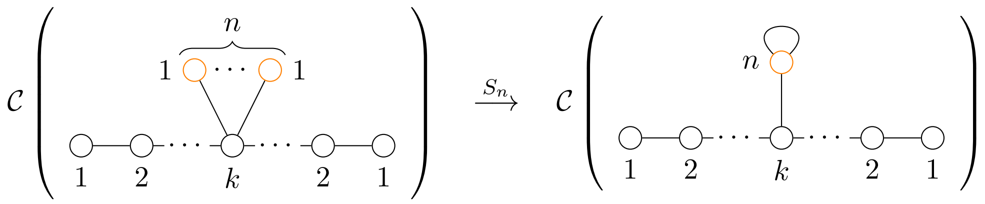

(3.1)

An application of the discrete quotients of Coulomb branches was to physically realise the results of Kostant-Brylinski [99], which relate certain nilpotent orbit closures under discrete quotients.

In this work the notion of a bouquet of U(1) gauge nodes in a unitary $3d\,\mathcal{N}=4$ quiver gauge theory is encompassed and extended to a *complete graph* of U(1) gauge nodes. There is a natural S_n permutation of these U(1) gauge nodes. This outer automorphism symmetry can be gauged and consequently there is a discrete S_n action on the Coulomb branch.

A second result of this work is to realise orbifold actions on the Coulomb branch by turning simply laced edges into non-simply laced edges [100]. The relationships between quivers with simply laced and non-simply laced edges were studied in [101, 102] and are studied further here.

These two new diagrammatic techniques, named *collapse* and *multi-lacing* respectively, are applied to various quivers and examples are presented for each technique applied on its own and also in combination.

There is a deep and rich connection between Coulomb branches and the mathematics of symplectic singularities, and in particular to slices in the nilpotent cone of semi-simple Lie algebras. The techniques of collapse and multi-lacing may be applied to quivers to study these moduli spaces. For example, the S_2 quotient of the Kleinian A-type singularity to the D-type singularity is constructed as a Coulomb branch. In addition many new discrete quotients of known moduli spaces such as $\overline{min.A_2}=a_2$, $\overline{min.A_3}=a_3$, and $\overline{minD_4}=d_4$ are constructed. Another outcome of this work is the Coulomb branch construction of a_2/S_4 and d_4/S_4, which appear respectively as a Słodowy slice in the nilpotent cone of $\mathfrak{e}_8$ between the nilpotent orbits with Bala-Carta labels $E_8(a_6)$ and $E_8(b_6)$ and as a Słodowy slice in the nilpotent cone of $\mathfrak{f}_4$ between the nilpotent orbits with Bala-Carter labels $F_4(a_3)$ and A_2 [6, 103]. One way of constructing d_4/S_4 as a Coulomb branch is through the discrete gauging of a bouquet. The discrete gauging of a bouquet is not amenable for the case of a_2/S_4. Instead, the isomorphism $S_4 \cong \mathbb{Z}_2^2 \rtimes S_3$ is employed. On the quiver, a combination of the two new techniques, orbifold and complete graph discrete quotients, are used to achieve the desired result. Specifically, we have the first construction of a_2/S_4 as a Coulomb branch and now two ways of constructing d_4/S_4.

Another outcome of this work is the discrete quotient on the Coulomb branch by a semi-direct product of discrete groups rather than a direct product of discrete groups.

The quivers for the $3d$ mirrors of certain Argyres-Douglas theories contain a complete graph [104, 105]. The discrete quotient on the Coulomb branch of the $3d$ mirrors are computed.

Outline of the chapter. This chapter is organised as follows. In Section 3.2 the complete graph quiver is introduced and the notation that is used throughout this paper is defined. The claim that there is an S_n quotient between the Coulomb branches of quivers with complete graphs and a $\mathrm{U}(n)$ gauge node with some number of adjoint hypermultiplets is stated. In Section 3.3 the monopole formula is introduced as well as the Molien sum on the monopole formula. The claim made in Section 3.2 is proved. The Molien sum on the monopole formula realising the orbifold relation between simply and non-simply laced quivers is also presented. In Section 3.4 the Abelianisation procedure is introduced. In Section 3.5 many examples of the S_n quotient are presented. These include the S_2 gauging of the A-type singularity to the D-type singularity, and, additionally, the $S_2 \times S_2$ gauging of the A_3 affine quiver. In Section 3.6 examples of $\mathbb{Z}_q$ quotient are presented. In Section 3.7 a combination of the S_n and $\mathbb{Z}_q$ quotients on the Coulomb branch are combined. In Section 3.8 the S_n quotient is generalised to other types of gauge group. In Section 3.9 conclusion are drawn and future work is discussed.

3.2 Discrete quotient on the quiver

Loops and complete graphs. The first family of quivers studied in this paper is $\mathcal{CG}_{n,k}$, the family of complete graphs shown in Figure 3.1.

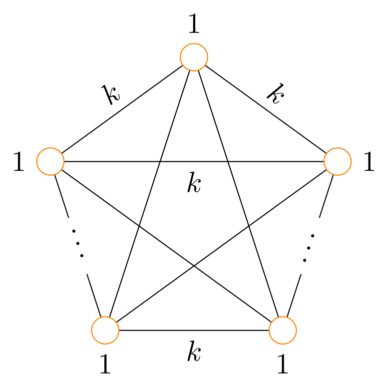

Figure 3.1: The complete graph quiver $\mathcal{CG}_{n,k}$ with n nodes of $\mathrm{U}(1)$ and edge multiplicity k. Henceforth $k = 2g - 2$.

The quiver $\mathcal{CG}_{n,k}$ consists of n nodes of $\mathrm{U}(1)$ with each pair of $\mathrm{U}(1)$s connected by k hypermultiplets transforming in the bi-fundamental representation. An overall $\mathrm{U}(1)$ acts freely and the faithfully acting gauge group is $\mathrm{U}(1)^n/\mathrm{U}(1)$. This family received some attention as the $3d$ mirror of the Argyres Douglas theories of type (A_{n-1}, A_{nk-1}) [104, 106], i.e. the Coulomb/Higgs branch of the $\mathcal{CG}_{n,k}$ theory is the Higgs/Coulomb branch of the

3d (A_{n-1}, A_{nk-1}) theory, respectively. For most quivers studied in this paper only even k is needed, and furthermore a convenient parametrisation is $k = 2g - 2$, where $g \in \mathbb{Z}^+$ is suggestive of the genus of a Riemann surface, as becomes clearer in Section 3.5.5. Note that there is an S_n permutation symmetry of the U(1) gauge nodes which comes from the outer automorphism symmetry of $\mathcal{CG}_{n,2g-2}$. Correspondingly, the Coulomb branch has this S_n symmetry, and one can construct many orbifolds by gauging a subgroup of this symmetry.

The second family of quivers studied here is the multi-loop quiver $\mathcal{ML}_{n,g}$ shown in Figure 3.2. This quiver consists of a $\mathrm{U}(n)$ gauge group with g hypermultiplets in the adjoint representation. As the centre U(1) is acting trivially on the matter content, the faithfully acting gauge group is $\mathrm{PSU}(n)$.

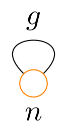

Figure 3.2: Multi-loop quiver $\mathcal{ML}_{n,g}$ of $\mathrm{U}(n)$ gauge group with g adjoints.

The two main results of this paper are

1. The Coulomb branches of $\mathcal{ML}_{n,g}$ and $\mathcal{CG}_{n,2g-2}$ are related by a quotient of the S_n symmetry:
$$\mathcal{C}(\mathcal{ML}_{n,g}) = \mathcal{C}(\mathcal{CG}_{n,2g-2})/S_n\,. \tag{3.2}$$
Here the edge multiplicity k is required to be even. Odd multiplicity gives non-integer g which makes the quiver of Figure 3.2 ill defined. This S_n action represented on quivers is the *collapse* of the $\mathcal{CG}_{n,2g-2}$ quiver to $\mathcal{ML}_{n,g}$.

2. Given a complete graph quiver $\mathcal{CG}_{n,k}$, if the edge multiplicity is increased to be q-fold, the quiver becomes $\mathcal{CG}_{n,qk}$, and the Coulomb branches are related by a quotient of $\mathbb{Z}_q^{n-1}$:
$$\mathcal{C}(\mathcal{CG}_{n,qk}) = \mathcal{C}(\mathcal{CG}_{n,k})/\mathbb{Z}_q^{n-1}\,. \tag{3.3}$$
This $\mathbb{Z}_q^{n-1}$ action represented on quivers is the *multi-lacing* of the $\mathcal{CG}_{n,k}$ quiver to $\mathcal{CG}_{n,qk}$.

There are some corollaries of these two results.

Combined action. Notice that the S_n symmetry is preserved after the $\mathbb{Z}_q^{n-1}$ quotient: $\mathcal{CG}_{n,1}$ and $\mathcal{CG}_{n,q}$ have the same outer-automorphism symmetry, so one can combine the two relations (3.2) and (3.3) above, and result in the following quotient relation:

$$\mathcal{C}(\mathcal{ML}_{n,g}) = \mathcal{C}(\mathcal{CG}_{n,1})/\mathbb{Z}_{2g-2}^{n-1} \rtimes S_n. \tag{3.4}$$

The composition is a semi-direct product, since the S_n symmetry also permutes these $n-1$ $\mathbb{Z}_q$s.

Connecting to a background quiver. The two families of quivers $\mathcal{CG}_{n,2g-2}$ and $\mathcal{ML}_{n,g}$ can be connected to a *pivot* node of a quiver $\mathcal{Q}_B$.

Then there are two families of quivers $\mathcal{Q}_{3.3a}$ and $\mathcal{Q}_{3.3b}$, shown in Figure 3.3a and Figure 3.3b respectively. The dotted lines in the quivers $\mathcal{Q}_{3.3a}$ and $\mathcal{Q}_{3.3b}$ refer to a link of any type to the same pivot node in $\mathcal{Q}_B$. For example, the dotted links could be a single bi-fundamental hypermultiplet, multiple bi-fundamental hypermultiplets, or directed non-simply laced edges. They can also be connected to multiple pivot nodes in $\mathcal{Q}_B$ as long as the links to that pivot are all the same for the U(1) nodes in the complete graph.

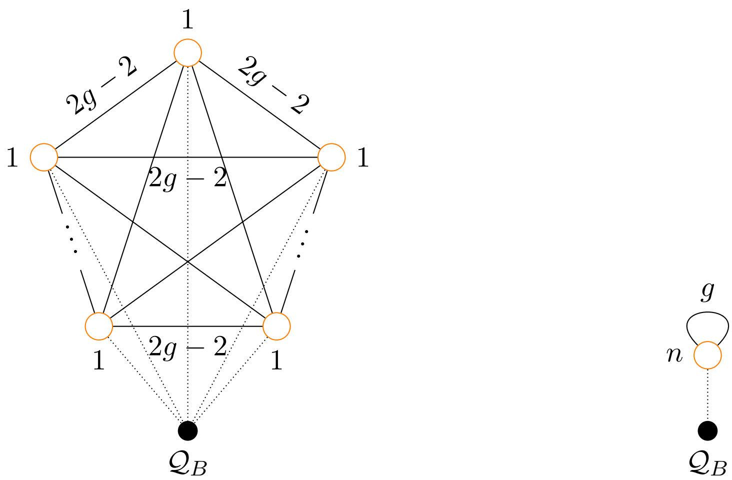

(a) (b)

Figure 3.3: a: Quiver $\mathcal{Q}_{3.3a}$ which has the complete graph subquiver $\mathcal{CG}_{n,2g-2}$, connecting to background $\mathcal{Q}_B$. b: Quiver $\mathcal{Q}_{3.3b}$ for U(n) gauge group with g adjoints, connecting to background $\mathcal{Q}_B$.

By adding this pivot node, the quiver outer-automorphism still contains the same S_n, hence the same quotient relation on the Coulomb branch holds:

$$\mathcal{C}(\mathcal{Q}_{3.3b}) = \mathcal{C}(\mathcal{Q}_{3.3a}\ )/S_n\,. \tag{3.5}$$

For the special case of $g = 1$ and each connection to some gauge node in $\mathcal{Q}_B$ is a single bi-fundamental, claim (3.5) reproduces the S_n quotient result for a bouquet of U(1) in [89–91].

Moreover, the complete graph part of $\mathcal{Q}_{3.3a}$ contains subgraphs which themselves are complete graphs of m nodes ($m \leq n$). So Claim (3.5) implies that any S_m with $m \leq n$ can be quotiented from $\mathcal{Q}_{3.3a}$. An important consequence of this relation is that every unitary quiver with a loop can be replaced by a quiver that has no loops, but instead admits a discrete permutation symmetry.

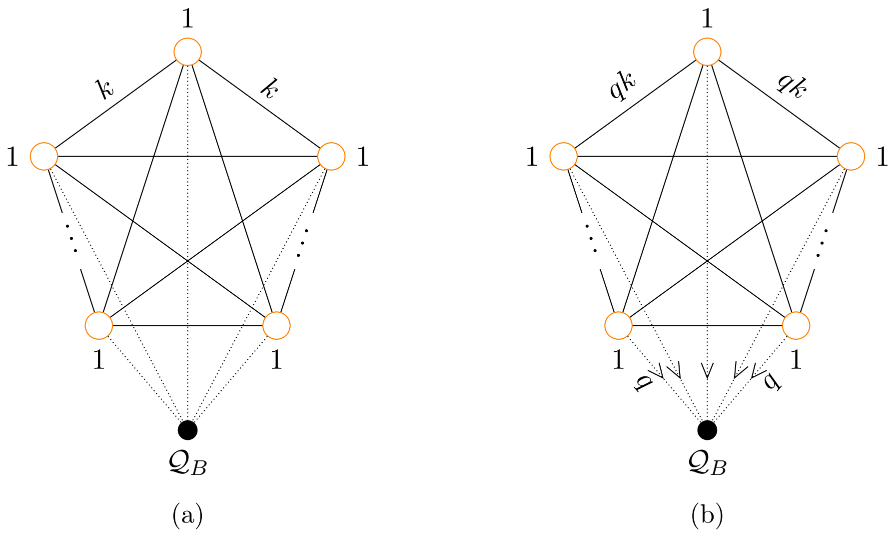

Figure 3.4: a: $\mathcal{CG}_{n,k}$ with simply laced edges connecting a simply laced $\mathcal{Q}_B$. b: $\mathcal{CG}_{n,qk}$ with q laced edges connecting a simply laced $\mathcal{Q}_B$.

The $\mathbb{Z}_q$ quotient relation also holds when connecting to a background quiver. The following claims are made[1]:

$$\mathcal{C}\left(\mathcal{Q}_{3.4b}\right) = \begin{cases} \mathcal{C}\left(\mathcal{Q}_{3.4a}/\mathbb{Z}_q^{n-1}\right) \,, & \text{when } \mathcal{Q}_B \text{ is empty or unframed}\,, \\ \mathcal{C}\left(\mathcal{Q}_{3.4a}/\mathbb{Z}_q^{n}\right) \,, & \text{when } \mathcal{Q}_B \text{ is framed}\,, \end{cases} \tag{3.6}$$

the reason for the different action for the framed and unframed $\mathcal{Q}_B$ is discussed in Section 3.3.3.

Notice that the S_n symmetry is preserved after $\mathbb{Z}_q^n$ quotient, and the S_n symmetry permutes these n $\mathbb{Z}_q$s. The following claims are made:

$$\mathcal{C}\left(\mathcal{Q}_{3.4b}/S_n\right) = \begin{cases} \mathcal{C}\left(\mathcal{Q}_{3.4a}/\mathbb{Z}_q^{n-1} \rtimes S_n\right) \,, & \text{when } \mathcal{Q}_B \text{ is empty or unframed}\,, \\ \mathcal{C}\left(\mathcal{Q}_{3.4a}/\mathbb{Z}_q^{n} \rtimes S_n\right) \,, & \text{when } \mathcal{Q}_B \text{ is framed}\,. \end{cases} \tag{3.7}$$

3.3 Generalised Molien sum and Coulomb branch Hilbert series

The Molien sum is a method to calculate the Hilbert series of an orbifold from a known Hilbert series, more details are in Appendix 6.2. In this section the generalised Molien sum on the monopole formula is introduced and (3.2) and (3.5) are proved using the Hilbert series.

[1]This claim does not rely on the complete graph structure. In fact, one can replace the complete graph with an arbitrary simply-laced Abelian quiver, and the quotient relation on Coulomb branch still holds.

3.3.1 Conformal dimension and monopole formula

The monopole formula, introduced in [32], is a method to calculate the Coulomb branch Hilbert series of a 3d $\mathcal{N}=4$ gauge theory. To evaluate the monopole formula, firstly the conformal dimension of the bare monopole operator [22] is determined. Further details about the monopole formula are in Appendix 6.1.

The conformal dimension for the $\mathcal{CG}_{n,2g-2}$ theory is computed as

$$\Delta(m_1,\cdots,m_n)=(g-1)\sum_{1\leq i,j\leq n}|m_i-m_j|. \tag{3.8}$$

where m_i labels the magnetic charges and $(m_1,\cdots,m_n)\in\mathrm{Hom}(\mathrm{U}(1),\mathrm{U}(n))=\Lambda_\omega^{\mathrm{U}(n)^\vee}=\mathbb{Z}^n$. The key point is that the $\mathcal{ML}_{n,g}$ theory has exactly the same conformal dimension.

Given this fact for the standalone quivers $\mathcal{CG}_{n,2g-2}$ and $\mathcal{ML}_{n,g}$ it is a simple extension to show that the conformal dimension when these quivers are attached to a background quiver $\mathcal{Q}_B$, as in quivers $\mathcal{Q}_{3.3b}$ and $\mathcal{Q}_{3.3a}$, is also the same,

$$\Delta(m_1,\ldots,m_n;\vec{B})=(g-1)\sum_{1\leq i,j\leq n}|m_i-m_j|+\sum_{1\leq j\leq l}\sum_{1\leq i\leq n}\Delta_j(m_i;\vec{B})+\Delta[\mathcal{Q}_B],. \tag{3.9}$$

Here, $\Delta[\mathcal{Q}_B]$ is the contribution from $\mathcal{Q}_B$. There could be links to each of the l gauge nodes in $\mathcal{Q}_B$, the contribution from these links to the j^{th} node in $\mathcal{Q}_B$ is denoted $\Delta_j(m_i;\vec{B})$ for $1\leq j\leq l$. The contribution $\Delta_j(m_i;\vec{B})$ takes the same functional form for all m_i. This is the only requirement for the links to $\mathcal{Q}_B$ in the quivers. So those links can be a single bi-fundamental hypermultiplet, multiple bi-fundamental hypermultiplets, and also directed non-simply laced edges, as long as they are all the same. Note that if a non-simply laced edge is used then these must all be directed in the same way for all connections to $\mathcal{Q}_B$.

The conformal dimensions for the $\mathcal{CG}_{n,2g-2}$ and the $\mathcal{ML}_{n,g}$ are the same, but the difference in Hilbert series for the Coulomb branch of $\mathcal{Q}_{3.3b}$ and $\mathcal{Q}_{3.3a}$ only comes from the magnetic lattice and the dressing factors.

3.3.2 Generalised Molien sum of S_n on the monopole formula

We take the specific action of S_n on the monopole formula and explain how the generalised Molien sum works.

Let us start with the quiver $\mathcal{Q}_{3.3a}$, which contains n identical U(1) nodes and a background $\mathcal{Q}_B$. Quiver $\mathcal{Q}_{3.3a}$ is unchanged under permutation of those n U(1) nodes, i.e. there is a $S_n\subset\mathrm{Out}(\mathcal{Q}_{3.3a})$.

We label the magnetic flux associated to the i-th node $\mathrm{U}(1)_i$ as m_i, and the collective magnetic fluxes associated to $\mathcal{Q}_B$ are denoted by $\vec{B}$. We label the dressing factor as $P_{\mathrm{U}(1)^n}=\frac{1}{(1-t^2)^n}$ and $P_B(\vec{B})$. The monopole formula of $\mathcal{Q}_{3.3a}$ can be written as:

$$\mathrm{HS}\left(\mathcal{C}(\mathcal{Q}_{3.3a})\right) = \sum_{m_1,\ldots,m_n,\vec{B}} P_{\mathrm{U}(1)^n} P_B(\vec{B}) \cdot z_1^{m_1} \cdots z_n^{m_n} Z(\vec{B}) \cdot t^{\Delta(m_1,\ldots,m_n;\vec{B})}, \tag{3.10}$$

where the z_i are topological fugacities for the $\mathrm{U}(1)_i$ and $Z(\vec{B})$ is a monomial of topological fugacities associated to gauge nodes in $\mathcal{Q}_B$. The action of S_n permutes magnetic fluxes m_i, topological fugacities z_i and Casimir invariants, however leaves $P_B(\vec{B})$ and $Z(\vec{B})$ invariant by construction. This can be implemented in the monopole formula by restricting it to the fixed loci of $\sigma \in S_n$, which is discussed below in detail.

Elements of S_n can be written as cycles: $\sigma = (i_1 \ \ldots \ i_{\sigma_1})(i_{\sigma_1+1} \ \ldots \ i_{\sigma_1+\sigma_2}) \cdots (i_{n-\sigma_k+1} \ \ldots \ i_n)$, where $\sum_{l=1}^{k} \sigma_l = n$. For example, $(1\ 3)(2\ 5\ 4) \in S_5$ acts on the magnetic fluxes as:

$$(m_1, m_2, m_3, m_4, m_5) \to (m_3, m_5, m_1, m_2, m_4). \tag{3.11}$$

Under the action of σ, the fixed locus for the magnetic fluxes is written as identifying the fluxes within the same cycle, i.e. $m_{i_1} = \cdots = m_{i_{\sigma_1}}, \ldots, m_{i_{n-\sigma_k+1}} = \cdots = m_{i_n}$. The same rule applies for the topological fugacities z_i.

The next step is to determine the dressing factors under σ. The Casimir invariants form the polynomial ring of $\mathbb{C}^n$. The degree of each coordinate is scaled by a factor of 2 and the Hilbert series $\frac{1}{(1-t^2)^n}$ is exactly the dressing factor of $\mathrm{U}(1)^n$. The Hilbert series of the invariant ring under S_n follows from the Molien formula:

$$\begin{aligned} \mathrm{HS}\left((\mathbb{C}^n)^{S_n}\right) &= \frac{1}{n!} \sum_{\sigma \in S_n} \frac{1}{\det(1 - t^2 \cdot \sigma)} \\ &= \frac{1}{n!} \sum_{\sigma \in S_n} \frac{1}{(1-t^{2\sigma_1}) \cdots (1-t^{2\sigma_k})} \\ &= \frac{1}{(1-t^2)\cdots(1-t^{2n})} \,. \end{aligned} \tag{3.12}$$

which is the dressing factor for the unbroken $\mathrm{U}(n)$. Hence, on the fixed loci of σ, the dressing factors turns into:

$$P_{\mathrm{U}(1)^n} = \frac{1}{(1-t^2)^n} \quad \xrightarrow{\sigma} \quad \frac{1}{\det(1-t^2\cdot\sigma)} = \frac{1}{(1-t^{2\sigma_1})\cdots(1-t^{2\sigma_k})} \tag{3.13}$$

Now the monopole formula under the action of σ is expressed. The fugacities z_i and $Z(\vec{B})$ are set to 1 for brevity, however recall that the z_i have the same behaviour as $t^{\Delta(m_1,\ldots,m_n;\vec{B})}$ under S_n and $Z(\vec{B})$ is invariant. The monopole formula under the element σ becomes:

$$\mathrm{HS}\left(\mathcal{C}(\mathcal{Q}_{3.3a})\right)^{\sigma} = \sum_{\vec{B}} \sum_{m_{i_1}=\ldots=m_{i_{\sigma_1}}} \cdots \sum_{m_{i_{n-\sigma_k+1}}=\ldots=m_{i_n}} \left(\prod_{l=1}^{k} \frac{1}{(1-t^{2\sigma_l})} \right) P_B(\vec{B}) \cdot t^{\Delta(m_1,\ldots,m_n;\vec{B})} \,. \tag{3.14}$$

According to Molien formula, the monopole formula applied to $\mathcal{C}\left(\mathcal{Q}_{3.3a}\right)/S_n$ is the average over the S_n action:

$$\mathrm{HS}\left(\mathcal{C}\left(\mathcal{Q}_{3.3a}/S_n\right)\right) = \frac{1}{n!}\sum_{\sigma\in S_n} \mathrm{HS}\left(\mathcal{C}\left(\mathcal{Q}_{3.3a}\right)\right)^{\sigma}. \tag{3.15}$$

This generalised Molien sum is realised through cycle index for special cases in [90] and also agrees with the Hilbert series of the wreathed quiver [97].

Proof of the S_n relation. In this paragraph, the claim (3.5) is proved at the level of the Hilbert series. For claim (3.5) to be true, the following must hold:

$$\mathrm{HS}\left(\mathcal{C}\left(\mathcal{Q}_{3.3a}/S_n\right)\right) = \mathrm{HS}\left(\mathcal{C}\left(\mathcal{Q}_{3.3b}\right)\right). \tag{3.16}$$

To begin with, the monopole formula of $\mathcal{Q}_{3.3b}$ can be written as:

$$\mathrm{HS}\left(\mathcal{C}(\mathcal{Q}_{3.3b})\right) = \sum_{\vec{B}} \sum_{m_1\geq\cdots\geq m_n} P_{\mathrm{U}(n)}(m_1,\ldots,m_n)P_B(\vec{B})\cdot t^{\Delta(m_1,\ldots,m_n;\vec{B})}. \tag{3.17}$$

where the magnetic fluxes are restricted to the principle Weyl chamber, and $P_{\mathrm{U}(n)}(m_1,\ldots,m_n)$ are the dressing factors of $\mathrm{U}(n)$. The value of $P_{\mathrm{U}(n)}$ is determined by the number of identical magnetic fluxes [32]. If the values of the fluxes $(m_1,\ldots,m_n)$ satisfy $m_{i_1}=\cdots=m_{i_{\sigma_1}}>\cdots>m_{i_{n-\sigma_k+1}}=\cdots=m_{i_n}$, then $P_{\mathrm{U}(n)}(m_1,\ldots,m_n)=\frac{1}{(1-t^2)\ldots(1-t^{2\sigma_1})}\cdots\frac{1}{(1-t^2)\ldots(1-t^{2\sigma_k})}$. A short-hand notation for the fixed loci of vector of magnetic fluxes under σ is introduced as:

$$(m,\sigma): \qquad m_{i_1}=\ldots=m_{i_{\sigma_1}},\ldots,m_{i_{n-\sigma_k+1}}=\ldots=m_{i_n}, \tag{3.18a}$$

$$(m;\sigma): \qquad m_{i_1}=\ldots=m_{i_{\sigma_1}}>\ldots>m_{i_{n-\sigma_k+1}}=\ldots=m_{i_n}, \quad \text{with all possible orderings of the cycles in } \sigma. \tag{3.18b}$$

For example, $(m,(1\ 3)(2\ 5\ 4))$ means $m_1=m_3,\ m_2=m_5=m_4$, and $(m;(1\ 3)(2\ 5\ 4))$ means $m_1=m_3>m_2=m_5=m_4 \bigcup m_2=m_5=m_4>m_1=m_3$. In addition $\sum_{(m,\sigma)}$ and $\sum_{(m;\sigma)}$ denotes the sum of the magnetic flux with respect to these conditions.

Without restricting the monopole formula (3.17) to the principal Weyl chamber, it can be expressed as:

$$\mathrm{HS}\left(\mathcal{C}(\mathcal{Q}_{3.3b})\right) = \sum_{\vec{B}}\sum_{\sigma\in S_n}\frac{\sigma_1!\cdots\sigma_k!}{n!}\sum_{(m;\sigma)}\frac{1}{(1-t^2)\cdots(1-t^{2\sigma_1})}\cdots\frac{1}{(1-t^2)\cdots(1-t^{2\sigma_k})}P_B(\vec{B})\cdot t^{\Delta(m_1,\ldots,m_n;\vec{B})}. \tag{3.19}$$

With (3.12), the monopole formula (3.19) is rewritten as:

$$\mathrm{HS}\left(\mathcal{C}(\mathcal{Q}_{3.3b})\right) = \sum_{\vec{B}}\sum_{\sigma\in S_n}\frac{\sigma_1!\cdots\sigma_k!}{n!}\sum_{(m;\sigma)}\left(\prod_{\sigma_i\in\sigma}\left(\frac{1}{\sigma_i!}\sum_{\rho'\in S_{\sigma_i}}\frac{1}{(1-t^{2\rho'_1})\cdots(1-t^{2\rho'_{l'}})}\right)\right) \tag{3.20}$$

$$\cdot P_B(\vec{B})\cdot t^{\Delta(m_1,\ldots,m_n;\vec{B})}$$

$$= \frac{1}{n!}\sum_{\vec{B}}\sum_{\sigma\in S_n}\sum_{\rho\in S_{\sigma_1}\times\ldots\times S_{\sigma_k}}\sum_{(m;\sigma)}\frac{1}{(1-t^{2\rho_1})\cdots(1-t^{2\rho_l})} \tag{3.21}$$
$$\cdot P_B(\vec{B})\cdot t^{\Delta(m_1,\ldots,m_n;\vec{B})}$$
$$= \frac{1}{n!}\sum_{\vec{B}}\sum_{\rho\in S_n}\sum_{\sigma\ni\rho}\sum_{(m;\sigma)}\frac{1}{(1-t^{2\rho_1})\cdots(1-t^{2\rho_l})}P_B(\vec{B})\cdot t^{\Delta(m_1,\ldots,m_n;\vec{B})}. \tag{3.22}$$

Here $(\rho'_1,\ldots,\rho'_{l'})$ are σ_i-partition corresponding to the sizes of cycles of $\rho'\in S_{\sigma_i}$, and $(\rho_1,\ldots,\rho_l)$ are n-partition corresponding to the sizes of cycles of $\rho\in S_{\sigma_1}\times\ldots\times S_{\sigma_k}$, the minimal permutation subgroup containing σ. A further bit of notation is that the sum over all $\sigma\in S_n$ whose minimal permutation subgroup contains $S_{\rho_1}\times\ldots\times S_{\rho_l}$ is denoted $\sum_{\sigma\ni\rho}$. Moreover, if follows that $\sum_{\sigma\in S_n}\sum_{\rho\in S_{\sigma_1}\times\ldots\times S_{\sigma_k}}$ is equivalent to $\sum_{\rho\in S_n}\sum_{\sigma\ni\rho}$. Also note that:

$$\sum_{(m,\rho)} t^{\Delta(m_1,\ldots,m_n;\vec{B})} = \sum_{\sigma\ni\rho}\sum_{(m;\sigma)} t^{\Delta(m_1,\ldots,m_n;\vec{B})}, \tag{3.23}$$

for example, $\sum_{(m,(1\ 3)(2\ 5\ 4))} = \sum_{m_1=m_3,m_2=m_5=m_4} = \sum_{m_1=m_2=m_3=m_4=m_5} + \sum_{m_1=m_3>m_2=m_5=m_4} + \sum_{m_1=m_3<m_2=m_5=m_4}$.
Combining (3.14), (3.15), (3.20) and (3.23), the following HS is obtained:

$$\begin{aligned}
\mathrm{HS}\left(\mathcal{C}(\mathcal{Q}_{3.3b})\right) &= \frac{1}{n!}\sum_{\vec{B}}\sum_{\rho\in S_n}\sum_{(m,\rho)}\frac{1}{(1-t^{2\rho_1})\cdots(1-t^{2\rho_l})}P_B(\vec{B})\cdot t^{\Delta(m_1,\ldots,m_n;\vec{B})}\\
&= \frac{1}{n!}\sum_{\vec{B}}\sum_{\sigma\in S_n}\sum_{(m,\sigma)}\frac{1}{(1-t^{2\sigma_1})}\cdots\frac{1}{(1-t^{2\sigma_k})}P_B(\vec{B})\cdot t^{\Delta(m_1,\ldots,m_n;\vec{B})}\\
&= \mathrm{HS}\left(\mathcal{C}(\mathcal{Q}_{3.3a}/S_n)\right),
\end{aligned} \tag{3.24}$$

here the first line to the second line is just a relabelling from ρ to σ. Hence, Claim (3.5) is proved at the level of the Hilbert series.

Ungauging. One can always ungauge on $\mathcal{Q}_B$ if it is non-empty. However, if $\mathcal{Q}_B$ is empty, one can set an arbitrary $m_i=0$ and take a $\frac{1}{1-t^2}$ factor away from the whole dressing factor. The proof proceeds analogous to the above. Hence, the Claim (3.2) is also verified on the level of the Hilbert series.

3.3.3 Generalised Molien sum of $\mathbb{Z}_q^n$ on the monopole formula

In this section, the assumption that the edges between the complete graph and $\mathcal{Q}_B$ and $\mathcal{Q}_B$ itself are simply laced is made. Apart from the outer-automorphism symmetry on the complete graph quiver, there is another discrete action $\mathbb{Z}_q^n$ acting on the Cartan of the gauge group. After the $\mathbb{Z}_q^n$ quotient, the edge multiplicity of edges in the complete graph increase q-fold, and the edge connecting complete graph and $\mathcal{Q}_B$ pick up a lace q pointing to $\mathcal{Q}_B$. The edges in the complete graph can also be thought of as becoming double q-laced. However, for Abelian nodes, one cannot distinguish between the edge multiplicity and charge multiplicity at the level of the Coulomb branch. If $\mathcal{Q}_B$ is empty or unframed, a $\mathrm{U}(1)\subset\mathrm{U}(1)^n$ is decoupled from complete graph, then the action reduced to $\mathbb{Z}_q^{n-1}$.

At the level of Hilbert series:

$$\mathrm{HS}\left(\mathcal{C}(\mathcal{Q}_{3.4b})\right) = \begin{cases} \mathrm{HS}\left(\mathcal{C}(\mathcal{Q}_{3.4a}/\mathbb{Z}_q^{n-1})\right)\,, & \text{when } \mathcal{Q}_B \text{ is empty or unframed}\,, \\ \mathrm{HS}\left(\mathcal{C}(\mathcal{Q}_{3.4a}/\mathbb{Z}_q^{n})\right)\,, & \text{when } \mathcal{Q}_B \text{ is framed}\,. \end{cases} \tag{3.25}$$

To show this, the refinement fugacities are turned back on. The $\mathbb{Z}_q^n$ acts on these fugacities in the following way:

$$\mathbb{Z}_q^n: \qquad (z_1,\dots,z_n) \to (\omega_q^{k_1} z_1,\dots,\omega_q^{k_n} z_n)\,, \tag{3.26}$$

where ω_q is the primitive q-th root of unity and $(k_1,\dots,k_n)\in\mathbb{Z}_q^n$. Similar to [102, 107], the Molien formula yields:

$$\begin{aligned} \mathrm{HS}\left(\mathcal{C}(\mathcal{Q}_{3.4a}/\mathbb{Z}_q^n)\right) &= \frac{1}{q^n}\sum_{k_1,\dots,k_n}\sum_{m_1,\dots,m_n} P(m_1,\dots,m_n)\cdot\omega_q^{m_1\cdot k_1} z_1^{m_1}\cdots\omega_q^{m_n\cdot k_n} z_n^{m_n}\cdot t^{\Delta(m_1,\dots,m_n)} \\ &= \sum_{m_1,\dots,m_n} P(m_1,\dots,m_n)\cdot z_1^{q\cdot m_1}\cdots z_n^{q\cdot m_n}\cdot t^{\Delta(q\cdot m_1,\dots,q\cdot m_n)} \\ &= \mathrm{HS}\left(\mathcal{C}(\mathcal{Q}_{3.4b})\right)\,. \end{aligned} \tag{3.27}$$

Considering the ungauging process: if $\mathcal{Q}_B$ is framed, there is no need to ungauge; if $\mathcal{Q}_B$ is empty or unframed, one can set one $m_i=0$ (or other choices so long as it cancels the same shift invariance), as a result, the $\mathbb{Z}_q$ action on z_i is trivial and the overall action becomes $\mathbb{Z}_q^{n-1}$:

$$\mathrm{HS}\left(\mathcal{C}(\mathcal{Q}_{3.4a}/\mathbb{Z}_q^{n-1})\right)|_{m_i=0} = \mathrm{HS}\left(\mathcal{C}(\mathcal{Q}_{3.4b})\right)|_{m_i=0}. \tag{3.28}$$

Hence, Claims (3.3) and (3.6) are verified on the level of the Hilbert series.

As we can see from the proof, this $\mathbb{Z}_q$ quotient has two origins: one is to increase the edge multiplicity q-times, the other is to increase the charge of hypermultiplets q-times. On the Coulomb branch geometry these two constructions have no difference, but can be distinguished by deformation and the corresponding Higgs branch.

3.4 Abelianisation

In this section the discrete action on the Coulomb branch of a 3d $\mathcal{N}=4$ theory with unitary gauge groups via the Abelianisation method introduced in [33] is discussed. From the monopole formula it is easy to read the representation of the monopole operators under continuous global symmetry, but it is hard to find the exact representation under the discrete action. Abelianisation provides a systemic way to find out the discrete action induced by quiver outer-automorphism.

Start with an Abelian theory of rank n, i.e, the gauge group is $\mathrm{U}(1)^n$, with hypermultiplets with charge $\rho\oplus\bar{\rho}$. The monopole operators transform under the topological $\mathrm{U}(1)^n_{top}$. For each topological charge $A\in\mathbb{Z}^n$, there exists a (bare) monopole operator v_A. The Coulomb branch chiral ring is generated by the set of bare monopole operators v_A and the set of

Casimir invariants ϕ_i of gauge group, which are subject to relations determined by the charge matrix ρ.

The simplest example is the theory of a single U(1) with no hypermultiplet. The (bare) monopole operator can be written as a holomorphic function of v_1 and v_{-1}: for a positive integer k, $v_k = v_1^k$ and $v_{-k} = v_{-1}^k$. Hence, the chiral ring generators are v_1, v_{-1}, ϕ. The relation between generators is $v_1 v_{-1} = 1$. The ring $\mathbb{C}[v_1, v_{-1}, \phi]/\langle v_1 v_{-1} = 1\rangle$ is exactly $T^*\mathbb{C}^\times$.

For a non-Abelian theory with unitary gauge group G of rank n, if the representation of hypermultiplets contains at least all the roots of G, one can always find a corresponding Abelian theory whose gauge group is the Cartan subgroup of the non-Abelian gauge group [108]. The charges of the hypermultiplets in this Abelian theory should add up to the charges of the representations of hypermultiplets under the Cartan subgroup, i.e. the bare monopole operators in both theories have the same conformal dimension contribution. The difference between the two Coulomb branch chiral rings is a quotient of the Weyl group $\mathcal{W}_G$.

For the most general case, the Weyl group action on the Coulomb branch is:

$$\phi_i \longleftrightarrow \phi_{\sigma(i)} \ , \qquad v_{(n_1,\ldots,n_k)} \longleftrightarrow v_{(n_{\sigma(1)},\ldots,n_{\sigma(k)})} \ . \tag{3.29}$$

3.5 Examples of S_n quotients

The S_n gauging on quivers which are or contain certain complete graphs are computed and the corresponding S_n on their Coulomb branches are studied. This action is studied through the Hilbert series computed with the monopole formula and through Abelianisation for each example.

3.5.1 From Kleinian A to Kleinian D – An S_2 gauging

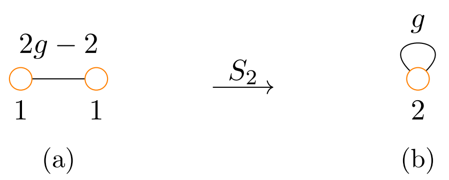

Figure 3.5: a: The Abelian quiver $\mathcal{CG}_{2,2g-2}$, whose Coulomb branch is the A_{2g-3} surface singularity. b: The quiver $\mathcal{ML}_{2,g}$, whose Coulomb branch is the D_{g+1} Kleinian singularity.

Consider the Abelian quiver $\mathcal{Q}_{3.5a} = \mathcal{CG}_{2,2g-2}$ of Figure 3.5a, whose Coulomb branch is the A-type singularity $A_{2g-3} \cong \mathbb{C}^2/\mathbb{Z}_{2g-2}$. The Coulomb branch of the quiver $\mathcal{Q}_{3.5b}$ in Figure 3.5b is the D-type singularity $D_{g+1} \cong \mathbb{C}^2/\mathrm{Dic}_{g-1}$. Embracing (3.5), one is led to an interesting relation between the two quivers of Figure 3.5: as a complete graph, $\mathcal{Q}_{3.5a}$ has an S_2 outer-automorphism. By gauging this S_2, in view of (3.5), $\mathcal{Q}_{3.5b}$ is obtained, a quiver with a single U(2) gauge node and with g hypermultiplets in the adjoint representation.

Hence, the following relationship between the Coulomb branches of these two quivers is found:

$$\mathcal{C}(\mathcal{Q}_{3.5b}) = \mathcal{C}(\mathcal{Q}_{3.5a})/S_2. \tag{3.30}$$

This, in fact, reproduces the well-known relation between the two Kleinian singularities:

$$D_{g+1} \cong A_{2g-3}/S_2\,, \tag{3.31}$$

but now it is phrased as an operation on quivers.

Monopole formula

Let us examine the relationship (3.30) using the Hilbert series, which for these singularities are:

$$\mathrm{HS}\left(A_{2g-3}\right) = \mathrm{PE}\left[t^2 + \left(q + \frac{1}{q}\right)t^{2g-2} - t^{4g-4}\right], \tag{3.32a}$$

$$\mathrm{HS}\left(D_{g+1}\right) = \mathrm{PE}\left[t^4 + t^{2g-2} + t^{2g} - t^{4g}\right], \tag{3.32b}$$

where q is the fugacity of the topological $\mathrm{U}(1)_J$. The global symmetry on A_{2g-3} is $\mathrm{U}(1)_J$, except for the special case of $g=2$, where the global symmetry is enhanced to $\mathrm{SU}(2)$. There is no continuous global symmetry on D_{g+1}, since the S_2 action breaks the $\mathrm{U}(1)_J$ symmetry.

Now the result is verified further from the monopole formula and generalised Molien sum. The magnetic fluxes of $\mathcal{Q}_{3.5a}$ are denoted as m_1 and m_2, and the overall $\mathrm{U}(1)$ is ungauged by taking $m_2 = 0$. The monopole formula is:

$$\mathrm{HS}\left(\mathcal{C}(\mathcal{Q}_{3.5a})\right) = \frac{1}{1-t^2}\sum_{m_1=-\infty}^{\infty} q^{m_1+m_2}\cdot t^{(2g-2)|m_1-m_2|}|_{m_2=0} = \mathrm{PE}\left[t^2 + \left(q+\frac{1}{q}\right)t^{2g-2} - t^{4g-4}\right], \tag{3.33}$$

reproducing the result in (3.32a). Using the same notation, the monopole formula of $\mathcal{Q}_{3.5b}$ is:

$$\mathrm{HS}\left(\mathcal{C}(\mathcal{Q}_{3.5b})\right) = \frac{1}{1-t^4} + \frac{1}{1-t^2}\sum_{m_1>m_2}^{\infty} t^{(2g-2)|m_1-m_2|}|_{m_2=0} = \mathrm{PE}\left[t^4 + t^{2g-2} + t^{2g} - t^{4g}\right], \tag{3.34}$$

reproducing the result in (3.32b). Let the non-trivial action of S_2 be denoted as $(1\ 2)$. Using (3.14), the monopole formula on the fixed loci $m_1 = m_2 = 0$ of $(1\ 2)$ is:

$$\begin{aligned}\mathrm{HS}\left(\mathcal{C}(\mathcal{Q}_{3.5a})\right)^{(1\ 2)} &= \frac{1-t^2}{1-t^4}\left(t^{(2g-2)|m_1-m_2|}\right)|_{m_1=m_2=0} \\ &= \frac{1}{1+t^2}\,.\end{aligned} \tag{3.35}$$

By applying the generalised Molien sum (3.15), there is agreement that:

$$\begin{aligned}\frac{1}{2}\left(\mathrm{HS}\left(\mathcal{C}(\mathcal{Q}_{3.5a})\right)|_{q=1}+\mathrm{HS}\left(\mathcal{C}(\mathcal{Q}_{3.5a})\right)^{(1\ 2)}\right)&=\frac{1}{2}\left(\frac{1-t^{4g-4}}{(1-t^2)(1-t^{2g-2})^2}+\frac{1}{1+t^2}\right)\\&=\mathrm{PE}\left[t^4+t^{2g-2}+t^{2g}-t^{4g}\right]\\&=\mathrm{HS}\left(\mathcal{C}(\mathcal{Q}_{3.5b})\right).\end{aligned}\tag{3.36}$$

From the PE, the numbers and representations/charges of the generators and relations at each degree are read off. From (3.32a), A_{2g-3} has one generator at degree 2 with charge 0, two generators at degree $2g-2$ with charge $+1$ and -1, and one relation between them at degree $4g-4$ with charge 0. From (3.32b), D_{g+1} has three generators at degree 4, $2g-2$, and $2g$ respectively; and one relation between them at degree $4g$. The explicit generators and relations for the A_{2g-3} and D_{g+1} singularities are given in Table 3.1a and Table 3.1b, respectively.

Generators	$\mathrm{U}(1)_J$ Charge	Degree
ϕ	0	2
u	1	$2g-2$
v	-1	$2g-2$
Relation		
$\phi^{2g-2}+uv=0$	0	$4g-4$

(a) A_{2g-3} singularity

Generators	Degree
x	4
w	$2g-2$
z	$2g$
Relation	
$z^2-xw^2+x^g=0$	$4g$

(b) D_{g+1} singularity

Table 3.1: Generators and relations: a for Kleinian A_{2g-3}; and b for Kleinian D_{g+1}.

Now let us construct the D_{g+1} surface singularity starting from the Kleinian A_{2g-3} singularity. The action of S_2 on the generators of A_{2g-3} is given by

$$\phi\to-\phi\,,\quad u\to v\,,\quad v\to u\,.\tag{3.37}$$

There are four fundamental invariants under this S_2 action: ϕ^2, $u+v$, $\phi(u-v)$, and uv. Together with the relations there are three independent generators: $\phi^2=x$, $u+v=2w$, and $\phi(u-v)=2z$. These have the same degrees as the generators of D_{g+1}. Moreover, the relation between x, w, and z is indeed $z^2-xw^2+x^g=0$, which coincides with the relation of the D_{g+1} singularity, cf. Table 3.1b.

Abelianisation

Now let us verify the generators and relations of the monopole operators via Abelianisation, as described in Section 3.4. For the Abelian theory $\mathcal{Q}_{3.5a}=\mathcal{CG}_{2,2g-2}$, the Casimir operators of the gauge group $\mathrm{U}(1)^2$ is labelled as ϕ_1 and ϕ_2, and the general monopole operators as

$v_{(n_1,n_2)}$, where $(n_1, n_2) \in \mathbb{Z}^2$. The chiral ring relations between these operators are:

$$v_{(n_1,n_2)}v_{(m_1,m_2)} = v_{(n_1+m_1,n_2+m_2)}(\phi_1 - \phi_2)^{(2g-2)\mathrm{ABS}_+(n_1-n_2,m_1-m_2)}\,, \tag{3.38a}$$

$$\text{with} \quad \mathrm{ABS}_+(n, m) := \max(n, 0) + \max(m, 0) - \max(n + m, 0)\,. \tag{3.38b}$$

The defining Coulomb branch relations are:

$$v_{(1,1)}v_{(-1,-1)} = 1\,, \tag{3.39a}$$

$$v_{(1,0)}v_{(-1,0)} = (\phi_1 - \phi_2)^{2g-2}\,, \tag{3.39b}$$

$$v_{(0,1)}v_{(0,-1)} = (\phi_1 - \phi_2)^{2g-2}\,, \tag{3.39c}$$

$$v_{(1,0)}v_{(0,1)} = v_{(1,1)}(\phi_1 - \phi_2)^{2g-2}\,, \tag{3.39d}$$

$$v_{(-1,0)}v_{(0,-1)} = v_{(-1,-1)}(\phi_1 - \phi_2)^{2g-2}\,, \tag{3.39e}$$

$$v_{(kn_1,kn_2)} = v^k_{(n_1,n_2)}\,. \tag{3.39f}$$

Here, (3.39f) reflects the holomorphicity of the chiral ring. From (3.39a) it is clear that the freely acting diagonal U(1) contributes to the relation of $T^*\mathbb{C}^\times$: $\mathbb{C}/[v_{(1,1)}, v_{(-1,-1)}, \phi_1+\phi_2]/\langle v_{(1,1)}v_{(-1,-1)} = 1\rangle$. Next, (3.39b) is the relation of the A_{2g-3} singularity: $\mathbb{C}/[v_{(1,0)}, v_{(-1,0)}, \phi_1-\phi_2]/\langle v_{(1,0)}v_{(-1,0)} = (\phi_1 - \phi_2)^{2g-2}\rangle$. The generators $v_{(1,0)}$, $v_{(-1,0)}$, $\phi_1 - \phi_2$ can be identified with u, v, ϕ, respectively, as in Table 3.1a. The relation (3.39c) is then derived from (3.39a) and (3.39b)

$$v_{(0,1)}v_{(0,-1)} = v_{(1,1)}v_{(-1,0)}v_{(-1,-1)}v_{(1,0)} = (\phi_1 - \phi_2)^{2g-2}\,. \tag{3.40}$$

Hence, the overall Coulomb branch of $\mathcal{Q}_{3.5a}$ is $T^*\mathbb{C}^\times \times A_{2g-3}$, in which $T^*\mathbb{C}^\times$ can be decoupled via the ungauging process. After the ungauging there is an identification $v_{n_1+k,n_2+k} \sim v_{n_1,n_2}$.

According to the statement above, the Coulomb branch of non-Abelian theory $\mathcal{Q}_{3.5b}$ is a quotient of the Coulomb branch of $\mathcal{Q}_{3.5a}$ by the Weyl group S_2. The nontrivial action of S_2 is simply permuting the two U(1)s in the Cartan subgroup:

$$v_{(n_1,n_2)} \longleftrightarrow v_{(n_2,n_1)}\,, \qquad \phi_1 \longleftrightarrow \phi_2\,, \tag{3.41}$$

which agrees with (3.37). The free part $T^*\mathbb{C}^\times$ is invariant under this action, and the singular part A_{2g-3} becomes D_{g+1}. Therefore, the overall Coulomb branch of $\mathcal{Q}_{3.5b}$ is $T^*\mathbb{C}^\times \times D_{g+1}$.

3.5.2 A_3 affine quiver with S_2 gauging

A similar analysis is repeated for the affine A_3 quiver. The Coulomb branch is the closure of the minimal nilpotent orbit of $\mathfrak{sl}_4$ which is denoted a_3.

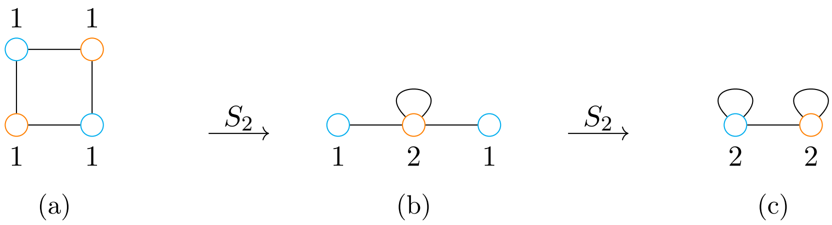

Figure 3.6: a: Quiver $\mathcal{Q}_{3.6a}$ is the affine A_3 quiver. The Coulomb branch is the closure of minimal nilpotent orbit a_3. The orange and cyan parts are two $\mathcal{CG}_{2,0}$ sub-graphs. b: Non-Abelian quiver $\mathcal{Q}_{3.6b}$, whose Coulomb branch is the closure of next-to-minimal nilpotent orbit $\overline{n.min.B_2}$. c: Non-Abelian quiver $\mathcal{Q}_{3.6c}$.

An S_2 quotient can be taken on this quiver if a pair of U(1)s diagonally opposite are treated as a sub-complete graph of $\mathcal{CG}_{2,0}$ on which the S_2 gauging occurs, as shown in Figure 3.6a and Figure 3.6b. Note that this is the only possibility, as the alternative, which takes a pair of U(1) on the same side as $\mathcal{CG}_{2,1}$ for the gauging, has odd edge multiplicity. Importantly, the magnetic quiver for $\overline{n.min.B_2}$ is found, which is consistent with the result of Kostant and Brylinski [99] and also consistent with previous studies on discrete actions on Coulomb branches of $3d$ $\mathcal{N}=4$ quiver gauge theories [97]. Furthermore, since there are two pairs of diagonally opposite U(1)s as two sub-complete graphs of $\mathcal{CG}_{2,0}$, an $S_2 \times S_2$ quotient can also be taken, the quiver is shown in Figure 3.6c.

Monopole formula

Let us derive the chiral ring relations of these three quivers via Hilbert series and show how the S_2 and $S_2 \times S_2$ quotients act on the generators. The unrefined Hilbert series

read:

$$\mathrm{HS}\left(\mathcal{C}\left(\mathcal{Q}_{3.6a}\right)\right) = \frac{(1+t^2)(1+8t^2+t^4)}{(1-t^2)^6}\,, \tag{3.42a}$$

$$\mathrm{HS}\left(\mathcal{C}\left(\mathcal{Q}_{3.6b}\right)\right) = \frac{(1+t^2)(1+3t^2+t^4)}{(1-t^2)^6}\,, \tag{3.42b}$$

$$\mathrm{HS}\left(\mathcal{C}\left(\mathcal{Q}_{3.6c}\right)\right) = \frac{1+3t^2+11t^4+10t^6+11t^8+3t^{10}+t^{12}}{(1-t^2)^3(1-t^4)^3}\,. \tag{3.42c}$$

The coefficient of t^2 term indicates global symmetry on the Coulomb branches are SU(4), SO(5) $\cong$ USp(4) and SU(2) $\times$ SU(2) respectively.

It is straightforward to show that these Hilbert series follow from the Molien sum relation (3.15):

$$\mathrm{HS}\left(\mathcal{C}\left(\mathcal{Q}_{3.6a}\right)\right)^{(1\ 3)} = \mathrm{HS}\left(\mathcal{C}\left(\mathcal{Q}_{3.6a}\right)\right)^{(2\ 4)} = \frac{1+t^2}{(1-t^2)^4}\,, \tag{3.43a}$$

$$\mathrm{HS}\left(\mathcal{C}\left(\mathcal{Q}_{3.6a}\right)\right)^{(1\ 3)(2\ 4)} = \frac{1+t^4}{(1+t^2)(1-t^4)^2}\,, \tag{3.43b}$$

$$\frac{1}{2}\left(\mathrm{HS}\left(\mathcal{C}\left(\mathcal{Q}_{3.6a}\right)\right) + \mathrm{HS}\left(\mathcal{C}\left(\mathcal{Q}_{3.6a}\right)\right)^{(1\ 3)}\right) = \frac{1}{2}\left(\mathrm{HS}\left(\mathcal{C}\left(\mathcal{Q}_{3.6a}\right)\right) + \mathrm{HS}\left(\mathcal{C}\left(\mathcal{Q}_{3.6a}\right)\right)^{(2\ 4)}\right)$$

$$
\begin{aligned}
&= \frac{1}{2}\left(\frac{(1+t^2)(1+8t^2+t^4)}{(1-t^2)^6}+\frac{1+t^2}{(1-t^2)^4}\right)\\
&= \frac{(1+t^2)(1+3t^2+t^4)}{(1-t^2)^6}\\
&= \mathrm{HS}\left(\mathcal{C}\left(\mathcal{Q}_{3.6b}\right)\right)\,, \qquad (3.43c)
\end{aligned}
$$

$$
\begin{aligned}
\frac{1}{4}\Big(\mathrm{HS}\left(\mathcal{C}\left(\mathcal{Q}_{3.6a}\right)\right)+\mathrm{HS}\left(\mathcal{C}\left(\mathcal{Q}_{3.6a}\right)\right)^{(1\ 3)} &+\mathrm{HS}\left(\mathcal{C}\left(\mathcal{Q}_{3.6a}\right)\right)^{(2\ 4)}+\mathrm{HS}\left(\mathcal{C}\left(\mathcal{Q}_{3.6a}\right)\right)^{(1\ 3)(2\ 4)}\Big)\\
&= \frac{1}{4}\left(\frac{(1+t^2)(1+8t^2+t^4)}{(1-t^2)^6}+2\frac{1+t^2}{(1-t^2)^4}+\frac{1+t^4}{(1+t^2)(1-t^4)^2}\right)\\
&= \frac{1+3t^2+11t^4+10t^6+11t^8+3t^{10}+t^{12}}{(1-t^2)^3(1-t^4)^3}\\
&= \mathrm{HS}\left(\mathcal{C}\left(\mathcal{Q}_{3.6c}\right)\right)\,, \qquad (3.43d)
\end{aligned}
$$

where (1 3) represents the permutation action between the orange $\mathrm{U}(1)^2$ and (2 4) represents the permutation action between the cyan $\mathrm{U}(1)^2$.

Now let us extract the information of the independent generators and relations of the first two quivers via the refined PL:

$$
\mathrm{PL}((3.42a)) = [1,0,1]_{\mathfrak{su}4}t^2 - [0,1,0]_{\mathfrak{su}4}t^4 + O(t^5)\,, \qquad (3.44a)
$$

$$
\mathrm{PL}((3.42b)) = [2,0]_{\mathfrak{usp}4}t^2 - ([0,0]_{\mathfrak{usp}4}+[0,1]_{\mathfrak{usp}4})t^4 + O(t^5)\,. \qquad (3.44b)
$$

As a result, the explicit generators and relations are derived as shown in Tables 3.2 and 3.3.

Generators	Reps of SU(4)	Degree
M_i^j	$[1,0,1]+[0,0,0]$	2
Relations		
$\mathrm{Tr}(M)=0$	$[0,0,0]+[0,2,0]+[1,0,1]$	2
$M_i^j M_k^l - M_i^l M_k^j = 0$ $(\mathrm{rk}(M)\le 1)$	$[0,1,0]$	4

Table 3.2: Generators and relations of Coulomb branch of $\mathcal{Q}_{3.6a}$, which is $a_3 \cong \mathbb{C}[M_i^j]/\langle \mathrm{tr}(M)=0,\ \mathrm{rk}(M)\le 1\rangle$, where $i,j=1,2,3,4$.

Generators	Reps of USp(4)	Degree
S_{ij}	$[2,0]$	2
Relations		
$\Omega^{jk}S_{ij}S_{kl}=0$	$[0,0]+[0,1]$	4

Table 3.3: Generators and relations of Coulomb branch of $\mathcal{Q}_{3.6b}$, which is a_3/S_2. The global symmetry is $\mathrm{SO}(5)\cong\mathrm{USp}(4)$. Ω is the standard skew-symmetric matrix.

In this case and examples following, it is more clear and systematic to see the orbifold action on the generators from the Abelianisation.

Abelianisation

Alternatively, Abelianisation can be used to inspect the quotients in Figure 3.6. For the Abelian theory $\mathcal{Q}_{3.6a}$, the Casimir operators of the orange $\mathrm{U}(1)^2$ are labelled as ϕ_1, ϕ_3, and for the cyan $\mathrm{U}(1)^2$ as ϕ_2, ϕ_4. A general monopole operator is denoted by $v_{(n_1,n_2,n_3,n_4)}$, where $(n_1, n_3) \in \mathbb{Z}^2$ are the magnetic fluxes for the orange $\mathrm{U}(1)^2$ gauge nodes and $(n_2, n_4) \in \mathbb{Z}^2$ are the magnetic fluxes for the cyan $\mathrm{U}(1)^2$ gauge nodes. The chiral ring relations are:

$$
\begin{aligned}
v_{(1,1,1,1)}v_{(-1,-1,-1,-1)} &= 1 \,, && \text{(3.45a)}\\
v_{(1,0,0,0)}v_{(-1,0,0,0)} &= (\phi_4-\phi_1)(\phi_1-\phi_2) \,, && \text{(3.45b)}\\
v_{(0,1,0,0)}v_{(0,-1,0,0)} &= (\phi_1-\phi_2)(\phi_2-\phi_3) \,, && \text{(3.45c)}\\
v_{(0,0,1,0)}v_{(0,0,-1,0)} &= (\phi_2-\phi_3)(\phi_3-\phi_4) \,, && \text{(3.45d)}\\
v_{(0,0,0,1)}v_{(0,0,0,-1)} &= (\phi_3-\phi_4)(\phi_4-\phi_1) \,, && \text{(3.45e)}\\
v_{(1,0,0,0)}v_{(0,1,0,0)} &= v_{(1,1,0,0)}(\phi_1-\phi_2) \,, && \text{(3.45f)}\\
v_{(0,1,0,0)}v_{(0,0,1,0)} &= v_{(0,1,1,0)}(\phi_2-\phi_3) \,, && \text{(3.45g)}\\
v_{(0,0,1,0)}v_{(0,0,0,1)} &= v_{(0,0,1,1)}(\phi_3-\phi_4) \,, && \text{(3.45h)}\\
v_{(0,0,0,1)}v_{(1,0,0,0)} &= v_{(1,0,0,1)}(\phi_4-\phi_1) \,, && \text{(3.45i)}\\
v_{(1,0,0,0)}v_{(0,1,0,0)}v_{(0,0,1,0)} &= v_{(1,1,1,0)}(\phi_1-\phi_2)(\phi_2-\phi_3) \,, && \text{(3.45j)}\\
v_{(0,1,0,0)}v_{(0,0,1,0)}v_{(0,0,0,1)} &= v_{(0,1,1,1)}(\phi_2-\phi_3)(\phi_3-\phi_4) \,, && \text{(3.45k)}\\
v_{(0,0,1,0)}v_{(0,0,0,1)}v_{(1,0,0,0)} &= v_{(1,0,1,1)}(\phi_3-\phi_4)(\phi_4-\phi_1) \,, && \text{(3.45l)}\\
v_{(0,0,0,1)}v_{(1,0,0,0)}v_{(0,1,0,0)} &= v_{(1,1,0,1)}(\phi_4-\phi_1)(\phi_1-\phi_2) \,, && \text{(3.45m)}\\
v_{(1,0,0,0)}v_{(0,1,0,0)}v_{(0,0,1,0)}v_{(0,0,0,1)} &= v_{(1,1,1,1)}(\phi_1-\phi_2)(\phi_2-\phi_3)(\phi_3-\phi_4)(\phi_4-\phi_1) \,, && \text{(3.45n)}\\
v_{(kn_1,kn_2)} &= v^k_{(n_1,n_2)} \,. && \text{(3.45o)}
\end{aligned}
$$

From (3.45a) it is clear that the freely acting diagonal $\mathrm{U}(1)$ contributes to the relation of $T^*\mathbb{C}^\times$:
$\mathbb{C}[v_{(1,1,1,1)}, v_{(-1,-1,-1,-1)}, \phi_1+\phi_2+\phi_3+\phi_4]/\langle v_{(1,1,1,1)}v_{(-1,-1,-1,-1)} = 1\rangle$. After decoupling this free $\mathrm{U}(1)$, there is the identification $v_{(n_1+k,n_2+k,n_3+k,n_4+k)} \sim v_{(n_1,n_2,n_3,n_4)}$. By rearranging the remaining generators into matrix form:

$$
\begin{pmatrix}
\phi_1-\phi_2 & v_{(0,1,0,0)} & v_{(0,1,1,0)} & v_{(1,0,0,0)}\\
v_{(0,-1,0,0)} & \phi_2-\phi_3 & v_{(0,0,1,0)} & v_{(0,0,1,1)}\\
v_{(0,-1,-1,0)} & v_{(0,0,-1,0)} & \phi_3-\phi_4 & v_{(0,0,0,1)}\\
v_{(-1,0,0,0)} & v_{(0,0,-1,-1)} & v_{(0,0,0,-1)} & \phi_4-\phi_1
\end{pmatrix} , \tag{3.46}
$$

The chiral ring relations (3.45b–3.45n) hold by requiring the rank of the matrix is no greater than 1. Hence the generators and relations can be identified with M_i^j in Table 3.2.

The non-trivial S_2 action which permutes the orange $\mathrm{U}(1)^2$ is given by

$$v_{(n_1,n_2,n_3,n_4)} \longleftrightarrow v_{(n_3,n_2,n_1,n_4)} \,, \qquad \phi_1 \longleftrightarrow \phi_3 \,, \tag{3.47}$$

and the non-trivial S_2 action permuting the cyan $\mathrm{U}(1)^2$ reads

$$v_{(n_1,n_2,n_3,n_4)} \longleftrightarrow v_{(n_1,n_4,n_3,n_2)} \,, \qquad \phi_2 \longleftrightarrow \phi_4 \,. \tag{3.48}$$

Having studied these simple examples, let us turn to another nice consequence of the statements in Section 3.2, where in the following example a known hypersurface is studied, but in a different light.

3.5.3 Symplectic hypersurfaces in 2 quaternionic dimensions and S_2 gauging

Symplectic singularities which are hypersurfaces are very rare. According to a conjecture by [109, 110] these are

1. Klein singularities (quaternionic dimension 1),
2. Intersections of Słodowy slices in the $\mathrm{Sp}(g)$ nilpotent cone (dimension 2),
3. The transverse slice between the regular and minimal orbits in G_2 (dimension 3).

It is easy to construct quivers such that their moduli spaces are symplectic hypersurfaces [111].

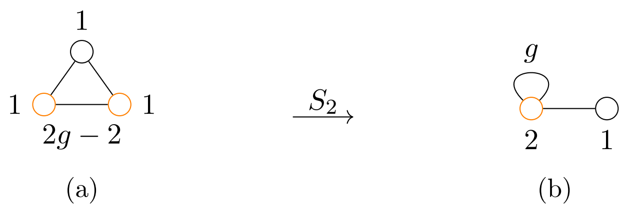

Figure 3.7: a: Quiver $\mathcal{Q}_{3.7a}$ is composed of two parts: the complete graph $\mathcal{CG}_{2,2g-2}$ in orange, and the background $\mathcal{Q}_B$, given by the uncoloured U(1) node. They are connected by edges of multiplicity 1. b: Quiver $\mathcal{Q}_{3.7b}$ is composed of $\mathcal{Q}_{3.5b}$, shown in orange, connecting to the same background quiver Q_B.

For case 2, the family of these symplectic hypersurfaces are the Coulomb branches of the multiloop quiver $\mathcal{Q}_{3.7b}$ on the RHS of Figure 3.7. This family of hypersurfaces was studied in [112] as the Higgs branch of a certain $4d$ $\mathcal{N}=2$ A_1 Class $\mathcal{S}$ theory on a Riemann surface of genus g and 1 puncture.

The Coulomb branch of this quiver was identified in [113] as $\mathcal{S}^{[2g]}_{[2g-2,1,1]}$, the intersection of the nilpotent cone of $\mathrm{Sp}(g)$ with the Słodowy slice to the orbit $[2g-2,1,1]$. Incidentally, this moduli space has a Higgs branch realisation by the S_2 quotient of the affine D_{g+1}

quiver:

$$\mathcal{S}^{[2g]}_{[2g-2,1,1]} = \mathcal{H}\left(\vphantom{\int} \right.$$ 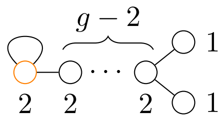 $$\left. \vphantom{\int} \right) = \mathcal{C}\left(\vphantom{\int} \right.$$ 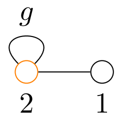 $$\left. \vphantom{\int} \right) . \tag{3.49}$$

Notice that the orange U(2) node of $\mathcal{Q}_{3.7b}$ has loops. According to the claim (3.5), the Coulomb branch of $\mathcal{Q}_{3.7b}$ admits a double-cover, whose quiver $\mathcal{Q}_{3.7a}$ is shown on the LHS of Figure 3.7:

$$\mathcal{C}\left(\mathcal{Q}_{3.7b}\right) \cong \mathcal{C}\left(\mathcal{Q}_{3.7a}\right)/S_2. \tag{3.50}$$

In $\mathcal{Q}_{3.7a}$, the orange U(1) nodes on the bottom together with the $2g$–2 edges can be treated as a complete graph. There is a S_2 symmetry permuting these two nodes. By gauging this S_2 symmetry, it becomes the orange U(2) node with g adjoints in quiver $\mathcal{Q}_{3.7b}$.

Monopole formula

Let us derive the chiral ring relations of these two quivers from Hilbert series and show how this S_2 quotient acts on the generators. Firstly, let us look at the refined Hilbert series of these two quivers:

$$\begin{aligned}\mathrm{HS}\left(\mathcal{C}\left(\mathcal{Q}_{3.7a}\right)\right) = &\left(1+t^2-\left(q+\frac{1}{q}\right)[1]t^{2g+1}-([2]+1)t^{4g-2}+([2]+1)t^{4g}\right.\\ &\left.+\left(q+\frac{1}{q}\right)[1]t^{6g-3}-t^{8g-4}-t^{8g-2}\right)\cdot \mathrm{PE}\left[([2]+1)t^2+\left(q+\frac{1}{q}\right)[1]t^{2g-1}\right],\end{aligned} \tag{3.51a}$$

$$\mathrm{HS}\left(\mathcal{C}\left(\mathcal{Q}_{3.7b}\right)\right) = \mathrm{PE}\left[[2]t^2+[1]t^{2g-1}-t^{4g}\right], \tag{3.51b}$$

where q is the fugacity for U(1), and $[n]$ refers to the character for the $n+1$ dimensional representation[2] of SU(2). The Coulomb branch global symmetry of $\mathcal{Q}_{3.7a}$ is $\mathrm{U}(2) \cong \mathrm{SU}(2) \times \mathrm{U}(1)$; while the Coulomb branch global symmetry of $\mathcal{Q}_{3.7b}$ is SU(2). The S_2 quotient breaks the U(1) global symmetry and leaves the SU(2) intact.

It is straightforward to verify that the monopole formula satisfies the generalised Molien sum (3.15):

$$\mathrm{HS}\left(\mathcal{C}\left(\mathcal{Q}_{3.7b}\right)\right) = \frac{1}{2}\left(\mathrm{HS}\left(\mathcal{C}\left(\mathcal{Q}_{3.7a}\right)\right)+\mathrm{HS}\left(\mathcal{C}\left(\mathcal{Q}_{3.7a}\right)\right)^{(1\ 2)}\right)|_{q=1}\,. \tag{3.52}$$

To extract the information about the independent generators and relations for each variety, the PL of the HS is taken:

$$\begin{aligned}\mathrm{PL}\left((3.51\mathrm{a})\right) = &([2]+1)t^2-t^4+\left(q+\frac{1}{q}\right)[1]\;t^{2g-1}-\left(q+\frac{1}{q}\right)[1]\;t^{2g+1}\\ &-([2]+1)t^{4g-2}+\mathrm{O}(t^{4g-1}),\end{aligned} \tag{3.53a}$$

$$\mathrm{PL}\left((3.51\mathrm{b})\right) = [2]\;t^2+[1]\;t^{2g-1}-t^{4g}\,. \tag{3.53b}$$

[2]Here, for a rank k Lie group, the Dynkin label $[n_1,\ldots,n_k]$ is used to represent both the irrep of corresponding highest weight and its character.

Building on this, the explicit generators and relations are derived as shown in Tables 3.4 and 3.5.

Generators	Reps of $(\mathrm{U}(1), \mathrm{SU}(2))$	Degree
Φ	$(0, [0])$	2
M_{ij}	$(0, [2])$	2
X_i	$(1, [1])$	$2g-1$
Y_i	$(-1, [1])$	$2g-1$
Relations		
$\epsilon^{ik}\epsilon^{jl}M_{ij}M_{kl} - f_1\Phi^2 = 0$	$(0, [0])$	4
$\epsilon^{ik}M_{ij}X_k - f_2\Phi X_j = 0$	$(1, [1])$	$2g+1$
$\epsilon^{ik}M_{ij}Y_k - f_2\Phi Y_k = 0$	$(-1, [1])$	$2g+1$
$X_iY_j - f_3\Phi^{2g-2}M_{ij} = 0$	$(0, [2])$	$4g-2$
$\epsilon^{ij}X_iY_j - f_4\Phi^{2g-1} = 0$	$(0, [0])$	$4g-2$

Table 3.4: Generators and relations of Coulomb branch of $\mathcal{Q}_{3.7a}$, with $f_{1,2,3,4}$ constants that depend on g.

Generators	Reps of SU(2)	Degree
M_{ij}	[2]	2
B_i	[1]	$2g-1$
Relation		
$\left(\epsilon^{ik}\epsilon^{jl}M_{ij}M_{kl}\right)^g - f\epsilon^{ik}\epsilon^{jl}M_{ij}B_kB_l = 0$	[0]	$4g$

Table 3.5: Generators and relations of Coulomb branch of $\mathcal{Q}_{3.7b}$, where f is a constant depending on g.

Next, let us construct $\mathcal{C}\left(\mathcal{Q}_{3.7b}\right)$ from $\mathcal{C}\left(\mathcal{Q}_{3.7a}\right)$. The S_2 action on the generators of $\mathcal{C}\left(\mathcal{Q}_{3.7a}\right)$ is given by:

$$\Phi \to -\Phi\,, \quad X_i \to Y_i\,, \quad Y_i \to X_i\,. \tag{3.54}$$

There are five fundamental invariants under the S_2 action: M_{ij}, Φ^2, X_i+Y_i, $\Phi(X_i-Y_i)$, and X_iY_j. Due to the relations, there are only two independent generators: M_{ij} and $X_i+Y_i = B_i$. Moreover, the relation between M_{ij} and B_i is indeed given by $\left(\epsilon^{ik}\epsilon^{jl}M_{ij}M_{kl}\right)^g - f\epsilon^{ik}\epsilon^{jl}M_{ij}B_kB_l = 0$.

Abelianisation

For the Abelian theory $\mathcal{Q}_{3.7a}$, the Casimir operators of the bottom $\mathrm{U}(1)^2$ are denoted as ϕ_1, ϕ_2, and for the top $\mathrm{U}(1)$ as ϕ_3. Likewise, a generic monopole operator is denoted by

$v_{(n_1,n_2,n_3)}$, with $(n_1, n_2, n_3) \in \mathbb{Z}^3$. The chiral ring relations for these operators are:

$$\begin{aligned} v_{(n_1,n_2,n_3)}v_{(m_1,m_2,m_3)} =& v_{(n_1+m_1,n_2+m_2,n_3+m_3)}(\phi_1-\phi_2)^{(2g-2)\mathrm{ABS}_+(n_1-n_2,m_1-m_2)} \\ &\cdot(\phi_2-\phi_3)^{\mathrm{ABS}_+(n_2-n_3,m_2-m_3)}(\phi_3-\phi_1)^{\mathrm{ABS}_+(n_3-n_1,m_3-m_1)} \ . \end{aligned} \tag{3.55}$$

The defining Coulomb branch relations are thus given by:

$$v_{(1,1,1)}v_{(-1,-1,-1)} = 1 \ , \tag{3.56a}$$
$$v_{(1,0,0)}v_{(-1,0,0)} = (\phi_1-\phi_2)^{2g-2}(\phi_3-\phi_1) \ , \tag{3.56b}$$
$$v_{(0,1,0)}v_{(0,-1,0)} = (\phi_1-\phi_2)^{2g-2}(\phi_2-\phi_3) \ , \tag{3.56c}$$
$$v_{(0,0,1)}v_{(0,0,-1)} = (\phi_2-\phi_3)(\phi_3-\phi_1) \ , \tag{3.56d}$$
$$v_{(1,0,0)}v_{(0,1,0)} = v_{(1,1,0)}(\phi_1-\phi_2)^{2g-2} \ , \tag{3.56e}$$
$$v_{(-1,0,0)}v_{(0,-1,0)} = v_{(-1,-1,0)}(\phi_1-\phi_2)^{2g-2} \ , \tag{3.56f}$$
$$v_{(1,0,0)}v_{(0,0,1)} = v_{(1,0,1)}(\phi_3-\phi_1) \ , \tag{3.56g}$$
$$v_{(-1,0,0)}v_{(0,0,-1)} = v_{(-1,0,-1)}(\phi_3-\phi_1) \ , \tag{3.56h}$$
$$v_{(0,1,0)}v_{(0,0,1)} = v_{(0,1,1)}(\phi_2-\phi_3) \ , \tag{3.56i}$$
$$v_{(0,-1,0)}v_{(0,0,-1)} = v_{(0,-1,-1)}(\phi_2-\phi_3) \ , \tag{3.56j}$$
$$v_{(1,0,0)}v_{(0,1,0)}v_{(0,0,1)} = v_{(1,1,1)}(\phi_1-\phi_2)^{2g-2}(\phi_2-\phi_3)(\phi_3-\phi_1) \ , \tag{3.56k}$$
$$v_{(-1,0,0)}v_{(0,-1,0)}v_{(0,0,-1)} = v_{(-1,-1,-1)}(\phi_1-\phi_2)^{2g-2}(\phi_2-\phi_3)(\phi_3-\phi_1) \ , \tag{3.56l}$$
$$v_{(kn_1,kn_2,kn_3)} = v^k_{(n_1,n_2,n_3)} \ . \tag{3.56m}$$

Here (3.56m) reflects the holomorphicity of the chiral ring. The freely acting diagonal U(1) is seen from (3.56a), which contributes to the relation of $T^*\mathbb{C}^\times$: $\mathbb{C}/[v_{(1,1,1)}, v_{(-1,-1,-1)}, \phi_1+\phi_2+\phi_3]/\langle v_{(1,1,1)}v_{(-1,-1,-1)} = 1\rangle$. After decoupling this $T^*\mathbb{C}^\times$, there is the identification $v_{(n_1+k,n_2+k,n_3+k)} \sim v_{(n_1,n_2,n_3)}$. Here $\phi_1-\phi_2$, $v_{(0,0,1)}$, $v_{(0,0,-1)}$, $\phi_1+\phi_2-2\phi_3$ can be rearranged and identified with Φ, M_{ij} in Table 3.4. Also there is an arrangement of $v_{(0,1,0)}$, $v_{(0,-1,0)}$, $v_{(1,0,0)}$, $v_{(-1,0,0)}$ into X_i, Y_i. Under this identification, the relations in Table 3.4 from (3.56b–3.56j) are recovered.

According to the statement above, the Coulomb branch of the non-Abelian theory $\mathcal{Q}_{3.7b}$ is a quotient of the Coulomb branch of $\mathcal{Q}_{3.7a}$ by the Weyl group S_2. The non-trivial S_2 action is simply permuting the two bottom U(1)s:

$$v_{(n_1,n_2,n_3)} \longleftrightarrow v_{(n_2,n_1,n_3)}, \ \phi_1 \longleftrightarrow \phi_2, \tag{3.57}$$

which agrees with (3.54). This action leads to the Coulomb branch of $\mathcal{Q}_{3.7b}$.

3.5.4 Complete graph of three nodes – $\mathcal{CG}_{3,2g-2}$ quiver with S_3 gauging

The quiver $\mathcal{Q}_{3.8a} = \mathcal{CG}_{3,2g-2}$ is the magnetic quiver of the *AD* theory (A_2, A_{6g-7}).

There is a clear S_3 automorphism acting on $\mathcal{Q}_{3.8a}$. From (3.5), by gauging this S_3, the quiver $\mathcal{Q}_{3.8b}$ is found which is a single U(3) node with g adjoints, shown in Figure 3.8.

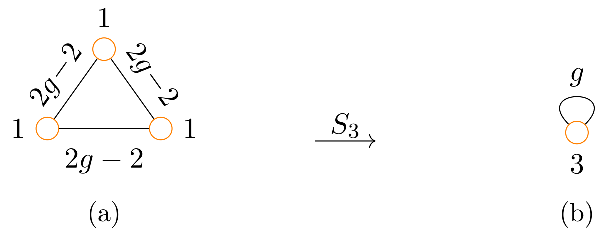

Figure 3.8: a: Abelian quiver $\mathcal{CG}_{3,2g-2}$. b: Quiver $\mathcal{ML}_{3,g}$.

Consequently, there exists the following relation between the Coulomb branches of the two quivers:

$$\mathcal{C}(\mathcal{Q}_{3.8b}) = \mathcal{C}(\mathcal{Q}_{3.8a})/S_3. \tag{3.58}$$

Again, Hilbert series and Abelianisation techniques are use in turn to shed light on the fine details.

Monopole formula

Let us examine the generators and relations via their Coulomb branch Hilbert series:

$$\begin{aligned}\mathrm{HS}\left(\mathcal{C}\left(\mathcal{Q}_{3.8a}\right)\right) = &\left(1 + 2t^{4g-4} - \left(z_1 + z_2 + z_1 z_2 + \frac{1}{z_1} + \frac{1}{z_2} + \frac{1}{z_1 z_2}\right) t^{8g-8} + 2t^{12g-12} + t^{16g-16}\right) \\ &\cdot \mathrm{PE}\left[2t^2 + \left(z_1 + z_2 + z_1 z_2 + \frac{1}{z_1} + \frac{1}{z_2} + \frac{1}{z_1 z_2}\right) t^{4g-4} - 2t^{4g-4}\right] ,\end{aligned} \tag{3.59a}$$

$$\mathrm{HS}\left(\mathcal{C}\left(\mathcal{Q}_{3.8b}\right)\right) = \frac{1 + 2t^{4g-2} + 2t^{4g} + t^{8g-2}}{(1-t^4)(1-t^6)(1-t^{4g-4})^2} , \tag{3.59b}$$

here z_1 and z_2 are the fugacities for the topological $\mathrm{U}(1)_1 \times \mathrm{U}(1)_2$. The Coulomb branch global symmetry of $\mathcal{Q}_{3.8a}$ is $\mathrm{U}(1)_1 \times \mathrm{U}(1)_2$. The S_3 quotient breaks the $\mathrm{U}(1)_1 \times \mathrm{U}(1)_2$ global symmetry, leaving behind no continuous Coulomb branch global symmetry for $\mathcal{Q}_{3.8b}$.

Again, it is straightforward to verify that the generalised Molien sum (3.15) is satisfied:

$$\begin{aligned}\mathrm{HS}\left(\mathcal{C}\left(\mathcal{Q}_{3.8b}\right)\right) = \frac{1}{2}\Big(&\mathrm{HS}\left(\mathcal{C}\left(\mathcal{Q}_{3.8a}\right)\right) + \mathrm{HS}\left(\mathcal{C}\left(\mathcal{Q}_{3.8a}\right)\right)^{(1\ 2)} + \mathrm{HS}\left(\mathcal{C}\left(\mathcal{Q}_{3.8a}\right)\right)^{(2\ 3)} + \mathrm{HS}\left(\mathcal{C}\left(\mathcal{Q}_{3.8a}\right)\right)^{(3\ 1)} \\ &+ \mathrm{HS}\left(\mathcal{C}\left(\mathcal{Q}_{3.8a}\right)\right)^{(1\ 2\ 3)} + \mathrm{HS}\left(\mathcal{C}\left(\mathcal{Q}_{3.8a}\right)\right)^{(1\ 3\ 2)}\Big) |_{z_1 = z_2 = 1}.\end{aligned} \tag{3.60}$$

As before, the PL enables us to extract the information on the independent generators and relations:

$$\begin{aligned}\mathrm{PL}\left((3.59a)\right) = 2t^2 &+ \left(z_1 + z_2 + z_1 z_2 + \frac{1}{z_1} + \frac{1}{z_2} + \frac{1}{z_1 z_2}\right) t^{4g-4} \\ &- \left(3 + z_1 + z_2 + z_1 z_2 + \frac{1}{z_1} + \frac{1}{z_2} + \frac{1}{z_1 z_2}\right) t^{8g-8} + \mathrm{O}(t^{8g-7}),\end{aligned} \tag{3.61a}$$

$$\mathrm{PL}\left((3.59b)\right) = t^4 + t^6 + 2t^{4g-4} + 2t^{4g-2} + 2t^{4g} - 3t^{8g-4} - 3t^{8g-2} - 3t^{8g} + \mathrm{O}(t^{8g+1}) . \tag{3.61b}$$

The explicit generators and relations are summarised in Tables 3.6 and 3.7.

Generators	Charge of $\mathrm{U}(1)_1 \times \mathrm{U}(1)_2$	Degree
$\Phi_1,\ \Phi_2,\ \Phi_3$	$(0,0)$	2
X_1	$(1,0)$	$4g-4$
X_2	$(0,1)$	$4g-4$
X_3	$(-1,-1)$	$4g-4$
Y_1	$(-1,0)$	$4g-4$
Y_2	$(0,-1)$	$4g-4$
Y_3	$(1,1)$	$4g-4$
Relations		
$\Phi_1+\Phi_2+\Phi_3=0$	$(0,0)$	2
$X_1Y_1-(\Phi_2\Phi_3)^{2g-2}=0$	$(0,0)$	$8g-8$
$X_2Y_2-(\Phi_3\Phi_1)^{2g-2}=0$	$(0,0)$	$8g-8$
$X_3Y_3-(\Phi_1\Phi_2)^{2g-2}=0$	$(0,0)$	$8g-8$
$Y_2Y_3-X_1\Phi_1^{2g-2}=0$	$(1,0)$	$8g-8$
$X_2X_3-Y_1\Phi_1^{2g-2}=0$	$(-1,0)$	$8g-8$
$Y_1Y_3-X_2\Phi_2^{2g-2}=0$	$(0,1)$	$8g-8$
$X_3X_1-Y_2\Phi_2^{2g-2}=0$	$(0,-1)$	$8g-8$
$Y_2Y_1-X_3\Phi_3^{2g-2}=0$	$(-1,-1)$	$8g-8$
$X_1X_2-Y_3\Phi_3^{2g-2}=0$	$(1,1)$	$8g-8$

Table 3.6: Generators and relations of Coulomb branch of $\mathcal{Q}_{3.8a}$. At degree 2, instead of two independent generators, three generators are used together with 1 relation to demonstrate the S_3 symmetry. When $g=2$, it reduces to the generators and relations of $a_2 \cong \mathbb{C}[M_i^j]/\langle \mathrm{tr}(M)=0,\ \mathrm{rk}(M)\le 1\rangle$, where $i,j=1,2,3$.

Generators	Degree
p_2	4
p_3	6
$u_1,\ u_2$	$4g-4$
$v_1,\ v_2$	$4g-2$
$w_1,\ w_2$	$4g$
Relations	
r_1, r_2, r_3	$8g-4$
r'_1, r'_2, r'_3	$8g-2$
r''_1, r''_2, r''_3	$8g$

Table 3.7: Generators and relations of Coulomb branch of $\mathcal{Q}_{3.8b}$.

Next, one can construct $\mathcal{C}\left(\mathcal{Q}_{3.8b}\right)$ from $\mathcal{C}\left(\mathcal{Q}_{3.8a}\right)$ explicitly. The S_3 action on the generators of $\mathcal{C}\left(\mathcal{Q}_{3.8a}\right)$ is given by:

$$\Phi_i \to -\Phi_{\sigma(i)}\ , \quad X_i \to X_{\sigma(i)}\ , \quad Y_i \to Y_{\sigma(i)}\ . \tag{3.62}$$

This action is induced from the S_3 subgroup of outer-automorphism of $\mathrm{SL}(3,\mathbb{C})$, for more details see Appendix 6.3. The generators are given by: $p_2 = \Phi_1^2+\Phi_2^2+\Phi_3^2$, $p_3 = \Phi_1\Phi_2(\Phi_1-\Phi_2)+\Phi_2\Phi_3(\Phi_2-\Phi_3)+\Phi_3\Phi_1(\Phi_3-\Phi_1)$, $u_1 = X_1+X_2+X_3$, $u_2 = Y_1+Y_2+Y_3$, $v_1 = X_1\Phi_1+X_2\Phi_2+X_3\Phi_3$, $v_2 = Y_1\Phi_1+Y_2\Phi_2+Y_3\Phi_3$, $w_1 = X_1(\Phi_2-\Phi_3)+X_2(\Phi_3-\Phi_1)+X_3(\Phi_1-\Phi_2)$ and $w_2 = Y_1(\Phi_2-\Phi_3)+Y_2(\Phi_3-\Phi_1)+Y_3(\Phi_1-\Phi_2)$. The 9 relations r_1, r_2, r_3, r_1', r_2', r_3', r_1'', r_2'' and r_3'' after the quotient can be worked out explicitly for small g.

Abelianisation

For the Coulomb branch of $\mathcal{Q}_{3.8a} \cong \mathcal{CG}_{3,2g-2}$, the Casimir operators of gauge group $\mathrm{U}(1)^3$ are labelled as ϕ_1, ϕ_2 and ϕ_3, and the generic monopole operator as $v_{(n_1,n_2,n_3)}$, with $(n_1,n_2,n_3)\in\mathbb{Z}^3$. The chiral ring relations between these operators are:

$$\begin{aligned} v_{(n_1,n_2,n_3)}v_{(m_1,m_2,m_3)} =& v_{(n_1+m_1,n_2+m_2,n_3+m_3)}(\phi_1-\phi_2)^{(2g-2)\mathrm{ABS}_+(n_1-n_2,m_1-m_2)} \\ &\cdot(\phi_2-\phi_3)^{(2g-2)\mathrm{ABS}_+(n_2-n_3,m_2-m_3)}(\phi_3-\phi_1)^{(2g-2)\mathrm{ABS}_+(n_3-n_1,m_3-m_1)} \end{aligned} \tag{3.63}$$

which allows for the extraction of the determining Coulomb branch relations:

$$v_{(1,1,1)}v_{(-1,-1,-1)} = 1\ , \tag{3.64a}$$
$$v_{(1,0,0)}v_{(-1,0,0)} = (\phi_1-\phi_2)^{2g-2}(\phi_3-\phi_1)^{2g-2}\ , \tag{3.64b}$$
$$v_{(0,1,0)}v_{(0,-1,0)} = (\phi_1-\phi_2)^{2g-2}(\phi_2-\phi_3)^{2g-2}\ , \tag{3.64c}$$
$$v_{(0,0,1)}v_{(0,0,-1)} = (\phi_2-\phi_3)^{2g-2}(\phi_3-\phi_1)^{2g-2}\ , \tag{3.64d}$$
$$v_{(1,0,0)}v_{(0,1,0)} = v_{(1,1,0)}(\phi_1-\phi_2)^{2g-2}\ , \tag{3.64e}$$
$$v_{(0,1,0)}v_{(0,0,1)} = v_{(0,1,1)}(\phi_2-\phi_3)^{2g-2}\ , \tag{3.64f}$$
$$v_{(0,0,1)}v_{(1,0,0)} = v_{(1,0,1)}(\phi_3-\phi_1)^{2g-2}\ , \tag{3.64g}$$
$$v_{(-1,0,0)}v_{(0,-1,0)} = v_{(-1,-1,0)}(\phi_1-\phi_2)^{2g-2}\ , \tag{3.64h}$$
$$v_{(0,-1,0)}v_{(0,0,-1)} = v_{(0,-1,-1)}(\phi_2-\phi_3)^{2g-2}\ , \tag{3.64i}$$
$$v_{(0,0,-1)}v_{(-1,0,0)} = v_{(-1,0,-1)}(\phi_3-\phi_1)^{2g-2}\ , \tag{3.64j}$$
$$v_{(1,0,0)}v_{(0,1,0)}v_{(0,0,1)} = v_{(1,1,1)}(\phi_1-\phi_2)^{2g-2}(\phi_2-\phi_3)^{2g-2}(\phi_3-\phi_1)^{2g-2}\ , \tag{3.64k}$$
$$v_{(-1,0,0)}v_{(0,-1,0)}v_{(0,0,-1)} = v_{(-1,-1,-1)}(\phi_1-\phi_2)^{2g-2}(\phi_2-\phi_3)^{2g-2}(\phi_3-\phi_1)^{2g-2}\ , \tag{3.64l}$$
$$v_{(kn_1,kn_2,kn_3)} = v^k_{(n_1,n_2,n_3)}\ . \tag{3.64m}$$

The freely acting $\mathrm{U}(1)$ is the diagonal $\mathrm{U}(1)$ as seen from (3.64a), which contributes to $T^*\mathbb{C}^\times = \mathbb{C}[v_{(1,1,1)}, v_{(-1,-1,-1)}, \phi_1+\phi_2+\phi_3]/\langle v_{(1,1,1)}v_{(-1,-1,-1)} = 1\rangle$. After decoupling this $T^*\mathbb{C}^\times$ there is the identification $v_{(n_1+k,n_2+k,n_3+k)} \sim v_{(n_1,n_2,n_3)}$. The generators $v_{(1,0,0)}$, $v_{(0,1,0)}$, $v_{(-1,-1,0)}$, $v_{(-1,0,0)}$, $v_{(0,-1,0)}$, $v_{(1,1,0)}$, $\phi_1-\phi_2$, $\phi_2-\phi_3$, $\phi_3-\phi_1$ can be identified with X_1, X_2, X_3, Y_1, Y_2, Y_3, Φ_3, Φ_1, Φ_2 respectively in Table 3.6. The relations (3.64b – 3.64j) can be repackaged into matrix form with constraint of rank no larger than 1:

$$\begin{pmatrix} (\phi_1-\phi_2)^2 & v_{(0,1,0)} & v_{(-1,0,0)} \\ v_{(0,-1,0)} & (\phi_2-\phi_3)^2 & v_{(0,0,1)} \\ v_{(1,0,0)} & v_{(0,0,-1)} & (\phi_3-\phi_1)^2 \end{pmatrix}, \tag{3.65}$$

they are exactly the generators and relations of $a_2/\mathbb{Z}^2_{2g-2}$, as in (6.14).

The S_3 Weyl group action on the Abelian Coulomb branch is:

$$\phi_i \longleftrightarrow \phi_{\sigma(i)}\ , \qquad v_{(n_1,n_2,n_3)} \longleftrightarrow v_{(n_{\sigma(1)},n_{\sigma(2)},n_{\sigma(3)})}, \tag{3.66}$$

which agrees with (3.62). This action leads to the Coulomb branch of $\mathcal{Q}_{3.8b}$.

Quotient by an S_2 subgroup

A quotient by an $S_2 \subset S_3$ symmetry can also be applied on the Coulomb branch of $\mathcal{Q}_{3.8a} \cong \mathcal{CG}_{3,2g-2}$. The quivers are shown in Figure 3.9.

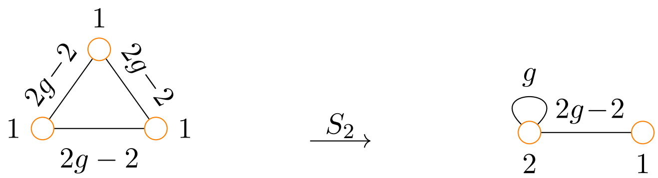

Figure 3.9: Magnetic quivers of the $S_2 \in S_3$ quotient on the Coulomb branch of $\mathcal{CG}_{3,2g-2}$.

The S_2 Weyl group action on the Abelian Coulomb branch is a subgroup action of S_3 in (3.66):

$$\phi_i \longleftrightarrow \phi_{\sigma(i)}\ , \quad v_{(n_1,n_2,n_3)} \longleftrightarrow v_{(n_{\sigma(1)},n_{\sigma(2)},n_3)}, \tag{3.67}$$

where $\sigma \in S_2 \cong \{\mathrm{Id},\ (1\ 2)\}$. The Hilbert series are detailed in Section 3.7.2.

3.5.5 3d mirror of $D_p(\mathrm{SU}(n))$ theories with S_m gauging

The complete graph can be found as a subquiver in the 3d mirror of $D_p(\mathrm{SU}(n))$. The $D_p(\mathrm{SU}(n))$ theories can be realised as 6d $\mathcal{N}=(2,0)$ theories compactified on a sphere with one Type I irregular puncture and one regular (1^n) maximal puncture [114]. The procedure to derive magnetic quivers for these theories are given in [105] and the resulting magnetic quiver takes the form of $\mathcal{Q}_{3.3a}$. In particular, the irregular puncture gives the complete graph part, and the full puncture gives the form of Q_B which is a linear quiver of $(1)-\cdots-(n-1)$ in this case.

Let us restrict to the case where $p \geq n$, here in the complete graph part of the magnetic quivers of $D_p(\mathrm{SU}(n))$ theories there are $m = \mathrm{GCD}(p,n)$ nodes with edge multiplicity $\frac{n(p-n)}{m^2}$. The $\mathcal{Q}_B$ is given, as before, by a linear quiver $(1)-\cdots-(n-1)$. Each U(1) node in the complete graph is connected to the $\mathrm{U}(n-1)$ in $\mathcal{Q}_B$ by $\frac{n}{m}$ bi-fundamentals. There are also $\frac{(n-m)(p-n-m)}{2m}$ free hypermultiplets together.

Then equation (3.5) implies one can gauge any $S_{\sigma_1} \times \cdots \times S_{\sigma_k}$ permutation subgroup of S_n of the 3d mirror of the $D_p(\mathrm{SU}(n))$ theories. For $D_{n(2g-1)}(\mathrm{SU}(n))$ theories, after gauging S_n, a magnetic quiver for Class $\mathcal{S}$ theories with genus g and one maximal regular (1^n) puncture is found.

Some examples are listed in the following.

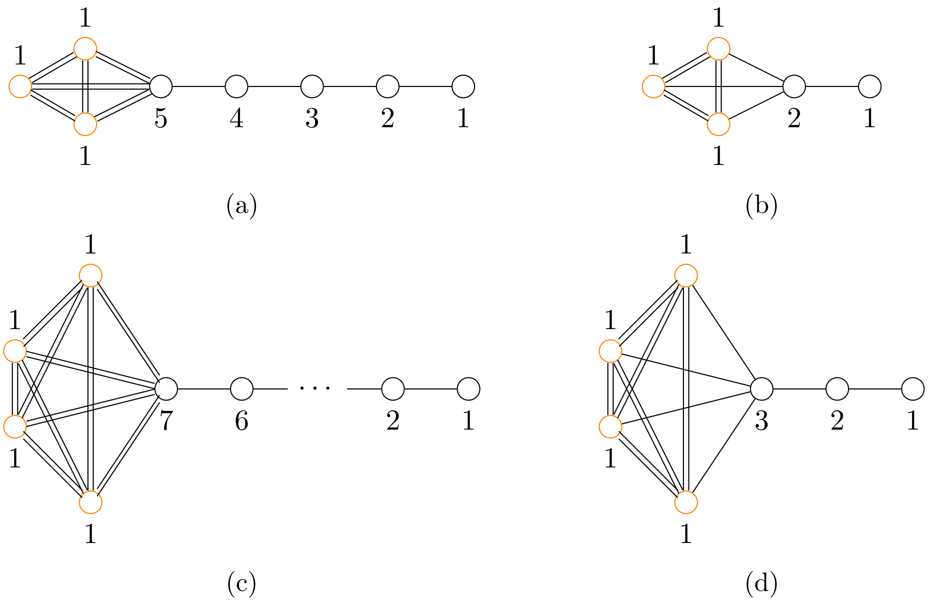

Figure 3.10: a: Magnetic Quiver for $D_9(\mathrm{SU}(6))$. b: Magnetic Quiver for $D_9(\mathrm{SU}(3))$. c: Magnetic Quiver for $D_{12}(\mathrm{SU}(8))$. d: Magnetic Quiver for $D_{12}(\mathrm{SU}(4))$.

- $\mathcal{Q}_{3.10a}$ and $\mathcal{Q}_{3.10b}$ give the magnetic quivers for $D_9(\mathrm{SU}(6))$ and $D_9(\mathrm{SU}(3))$ theories. Both of them can be quotiented by S_2 or S_3. For $D_9(\mathrm{SU}(3))$ theory, the results after the quotient are shown in Figure 3.11. The same operation can be done for $D_9(\mathrm{SU}(6))$.

- $\mathcal{Q}_{3.10c}$ and $\mathcal{Q}_{3.10d}$ gives the magnetic quivers for $D_{12}(\mathrm{SU}(8))$ and $D_{12}(\mathrm{SU}(4))$ theories. Both of them can be quotiented by S_2, $S_2 \times S_2$, S_3, or S_4. For $D_{12}(\mathrm{SU}(4))$ theory, the results after the quotient are shown in Figure 3.12. The same operation can be done for $D_{12}(\mathrm{SU}(8))$.

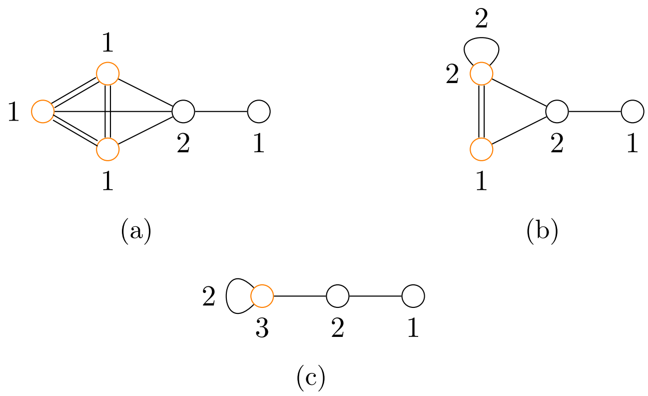

Figure 3.11: a: Magnetic Quiver for $D_9(\mathrm{SU}(3))$. b: S_2 quotient on Coulomb branch of $\mathcal{Q}_{3.11a}$. c: S_3 quotient on Coulomb branch of $\mathcal{Q}_{3.11a}$.

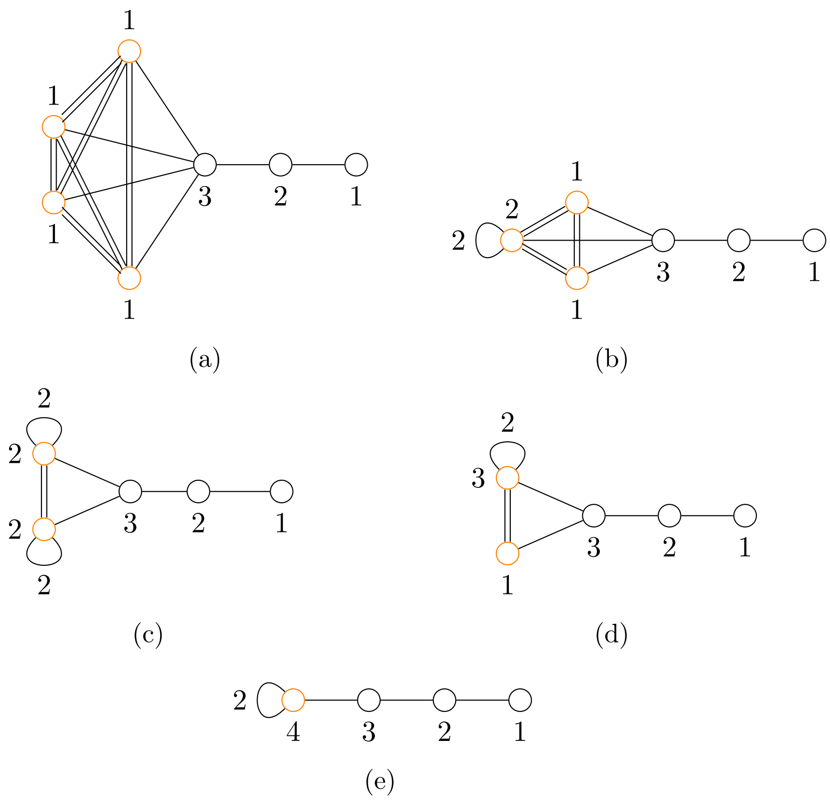

Figure 3.12: a: Magnetic Quiver for $D_{12}(\mathrm{SU}(4))$. b: S_2 quotient on Coulomb branch of $\mathcal{Q}_{3.12a}$. c: $S_2 \times S_2$ quotient on Coulomb branch of $\mathcal{Q}_{3.12a}$. d: S_3 quotient on Coulomb branch of $\mathcal{Q}_{3.12a}$. e: S_4 quotient on Coulomb branch of $\mathcal{Q}_{3.12a}$.

The unrefined Coulomb branch Hilbert series for $\mathcal{Q}_{3.11a}$ and the S_2 and S_3 quotients $\mathcal{Q}_{3.11b}$ and $\mathcal{Q}_{3.11c}$ are computed using monopole formula and Molien sums. Note that in the S_3 quotient, the element (1 2), (1 3), and (2 3) give the same contribution, as do the pair (1 2 3) and (1 3 2). The Hilbert Series after the action of an element in S_n only depends on the conjugacy class of the element.

$$
\mathrm{HS}\left(\mathcal{C}(\mathcal{Q}_{3.11a})\right) = \frac{\begin{pmatrix} 1+4t^2+10t^4+32t^6+65t^8+104t^{10}+153t^{12}+150t^{14} \\ +153t^{16}+104t^{18}+65t^{20}+32t^{22}+10t^{24}+4t^{26}+t^{28} \end{pmatrix}}{(1-t^4)^{-1}(1-t^2)^6(1-t^6)^5}, \tag{3.68a}
$$

$$
\begin{aligned}
\mathrm{HS}\left(\mathcal{C}(\mathcal{Q}_{3.11b}/S_2)\right) &= \frac{1}{2}\left(\mathrm{HS}\left(\mathcal{C}(\mathcal{Q}_{3.11a})\right) + \mathrm{HS}\left(\mathcal{C}(\mathcal{Q}_{3.11a})\right)^{(1\ 2)}\right) \\
&= \frac{1}{2}\left(\mathrm{HS}\left(\mathcal{C}(\mathcal{Q}_{3.11a})\right) + \frac{(1-t^4)(1+2t^2+4t^4+8t^6+7t^8+8t^{10}+4t^{12}+2t^{14}+t^{16})}{(1-t^2)^6(1-t^6)^3}\right) \\
&= \frac{\begin{pmatrix} 1+3t^2+7t^4+19t^6+34t^8+52t^{10}+71t^{12}+70t^{14} \\ +71t^{16}+52t^{18}+34t^{20}+19t^{22}+7t^{24}+3t^{26}+t^{28} \end{pmatrix}}{(1-t^4)^{-1}(1-t^2)^6(1-t^6)^5},
\end{aligned} \tag{3.68b}
$$

$$
\begin{aligned}
\mathrm{HS}\left(\mathcal{C}(\mathcal{Q}_{3.11c}/S_3)\right) &= \frac{1}{6}\Big(\mathrm{HS}\left(\mathcal{C}(\mathcal{Q}_{3.11a})\right) + \mathrm{HS}\left(\mathcal{C}(\mathcal{Q}_{3.11a})\right)^{(1\ 2)} + \mathrm{HS}\left(\mathcal{C}(\mathcal{Q}_{3.11a})\right)^{(2\ 3)} \\
&\quad + \mathrm{HS}\left(\mathcal{C}(\mathcal{Q}_{3.11a})\right)^{(1\ 3)} + \mathrm{HS}\left(\mathcal{C}(\mathcal{Q}_{3.11a})\right)^{(1\ 2\ 3)} + \mathrm{HS}\left(\mathcal{C}(\mathcal{Q}_{3.11a})\right)^{(1\ 3\ 2)}\Big) \\
&= \frac{1}{6}\Big(\mathrm{HS}\left(\mathcal{C}(\mathcal{Q}_{3.11a})\right) + 3\frac{(1-t^4)(1+2t^2+4t^4+8t^6+7t^8+8t^{10}+4t^{12}+2t^{14}+t^{16})}{(1-t^2)^6(1-t^6)^3}
\end{aligned} \tag{3.68c}
$$

$$
\begin{aligned}
&+2\frac{1-t^4}{(1-t^2)^7}\Big) \\
&= \frac{(1-t^8)\begin{pmatrix} 1+2t^2+3t^4+5t^6+8t^8+11t^{10}+14t^{12} \\ +11t^{14}+8t^{16}+5t^{18}+3t^{20}+2t^{22}+t^{24} \end{pmatrix}}{(1-t^2)^6(1-t^6)^5}.
\end{aligned} \tag{3.68d}
$$

Both $\mathcal{Q}_{3.11a}$ and $\mathcal{Q}_{3.11c}$ admit a well-defined 4d construction, in the sense that they are magnetic quivers for such 4d $\mathcal{N}=2$ SCFTs. In contrast, it remains to be explored if $\mathcal{Q}_{3.11b}$ also is a magnetic quiver of some 4d theory (compactified from 6d). An intuitive guess is that all these theories can be compactified on a genus g Riemann surface with certain number of punctures, the genus g contributes to the number of loops, and the punctures should encode the partition data of the subgroups of S_3. The investigation of the discrete quotient in the 4d point of view is left to future work.

3.5.6 Pure $\mathrm{U}(1)^3$ with S_3 gauging – D-brane physics

In this section a well-studied case is used to show the claim and Molien sum technique also work for bad quivers. The quiver before discrete gauging consists of three disconnected U(1) nodes. After S_2 gauging is one U(2) node with one adjoint and one U(1) node. After S_3 gauging is U(3) node with one adjoint.

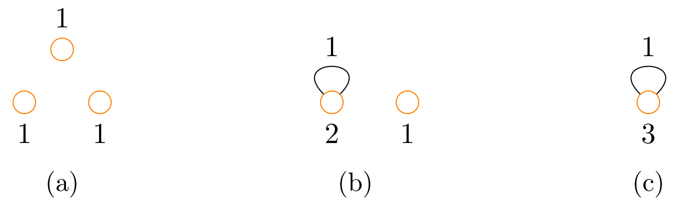

Figure 3.13: a: $\mathcal{CG}_{3,0}$. b: $\mathcal{ML}_{2,1}$ with $\mathcal{CG}_{1,0}$. c: $\mathcal{ML}_{3,1}$.

In this case, the supersymmetry is enhanced to $\mathcal{N} = 8$, the Coulomb branch receives no quantum correction. The discrete gauging between each quiver simply reflects the classical description: $(\mathbb{R}^3 \times S^1)^r/\mathcal{W}_G$, where $\mathcal{W}_G$ is the Weyl group of the gauge group. In [38], it is expressed as the cotangent bundle of the maximal torus of the Langlands (GNO) dual group of the gauge group: $T^*T^\vee/\mathcal{W}$. Applying this description to the quivers above, the following is found:

$$\mathcal{C}\left(\mathcal{CG}_{3,0}\right) = T^*(\mathbb{C}^\times)^3 \tag{3.69a}$$

$$\mathcal{C}\left(\mathcal{CG}_{3,0}/S_2\right) = \mathcal{C}\left(\mathcal{ML}_{2,1} \times \mathcal{CG}_{1,0}\right) = T^*(\mathbb{C}^\times)^2/S_2 \times T^*\mathbb{C}^\times \tag{3.69b}$$

$$\mathcal{C}\left(\mathcal{CG}_{3,0}/S_3\right) = \mathcal{C}\left(\mathcal{ML}_{3,1}\right) = T^*(\mathbb{C}^\times)^3/S_3 \tag{3.69c}$$

The monopole formula diverges when applied to these quivers:

$$\mathrm{HS}\left(\mathcal{C}\left(\mathcal{CG}_{3,0}\right)\right) = \frac{1}{(1-t^2)^3} \sum_{m_1,m_2,m_3} z_1^{m_1} z_2^{m_2} z_3^{m_3} \tag{3.70a}$$

$$\mathrm{HS}\left(\mathcal{C}\left(\mathcal{CG}_{3,0}/S_2\right)\right) = \frac{1}{1-t^2} \sum_{m_3} z_3^{m_3} \left(\frac{1}{(1-t^2)(1-t^4)} \sum_{m_1=m_2} z^{m_1+m_2} + \frac{1}{(1-t^2)^2} \sum_{m_1>m_2} z^{m_1+m_2} \right) \tag{3.70b}$$

$$\begin{aligned} \mathrm{HS}\left(\mathcal{C}\left(\mathcal{CG}_{3,0}/S_3\right)\right) = & \frac{1}{(1-t^2)(1-t^4)(1-t^6)} \sum_{m_1=m_2=m_3} z^{m_1+m_2+m_3} \\ & + \frac{1}{(1-t^2)^2(1-t^4)} \left(\sum_{m_1>m_2=m_3} + \sum_{m_1=m_2>m_3} \right) z^{m_1+m_2+m_3} \\ & + \frac{1}{(1-t^2)^3} \sum_{m_1>m_2>m_3} z^{m_1+m_2+m_3} \end{aligned} \tag{3.70c}$$

The reason is that there are no less than one freely acting U(1)s in each quiver. However, the divergent monopole formula is still a valid tool. For example, the Coulomb branch of pure U(1) theory is $\mathbb{C}[\phi, u_-, u_+]/\langle u_-u_+ - 1\rangle$. The monopole formula for this theory is $\frac{1}{1-t^2}\sum_{m_1} z^{m_1}$, This can be interpreted as: for any fixed monopole charge m_1, there is one monopole operator $u_+^{m_1}\phi^n = u_-^{-m_1}\phi^n$ at degree $2n$. From the geometry point of view, there is a $\mathbb{C}$ fibring over $\mathbb{C}^\times$.

After demonstrating the S_n quotient, now let us demonstrate the $\mathbb{Z}_q$ quotient.

3.6 Examples of $\mathbb{Z}_q$ quotient

The $\mathbb{Z}_q$ gauging on quivers which are or contain certain complete graphs are computed and the corresponding $\mathbb{Z}_q$ quotients on their Coulomb branches are studied. This action is studied through the Hilbert series computed with the monopole formula for each example.

3.6.1 Kleinian A with $\mathbb{Z}_q$ quotient

Now let us look at the simplest example of Claim (3.3). The $A_{k-1} \cong \mathbb{C}^2/\mathbb{Z}_k$ singularity can be realised through the Coulomb branch of an Abelian quiver $\mathcal{CG}_{2,k}$, as $\mathcal{Q}_{3.14a}$ in Figure 3.14.

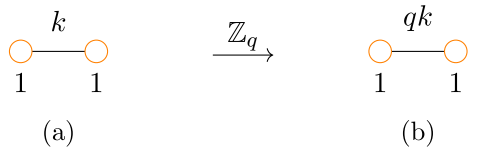

Figure 3.14: a: Quiver $\mathcal{CG}_{2,k}$, whose Coulomb branch is the A_{k-1} singularity. b: Quiver $\mathcal{CG}_{2,kq}$ of (3.2), whose Coulomb branch is the A_{kq-1} singularity.

Since A_{kq-1} is a $\mathbb{Z}_q$ quotient of A_{k-1}, the Coulomb branch of $\mathcal{CG}_{2,kq}$ is a $\mathbb{Z}_q$ quotient of the Coulomb branch of $\mathcal{CG}_{2,k}$:

$$\mathcal{C}\left(\mathcal{CG}_{2,kq}\right) = \mathcal{C}\left(\mathcal{CG}_{2,k}\right)/\mathbb{Z}_q. \tag{3.71}$$

The $\mathbb{Z}_q$ action on $\mathcal{C}\left(\mathcal{CG}_{2,k}\right) = A_{k-1} \cong \mathbb{C}[\phi, u, v]/\langle \phi^k - uv\rangle$ is given by:

$$u \to \omega_q \cdot u, \;\; v \to \omega_q^{-1} \cdot v\ , \tag{3.72}$$

and the fundamental invariants are $u^q = u'$, $v^q = v'$, subject to $uv = \phi^k$. This agrees with $\mathcal{C}\left(\mathcal{CG}_{2,kq}\right) = A_{kq-1} \cong \mathbb{C}[\phi, u', v']/\langle \phi^{kq} - u'v'\rangle$. The $\mathbb{Z}_q$ action can also be implemented in the Hilbert series: it acts on the $\mathrm{U}(1)_J$ fugacity as in (3.26):

$$z \to \omega_q \cdot z\ . \tag{3.73}$$

Combined with the Molien sum (3.27), the Hilbert Series of $\mathcal{C}\left(\mathcal{CG}_{2,kq}\right)$ is obtained from the Hilbert Series of $\mathcal{C}\left(\mathcal{CG}_{2,k}\right)$:

$$\begin{aligned}
\mathrm{HS}(A_{kq-1}) &= \frac{1}{q}\sum_{i=1}^{q} \mathrm{HS}(A_{k-1})|_{z\to\omega_q^i\cdot z} \\
&= \frac{1}{q}\sum_{i=1}^{q} \mathrm{PE}\left[t^2 + (\omega_q^i \cdot z + \frac{1}{\omega_q^i \cdot z})t^k - t^{2k}\right] \\
&= \mathrm{PE}\left[t^2 - (z^q + \frac{1}{z^q})t^{kq} - t^{2kq}\right].
\end{aligned} \tag{3.74}$$

From the quivers in Figure 3.14, the $\mathbb{Z}_q$ quotient can be implemented through the edge multiplicity k. On the Coulomb branch level, instead of q-times the edge multiplicity, the action (3.73) can also be interpreted as q-times the charge (double q lace) of hypermultiplets under the gauge $\mathrm{U}(1)^2$. The edge multiplicity and double lace on Coulomb branch cannot be distinguished; the difference is manifest on the Higgs branch, which is left to future work. Moreover, the two potential theory also differ in their higher symmetries, as recently analysed in [102, 107, 115].

3.6.2 $\mathbb{H}^2$ with $\mathbb{Z}_q$ quotient

As an extension of the A-type singularity to 4 complex dimensions, there is $\mathbb{C}^4/\mathbb{Z}_q$ with the action of $\mathbb{Z}_q$: $\mathrm{diag}(\omega_q, \omega_q, \omega_q^{-1}, \omega_q^{-1})$. The magnetic quiver of this singularity is $\mathcal{Q}_{3.15b}$. The Coulomb branch of $\mathcal{Q}_{3.15b}$ can be seen as a $\mathbb{Z}_q$ quotient on the Coulomb branch of $\mathcal{Q}_{3.15a}$ by the Claim (3.6):

$$\mathcal{C}\left(\mathcal{Q}_{3.15b}\right) = \mathcal{C}\left(\mathcal{Q}_{3.15a}\right)/\mathbb{Z}_q \tag{3.75}$$

here the middle node is treated as the background quiver.

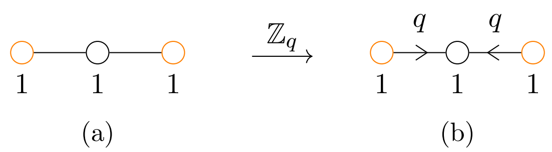

Figure 3.15: a: Quiver $\mathcal{Q}_{3.15a}$ is an Abelian linear quiver of three nodes. The Coulomb branch is $\mathbb{H}^2 \cong \mathbb{C}^4$. b: Quiver $\mathcal{Q}_{3.15b}$ has two q laced edges pointing to the middle $\mathrm{U}(1)$. The Coulomb branch is $\mathbb{C}^4/\mathbb{Z}_q$.

This construction can be further extended to $2n$ complex dimensions: i.e. $\mathbb{C}^{2n}/\mathbb{Z}_q$ with the action $\mathrm{diag}(\omega_q, \cdots, \omega_q, \omega_q^{-1}, \cdots, \omega_q^{-1})$. The Coulomb branch construction is shown in Figure 3.16 and the Coulomb branches obey the relation:

$$\mathcal{C}\left(\mathcal{Q}_{3.16b}\right) = \mathcal{C}\left(\mathcal{Q}_{3.16a}\right)/\mathbb{Z}_q. \tag{3.76}$$

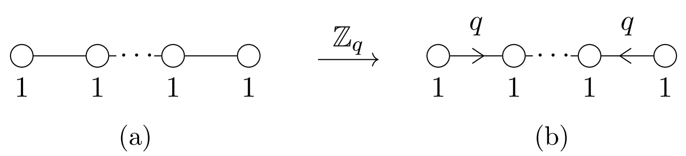

Figure 3.16: a: Quiver $\mathcal{Q}_{3.16a}$ is an linear Abelian quiver composed of $n+1$ nodes. The Coulomb branch is $h_{n,1} = \mathbb{H}^n \cong \mathbb{C}^{2n}$. b: Quiver $\mathcal{Q}_{3.16b}$ has two q laced edges pointing to the middle, as leftmost and rightmost. The Coulomb branch is $h_{n,q} = \mathbb{C}^{2n}/\mathbb{Z}_q$. The $h_{n,q}$ appears an elementary slice in the affine Grassmannian, and in more general symplectic singularities.

In this case, however, the leftmost and rightmost nodes cannot be seen as identical, so the quiver does not fit the Claim (3.6). But, since the proof of Claim (3.6) only assumes the subquiver to be an Abelian instead of a complete graph, it can be applied to any simply-laced Abelian subquiver.

3.6.3 a_2 with $\mathbb{Z}_q^2$ gauging

Another interesting example of (3.3) is the quotient on $\mathcal{CG}_{3,1}$. The Coulomb branch of $\mathcal{CG}_{3,1}$ is a_2, the closure of minimal nilpotent orbit of $\mathfrak{sl}_3$. The coordinate ring of this Coulomb branch is written as $\mathbb{C}[M^i_j]/\langle \mathrm{Tr}(M) = 0,\ \mathrm{rk}(M) \leq 1\rangle$, where $i, j = 1, 2, 3$. According to Claim (3.3), there is the following relationship:

$$\mathcal{C}\left(\right) = \mathcal{C}\left(\right) /\mathbb{Z}_q^2. \tag{3.77}$$

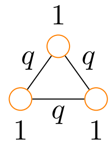

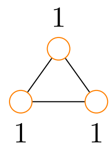

The Coulomb branch ring of $\mathcal{CG}_{3,q}$ is the ring of invariants $\mathbb{C}[M^j_i]^{\mathbb{Z}_q\times\mathbb{Z}_q}/\langle \mathrm{Tr}(M) = 0,\ \mathrm{rk}(M) \leq 1\rangle$. The $\mathbb{Z}_q \times \mathbb{Z}_q$ action is given by: $M^j_i \to \omega_q^{k_i - k_j} M^j_i$, with $(k_i, k_j) \in \mathbb{Z}_q^2$.

3.7 Examples of combined S_n and $\mathbb{Z}_q$ quotients

After studying the S_n and $\mathbb{Z}_q$ quotients individually, it is time to explore the combined action.

3.7.1 Kleinian review: Dih or Dic

In Section 3.5.1, we showed the S_2 quotient relation between A_{2g-3} and D_{g+1} through quivers. The Claim (3.4) indicates that $\mathcal{C}(\mathcal{CG}_{2,k}) \cong A_{k-1}$ and $\mathcal{C}(\mathcal{ML}_{2,qk+1}) \cong D_{qk+2}$ are related by a $\mathbb{Z}_{2q} \rtimes S_2 \cong Dih_{2q}$ quotient. However, this claim might be confusing without specifying the module of the group action. For example, when $k = 1$, the two Coulomb branches $A_0 \cong \mathbb{C}^2$ and $D_{q+2} \cong \mathbb{C}^2/Dic_{2q}$ are related by the non-split extension $\mathbb{Z}_{2q}.S_2 = Dic_q$ instead of the split extension $\mathbb{Z}_{2q} \rtimes S_2 = Dih_{2q}$. To fit the claim, we should take the module of the generators $\mathrm{span}[u, v, \phi]$ instead of $\mathbb{C}^2$, then the actions are:

$$\sigma = \begin{pmatrix} \omega_{2q} & 0 & 0 \\ 0 & \omega_{2q}^{-1} & 0 \\ 0 & 0 & 1 \end{pmatrix}, \quad \tau = \begin{pmatrix} 0 & 1 & 0 \\ 1 & 0 & 0 \\ 0 & 0 & -1 \end{pmatrix}, \tag{3.78}$$

which exactly generate the group $Dih_{2q} = \langle \sigma, \tau | \sigma^{2q} = \tau^2 = \sigma\tau\sigma\tau = \mathrm{Id}\rangle$.

3.7.2 A_2 affine quiver with S_4 gauging

In this section the combined discrete quotient on the Coulomb branch of the affine A_2 quiver $\mathcal{CG}_{3,1}$ is studied. As in Section 3.6.3, a $\mathbb{Z}_q^2$ quotient on a_2 is performed, which takes the $\mathcal{CG}_{3,1}$ quiver to the $\mathcal{CG}_{3,q}$ quiver. Recalling Section 3.5.4, a further S_3 quotient on the Coulomb branch of $\mathcal{CG}_{3,2g-2}$ is performed, which results in the $\mathcal{ML}_{3,g}$ quiver – a single U(3) gauge node with g adjoint hypermultiplets.

Let us consider the simplest example of the combined action. A S_2 or S_3 symmetry can be quotiented from $\mathcal{CG}_{3,2}$, the corresponding quivers are shown in Table 3.8. According to Claim (3.7), the Coulomb branches are $a_2/\mathbb{Z}_2^2 \rtimes S_2$ and $a_2/\mathbb{Z}_2^2 \rtimes S_3$ respectively. There are surprising examples due to the coincidences of the group action: $\mathbb{Z}_2^2 \rtimes S_2 \cong Dih_4$ and $\mathbb{Z}_2^2 \rtimes S_3 \cong S_4$. The latter leads to a recently studied symplectic singularity [103]. The details are discussed below.

In terms of gauging outer automorphism symmetries both S_2 and S_3 could be gauged on the Coulomb branch of $\mathcal{CG}_{3,2}$, but not on $\mathcal{CG}_{3,1}$ due to its odd edge multiplicity.

The Hilbert series of all possible combinations of $\mathbb{Z}_2^2$ and S_2 and S_3 gaugings on a_2 are computed. The quivers, unrefined HS, and the volume of the Coulomb branches are provided in Table 3.8.

Label	Quiver	Discrete Quotient	HS	Volume
$\mathcal{C}(\mathcal{CG}_{3,1}) = a_2$	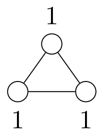		$\frac{1+4t^2+t^4}{(1-t^2)^4}$	$\frac{3}{8}$
$\mathcal{C}(\mathcal{CG}_{3,2}) = a_2/\mathbb{Z}_2^2$	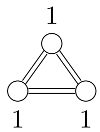	$\mathbb{Z}_2^2 \cong Klein_4$	$\frac{1+4t^4+t^8}{(1-t^2)^2(1-t^4)^2}$	$\frac{3}{32}$
$a_2/\mathbb{Z}_2^2 \rtimes S_2$	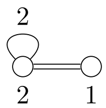	$\mathbb{Z}_2^2 \rtimes S_2 \cong Dih_4$	$\frac{1+t^2+2t^4+4t^6+2t^8+t^{10}+t^{12}}{(1-t^4)^4}$	$\frac{3}{64}$
$a_2/\mathbb{Z}_2^2 \rtimes S_3 \cong a_2/S_4$	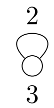	$\mathbb{Z}_2^2 \rtimes S_3 \cong S_4$	$\frac{1+2t^6+2t^8+t^{14}}{(1-t^4)^3(1-t^6)}$	$\frac{1}{64}$

Table 3.8: Quivers from discrete quotient of a_2.

Note that the ratios of the volumes[3] of the moduli spaces is also consistent with the gaugings performed. Indeed, $\frac{\mathrm{vol}^{-1}(a_2/\mathbb{Z}_2^2)}{\mathrm{vol}^{-1}(a_2)} = 4$, $\frac{\mathrm{vol}^{-1}(a_2/\mathbb{Z}_2^2 \rtimes S_2)}{\mathrm{vol}^{-1}(a_2)} = 8$, and $\frac{\mathrm{vol}^{-1}(a_2/\mathbb{Z}_2^2 \rtimes S_3)}{\mathrm{vol}^{-1}(a_2)} = 24$.

In addition, full details of the computation of the Hilbert Series of these quotients using the Molien sum (3.15) and (3.27) are provided. Here, the fugacities (z_1', z_2', z_3') for $\mathcal{CG}_{3,1}$, and rescaled fugacities $(z_1, z_2, z_3) = ({z_1'}^2, {z_2'}^2, {z_3'}^2)$ for $\mathcal{CG}_{3,2}$ are turned on. The quiver is ungauged by setting $m_3 = 0$ and $z_3' = z_3 = 1$:

$$\begin{aligned}
\mathrm{HS}(a_2) &= \frac{1}{(1-t^2)^2} \sum_{m_1,m_2} {z_1'}^{m_1} {z_2'}^{m_2} t^{|m_1|+|m_2|+|m_1-m_2|} \\
&= \frac{1 + 2t^2 - (z_1' + z_2' + z_1'z_2' + \frac{1}{z_1'} + \frac{1}{z_2'} + \frac{1}{z_1'z_2'})t^4 + 2t^6 + t^8}{(1 - z_1't^2)(1 - z_2't^2)(1 - z_1'z_2't^2)(1 - \frac{t^2}{z_1'})(1 - \frac{t^2}{z_2'})(1 - \frac{t^2}{z_1'z_2'})} \qquad (3.79a) \\
\mathrm{HS}(a_2/\mathbb{Z}_2^2) &= \frac{1}{4} \sum_{i=1}^{2} \sum_{j=1}^{2} \mathrm{HS}(a_2)|_{z_1' \to \omega_2^i \cdot z_1', z_2' \to \omega_2^j \cdot z_2'}
\end{aligned}$$

[3]The (inverse) volume of the Coulomb branches can be calculated from Hilbert series as $\mathrm{vol}^{-1} = \lim_{t\to 1}(1-t)^d \mathrm{HS}$, where d is the complex dimension of the Coulomb branch. If two space are related by a G quotient, then the ratio between the volumes should be the order $|G|$.

$$= \frac{1}{(1-t^2)^2} \sum_{m_1,m_2} {z'_1}^{2m_1} {z'_2}^{2m_2} t^{2|m_1|+2|m_2|+2|m_1-m_2|}|_{{z'_1}^2=z_1,{z'_2}^2=z_2}$$

$$= \frac{1+2t^4-(z_1+z_2+z_1z_2+\frac{1}{z_1}+\frac{1}{z_2}+\frac{1}{z_1z_2})t^8+2t^{12}+t^{16}}{(1-z_1t^4)(1-z_2t^4)(1-z_1z_2t^4)(1-\frac{t^4}{z_1})(1-\frac{t^4}{z_2})(1-\frac{t^4}{z_1z_2})(1+t^2)^{-2}} \tag{3.79b}$$

$$\mathrm{HS}(a_2/\mathbb{Z}_2^2 \rtimes S_2) = \frac{1}{2}\left(\mathrm{HS}(a_2/\mathbb{Z}_2^2) + \mathrm{HS}(a_2/\mathbb{Z}_2^2)^{(1\ 2)}\right)$$

$$= \frac{1}{2}\left(\mathrm{HS}(a_2/\mathbb{Z}_2^2) + \frac{1}{1-t^4}\sum_{m_1=m_2} z_1^{m_1} z_2^{m_2} t^{2|m_1|+2|m_2|+2|m_1-m2|}\right)|_{z_1=z_2=z}$$

$$= \frac{1+t^2+2t^4+(2+z+\frac{1}{z})t^6+2t^8+t^{10}+t^{12}}{(1-zt^4)(1-z^2t^4)(1-\frac{1}{z}t^4)(1-\frac{1}{z^2}t^4)} \tag{3.79c}$$

$$\mathrm{HS}(a_2/\mathbb{Z}_2^2 \rtimes S_3) = \frac{1}{6}\Big(\mathrm{HS}(a_2/\mathbb{Z}_2^2) + \mathrm{HS}(a_2/\mathbb{Z}_2^2)^{(1\ 2)} + \mathrm{HS}(a_2/\mathbb{Z}_2^2)^{(1\ 3)} + \mathrm{HS}(a_2/\mathbb{Z}_2^2)^{(2\ 3)}$$

$$+\mathrm{HS}(a_2/\mathbb{Z}_2^2)^{(1\ 2\ 3)} + \mathrm{HS}(a_2/\mathbb{Z}_2^2)^{(1\ 3\ 2)}\Big)$$

$$= \frac{1}{6}\Bigg(\mathrm{HS}(a_2/\mathbb{Z}_2^2) + \frac{1}{1-t^4}\Big(\sum_{m_1=m_2} + \sum_{m_1=0,m_2} + \sum_{m_1,m_2=0}\Big) z_1^{m_1} z_2^{m_2} t^{2|m_1|+2|m_2|+2|m_1-m2|}$$

$$+\frac{1-t^2}{1-t^6} + \frac{1-t^2}{1-t^6}\Bigg)|_{z_1=z_2=1}$$

$$= \frac{1+2t^6+2t^8+t^{14}}{(1-t^4)^3(1-t^6)}\,. \tag{3.79d}$$

Note that in (3.79d), the elements (1 2), (1 3) and (2 3) give the same contribution, so do the elements (1 2 3) and (1 3 2). In general, the elements in the same conjugacy of S_n class give the same contribution.

Finally, a comment on the $a_2/\mathbb{Z}_2^2 \rtimes S_3$. This case raises a special interest due to the accidental identification of the discrete symmetry $\mathbb{Z}_2^2 \rtimes S_3$ with S_4. This symplectic singularity is also found and constructed explicitly as part of the nilpotent cone of $\mathfrak{e}_8$ in [103], as the slice between $E_8(a_6)$ and $E_8(b_6)$. The original construction is given in Appendix 6.3. By comparing the Hilbert series with the generators and relations, the claim that the quiver and the Hilbert Series presented in the last row of Table 3.8 are indeed the magnetic quiver and Hilbert Series for a_2/S_4, respectively is made.

In addition, the Hasse diagram and decorated quiver description of a_2/S_4 is given in Figure 3.17.

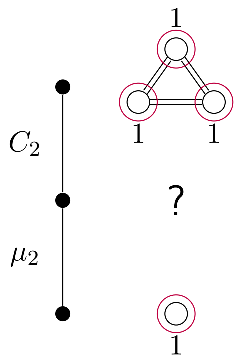

Figure 3.17: Hasse diagram of a_2/S_4.

In the diagram, C_2 is the Kleinian singularity A_3 with an intrinsic symmetry S_2. This means, winding around the base leaf, there is a monodromy of S_2 acting on A_3 and 2 FI parameters are frozen to take the same value. More dedtails are explained in next chapter. μ_2 is a non-normal slice with normalisation A_3[4]. The decorated quiver with a simply-laced bouquet is introduced and discussed in [8, 116]. The investigation of the decorated quiver with a non-simply-laced bouquet or complete graphs is left for future work.

3.7.3 A_3 affine quiver with S_2 and $\mathbb{Z}_2$ gauging

A similar analysis for the affine A_3 quiver: $\mathcal{CG}_{4,1}$ is performed. The Coulomb branch is the closure of the minimal nilpotent orbit of A_3, which is denoted a_3. Hence, for a_3, quotients by S_2, S_2^2, $\mathbb{Z}_2^3$, and products thereof can be taken. The quotient of S_2 and S_2^2 are discussed above in Section 3.5.2. The resulting quivers, unrefined HS, and volume of the resulting moduli space are summarised in Table 3.9.

[4]The slice C_2 can be generalised to C_p. The ring of C_p is locally the same as D_{p+1}. Geometrically there is a monodromy map changing the canonical set of generators of D_{p+1}. It appears as the top slice of the $a_2/\mathbb{Z}_p^2 \rtimes S_3$ Hasse diagram. The non-normal slice μ_2 can be generalised to μ_p, whose normalisation is A_{2p-1}. The ring of μ_p is $\mathbb{C}[s^2t^2, s^3t^3, s^{2p}, t^{2p}, s^{2p+1}t, st^{2p+1}]$. It appears as the bottom slice of the $a_2/\mathbb{Z}_p^2 \rtimes S_3$ Hasse diagram.

Label	Quiver	Discrete Quotient	HS	Volume
a_3	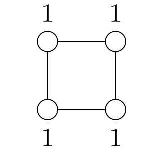		$\frac{(1+t^2)(1+8t^2+t^4)}{(1-t^2)^6}$	$\frac{5}{8}$
$a_3/S_2 \cong \overline{\text{n.min } B_2}$	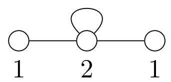	S_2	$\frac{(1+t^2)(1+3t^2+t^4)}{(1-t^2)^6}$	$\frac{5}{16}$
$a_3/S_2 \times S_2$	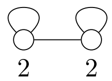	$S_2 \times S_2 \cong \text{Klein}_4$	$\frac{1+3t^2+11t^4+10t^6+11t^8+3t^{10}+t^{12}}{(1-t^2)^3(1-t^4)^3}$	$\frac{5}{32}$
$a_3/\mathbb{Z}_2^3$	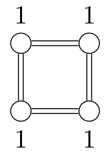	$\mathbb{Z}_2^3$	$\frac{(1+t^4)(1+8t^4+t^8)}{(1-t^2)^3(1-t^4)^3}$	$\frac{5}{64}$
$a_3/\mathbb{Z}_2^3 \rtimes S_2$	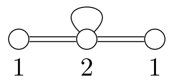	$\mathbb{Z}_2^3 \rtimes S_2 \cong \mathbb{Z}_2 \times Dih_4$	$\frac{(1+t^4)(1-t^2+5t^4-t^6+t^8)}{(1-t^2)^3(1-t^4)^3}$	$\frac{5}{128}$
$a_3/\mathbb{Z}_2^3 \rtimes S_2 \times S_2$	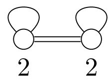	$\mathbb{Z}_2^3 \rtimes S_2 \times S_2$	$\frac{1-2t^2+6t^4-4t^6+8t^8-4t^{10}+6t^{12}-2t^{14}+t^{16}}{(1-t^2)^3(1-t^4)^2(1-t^8)}$	$\frac{5}{256}$

Table 3.9: Quivers from discrete quotient of a_3.

Again, one verifies that the (inverse) volume ratios agree with the order of the quotient group: $\frac{\text{vol}^{-1}(a_3/S_2)}{\text{vol}^{-1}(a_3)} = 2$, $\frac{\text{vol}^{-1}(a_3/S_2\times S_2)}{\text{vol}^{-1}(a_3)} = 4$, $\frac{\text{vol}^{-1}(a_3/\mathbb{Z}_2^3)}{\text{vol}^{-1}(a_3)} = 8$, $\frac{\text{vol}^{-1}(a_3/\mathbb{Z}_2^3\rtimes S_2)}{\text{vol}^{-1}(a_3)} = 16$, and $\frac{\text{vol}^{-1}(a_3/\mathbb{Z}_2^3\rtimes S_2\times S_2)}{\text{vol}^{-1}(a_3)} = 32$.

3.7.4 D_4 affine quiver with S_4 gauging

The Coulomb branch of the D_4 affine quiver is d_4, the closure of the minimal nilpotent orbit of $\mathfrak{so}_8$. The quiver has a natural S_4 action that permutes the 4 U(1) nodes. By gauging this S_4 and its subgroups, the orbifolds of d_4 by the subgroup that is gauged can be obtained, the quivers are labelled by (1) in Table 3.10. This construction is well-studied in [89–91, 97, 117]. Here a different realisation of the orbifold of d_4 by S_4 and its subgroups is provided by using both the $\mathbb{Z}_q$ and the S_n quotients, the quivers are labelled by (2) in the Table 3.10. The symplectic singularity in the last row of this table is also found and constructed explicitly as part of the nilpotent cone of $\mathfrak{f}_4$ in [103], as the slice between $E_8(a_6)$ and $E_8(b_6)$.

Label	Quiver	Discrete Quotient	HS	Volume
d_4	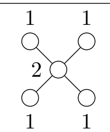		$\frac{(1+t^2)(1+17t^2+48t^4+17t^6+t^8)}{(1-t^2)^{10}}$	$\frac{21}{128}$
$d_4/S_2(1)$	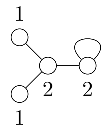	S_2	$\frac{(1+t^2)(1+10t^2+20t^4+10t^6+t^8)}{(1-t^2)^{10}}$	$\frac{21}{256}$
$d_4/S_2(2)$	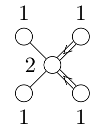	$\mathbb{Z}_2 \cong S_2$	$\frac{(1+3t^2+6t^4+3t^6+t^8)(1+8t^2+55t^4+64t^6+55t^8+8t^{10}+t^{12})}{(1-t^2)^5(1-t^4)^5}$	$\frac{21}{256}$
$d_4/S_2\times S_2(1)$	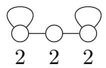	$S_2\times S_2$	$\frac{1+10t^2+55t^4+150t^6+288t^8+336t^{10}+288t^{12}+150t^{14}+55t^{16}+10t^{18}+t^{20}}{(1-t^2)^5(1-t^4)^5}$	$\frac{21}{512}$
$d_4/S_2\times S_2(2)$	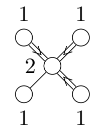	$\mathbb{Z}_2^2 \cong S_2\times S_2$	$\frac{1+5t^2+45t^4+130t^6+314t^8+354t^{10}+314t^{12}+130t^{14}+45t^{16}+5t^{18}+t^{20}}{(1-t^2)^5(1-t^4)^5}$	$\frac{21}{512}$
$d_4/S_3(1)$	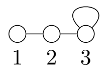	S_3	$\frac{(1+t^2)(1+3t^2+6t^4+3t^6+t^8)}{(1-t^2)^{10}}$	$\frac{7}{256}$
$d_4/S_3(2)$	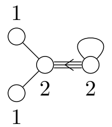	$\mathbb{Z}_3\rtimes S_2 \cong S_3$	$\frac{(1+t^2)(1+9t^2+31t^4+119t^6+234t^8+392t^{10}+645t^{12}+540t^{14}+645t^{16}+392t^{18}+234t^{20}+119t^{22}+31t^{24}+9t^{26}+t^{28})}{(1-t^2)^5(1-t^6)^5}$	$\frac{7}{256}$
$d_4/S_4(1)$	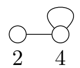	S_4	$\frac{1+3t^2+13t^4+25t^6+46t^8+48t^{10}+46t^{12}+25t^{14}+13t^{16}+3t^{18}+t^{20}}{(1-t^2)^5(1-t^4)^5}$	$\frac{7}{1024}$
$d_4/S_4(2)$	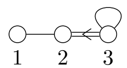	S_4	$\frac{1+3t^2+13t^4+25t^6+46t^8+48t^{10}+46t^{12}+25t^{14}+13t^{16}+3t^{18}+t^{20}}{(1-t^2)^5(1-t^4)^5}$	$\frac{7}{1024}$

Table 3.10: Quivers from discrete quotient of d_4.

A particularly interesting case is the symplectic singularity d_4/S_4, where the action matches for both cases (1) and (2), shown in the last two rows of Table 3.10. Therefore there are two different constructions of this singularity. One is a unitary quiver with an adjoint loop, and the other is a non-simply laced unitary quiver with adjoint. The Hasse diagrams are shown in Figure 3.18 and Figure 3.19, where one can observe that it is computed in two different ways, starting from each corresponding quiver. The decoration on nodes is introduced in [116] as a combinatorial tool to calculate the Hasse diagram. In a quiver, by definition of decoration, a multi-loop part $\mathcal{ML}_{n,g}$ can be replaced by a complete graph $\mathcal{CG}_{n,2g-2}$ with all nodes decorated in the same coluor. The Higgs branches of decorated quivers are discussed in more details in next chapter.

The Hasse diagram can be derived from the decorated quiver technique:

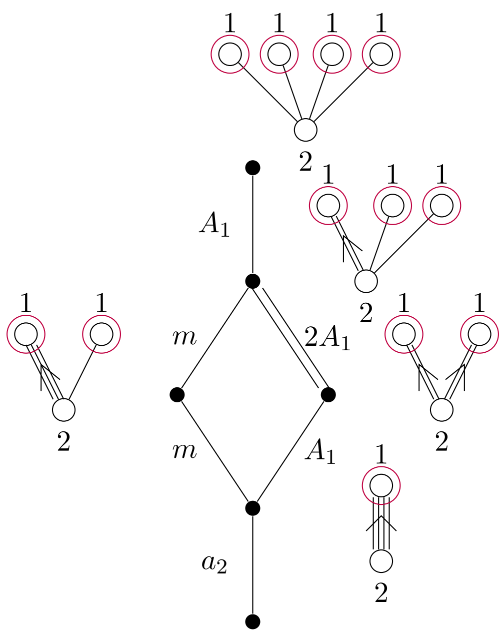

Figure 3.18: Hasse diagram and decorated quiver of $d_4/S_4(1)$.

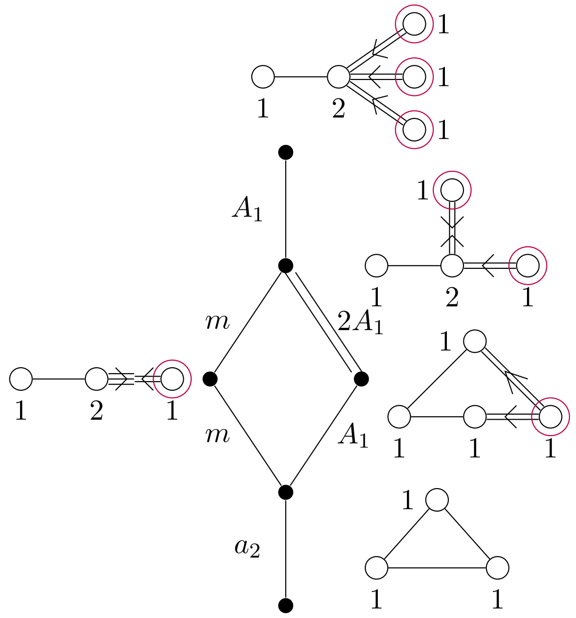

Figure 3.19: Hasse diagram and decorated quiver of $d_4/S_4(2)$. Note the generalised edges are defined in [3].

3.7.5 $\mathcal{CG}_{4,2}$ quiver with S_4 gauging

As a next example, consider the $\mathcal{CG}_{4,2}$ quiver, for which one can quotient S_2, $S_2 \times S_2$, S_3, or S_4. The resulting quivers are collected in Table 3.11.

Label	Quiver	Discrete Quotient	HS	Volume
$\mathcal{CG}_{4,2}$	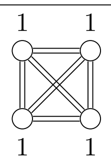		$\frac{1+6t^6+5t^8+5t^{12}+6t^{14}+t^{20}}{(1-t^2)^3(1-t^6)^2(1-t^8)}$	$\frac{1}{96}$
$\mathcal{CG}_{4,2}/S_2$	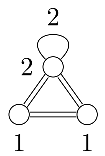	S_2	$\frac{1+4t^6+5t^8+2t^{10}+2t^{12}+5t^{14}+4t^{16}+t^{22}}{(1-t^2)^2(1-t^4)(1-t^6)^2(1-t^8)}$	$\frac{1}{192}$
$\mathcal{CG}_{4,2}/S_2\times S_2$	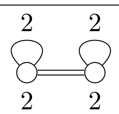	$S_2\times S_2$	$\frac{1+2t^6+6t^8+2t^{10}+2t^{12}+2t^{14}+6t^{16}+2t^{18}+t^{24}}{(1-t^2)(1-t^4)^2(1-t^6)^2(1-t^8)}$	$\frac{1}{384}$
$\mathcal{CG}_{4,2}/S_3$	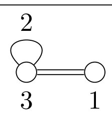	S_3	$\frac{1+2t^6+3t^8+4t^{10}+2t^{12}+2t^{14}+4t^{16}+3t^{18}+2t^{20}+t^{26}}{(1-t^2)(1-t^4)(1-t^6)^3(1-t^8)}$	$\frac{1}{576}$
$\mathcal{CG}_{4,2}/S_4$	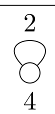	S_4	$\frac{1+2t^8+3t^{10}+4t^{12}+t^{14}+2t^{16}+t^{18}+4t^{20}+3t^{22}+2t^{24}+t^{32}}{(1-t^4)(1-t^6)^3(1-t^8)^2}$	$\frac{1}{2304}$

Table 3.11: Quivers from discrete quotient of $\mathcal{CG}_{4,2}$.

Again, one verifies straightforwardly that the computed (inverse) volume ratios agree with the orders of the quotient groups: $\frac{\mathrm{vol}^{-1}(\mathcal{CG}_{4,2}/S_2)}{\mathrm{vol}^{-1}(\mathcal{CG}_{4,2})} = 2$, $\frac{\mathrm{vol}^{-1}(\mathcal{CG}_{4,2}/S_2\times S_2)}{\mathrm{vol}^{-1}(\mathcal{CG}_{4,2})} = 4$, $\frac{\mathrm{vol}^{-1}(\mathcal{CG}_{4,2}/S_3)}{\mathrm{vol}^{-1}(\mathcal{CG}_{4,2})} =$

6, and $\frac{\mathrm{vol}^{-1}(\mathcal{CG}_{4,2}/S_4)}{\mathrm{vol}^{-1}(\mathcal{CG}_{4,2})} = 24$.

3.7.6 Orbifolds and covers of a hypersurface

Recalling the hypersurface $\mathcal{Q}_{3.7b}$ and its cover $\mathcal{Q}_{3.7a}$, one can study all possible discrete quotients of the latter. Specifically, this is a complete graph with only two nodes and edge multiplicity $2g-2$, and connected to a background U(1) gauge node. The $\mathbb{Z}_2$ quotient can be taken by either changing the edge multiplicity and changing the connection into non-simply laced, or quotient S_2 by merging the two edges. See Table 3.12 for a summary.

Label	Quiver	Discrete Quotient	HS	Volume
$\mathcal{C}(\mathcal{Q}_{3.7a})$	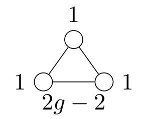		$\frac{1+t^2+2t^{2g-1}-2t^{2g+1}-t^{4g-2}-t^{4g}}{(1-t^2)^3(1-t^{2g-1})^2}$	$\frac{g}{(2g-1)^2}$
$\mathcal{C}(\mathcal{Q}_{3.7b}) = \mathcal{C}(\mathcal{Q}_{3.7a})/S_2$	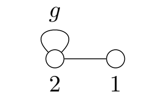	S_2	$\frac{1-t^{4g}}{(1-t^2)^3(1-t^{2g-1})^2}$	$\frac{g}{2(2g-1)^2}$
$\mathcal{C}(\mathcal{Q}_{3.7a})/\mathbb{Z}_2$	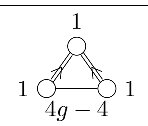	$\mathbb{Z}_2$	$\frac{1+t^2+4t^{4g-2}-4t^{4g}-t^{8g-4}-t^{8g-2}}{(1-t^2)^3(1-t^{4g-2})^2}$	$\frac{g}{2(2g-1)^2}$
$\mathcal{C}(\mathcal{Q}_{3.7a})/\mathbb{Z}_2 \rtimes S_2$	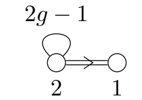	$\mathbb{Z}_2 \rtimes S_2$	$\frac{(1-t^{4g})(1-t^{8g-4})}{(1-t^2)^3(1-t^{4g-2})^3}$	$\frac{g}{4(2g-1)^2}$
$\mathcal{C}(\mathcal{Q}_{3.7a})/\mathbb{Z}_q$	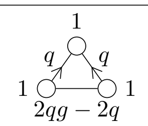	$\mathbb{Z}_q$	$\frac{1+t^2+2qt^{2qg-q}-2qt^{2qg-q+2}-t^{4qg-2q}-t^{4qg-2q+2}}{(1-t^2)^3(1-t^{2qg-q})^2}$	$\frac{g}{q(2g-1)^2}$
$\mathcal{C}(\mathcal{Q}_{3.7a})/\mathbb{Z}_q \rtimes S_2$	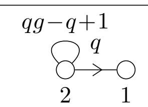	$\mathbb{Z}_q \rtimes S_2$	$\frac{1+(q-1)t^{2qg-q}-qt^{2qg-q+2}-qt^{4qg-2q}-(q-1)t^{4qg-2q+2}+t^{6qg-3q+2}}{(1-t^2)^3(1-t^{2qg-q})^3}$	$\frac{g}{2q(2g-1)^2}$

Table 3.12: Quivers from discrete quotients of a_2.

The most interesting case is the moduli space $\mathcal{C}(\mathcal{Q}_{3.7a})/\mathbb{Z}_q \rtimes S_2$. The Hilbert series indicates that it is a complete intersection: it has 3 generators in adjoint representation of SU(2) at degree 2, and 3 generators in adjoint representation of SU(2) at degree $4g-2$. Also there is one relation in the trivial representation at degree $4g$, and another relation in the trivial representation at degree $8g-4$.

3.8 Generalisations

It is straightforward to generalise the S_n quotient to quivers with other types of gauge groups with multiple adjoint hypermultiplets[5]; see Table 3.13. For instance, Figures 3.20, 3.21, and 3.22 illustrate such cases. The proof proceeds analogous to that Section 3.3.2.

[5] This is the natural generalisation of the bouquets with different gauge nodes of [90].

The following results are found:

$$\mathcal{C}(\mathcal{Q}_{3.20b}) = \mathcal{C}(\mathcal{Q}_{3.20a})/S_n \tag{3.80}$$
$$\mathcal{C}(\mathcal{Q}_{3.21b}) = \mathcal{C}(\mathcal{Q}_{3.21a})/S_n \tag{3.81}$$
$$\mathcal{C}(\mathcal{Q}_{3.22b}) = \mathcal{C}(\mathcal{Q}_{3.22a})/S_n. \tag{3.82}$$

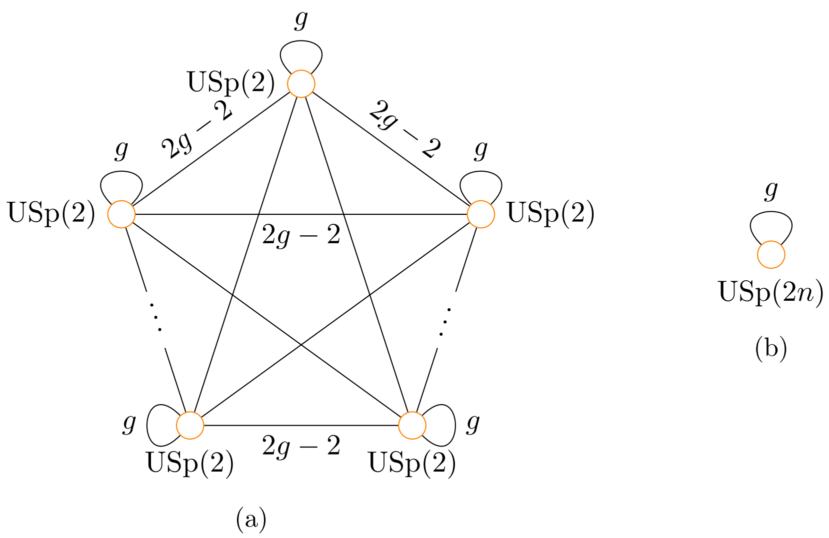

Figure 3.20: a: Complete graph quiver with n nodes of USp(2) with g adjoints and edges of multiplicity $2g-2$ connecting all pairs. b: Quiver for USp($2n$) gauge group with g adjoints.

USp(4) **Example.** USp(4) is used as an example to demonstrate the generalisation. A S_2 quotient on the Coulomb branch can be performed as follows:

$$\mathcal{C}\left(\mathcal{Q}_{\mathrm{USp}}(2,g)\right) = \mathcal{C}\left(\begin{array}{ccc} g & 2g-2 & g \\ \mathrm{USp}(2) & & \mathrm{USp}(2)\end{array}\right) \xrightarrow{S_2} \mathcal{C}\left(\mathcal{Q}_{\mathrm{USp}}(2,g)/S_2\right) = \mathcal{C}\left(\begin{array}{c} g \\ \mathrm{USp}(4)\end{array}\right). \tag{3.83}$$

The Hilbert series for the two Coulomb branches are calculated by an S_2 Molien sum

$$\begin{aligned}
\mathrm{HS}\left(\mathcal{C}\left(\mathcal{Q}_{\mathrm{USp}}(2,g)\right)\right) &= \frac{1}{(1-t^4)^2} + \left(\frac{1}{(1-t^2)(1-t^4)}\sum_{m_1=0,m_2>0} + \frac{1}{(1-t^2)(1-t^4)}\sum_{m_1>0,m2=0}\right. \\
&\quad \left. + \frac{1}{(1-t^2)^2}\sum_{m_1,m_2>0}\right) t^{(4g-4)(|m_1|+|m_2|)+(2g-2)(|m_1-m_2|+|m_1+m_2|)} \\
&= \frac{1+t^{8g-8}+2t^{8g-6}+2t^{12g-10}+t^{12g-8}+t^{20g-16}}{(1-t^4)^2(1-t^{8g-8})(1-t^{12g-12})}.
\end{aligned} \tag{3.84a}$$

$$\begin{aligned}
\mathrm{HS}\left(\mathcal{C}\left(\mathcal{Q}_{\mathrm{USp}}(2,g)/S_2\right)\right) &= \frac{1}{2}\left(\mathrm{HS}\left(\mathcal{Q}_{\mathrm{USp}}(2,g)\right) + \frac{1}{1-t^8} + \frac{1}{1-t^4}\right. \\
&\quad \left. \sum_{m_1=m_2>0} t^{(4g-4)(|m_1|+|m_2|)+(2g-2)(|m_1-m_2|+|m_1+m_2|)}\right)
\end{aligned} \tag{3.84b}$$

$$= \frac{1+t^{8g-6}+t^{8g-4}+t^{8g-2}+t^{12g-10}+t^{12g-8}+t^{12g-6}+t^{20g-12}}{(1-t^4)(1-t^8)(1-t^{8g-8})(1-t^{12g-12})}. \tag{3.84c}$$

and the last line agrees with the direct monopole formula evaluation of the USp(4) theory. Thus, validating the discrete quotient proposal. It then also follows that the (inverse) volume ratio agrees with the order quotient group: $\frac{\mathrm{vol}^{-1}\left(\mathcal{Q}_{\mathrm{USp}}(2,g)/S_2\right)}{\mathrm{vol}^{-1}\left(\mathcal{Q}_{\mathrm{USp}}(2,g)\right)} = 2$.

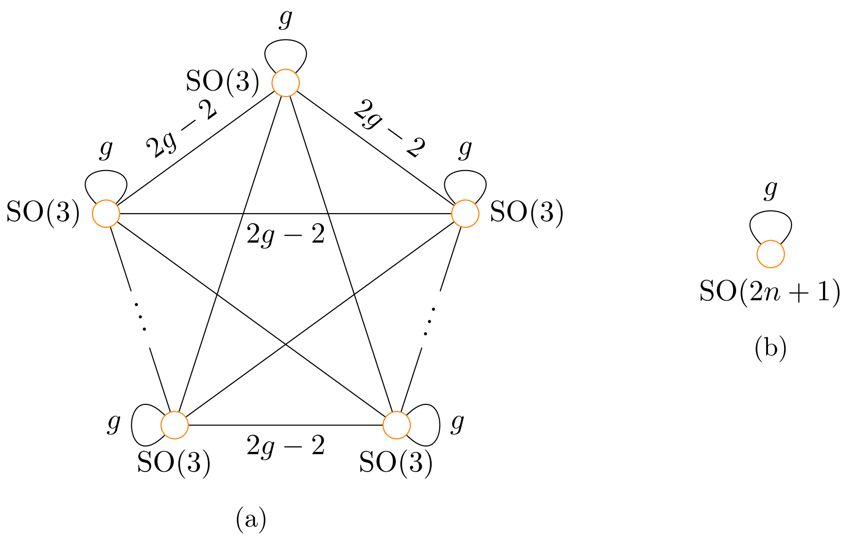

Figure 3.21: a: Complete graph quiver with n nodes of SO(3) with g adjoints and edges of multiplicity $2g-2$ connecting all pairs. b: Quiver for SO($2n+1$) gauge group with g adjoints.

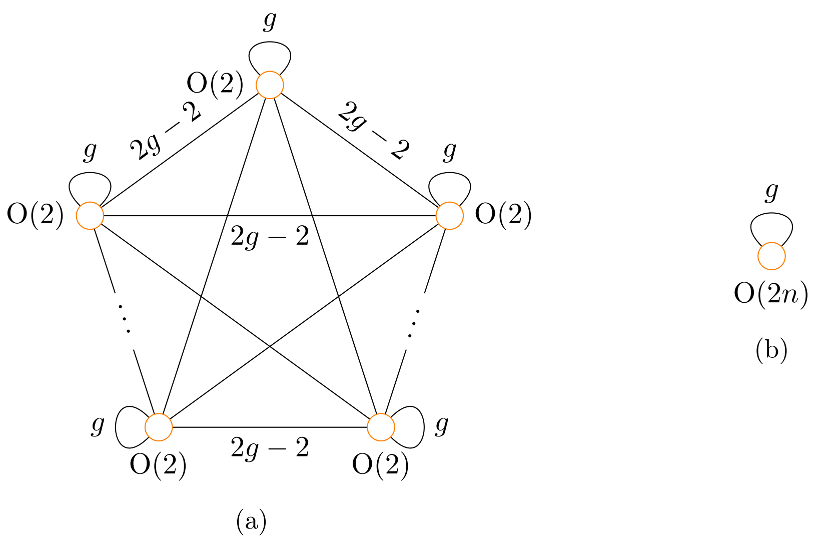

Figure 3.22: a: Complete graph quiver with n nodes of O(2) with edges of multiplicity $2g-2$ connecting all pairs. b: Quiver for O($2n$) gauge group with g adjoints.

As in [90], this statement can be further generalised to symplectic gauge groups with g hypermultiplets in the traceless second rank anti-symmetric product Λ^2, and special orthogonal groups with g hypermultiplets in traceless second rank symmetric product S^2;

see Table 3.13. Again, the proof proceeds analogous to that in Section 3.3.2. The following results are found:

$$\mathcal{C}(\mathcal{Q}_{3.23b}) = \mathcal{C}(\mathcal{Q}_{3.23a})/S_n \tag{3.85}$$

$$\mathcal{C}(\mathcal{Q}_{3.24b}) = \mathcal{C}(\mathcal{Q}_{3.24a})/S_n \tag{3.86}$$

$$\mathcal{C}(\mathcal{Q}_{3.25b}) = \mathcal{C}(\mathcal{Q}_{3.25a})/S_n. \tag{3.87}$$

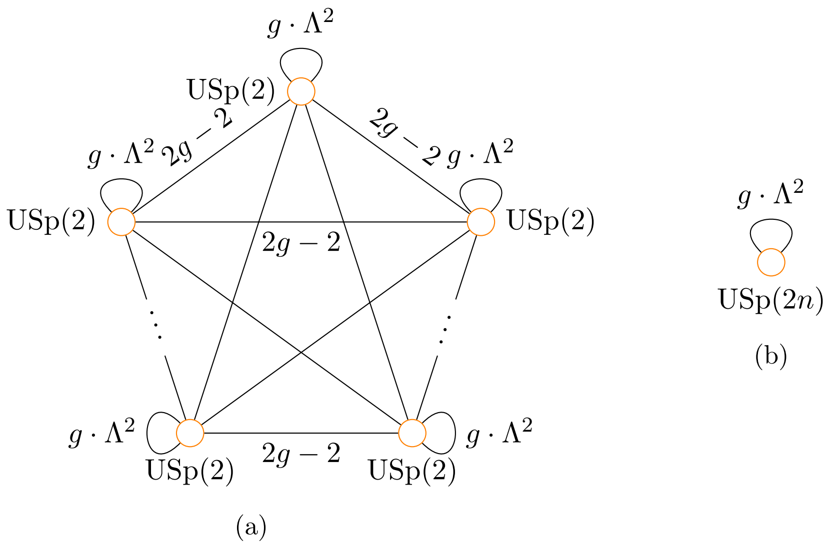

Figure 3.23: a: Complete graph quiver with n nodes of USp(2) and edges of multiplicity $2g-2$ connecting all pairs. b: Quiver for USp($2n$) gauge group with $g \cdot \Lambda^2$ hypermultiplets.

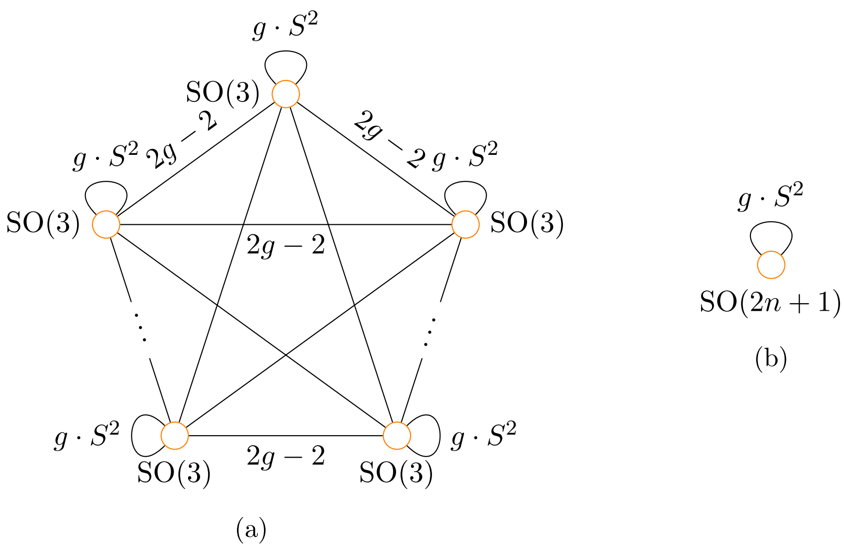

Figure 3.24: a: Complete graph quiver with n nodes of SO(3) with $g \cdot S^2$ hypermultiplets and edges of multiplicity $2g-2$ connecting all pairs. b: Quiver for SO($2n+1$) gauge group with $g \cdot S^2$ hypermultiplets.

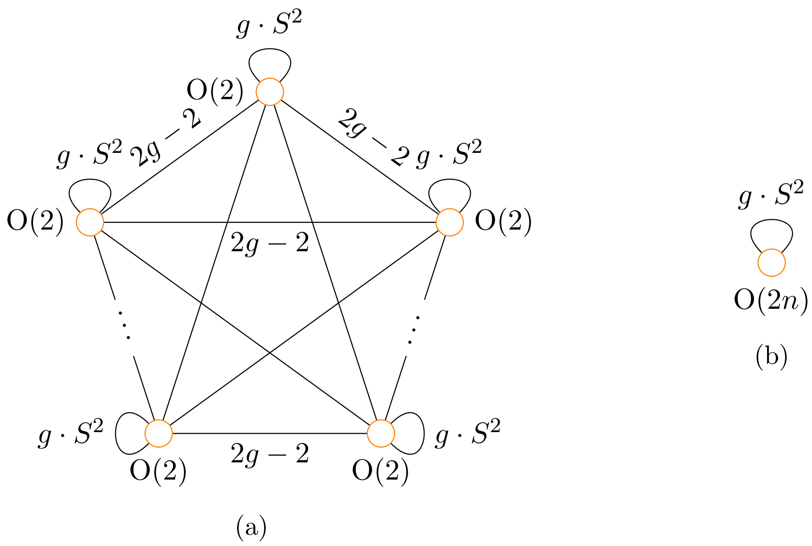

Figure 3.25: a: Complete graph quiver with n nodes of $\mathrm{O}(2)$ with edges of multiplicity $2g-2$ connecting all pairs. b: Quiver for $\mathrm{O}(2n)$ gauge group with g S^2 hypermultiplets.

Those generalizations of S_n quotient to orthosymplectic quivers are summarised in Table 3.13.

G	G'	V
$\mathrm{U}(1)$	$\mathrm{U}(n)$	adj
$\mathrm{USp}(2)$	$\mathrm{USp}(2n)$	$adj,\ \Lambda^2$
$\mathrm{SO}(3)$	$\mathrm{SO}(2n+1)$	$adj,\ S^2$
$\mathrm{O}(2)$	$\mathrm{O}(2n)$	$adj,\ S^2$

Table 3.13: The rank 1 gauge nodes G of the complete graph and the rank n gauge node G' after S_n quotient. V is the allowed representation of the loop attached to G and G'.

Weyl group quotient. In this section, only connected gauge groups are considered. Note that

$$\mathcal{C}\left(\mathcal{CG}_{2,4g-4}\right) = \mathcal{C}\left(\underset{1 \qquad 1}{\overset{4g-4}{\circ\!-\!\!-\!\!-\!\circ}} \right) \quad \xrightarrow{S_2} \quad \mathcal{C}\left(\mathcal{ML}_{\mathrm{USp}(2),g}\right) = \mathcal{C}\left(\underset{\mathrm{USp}(2)}{\overset{g}{\circ}} \right) . \tag{3.88}$$

This means that every $\mathrm{USp}(2)$ node can be acquired from a S_2 quotient of $\mathcal{CG}_{2,4g-4}$. Together with S_n, one may expect an Abelian theory $\mathcal{T}_w$ (not necessarily a quiver), such that the $S_2^n \rtimes S_n = \mathcal{W}_{\mathrm{USp}(2n)}$ quotient of the Coulomb branch of $\mathcal{T}_w$ is the Coulomb branch of $\mathcal{ML}_{\mathrm{USp}(2n),g}$.

Now this result is generalised as follows: Suppose that the non-zero weights of the matter representation $\mathcal{R}$ contains all the non-zero roots of the gauge group G_i, then the Coulomb branch can be written as the Coulomb branch of an Abelian theory quotient the Weyl group of G_i [108]. The Abelian theory $\mathcal{T}_w$ is given by rank(G_i) copies of U(1) gauge groups, and the hypermultiplet charges are given by non-zero weights in the original theory, minus one copy of the non-zero weights in the adjoint representation, i.e.

$$\mathcal{C}\left(\mathcal{Q}_G\right) = \mathcal{C}\left(\mathcal{T}_w / \mathcal{W}_{G_i}\right). \tag{3.89}$$

This generalises (3.5) in two ways. Firstly, in (3.89) any representation "larger" than the adjoint can be included. Secondly, the gauge group G can be any type.

In the orthogonal or symplectic case, from the Abelian theory the $\mathbb{Z}_2$ factors in the Weyl group of G_i can be understood as the $\mathbb{Z}_2$ automorphisms between $\mathcal{N}_i$ and $\bar{\mathcal{N}}_i$ of the hypermultiplet representations $\mathcal{R}_i = \mathcal{N}_i \oplus \bar{\mathcal{N}}_i$. Thus, after the quotient half-hypermultiplets appear in the orthosymplectic quivers.

It is straightforward to see that in quivers Figure 3.2 and Figure 3.3b the requirement for the hypermultiplet representations is satisfied. The requirement for a "larger" representation can be understood in the following way. For an Abelian theory, there is no negative contribution to the conformal dimension. In the corresponding non-Abelian theory, the negative contribution from the vector multiplet needs to be fully compensated. In general, for quivers with hypermultiplets representation "smaller" than the adjoint, one can only expect the Coulomb branch is birational to the Abelianized Coulomb branch [33].

The simplest example for orthosymplectic quivers are shown in Figure 3.26.

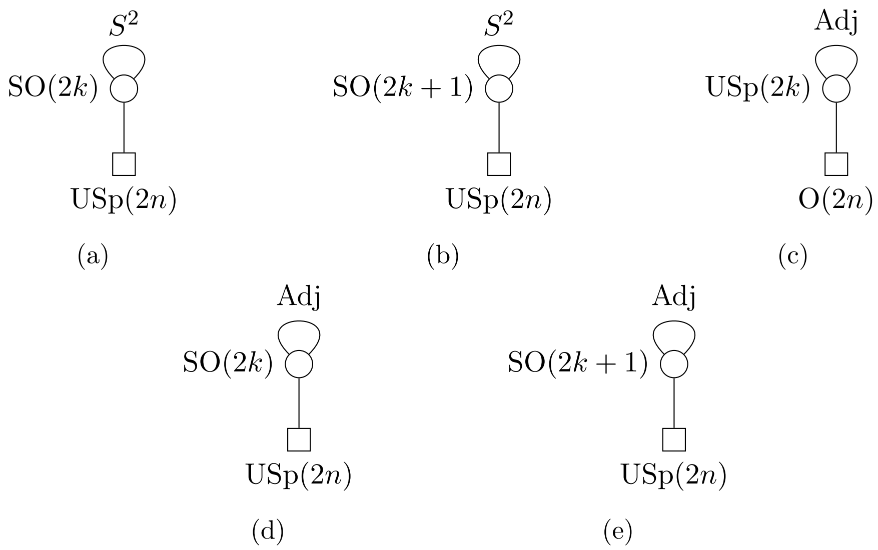

Figure 3.26: ADHM-like quivers.

With (3.89), the Coulomb branches of those quivers are summarised in Table 3.14a. For completeness, the Weyl groups are listed in Table 3.14b.

Quiver	Coulomb branch
$\mathcal{Q}_{3.26a}$	$(A_{2n+3})^k/\mathcal{W}_{D_k}$
$\mathcal{Q}_{3.26b}$	$(A_{2n+3})^k/\mathcal{W}_{B_k}$
$\mathcal{Q}_{3.26c}$	$(A_{2n-1})^k/\mathcal{W}_{C_k}$
$\mathcal{Q}_{3.26d}$	$(A_{2n-1})^k/\mathcal{W}_{D_k}$
$\mathcal{Q}_{3.26e}$	$(A_{2n-1})^k/\mathcal{W}_{B_k}$

(a)

G	$\mathcal{W}_G$	$\lvert\mathcal{W}_G\rvert$
A_k	S_k	$k!$
B_k	$\mathbb{Z}_2^k \rtimes S_k$	$2^k \cdot k!$
C_k	$\mathbb{Z}_2^k \rtimes S_k$	$2^k \cdot k!$
D_k	$\mathbb{Z}_2^{k-1} \rtimes S_k$	$2^{k-1} \cdot k!$

(b) The Weyl group of classical Lie algebras.

Table 3.14: a: The Coulomb branches of the quivers in Figure 3.26. b: The Weyl group of classical Lie algebras.

3.9 Conclusions and outlook

In this work, the S_n discrete quotient on the Coulomb branch of 3d $\mathcal{N}=4$ quiver with a bouquet of n U(1) is generalised to any quiver with a complete graph of n U(1). This result is proven on the level of the monopole formula by using the generalised Molien sum. This S_n plays the role of both outer-automorphism of the quiver and Weyl group of gauge group. This result is also generalised to complete graphs of any rank 1 nodes with loops in certain representations.

Another discrete action considered is $\mathbb{Z}_q^{n-1}$. This can be achieved by changing the edge multiplicity to q-fold or the charge to q-times. These two operations on quivers cannot be distinguished on Coulomb branch level, but can be distinguished by their Higgs branches. The idea behind both actions is to reflect the discrete action on the magnetic lattices into an action on the Coulomb branch geometry. Further, $\mathbb{Z}_q^{n-1}$ and S_n can be combined into $\mathbb{Z}_q^{n-1} \rtimes S_n$ action on the Coulomb branch.

These results are expanding our knowledge of relations between different quivers. It allows us to determine whether a Coulomb branch can be obtained as an orbifold of another, and construct new quivers following the rules. For example, a quiver construction of a_2/S_4 and a new quiver construction of d_4/S_4 were obtained in this paper.

There are plenty of directions to explore in the future. First of all, the Hasse diagrams of Coulomb branches of quivers with g adjoint hypermultiplets is not fully understood yet. Secondly, for the theories which cannot be Abelianised into a well-defined theory in the sense of [108], it is an open challenge to derive the S_n action on the chiral ring generators. Thirdly, it is interesting to classify all quivers whose Coulomb branches are orbifolds of flat space. For example, the orbifold quivers for the complex reflection groups are analysed in an upcoming work. Finally, it remains to be explored what those discrete actions on quivers imply on 4d theories. That is to say, the discrete action is well-defined on the magnetic quiver, but to what extend can this be transferred to the 4d $\mathcal{N}=2$ theory (Argyres-Douglas or class $\mathcal{S}$).

Chapter 4

Quiver subtraction on the Higgs branch

This chapter classifies all Higgs branch Higgsing patterns for simply-laced unitary quiver gauge theories with eight supercharges (including multiple loops) and introduces a Higgs branch subtraction algorithm. All possible minimal transitions are given, identifying differences between slices that emerge on the Higgs and Coulomb branches. In particular, the algorithm is sensitive to global information including monodromies and Namikawa-Weyl groups. Guided by symplectic duality, the algorithm further determines the global symmetry on the Coulomb branch, and verifies the exclusion of C type or F_4 global symmetry for (simply-laced) unitary quiver gauge theories. The Higgs branches of some unitary quivers are verified to give slices in the nilpotent cones of exceptional simple Lie algebras.

4.1 Introduction

A hall-mark of supersymmetric theories is the existence of a large continuous space of supersymmetric vacua. For theories with 8 supercharges in space-time dimension $d = 3, 4, 5, 6$, this moduli space of vacua contains maximal branches like the Higgs and Coulomb branch. By virtue of an $\mathrm{SU}(2)_R$ symmetry these Higgs branches exhibit strongly restricted geometric structures - known as singular hyper-Kähler spaces or symplectic singularities. In contrast, for $d = 3, 4, 5$ theories, the Coulomb branches of theories with 8 supercharges do not exhibit uniform behaviour across dimensions. Higgs branches $\mathcal{H}$ are therefore exceedingly useful objects in the study of the vast landscape of supersymmetric theories with 8 supercharges across various dimensions.

Owing to the high amount of supersymmetry, the Higgs branches $\mathcal{H}$ of theories with eight supercharges are understood as a stratification of leaves related under a partial order and transverse slices. Physically, each leaf represents a set of massless states, where moving within a leaf changes the mass of massive states but preserves the massless states. Hence, it is justified to call each leaf a phase of the theory. A slice, which in many instances can be represented as a moduli space of a quiver (either Higgs or Coulomb branch), is a set of moduli that, if tuned, changes the set of massless states and gives rise to a (second order) phase transition. In most cases, the mechanism in which the states acquire mass is the Brout-Englert-Guralnik-Higgs-Hagen-Kibble mechanism [118–121] (hereafter Higgs mechanism for short), but more general cases include, for example, small instanton transitions. The structure of the Higgs branch may be summarised in a Hasse diagram which displays the partial order of the leaves together with the slices between them. For Lagrangian theories, the Higgs branch Hasse diagram can be simply derived from the Higgs mechanism. Starting with a Lagrangian theory with gauge group G, each leaf in the Higgs branch Hasse diagram corresponds to a now partially Higgsed theory with gauge group $H \subset G$. The slice between them corresponds to a gauge theory with gauge group C, the commutant of H inside G, coupled to matter that is derived from the embedding of $H \subset G$. In practice, the gauge group C turns out to be of classical type.

While the Higgs mechanism is intuitive and familiar for Lagrangian theories, the derivation of the Higgs branch stratification for strongly-coupled and/or non-Lagrangian theories is beyond classical analysis. The characterisation of a leaf as a set of massless states remains, but does not necessarily enjoy a Lagrangian interpretation. The slices in turn are of non-classical nature, associated for example with the exceptional groups $E_{6,7,8}$, F_4, and G_2.

The magnetic quiver program (see [45, 51–55] and subsequent works) has opened a window to the systematic exploration of such Higgs branches. This includes the understanding of discrete and continuous actions on the moduli space as well as probing its structure. Based on progress involving 3d $\mathcal{N} = 4$ Coulomb branches (see [22, 32, 33, 39, 40, 75, 78, 82, 100, 122–124] and later works), the magnetic quiver toolbox has been expanded by several key techniques — among them: quiver subtraction [23, 93] and the decay and fission algorithm [24, 25]. Although both techniques produce the same stratification, they arise from entirely different principles.

The same ideas can be realised purely mathematically by viewing the Higgs branch from the algebro-geometric perspective. The coordinate ring of $\mathcal{H}$ has several Poisson ideals, partially ordered by inclusion, which correspond to singular loci in the geometry [125]. From the point of view of representation theory, each point on $\mathcal{H}$ gives an equivalence class of representations of the quiver algebra. These representations are preserved by some symmetry group, thus partially ordered by inclusion relations of the groups.

Based on intuition from brane systems, quiver subtraction postulates subtraction rules that allow for the derivation of the Coulomb branch Hasse diagram of the magnetic quiver.[1] It has been understood only recently that the Coulomb branch stratification can be derived without relying on subtraction rules — this is the essence of the decay and fission algorithm, which is the natural setting for the Higgs mechanism along the Coulomb branch.

However, a basic question remains: how does one derive the Higgs branch stratification directly from the (electric) theory? For concreteness, focus on unitary 3d $\mathcal{N} = 4$ quiver gauge

[1] This is, of course, equivalent to the Higgs branch Hasse diagram of the electric theory in the magnetic quiver context.

theories[2] — this is precisely the setting where the Coulomb branch techniques are the most developed. For such quivers a variety of results exist in the literature. In mathematics, these Higgs branches are known as Nakajima quiver varieties [126, 127] and their stratification data has been partially established in [128, 129]. Specifically, the latter computes the quivers after the partial Higgs mechanism along the Higgs branch. In other words, this algorithm establishes the stratification, but does not provide the geometric information on the minimal degeneration (the minimal Higgs mechanism).[3] In physics, minimal transitions along the Higgs branch have been studied in D5-D3-NS5 brane systems in [95, 131, 132] and sometimes go under the name Kraft-Procesi transitions.[4] Therein, hints appeared that one might be able to recast the Higgs branch transitions as subtractions according to a set of rules — such rules are the main results presented in this work. This is more than just a rewriting for a variety of reasons:

1. The Higgs branch subtraction algorithm offers the transition data at every step, allowing for a complete construction of the Higgs branch Hasse diagram and extending the algorithm of [128, 129] via physical reasoning.
2. The Higgs branch subtraction algorithm naturally displays the partial order of the Hasse diagram, which is otherwise not always transparent.
3. The global structure (monodromies, etc.) can be naturally extracted from the Higgs branch subtraction algorithm by utilising intuition from moduli spaces of instantons, symmetric products, and decorated magnetic quivers.

The algorithm introduced in this paper further illuminates the role in gauge theory of various concepts from the mathematics literature. For instance, monodromies [6, 135] in symplectic singularities are translated into *decorations* on the quivers appearing in the Higgs branch subtraction. Similarly, the so-called Namikawa-Weyl group [136, 137] is a discrete group acting on deformation/resolution parameters, such as FI-terms for the Higgs branch or masses for the Coulomb branch. The Higgs branch subtraction algorithm offers a simple way to extract the Namikawa-Weyl group.

The rules given in this paper lead to several new examples of theories whose Higgs and Coulomb branches arise as Słodowy intersections in the nilpotent cones (nilcones) of simple Lie algebras. Nilcones are among the most studied symplectic singularities in the mathematics literature – in some sense, their associated minimal nilpotent orbits act as units from which most other symplectic singularities encountered in physics can be constructed. Moreover, their Hasse diagrams, encoding precisely this singular stratification (alongside additional data such as the canonical quotient of Lusztig) are well known. Attempts to identify singular-symplectic properties of the moduli spaces of gauge theories with eight supercharges thus often begin with a variation on nilcone divination, and it is for this reason that examples of theories with Higgs/Coulomb branches as Słodowy intersections

[2] i.e. the gauge group factors are only of the type $\mathrm{U}(n_i)$ and the matter content is restricted to bifundamental and adjoint hypermultiplets. The former are called edges, while the latter are loops. Both of which may have multiplicity.

[3] This missing information on transition types is subject of an upcoming work [130].

[4] Similar types of Higgsing have appeared in other Type II brane systems [133, 134].

are so useful.

It is worth noting that the Nakajima quiver varieties studied in the mathematics literature are often constructed so as to avoid loops, which are known to introduce further complexities. From the physics perspective, loops on gauge nodes simply correspond to hypermultiplets in the adjoint representation of the gauge group, and as such the Higgs branch subtraction algorithm introduced in this work is equally as effective when applied to quivers with loops as to those without.

The remainder is organised as follows: in Section 4.2 the rules for Higgs branch subtraction are introduced; these determine the local structure. The global structure of the Higgs branch is then subject of Section 4.3. For the convenience of the reader, Section 6.4 provides a summary of the rules for the Higgs branch subtraction algorithm. Equipped with all relevant techniques, several examples are discussed in Section 4.4 and serve as non-trivial consistency checks of the rules proposed here. Lastly, a summary and outlook is provided in Section 4.5. The main body is supplemented by a number of appendices that cover background material.

4.2 Incomplete Local Rules for Higgs Branch Quiver Subtraction

This section presents a set of *local* rules delineating all possible quiver subtractions on the Higgs branch of the 3d $\mathcal{N}=4$ gauge theories considered here, along with justifications via explicit calculations using the classical Higgs mechanism. The subtraction slices themselves are the Higgs branches of minimal degenerate transverse theories; by sequential application of the relevant rules, the full local information of all minimal degenerate slices in the Higgs branch Hasse diagram can be specified. It is important to note here the distinction between the *local* and *global* structure of the Higgs branch, with the latter given a more exhaustive treatment in Section 4.3; *global* structure is sensitive to monodromies, which generically change the subtraction slice via the action of a discrete group. The local rules presented in this section are for this reason incomplete, and are included only as part of the derivation of the full global rules of Section 4.3. A proof of completeness of the local rules is offered in the work of Gwyn Bellamy and Travis Schedler [130].

All 3d $\mathcal{N}=4$ quiver gauge theories considered in this work are unframed simply-laced quivers with gauge group $G=\prod_i \mathrm{U}(n_i)/\mathrm{U}(1)$; where each node in the quiver contributes a 3d $\mathcal{N}=4$ $\mathrm{U}(n_i)$ vector multiplet. A simply-laced quiver is one in which all 3d $\mathcal{N}=4$ hypermultiplets (i.e. the quiver's edges) are in either the bi-fundamental or adjoint representation of the gauge group(s). Two gauge nodes connected by k edges are said to be connected by an edge of multiplicity k. Graphically, each node takes the form as shown in Figure 4.1a.

Without loss of generality, framed quivers can be treated as unframed quivers by absorption of all flavour nodes in a single $\mathrm{U}(1)$ gauge node, as in Figure 4.1b. This is called the

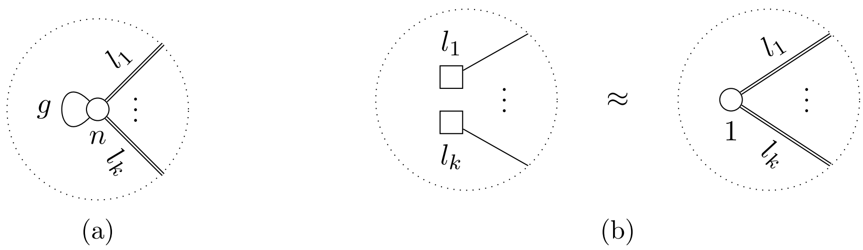

Figure 4.1: a: A $\mathrm{U}(n)$ gauge node with g loops (g hypermultiplets in the adjoint representation of $\mathrm{U}(n)$). This gauge node is in general connected to k other gauge nodes with simply laced edges of multiplicity $l_1, \cdots, l_k$, respectively. b: The "equivalence" between framed and unframed quivers. The difference is a $T^*\mathbb{C}^\times$ factor on the Coulomb branch, which is invisible to the Hasse diagram as it is non-singular. The Higgs branch is unchanged.

"Crawley-Boevey move" in the mathematics literature [128], and results in the Coulomb branch picking up a non-singular factor of $T^*\mathbb{C}^\times$ while leaving the Higgs branch unchanged.

4.2.1 Local Rules for Minimal Higgsing

Along the Higgs branch, the Higgs mechanism breaks the gauge group of the theory to a subgroup by giving non-zero VEVs to a gauge-invariant combination of the hypermultiplet scalars [118–121]. All vector multiplets not in the adjoint representation of the unbroken residual gauge group become massive, absorbing hypermultiplet scalars in the same representation. In this paper all allowed unbroken subgroups are continuous. In general, the Higgsing pattern for a given theory can be quite complicated and so it is convenient to organise this into a Hasse diagram. The vertices of the Hasse diagram are labelled by the residual (massless) theories after Higgsing and the edges are labelled by the minimal transitions between the theories.

Suppose the original gauge group is G, the unbroken subgroup is H, and the (reduced) normaliser is $T = N_G(H)/H$. Then the transverse slice is the Higgs branch (up to normalisation) of the transverse theory with gauge group T and hypermultiplets charged trivially under H and non-trivially under T.

There are three types of local minimal transition, which are encoded in the following rules:

Local Rule 1: Adjoint Higgsing

The local Rule 1, which is a consequence of the adjoint Higgs mechanism, applies to a $\mathrm{U}(n)$ gauge node with g adjoint loops. As shown in Figure 4.2a, the $\mathrm{U}(n)$ node splits into a $\mathrm{U}(n-m)$ and a $\mathrm{U}(m)$ node (with integer m such that $1 \leq m \leq \frac{n}{2}$), each with g adjoint loops and connected via $2g-2$ bi-fundamental hypermultiplets. For $n = 2m$ the reduced normaliser is $T = S_2 \subset S_n$, where S_n is the Weyl group of $\mathrm{U}(n)$. Hence the transverse theory is an S_2 gauge theory with g hypermultiplets in the sign representation of S_2. The Higgs branch of this transverse theory is $c_g \cong \mathbb{C}^{2g}/\mathbb{Z}_2$, which is the slice associated to the transition. For $n \neq m$, although the reduced normaliser is trivial the corresponding transverse gauge theory is not — the slice is actually the non-normal variety m_g, with normalisation $\mathbb{C}^{2g}$. More details on the non-normal variety m_g are provided below and in Appendix 6.6.

Note that repeated application of this rule to the node of rank n in Figure 4.2a recovers the complete graph quiver $\mathcal{CG}_{n,2g-2}$ [1] describing n gauge nodes of U(1) each with g adjoint loops on each node and $2g-2$ edges between each pair.

The following describes a computation of this rule via the Higgs mechanism. The gauge group breaks as

$$\mathrm{U}(n) \to \mathrm{U}(n-m) \times \mathrm{U}(m). \tag{4.1}$$

After breaking, all vector multiplets not in the adjoint representation of the unbroken residual group become massive, by absorbing hypermultiplets in the same representation. The adjoint representation decomposes as:

$$\mathsf{Adj}_{\mathrm{U}(n)} \to \mathsf{Adj}_{\mathrm{U}(n-m)} + \mathsf{Adj}_{\mathrm{U}(m)} + \mathsf{F}_{\mathrm{U}(n-m)} \times \bar{\mathsf{F}}_{\mathrm{U}(m)} + \bar{\mathsf{F}}_{\mathrm{U}(n-m)} \times \mathsf{F}_{\mathrm{U}(m)}. \tag{4.2}$$

This Higgsing pattern is incomplete, i.e. the moment map (in the adjoint representation of $\mathrm{U}(n)$) has a trivial trace contribution. Each adjoint of $\mathrm{U}(n)$ thus contributes a free sector $\mathbb{C}^2$, which is the trace of the $\mathrm{U}(n)$ adjoint matrix together with its conjugate. After branching into $\mathrm{U}(n-m)\times\mathrm{U}(m)$ the free sector becomes $\mathbb{C}^2\times\mathbb{C}^2$ as the trace and conjugate of the $\mathrm{U}(n-m)$ and $\mathrm{U}(m)$ adjoint matrices. The free sectors are removed by requiring the traces to be zero. This is equivalent to using $\mathrm{U}(n) \simeq \mathrm{SU}(n) \times \mathrm{U}(1)$. Hence, the transverse theory has a $2g$-dimensional Higgs branch, which is the difference between the singular sectors before and after breaking.

Transverse Slice c_g/m_g. Now consider the chiral ring of the slice. Note that the singlets live in the Cartan subalgebra and its conjugate, and hence the action of the gauge group $\mathrm{U}(n)$ can be reduced to the action of the Weyl group S_n, which permutes the diagonal elements. The singlets are invariant under the residual group $\mathrm{U}(m) \times \mathrm{U}(n-m)$, which is reduced to $S_m \times S_{n-m}$. The invariant $2g$ complex-dimensional sub vector space spanned by the singlets can be written as $V = \prod_i^g V_i$, where each V_i is a 2 complex-dimensional subspace parameterised by the coordinates (x_i, y_i) and takes the form (tracelessness is required to remove the free sector):

$$V_i = (\underbrace{mx_i, my_i, \cdots, mx_i, my_i}_{n-m}, \underbrace{-(n-m)x_i, -(n-m)y_i, \cdots, -(n-m)x_i, -(n-m)y_i}_{m}). \tag{4.3}$$

The invariant ring of V under the action of S_n gives exactly the ring of the non-normal slice m_g for $m \neq n-m$ and the c_g singularity for $m = n-m$:

$$V/S_n = \begin{cases} m_g & \text{when } m \neq n-m\,, \\ c_g & \text{when } m = n-m\,. \end{cases} \tag{4.4}$$

Note that for $m = n - m$, the action of S_n is reduced to the action of the normaliser $T = S_2$.

Local Rule 2: Bi-fundamental Higgsing

Rule 2, which is a consequence of the bi-fundamental Higgs mechanism, applies when two nodes $\mathrm{U}(n_1)$ and $\mathrm{U}(n_2)$ are connected by $g+1$ edges. Here the edge parametrisation is such that after the transition g loops remain, as shown in Figure 4.2b. The transition involves adding an additional $\mathrm{U}(m)$ node for any integer m in the range $1 \leq m \leq \min(n_1, n_2)$. The ranks of the $\mathrm{U}(n_1)$ and $\mathrm{U}(n_2)$ gauge nodes are reduced by m each with g–1 hypermultiplets connecting them to the $\mathrm{U}(m)$ gauge node. The requirement that the multiplicities are non-negative implies that $g \geq 1$ for a transition to happen. The transverse slice is the a_g singularity.

To demonstrate this, the Higgsing pattern is considered. The gauge group breaks as:

$$\mathrm{U}(n_1) \times \mathrm{U}(n_2) \to \mathrm{U}(n_1 - m) \times \mathrm{U}(n_2 - m) \times \mathrm{U}(m) \tag{4.5}$$

and the relevant representations decompose as follows:

$$\mathsf{Adj}_{\mathrm{U}(n_i)} \to \mathsf{Adj}_{\mathrm{U}(n_i-m)} + \mathsf{Adj}_{\mathrm{U}(m)} + \mathsf{F}_{\mathrm{U}(n_i-m)} \times \bar{\mathsf{F}}_{\mathrm{U}(m)} + \bar{\mathsf{F}}_{\mathrm{U}(n_i-m)} \times \mathsf{F}_{\mathrm{U}(m)}\,, \tag{4.6}$$

$$\mathsf{F}_{\mathrm{U}(n_1)} \times \bar{\mathsf{F}}_{\mathrm{U}(n_2)} \to \mathsf{F}_{\mathrm{U}(n_1-m)} \times \bar{\mathsf{F}}_{\mathrm{U}(n_2-m)} + \mathsf{F}_{\mathrm{U}(n_1-m)} \times \bar{\mathsf{F}}_{\mathrm{U}(m)} + \bar{\mathsf{F}}_{\mathrm{U}(n_2-m)} \times \mathsf{F}_{\mathrm{U}(m)} + \mathsf{Adj}_{\mathrm{U}(m)}\,. \tag{4.7}$$

The part of hypermultiplets getting vevs is $2(\mathsf{F}_{\mathrm{U}(n_1-m)} \times \bar{\mathsf{F}}_{\mathrm{U}(m)} + \bar{\mathsf{F}}_{\mathrm{U}(n_2-m)} \times \mathsf{F}_{\mathrm{U}(m)})$ and $2\mathsf{Adj}_{\mathrm{U}(m)}$.

Transverse Slice a_g. The transverse slice is determined as follows. For the same reason as in Section 4.2.1, each adjoint of the residual $\mathrm{U}(m)$ contributes a trace part as a singlet which enters the transverse theory as matter content. $g+1$ copies of bi-fundamental hypermultiplets between $\mathrm{U}(n_1)$ and $\mathrm{U}(n_2)$ provides $g+1$ such singlets. The normaliser is $T = \mathrm{U}(1)$. The trace part has charge 1 under T. Hence, the transverse theory is SQED with $g+1$ flavours, whose Higgs branch is a_g.

Local Rule 2 with Adjoint Loops. There exists a subtlety in the application of Rule 2 to subquivers with adjoint loops. If the node with higher rank has adjoint loops (e.g. take $n_1 > n_2$ in Figure 4.3 with the requirement $k_1 \neq 0$, $k_2 = 0$) then Rule 2 is *not* a minimal transition, and Rule 1 is. If the node with lower (or equal) rank has adjoint loops (e.g. take $n_1 > n_2$ in Figure 4.3 with $k_1 = 0$, $k_2 \neq 0$), then Rule 2 is minimal *only* with precisely $m = \min(n_1, n_2)$, instead of any $1 \leq m \leq \min(n_1, n_2)$, i.e, only a subtraction of the maximum number of subquivers is minimal. The number of adjoint loops on the $\mathrm{U}(m)$ nodes are also inherited by the new $\mathrm{U}(m)$ node after contracting — this is the non-Abelian analog of bullet point 2 below. See Figure 4.7 for an example. Otherwise, if $m < \min(n_1, n_2)$, the transition can be treated as a combination of Rule 1 and Rule 2, which is not a minimal transition. For this non-minimal transition, an example is shown in Figure 4.9a.

Local Rule 3: *ADE* Higgsing

Rule 3 applies when there is an affine ADE-shaped sub-quiver with each node's rank no less than n times the dual Coxeter label of the affine ADE Dynkin diagram, i.e, it contains n copies of Q_{ADE}.[5] The transition is shown in Figure 4.2c.

This rule can be derived from the Higgs mechanism as follows. Given a quiver $\mathcal{Q}$, suppose that it contains a sub-quiver of the form of some rank k ADE finite quiver. Let the gauge group coming from this sub-quiver be a gauge subgroup $G = \mathrm{U}(n_0) \times \cdots \times \mathrm{U}(n_k)$ with $n \leq \min(n_0/h_0^\vee, \cdots, n_k/h_k^\vee) < n+1$, where $h_i^\vee$ are the dual Coxeter labels for the rank k ADE group.[6] The aim is to Higgs $1 \leq m \leq n$ copies of this ADE sub-quiver in the sense of Figure 4.2c. If the subquiver to be subtracted has ranks $h_i^\vee$ at the i-th node, then the gauge groups breaks as

$$\mathrm{U}(n_0) \times \cdots \times \mathrm{U}(n_k) \to \mathrm{U}\left(n_0 - m h_1^\vee\right) \times \cdots \times \mathrm{U}\left(n_k - m h_k^\vee\right) \times \mathrm{U}(m) \tag{4.8}$$

and the adjoint representations decompose as follows:

$$\begin{aligned} \mathsf{Adj}_{\mathrm{U}(n_i)} \to\ & \mathsf{Adj}_{\mathrm{U}\left(n_i - m h_i^\vee\right)} + (h_i^\vee)^2 \cdot \mathsf{Adj}_{\mathrm{U}(m)} \\ & + h_i^\vee \left(\mathsf{F}_{\mathrm{U}\left(n_i - m h_i^\vee\right)} \times \overline{\mathsf{F}}_{\mathrm{U}(m)} + \mathsf{F}_{\mathrm{U}(m)} \times \overline{\mathsf{F}}_{\mathrm{U}\left(n_i - m h_i^\vee\right)} \right) \end{aligned} \tag{4.9}$$

and the bifundamental hypermultiplets (whenever there exits one between node i and j) decomposes

$$\begin{aligned} \mathsf{F}_{\mathrm{U}(n_i)} \times \overline{\mathsf{F}}_{\mathrm{U}(n_j)} \to\ & \mathsf{F}_{\mathrm{U}(n_i - m h_i^\vee)} \times \overline{\mathsf{F}}_{\mathrm{U}(n_j - m h_j^\vee)} + h_i^\vee h_j^\vee \cdot \mathsf{Adj}_{\mathrm{U}(m)} \\ & + h_j^\vee \cdot \mathsf{F}_{\mathrm{U}\left(n_i - m h_i^\vee\right)} \times \overline{\mathsf{F}}_{\mathrm{U}(m)} + h_i^\vee \cdot \mathsf{F}_{\mathrm{U}(m)} \times \overline{\mathsf{F}}_{\mathrm{U}\left(n_j - m h_j^\vee\right)} . \end{aligned} \tag{4.10}$$

Let c_{ij} be the Cartan matrix for the affine Dynkin diagram. It has a zero eigenvector given by $h^\vee$ such that $\sum_{j=0}^k c_{ij} h_j^\vee = 0$. The conventions are such that the index $j = 0$ denotes the affine node for which $h_0^\vee = 1$. To verify the consistent Higgsing, count the multiplicities. To begin with, consider $\mathsf{Adj}_{\mathrm{U}(m)}$ for which one finds $\frac{1}{2}\sum_{i,j=0}^k h_i^\vee (2\delta_{ij} - c_{ij}) h_j^\vee - \sum_{i=0}^k (h_i^\vee)^2 = 0$ from the hypermultiplets minus vector multiplets. As the Higgsing pattern makes one $\mathsf{Adj}_{\mathrm{U}(m)}$ survive, one vector multiplet and one adjoint hypermultiplet are present. Next, consider the bifundamental $\mathsf{F}_{\mathrm{U}\left(n_i - m h_i^\vee\right)} \times \overline{\mathsf{F}}_{\mathrm{U}(m)}$ for which the multiplicity reads $\frac{1}{2}\sum_{j=0}^k (2\delta_{ij} - c_{ij}) h_j^\vee - h_i^\vee = 0$; again from hypermultiplets minus vector multiplets. In conclusion, the Higgsing reduces the quiver precisely to the one shown in Figure 4.2c.

[5] Here the label Q_{ADE} is used to denote a minimal balanced affine ADE quiver. The ADE affine Dynkin quivers with their dual Coxeter labels are shown in Table 4.1.

[6] In other words, the maximal balanced rank k affine ADE quiver contained in $\mathcal{Q}$ has n times the rank of the minimal balanced Q_{ADE}.

Transverse Slice ADE. All of the singlets that are not charged under $H = \mathrm{U}\left(n_0 - mh_0^\vee\right)\times \cdots \times \mathrm{U}\left(n_k - mh_k^\vee\right) \times \mathrm{U}(m)/\mathrm{U}(1)$ form the quiver data of Q_{ADE}. The vector multiplet decomposition (4.9) yields $\sum_{j=0}^{k}(h_j^\vee)^2 - 1$ singlets (after taking away the vectormultiplets of the residual theory), which is precisely the dimension of the $T = \prod_{i=0}^{k}\mathrm{U}(h_i^\vee)/\mathrm{U}(1)$ vector multiplets. Analogously, the hypermultiplet decomposition (4.10) yields $\frac{1}{2}h_i^\vee(2\delta_{ij} - c_{ij})h_j^\vee$, which is in the form of the matter content of the Q_{ADE} quiver. Hence, the transverse theory is the Q_{ADE} quiver, whose Higgs branch is the ADE singularity.

Local Rule 3 with Adjoint Loops. Similar to the case of local Rule 2, local Rule 3 presents a subtlety when applied to affine ADE Dynkin subquivers with adjoint loops. If there are adjoint loops on the node(s) of the affine ADE Dynkin subquiver that have dual Coxeter number larger than 1, then Rule 3 does *not* give rise to minimal transition. In this case, Rule 1 must be applied first.

If there are adjoint loops on the node(s) of the subquiver that have dual Coxeter number 1, and all such node(s) have rank exactly n, then Rule 3 is minimal only for $m = n$. This means that only $m = n$ copies of the Q_{ADE} subquiver can be subtracted, instead of any $1 \leq m \leq n$. The slice is of course the corresponding ADE singularity. The number of adjoint loops on the $\mathrm{U}(m)$ nodes are also inherited by the new $\mathrm{U}(m)$ node after contracting — this is the non-Abelian analog of Remark 2 below. See Figure 4.8 for an example. Otherwise, if $m < n$, the transition can be treated as a combination of Rule 1 and Rule 3, which is not a minimal transition. For this non-minimal transition, an example is shown in Figure 4.9b.

Remarks

A few comments are in order.

1. **Branching of External Edges.** The three rules above omit the discussion of the decomposition of the external edges connecting from the background to the subquiver. A simple principle to keep in mind is that all those edges are inherited by the new node after contracting, which is equivalent to the requirement of re-balancing.

2. **Number of Loops.** The adjoint loops on the $\mathrm{U}(1)$ nodes are also inherited by the new node after contracting. These loops contribute to the free sector. At each leaf, the local geometry can be written as: $\mathcal{M}_{\text{Sing.}} \times \mathbb{H}^l$, where l is the number of $\mathrm{U}(1)$ adjoint loops. The dimension of the singular and free sectors must sum to the Higgs branch dimension, i.e, $\dim_{\mathbb{H}}\mathcal{M}_{\text{Sing.}} + l = \dim_{\mathbb{H}}\mathcal{H}$.

3. **Degeneracy of Rules.** When $g = 1$, Rule 1 can be treated as the A_0 limit of Rule 3 and Rule 2 can be treated as the A_1 limit of Rule 3.

4. **Bad Theories and Incomplete Higgsing** The algorithm presented in this paper is equally effective at determining the singular structure of the Higgs branch of a theory regardless of whether it is *good*, *bad*, or *ugly* in the sense of [22]. In any case, repeated application of the algorithm reaches a quiver that cannot be operated on

Label	Affine Dynkin Diagrams	HS
A_n	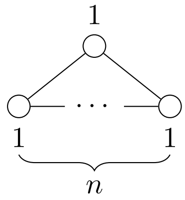	$\frac{1-t^{2n+2}}{(1-t^2)(1-t^{n+1})^2}$
D_n $n \geq 4$	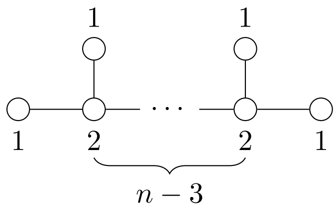	$\frac{1-t^{4n-4}}{(1-t^4)(1-t^{2n-4})(1-t^{2n-2})}$
E_6	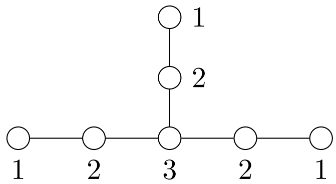	$\frac{1-t^{24}}{(1-t^6)(1-t^8)(1-t^{12})}$
E_7	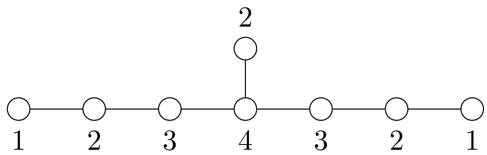	$\frac{1-t^{36}}{(1-t^8)(1-t^{12})(1-t^{18})}$
E_8	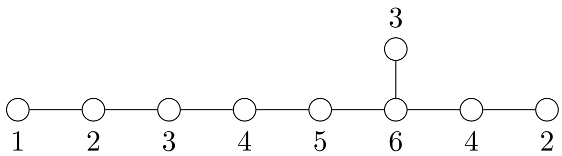	$\frac{1-t^{60}}{(1-t^{12})(1-t^{20})(1-t^{30})}$

Table 4.1: Affine Dynkin diagrams with dual Coxeter labels $h_i^\vee$. Note that $h_0^\vee = 1$ for the affine node. Subtraction of these quivers gives ADE surface singularities listed in the first column, alongside their Higgs branch Hilbert series in the third.

by the three above rules. This quiver is hence a top leaf on the Higgs branch, which is a non-singular phase.

Incomplete Higgsing corresponds to the case where the final quiver at the top leaf is *bad*. Note that for an unframed quiver this condition should be relaxed to the following: if the final quiver of the top leaf is still bad after ungauging a U(1), then there is incomplete Higgsing.

It is a simple exercise to construct a family of quivers with the same Higgs branch by adding a quiver with trivial Higgs branch on top of an original quiver. The Coulomb branches of the theories in this family also have the same singular structure, but differ in the smooth factor [138].

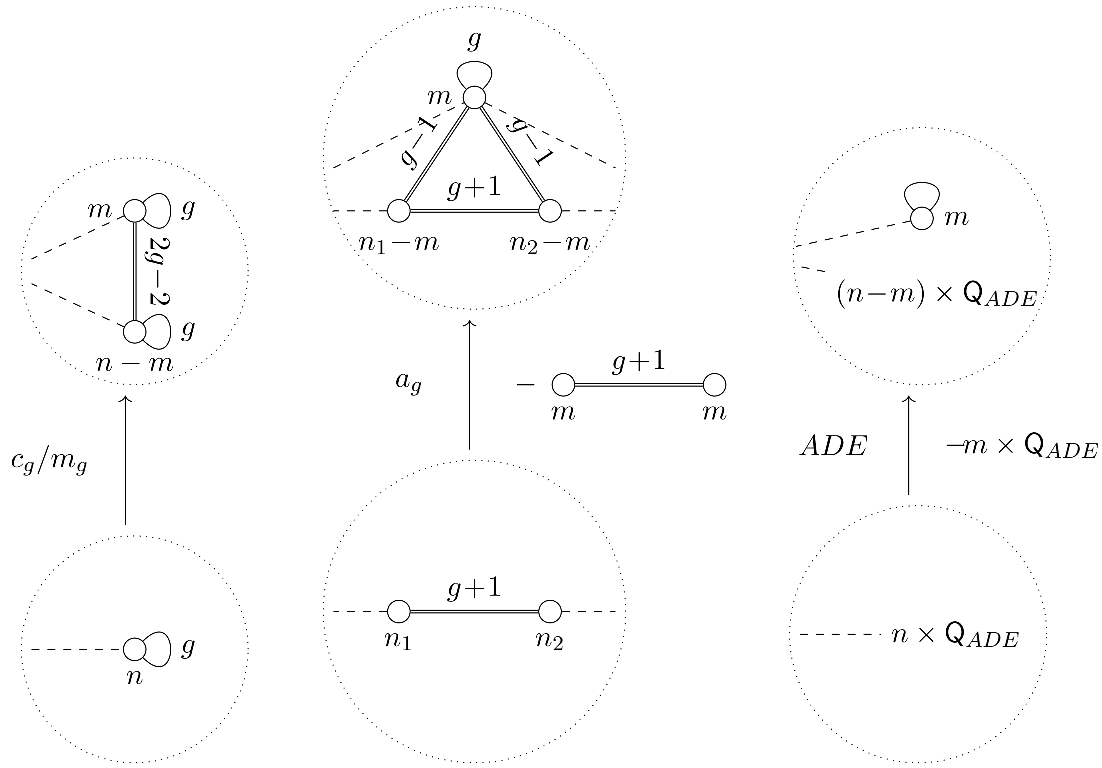

(a) Rule 1 (b) Rule 2 (c) Rule 3

Figure 4.2: a: Rule 1 — The U(n) node with g loops splits into two nodes of U(m) and U($n-m$) with g loops. Between them, there are $2g-2$ edges connecting the two nodes. The transverse slice is $c_g \cong \mathbb{C}^{2g}/\mathbb{Z}_2$ if $m = n-m$, and is m_g (whose normalisation is $\mathbb{C}^{2g}$) if $m \neq n-m$. The dashed lines denote the possible edges connecting to the rest of the quiver. b: Rule 2 — U(n_1) and U(n_2) nodes connected by $g+1$ edges splits into U(n_1-m), U(n_2-m), and U(m) gauge nodes. The U(n_1-m) and U(n_2-m) gauge nodes have $g+1$ edges between them and $g-1$ edges extending to the U(m) node, which has g loops on it. This transition can be visualised as a subtraction of a quiver of two U(m) nodes connected by $g+1$ edges contracting into a node of U(m) with g loops. The transverse slice is a_g. c: Rule 3 — It can be visualised as the subtraction of m copies of an Q_{ADE} sub-quiver, leaving a U(m) node with a loop. The transverse slice is the corresponding ADE Klein singularity. Note that the slice here denoted m_1 is more often in the quiver literature given the name m.

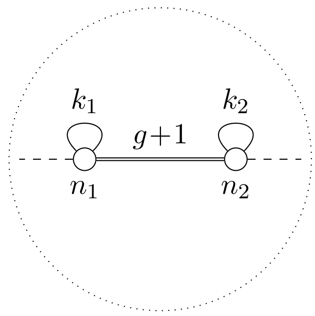

Figure 4.3: For this quiver, either Rule 1 or 2 are minimal transitions depending on the values of $n_{1,2}$, $k_{1,2}$. For $n_1 > n_2$ and $k_1 \neq 0$, $k_2 = 0$, Rule 1 is minimal, while Rule 2 is not. For $n_1 > n_2$ and $k_1 = 0$, $k_2 \neq 0$, Rule 2 is minimal for $m = \min(n_1, n_2)$.

4.2.2 Examples of Local Subtraction

This section presents simple examples of the rules introduced above.

Disclaimer. The examples in this section are only applications of the (incomplete) local rules, and not the full global rules introduced in Section 4.3 (in other words, they do not contain decorations); they are simply presented as instances of the local rules above, without consideration for global phenomena such as monodromies. The slices in the examples here have been chosen such that they are not altered by monodromies, however those considered later on in this work do in some cases significantly differ from the naïve local viewpoint, as explained in Section 4.3.

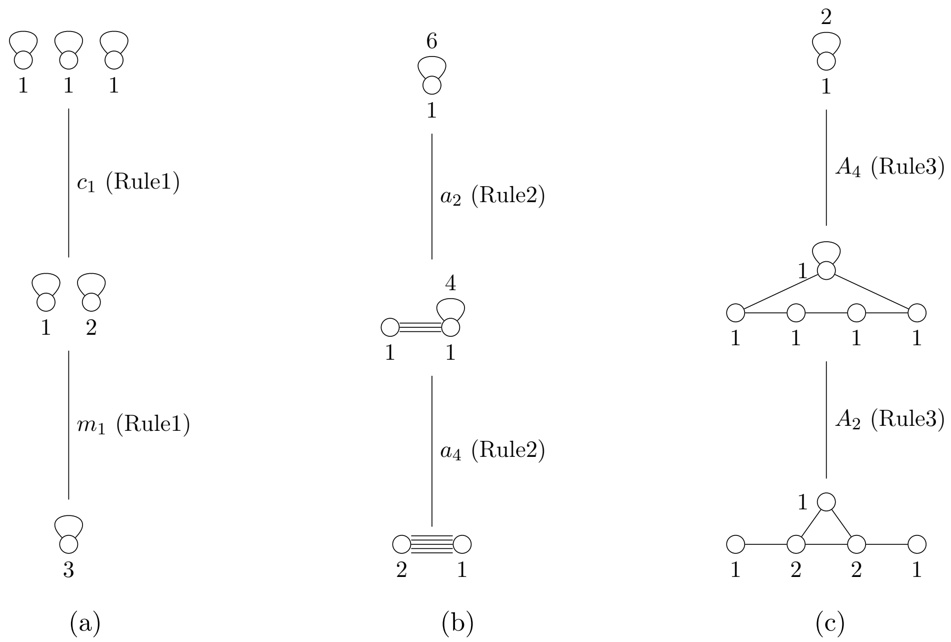

Figure 4.4: (a): Hasse diagram of U(3) with an adjoint loop, recovered by applying Rule 1 twice. (b): Hasse diagram of U(2) with 5 flavours (unframed), recovered by applying Rule 2 twice. (c): Hasse diagram of the (unframed) electric quiver for the Słodowy slice $\mathcal{S}^{A_4}_{(5),(3,1^2)}$ in the A_4 nilcone, recovered by applying Rule 3 twice. Note the addition of adjoint loops on U(1) nodes as explained in Paragraph 2.

In Figure 4.4 the examples each involve one rule only. The theory in Figure 4.4a is Higgsed to its Levi subgroup $\mathrm{U}(1)^3$, which is an incomplete Higgsing. The theories in Figure 4.4b and Figure 4.4c can be treated as complete Higgsing after factoring out the centre-of-mass U(1).

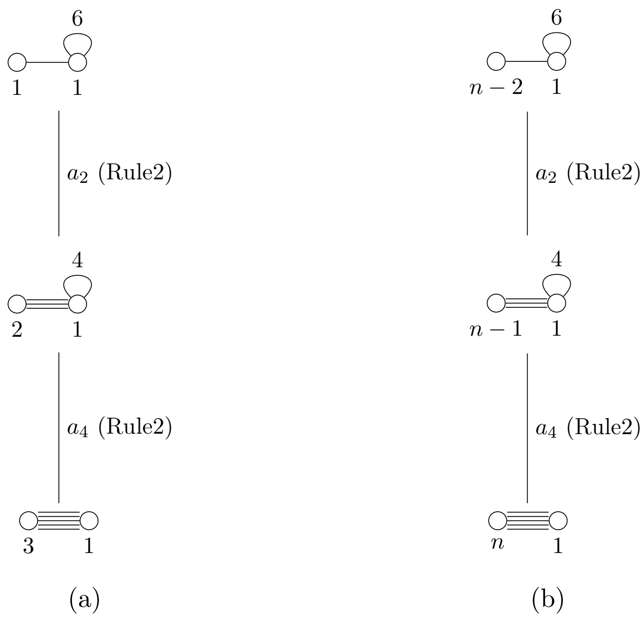

Figure 4.5: (a): Hasse diagram of U(3) with 5 flavours (unframed) showing incomplete Higgsing. (b): Hasse diagram of U(n) with 5 flavours (unframed), where $n > 3$ gives incomplete Higgsing.

Figure 4.5a and Figure 4.5b are extensions of Figure 4.4b — they have the same Higgs branch, shown from repeated application of Rule 2. Each leaf in Figure 4.5a is ugly, while each leaf in Figure 4.5b is bad for $n > 3$, implying incomplete Higgsing.

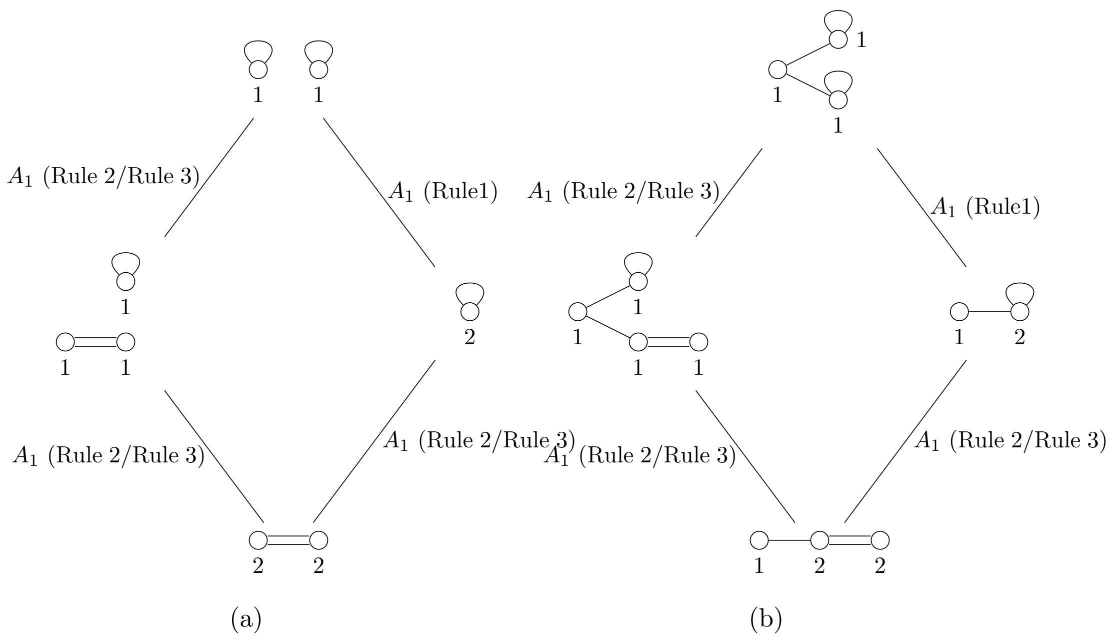

Figure 4.6: (a): The affine A_1 quiver with doubled node numbers. The Higgs branch is the 2$^{\text{nd}}$ symmetric product of the A_1 singularity. (b): This quiver is provided in [4, 5] as the 3d mirror of the ADHM quiver. Both quivers in (a) and (b) have the same Higgs branch and the same singular part of the Coulomb branch. Note that (a) has incomplete Higgsing, while (b) can be completely Higgsed.

Figure 4.6 gives two examples of quivers with the Higgs branch as the 2^{nd} symmetric product of the A_1 singularity, which is an orbifold of $\mathbb{C}^4$ by the dihedral group Dih_4 of order 8. Especially Figure 4.6a is the case that all the nodes are balanced but the theory has incomplete Higgsing.

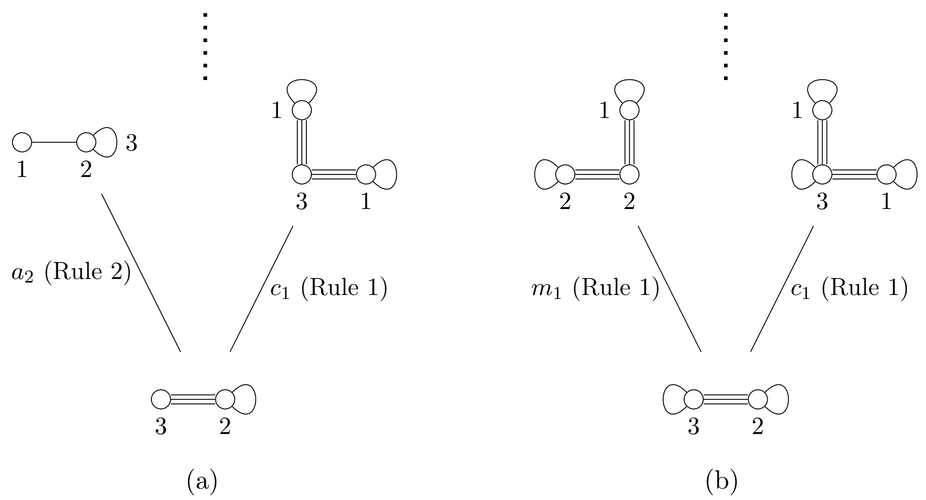

Figure 4.7: Examples of Rule 2 involving loops. In (a), the loop is on the node with lower rank - Rule 2 can be applied with $m = 2$. In (b), the loop on the higher rank node means that Rule 2 no longer gives a minimal transition.

Figure 4.7 gives examples of Rule 2 involving one loop. For brevity, only bottom slices are considered. In Figure 4.7a, Rule 2 can be applied only with $m = 2$, in contrast with Figure 4.7b, where the node with higher rank has an adjoint loop and so Rule 2 cannot be minimal transition before Rule 1 is applied.

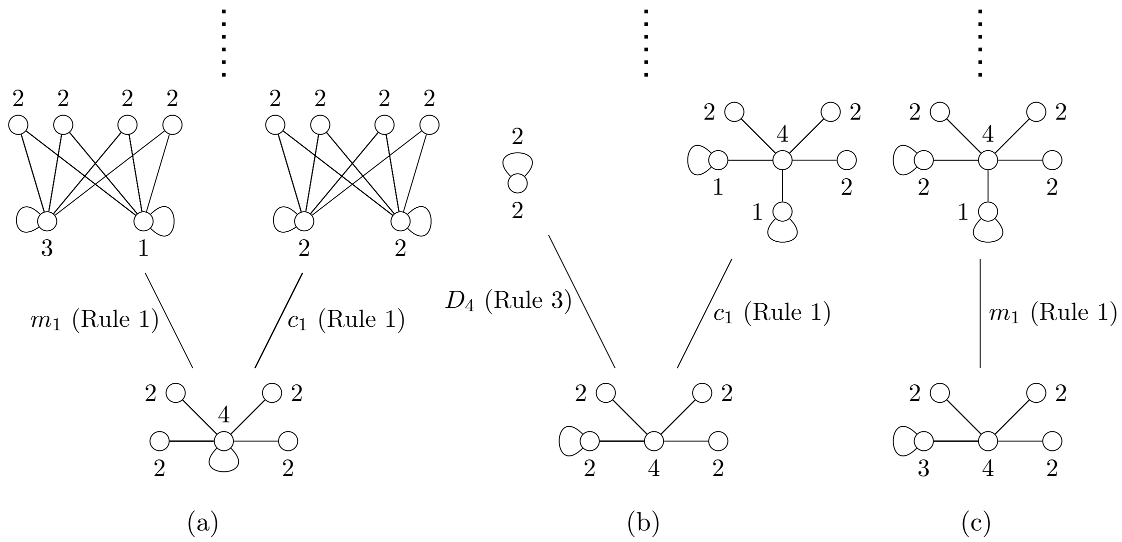

Figure 4.8: Examples of quivers containing at least the affine D_4 quiver with node numbers doubled, i.e, at least 2 copies of Q_{D_4}. An additional loop is added. Recall that for Q_{D_4}, the dual Coxeter labels are 2 for the middle node and 1 for each of the other nodes. In (a), the loop is on the node with label 2 and Rule 3 is not minimal transition. In (b), the loop is on one of the nodes with label 1, also the rank of the node is exactly 2 and Rule 3 can be applied by subtracting exactly 2 copies of Q_{D_4}. In (c), although the loop is on a node with dual Coxeter label 1 in the Q_{D_4} quiver, the node is of rank-3 which does not coincide with the number of copies (2) of Q_{D_4} present. Rule 3 is thus not a minimal transition.

In Figure 4.8, examples of Rule 3 involving a loop are shown. In Figure 4.8a and Figure 4.8c, Rule 3 is not a minimal transition. In Figure 4.8b, Rule 3 with $m = 2$ is a minimal transition.

Figure 4.9, shows why only the maximal number of subtractions is possible for minimal Higgsing; otherwise, it is equivalent to using Rule 1 to split the node and then using Rules 2 or 3 to do the subtraction (as shown in the left direction in the Hasse diagrams).

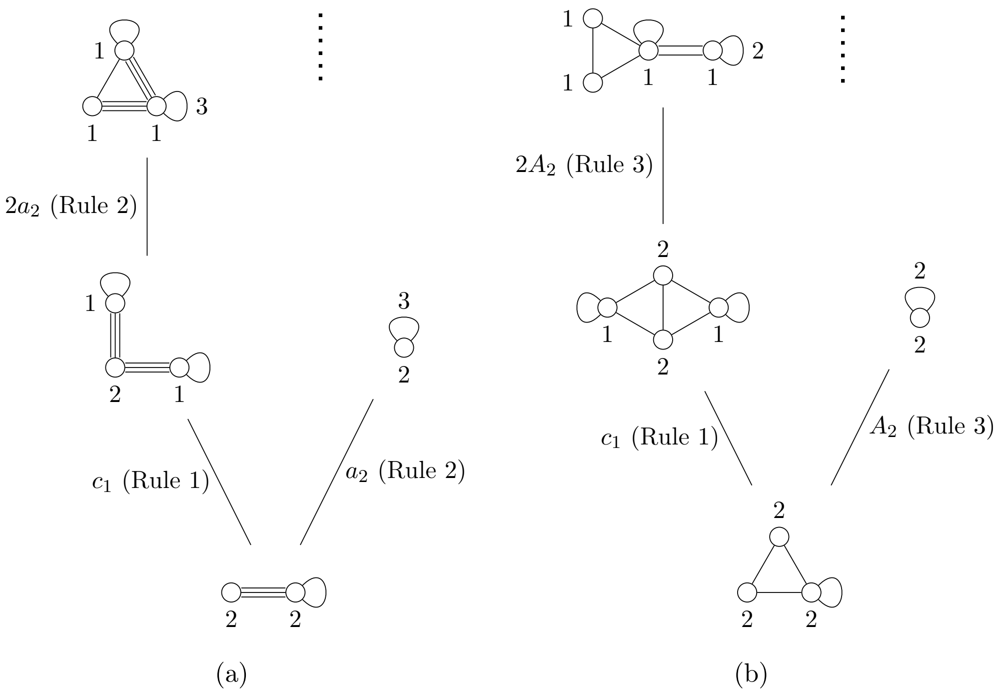

Figure 4.9: Examples of Rules 2 and 3 involving a loop. If Rules 2 and 3 are applied, only the maximum number of subtractions give rise to a minimal transition. Subtracting a non-maximal number of sub-diagrams is a non-minimal transition, and arises as the use of Rule 1 followed by Rules 2/3. The appearance of two unions of cones in the transition is explained in Section 4.3.2. In the figure, only the relevant part of the Hasse diagram is shown for brevity.

4.3 Full Global Rules and Decoration

In Section 4.2 a set of rules were introduced for computing the slices associated with subtracted theories on the Higgs branch locally. However, the stratification of a symplectic singularity in general admits non-trivial global structure which is not captured by this algorithm; the following section demonstrates that the global structure plays a crucial role in determining the Hasse diagram and promotes the local rules introduced in Section 4.2 to a full global argument.

Recall that a slice in a symplectic singularity is transverse to a local base leaf in some other higher dimensional leaf. In general, the local structure of a slice can be seen from any given point of the base leaf. If the global structure is trivial, moving around the base leaf does not change the appearance of the slice. However, non-trivial global structure means that moving on a closed path on the base leaf results in a non-trivial action, called a monodromy map, on the chiral ring of the slice [6, 139, 140].[7]
This global information can be recorded via a decoration in analogy to those used in top-down Coulomb branch quiver subtraction [8, 116].

[7]Moreover, the Weyl symmetry of the deformation parameters is also reduced under this action.

Decorated quivers were introduced to capture quotients of S_n outer-automorphisms on the Coulomb branch. In brane systems, Coulomb branch decoration corresponds to the indistinguishability of multiple branes or sub-brane systems. The Higgs branch decoration introduced here replaces the quotient that arises on the Coulomb branch with the action of a discrete symmetry on the Higgs branch. There is currently no brane-system interpretation of Higgs branch decoration.

4.3.1 Global Rules

As mentioned above, the local rules introduced in Section 4.2 are incomplete since they lack information relating to the global structure of the symplectic singularity. The introduction of decorations ameliorates this — giving the final form of the rules in Figure 4.11 — although they in general add further complexity to the subtraction process and mandate extra care when a single quiver (or even a single node) contains multiple decorations. The decoration rules introduced below are supported via non-trivial examples involving nilpotent cones as given in Section 4.4.

Higgs Branch Decoration Firstly, recall that the rules of Section 4.2 identify, for a given quiver $\mathcal{Q}$, several possible sub-quivers whose subtraction yields a transition on the Higgs branch. The most rigorous way in which to think about the decoration associated to this transition is the following.

1. Take all sub-quivers of $\mathcal{Q}$ that admit a subtraction and decorate them in the sense shown in Figure 4.10 (do not add another decoration to a sub-quiver if it is already decorated in its entirety[8]).

2. The application of the subtraction rules of Section 4.2 causes the decoration to be "inherited" by the subtraction products, as shown in Figure 4.11.

3. After a subtraction, the process of identifying new sub-quivers to be subtracted begins again, and new decorations need be applied.

Take as an example Rule 3, shown rightmost in Figure 4.11. If $m \geq 2$ one can apply Rule 1 (shown leftmost in Figure 4.11) to the node of rank m and split it into two nodes of rank m' and $m - m'$ for some $1 \leq m' < m$. In this case, *no new decoration should be applied*, since all nodes undergoing the transition (in this case just the single node of rank m) are already decorated by the decoration introduced in the initial subtraction. Similarly, further ADE subtractions to the same set of nodes as the initial subtraction also do not introduce a new decoration. A non-trivial example of this can be seen in Figure 4.37a, in which only one decoration has been used throughout.

This rather formal approach to decoration is in practice not the most intuitive, and it is common to think of subtraction products as 'picking up' a decoration in the process of

[8] That is to say, if the sub-quivers given in the bottom row of Figure 4.2 are decorated as in Figure 4.11, do not add any further decorations. (The decorations in the lower row of Figure 4.11 are in fact formally trivial, as shown in Figure 4.10.)

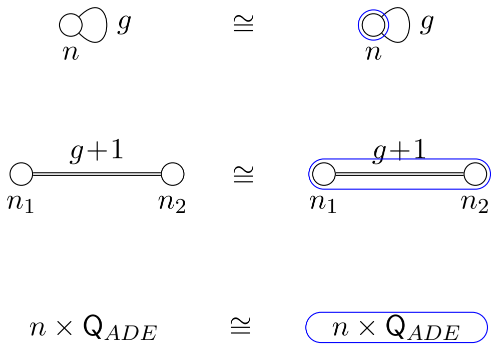

Figure 4.10: A (formally trivial) decoration is assigned to each sub-quiver that is not already entirely decorated.

subtraction instead of inheriting the decorations applied to sub-quivers beforehand. Indeed, the process of allocating decorations to subquivers before performing a subtraction does not modify the quiver as it introduces no global information, in other words, only the decorations in the upper row of Figure 4.11 are non-trivial[9]. Of course, it is easiest to understand the process of decoration via illustrations, and the reader is encouraged to consider the numerous Hasse diagrams in this paper for examples of the rules in action.

If a quiver $\mathcal{Q}$ contains different sub-quivers (each not already entirely decorated) then each sub-quiver picks up a new decoration in the process of subtraction. Such an example is given in Figure 4.12, which shows the formal process of first assigning decorations to each of the nodes of ranks n_1 and n_2 before performing both subtractions. Note that the transition in Figure 4.12 is not minimal.

Merging of Decoration. The next example of decoration consists of the case in which two decorations are applied to the same node, as shown in Figure 4.13. In this case, the two decorations can be said to 'merge', forming a new decorated node. Note that decoration merging is only applied in the situation in which it is a single node that holds two decorations. It is not uncommon to have quivers with overlapping decorations arising from ADE affine Dynkin subquivers that share nodes. In these cases, the two decorations are not inherited, leading to no merging, but instead the creation of a third decoration overlapping the other two. An example of such a case is provided in Figure 4.14, contrasting with the case in Figure 4.13 in which merging is allowed.

4.3.2 Monodromy Map and Union

The decoration determines the non-trivial global structure of the slice in one of the following two ways:

1. The slice is locally ADE or a_g and the corresponding quiver contains n identically decorated identical nodes. There is a monodromy map of (up to) S_n. The slices are

[9]This is somewhat similar to the redundancy of a decoration on a node of rank 1 in a bouquet of a single node in Coulomb-branch quiver subtraction

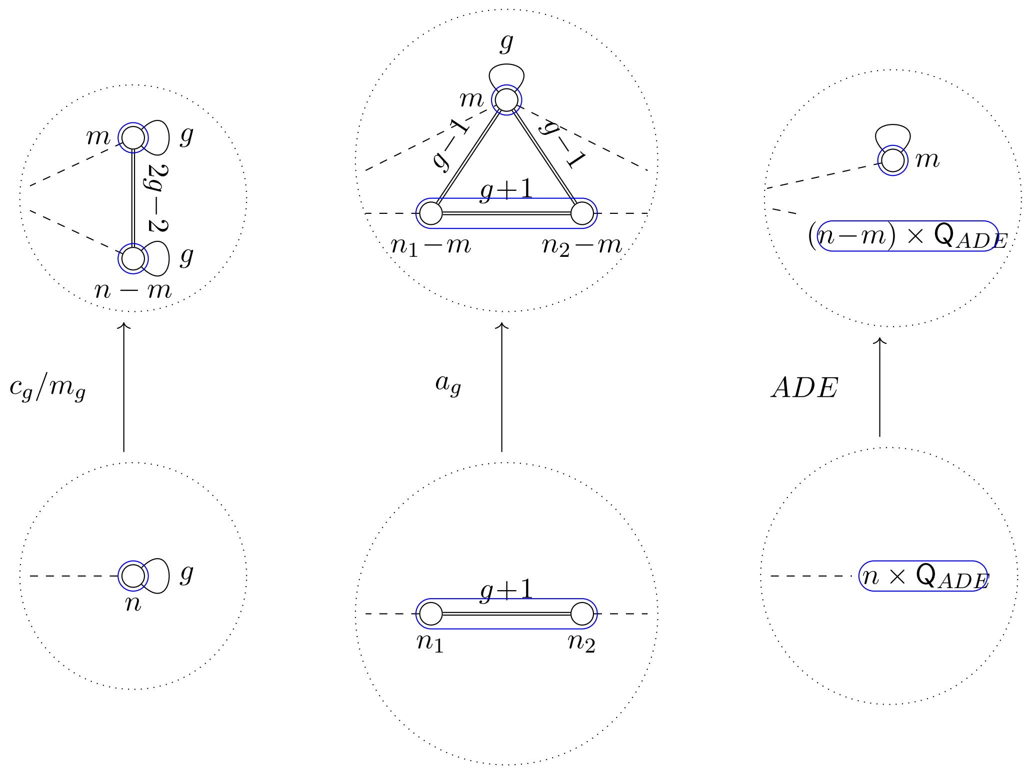

Figure 4.11: Decorations are inherited from the original theory before subtraction. The decorations in the bottom row are trivial, but become non-trivial in the rows above upon application of the subtraction rules.

shown in Table 4.2.

2. The slice is locally k copies of ADE or a_g and the corresponding quiver for each copy has the same decoration. The n-copies become a union that intersects at the singular point.

The two cases can take place simultaneously. For the first case, if the slice is of type ADE then the monodromy map is actually a subgroup of the automorphism of the corresponding Dynkin diagram [6], so it often happens that the actual monodromy map is smaller than the decoration indicates. Here there is a connection between the decoration and folding on the finite Dynkin diagram[10] as in Table 4.3.

The origin of the discrete symmetry is the action of Weyl group on the unbroken subgroup. There are in general different ways to embed the unbroken groups into the original group and these different embeddings are related by the action of Weyl group. For example, there are $n!$ different ways to embed $\mathrm{U}(1)^n$ into $\mathrm{U}(n)$: each $\mathrm{U}(1)\subset\mathrm{U}(1)^n$ is assigned to a certain $\mathrm{U}(1)$ in the Cartan subgroup of $\mathrm{U}(n)$. These embeddings are exchanged into each other under the action of $\mathcal{W}_{\mathrm{U}(n)}=S_n$. From the point of view of the stratification, going around a closed path on the base leaf corresponds to changing the embedding. This action also acts on the deformation space, as is discussed in the following subsection.

[10]The relation between quiver folding and Coulomb branch geometry was studied in [97].

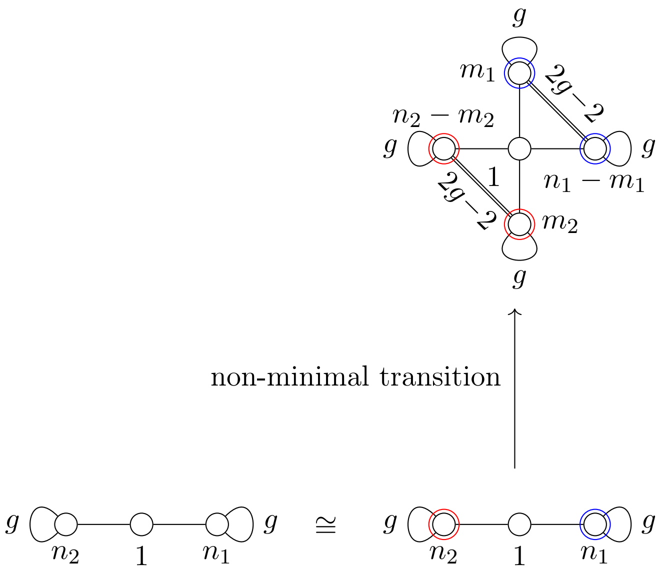

Figure 4.12: An example of a single quiver with different decorations on different subquivers (nodes). Note that the transition shown here is non-minimal (in other words, the transition is the result of several applications of the rules).

4.3.3 Namikawa Weyl Group

Despite its use in the theory of symplectic singularities, the Namikawa-Weyl group [136, 137], which arises as the reflection group acting on deformation parameters, has heretofore gone largely unmentioned in the physics literature. However, the Namikawa-Weyl group plays an important physical role in the moduli spaces of vacua of 3d $\mathcal{N} = 4$ gauge theories: on the Higgs branch it is the reflection group acting on FI parameters, while on the Coulomb branch it is the reflection group acting on mass parameters. In other words, the Namikawa-Weyl group acts to exchange different chambers of deformation parameters associated to a generic symplectic singularity; under symplectic duality [69], the Namikawa-Weyl group of one branch is exchanged with the Weyl group of the global symmetry of the other. This translates to a D3-/D5-/NS5-brane system as follows. The Weyl group of the heavy D5-branes is the Weyl group of the Higgs branch global symmetry, which under symplectic duality corresponds to the Namikawa-Weyl group of mass parameters on the Coulomb branch. Conversely, the Weyl group of the NS5-branes corresponds to the Namikawa-Weyl group of FI parameters on the Higgs branch.

In the Hasse diagram, the Namikawa-Weyl group $\mathcal{W}^X$ (of the symplectic singularity X) appears as the Weyl group of the Lie group associated to the slices from the top of the diagram to the quaternionic codimension-1 subvarieties [141] [11]:

$$\mathcal{W}^X = \prod_i \mathcal{W}_i, \tag{4.11}$$

[11] Namikawa Weyl groups are not defined for non-normal varieties. However, the Higgs branch of a unitary quiver is always normal and the only (quaternionic) one-dimensional normal symplectic singularities are Kleinian singularities, so there is no ambiguity in this statement.

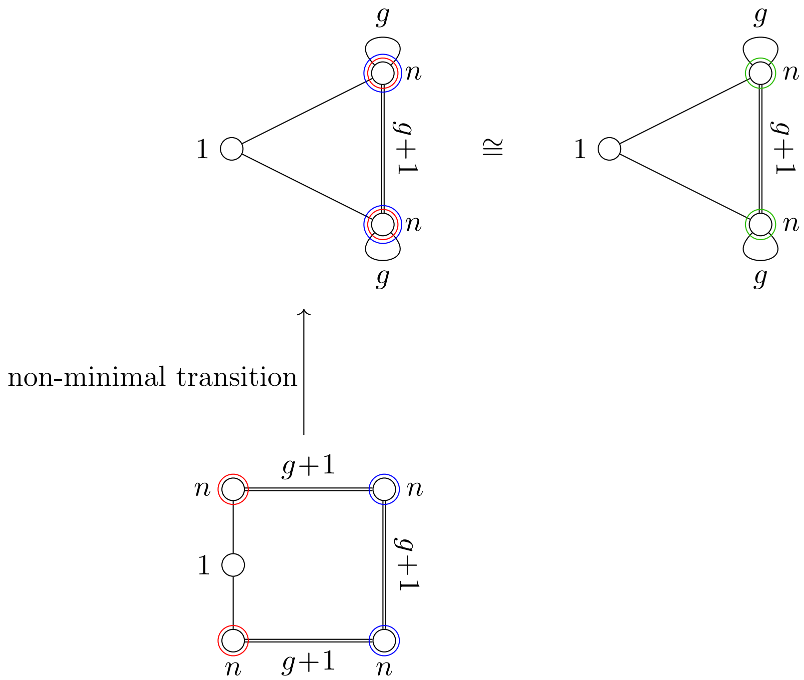

Figure 4.13: The procedure of decoration merging for individual nodes that are decorated twice. Such situations arise in the event that two individually-decorated nodes connected via $g+1$ links undergo an a_g transition.

where i runs over all quaternionic 1-dimensional top slices, and $\mathcal{W}_i$ is the Weyl group associated with the slice.

From the brane system picture, (4.11) is a simple consequence of the Kraft-Procesi transition. When there are more than one D5/NS5 branes with the same linking number in the same segment between two NS5/D5 branes, there is a valid transition to codimension-1 subvarieties. A natural Weyl symmetry acting on the D5/NS5 branes gives the Weyl symmetry of the deformation parameters. The direct product of all such Weyl symmetry gives the whole Weyl symmetry of the deformation parameters.

Using the above formula, it is simple to calculate the Namikawa-Weyl group for a given Higgs branch from its Hasse diagram. To find each $\mathcal{W}_i$, first take the decorated quiver whose Higgs branch corresponds to the given 1-dimensional slice — $\mathcal{W}_i$ is then the Weyl group of the Lie algebra given by the folded Dynkin diagram associated to the decorated quiver, according to the correspondence in Tables 4.2 and 4.3. For example, the A_n slice gives the Namikawa-Weyl group $\mathcal{W}_{A_n} = S_n$, and C_n slice gives the Namikawa-Weyl group $\mathcal{W}_{B_n}$. Given a Higgs branch Hasse diagram, the Coulomb branch global symmetry is determined up to an ambiguity between the $\mathfrak{b}$ and $\mathfrak{c}$ algebras. Thus it seems natural to conjecture that the algebra of the Coulomb branch global symmetry is precisely that of the Higgs branch's top slices. For simply-laced unitary quivers, the continuous Coulomb branch symmetry takes the form:

$$G_{\mathcal{C}} = \prod_i G_i, \tag{4.12}$$

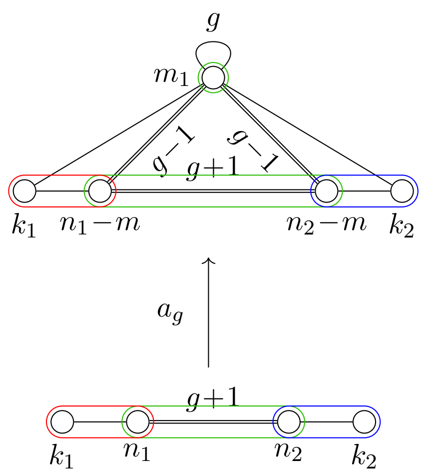

Figure 4.14: An example in which the blue and red decorations are not inherited.

where G_i is one of the U(1), SU(n), SO(n), G_2, E_6, E_7, E_8 determined by $\mathcal{Q}_i$. The absence of Sp(n) and F_4 is due to the fact that the corresponding folded quivers cannot be constructed by adding decorations to single nodes, but to legs of multiple nodes.

Label	Quivers
$C_n \cong D_{n+1}$ with S_2	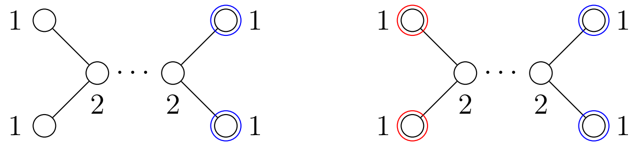
$C_2 \cong A_3$ with S_2	
$G_2 \cong D_4$ with S_3	
$B_n \cong A_{2n-1}$ with S_2	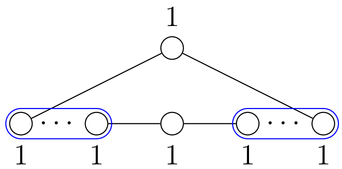
$F_4 \cong E_6$ with S_2	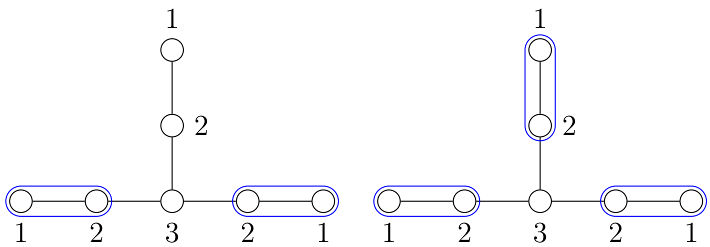
$a_g^+ \cong a_g$ with S_2	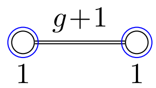

Table 4.2: The Higgs branches of the quivers on the right are labelled by the first column. In each case, the decorations give a monodromy on the corresponding slice. The third column shows that in some cases adding further decorations does not alter the Higgs branch monodromy. As the decorations on B_n and F_4 slices involve multiple nodes, they do not appear for a unitary quiver gauge theory. The last row shows the slice a_g^+ constructed as a Higgs branch.

G to G'	G Dynkin Diagram	G' Dynkin Diagram
D_{n+1} to B_n	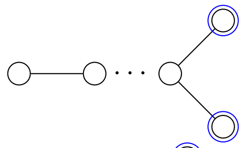	
D_4 to G_2	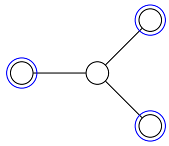	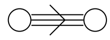
A_{2n-1} to C_n	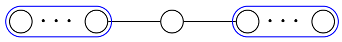	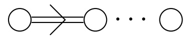
E_6 to F_4	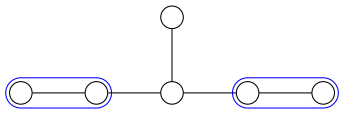	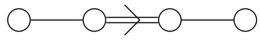

Table 4.3: Foldings of Lie algebras and their finite Dynkin diagrams. The automorphism subgroups for the folding are indicated from decoration.

$\mathfrak{g}$	Weyl group
U(1)	Trivial
SU(n)	S_n
SO($2n+1$)	$\mathbb{Z}_2^n \rtimes S_n$
Sp(n)	$\mathbb{Z}_2^n \rtimes S_n$
SO($2n$)	$\mathbb{Z}_2^{n-1} \rtimes S_n$

$\mathfrak{g}$	Weyl group
E_6	$\mathcal{W}_{E_6}$
E_7	$\mathcal{W}_{E_7}$
E_8	$\mathcal{W}_{E_8}$
F_4	$\mathcal{W}_{F_4}$
G_2	$\mathrm{Dih}_6 = \mathbb{Z}_6 \rtimes \mathbb{Z}_2$

Table 4.4: Table of Weyl groups for semi-simple Lie algebras: left side lists classical algebras, while right side contains exceptional algebras.

4.3.4 Global Structure in Practice

This section further studies the global structure of the Higgs branch and considers several examples.

From A_3 to C_2. The following is one of the simplest cases in which the monodromy map appears. The two examples in Figure 4.15 manifestly have the same local slices; however, the top slice in Figure 4.15b has a non-trivial global structure determined by the decoration, changing the corresponding slice from A_3 to C_2.

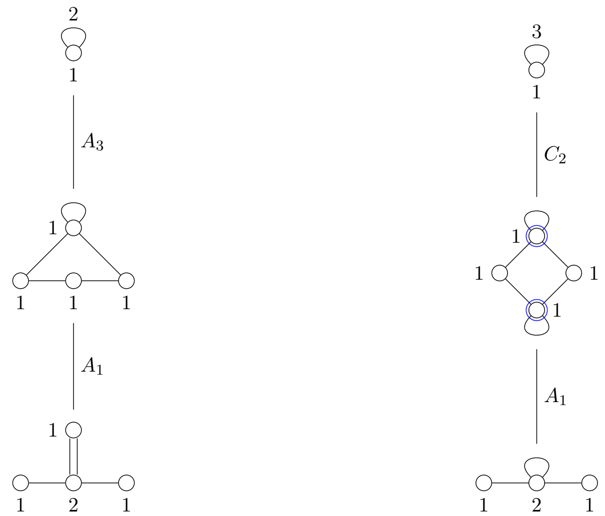

(a) (b)

Figure 4.15: (a): The Higgs branch of the quiver at the bottom of the Hasse diagram is the Słodowy Slice $\mathcal{S}^{[4]}_{[2,1^2]}$ in the A_3 nilcone. (b): The Higgs branch of the quiver at the bottom of the Hasse diagram is the Słodowy Slice $\mathcal{S}^{[4]}_{[2,1^2]}$ in the C_2 nilcone.

Consider how the decoration affects the operators in the chiral ring of Figure 4.15b; Figure 4.16 shows the hypermultiplets rewritten in terms of $3d\,\mathcal{N}=2$ multiplets (note that the free chiral hypermultiplets are omitted since they shall not appear in the F-term equations and GIOs).

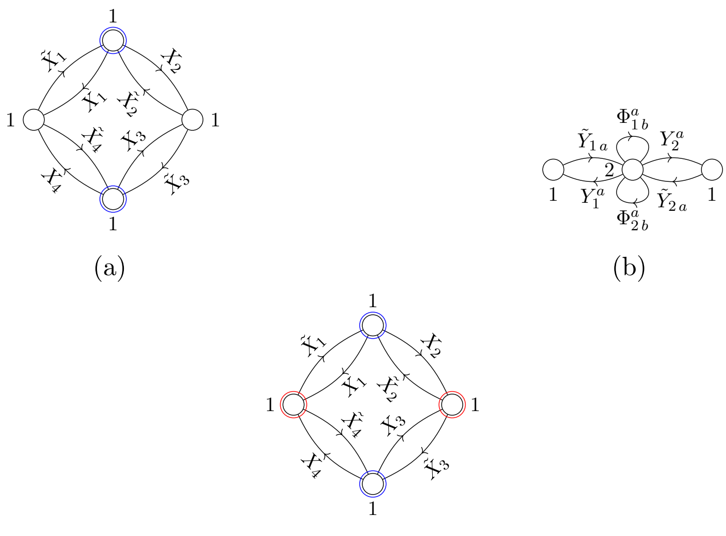

(a) (b)

(c)

Figure 4.16: (a): the non-trivial hypermultiplets of the middle leaf of Figure 4.15b in $3d$ $\mathcal{N}=2$ representation. (b): the hypermultiplets of bottom leaf of Figure 4.15b in $3d\,\mathcal{N}=2$ representation.(c): The same quiver as in (a), but with a further decoration added to the previously undecorated U(1) nodes.

The non-trivial Higgs branch operators in Figure 4.16a are given in Table 4.5.

Generators	Chiral Polynomials	Degree
x	$X_4\tilde{X}_3X_2\tilde{X}_1$	4
y	$X_1\tilde{X}_2X_3\tilde{X}_4$	4
z	$X_1\tilde{X}_1$	2
	Relations (F-term)	
	$X_1\tilde{X}_1 = X_2\tilde{X}_2 = X_3\tilde{X}_3 = X_4\tilde{X}_4$	2
Relations (GIOs)		
$xy = z^4$		8

Table 4.5: Chiral ring operators of Figure 4.16a, the middle leaf in Figure 4.15b.

The monodromy group action exchanges the two decorated U(1) nodes, which is inherited from the S_2 Weyl action of the original U(2) exchanging the two U(1)s in its Cartan matrix. Under this action, the scalars transform as:

$$\tilde{X}_1 \longleftrightarrow \tilde{X}_4,\ X_1 \longleftrightarrow X_4,\ X_2 \longleftrightarrow X_3,\ \tilde{X}_2 \longleftrightarrow \tilde{X}_3. \tag{4.13}$$

Note that this is not a gauge transformation but an equivalence between two choices of fields to describe the Higgs branch, so no quotient is taken under this action. The induced action on the GIOs is $x \longleftrightarrow y$, which thus gives a ring isomorphism (i.e. the Higgs branch is still the A_3 singularity under the change of embedding but the canonical sets of generators are different). This is a monodromy map as it 'moves around' the singular locus of the base leaf, modifying the deformation space as described in [6, 130, 141]. Roughly speaking, the two locally separated $\mathbb{P}^1$s in the fully resolved Higgs branch are connected globally, which means that going around the singular locus of the base leaf connects one $\mathbb{P}^1$ to another. Turning on FI parameters, the F-term equations are modified to the following:

$$-\tilde{X}_1X_1 + \tilde{X}_2X_2 = \zeta_{12}\,, \tag{4.14a}$$
$$-X_2\tilde{X}_2 - X_3\tilde{X}_3 = \zeta_{23}\,, \tag{4.14b}$$
$$\tilde{X}_3X_3 - \tilde{X}_4X_4 = \zeta_{34}\,, \tag{4.14c}$$
$$X_4\tilde{X}_4 + X_1\tilde{X}_1 = \zeta_{41}\,. \tag{4.14d}$$

The constraint $\zeta_{12} + \zeta_{23} + \zeta_{34} + \zeta_{41} = 0$ is manifest. The linear space defined by the constraint equation can be regarded as weight space of A_3 and has the permutation symmetry S_4. The algebraic equations are deformed to:

$$xy = z(z - \zeta_{12})(z - \zeta_{13})(z - \zeta_{14}). \tag{4.15}$$

The action (4.13) induces a map on the FI terms as:

$$\zeta_{12} \longleftrightarrow \zeta_{34}, \quad \zeta_{23} \;\text{ and }\; \zeta_{41} \;\text{ invariant.} \tag{4.16}$$

This map can be treated as an orientifold action on the deformation space, reducing the A_3 weight space to B_2 weight space, and folding the Higgs branch Namikawa-Weyl group from $\mathcal{W}_{A_3} \cong S_4$ to $\mathcal{W}_{B_2} \cong \mathbb{Z}_2^2 \rtimes S_2$.

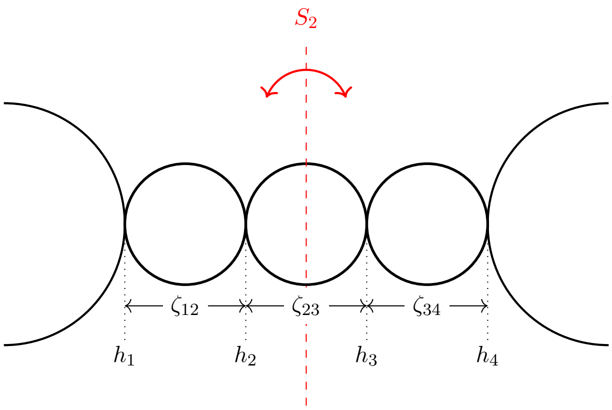

Figure 4.17: Schematic illustration of A_3 resolution under S_2 action. The FI parameters are the diameters of the $\mathbb{P}_1$ fibers.

Now consider what happens if another set of decorations are placed on the two undercoated U(1)s in Figure 4.16a, as shown in Figure 4.16c. Interestingly, this new decoration does not give rise to a new S_2 monodromy map but in fact reproduces the same map as the first. This is of course expected from the fact that the A_3 finite Dynkin diagram has a single S_2 outer automorphism.
This retention of the original S_2 action is also manifest from the deformation parameters of Figure 4.16b, the bottom leaf of Figure 4.15b. The F-term equations read:

$$Y_1^a \tilde{Y}_{1\,a} = \zeta_1\,, \tag{4.17a}$$

$$-Y_2^a \tilde{Y}_{2\,a} = \zeta_2\,, \tag{4.17b}$$

$$-\tilde{Y}_{1\,b} Y_1^a + \tilde{Y}_{2\,b} Y_2^a + \Phi^a_{1\,c}\Phi^c_{2\,b} - \Phi^a_{2\,c}\Phi^c_{1\,b} = \zeta_{12}\mathbb{1}^a_b\,. \tag{4.17c}$$

Which gives rise to the constraint $\zeta_1 + \zeta_2 + 2\zeta_{12} = 0$. This can be thought of as the weight space of B_2, thus has the symmetry $\mathcal{W}_{B_2} \cong \mathbb{Z}_2^2 \rtimes S_2$. The constraint is invariant under $\zeta_1 \leftrightarrow \zeta_2$ and $(\zeta_1,\ \zeta_2,\ \zeta_{12}) \mapsto (\zeta_1,\ -\zeta_2,\ \zeta_2 + \zeta_{12})$, which generates $\mathcal{W}_{B_2}$.

Now we elaborate how the F-term equations of Figure 4.16b reduce to F-term equations of Figure 4.16a. Firstly the following component scalars are identified:

$$\tilde{Y}_{1\,1} = \tilde{X}_1,\ Y_1^1 = X_1, \tag{4.18a}$$

$$\tilde{Y}_{1\,2} = \tilde{X}_4,\ Y_1^2 = X_4, \tag{4.18b}$$

$$\tilde{Y}_{2\,1} = \tilde{X}_2,\ Y_2^1 = X_2, \tag{4.18c}$$

$$\tilde{Y}_{2\,2} = \tilde{X}_3,\ Y_2^2 = X_3. \tag{4.18d}$$

Then, to move along the base leaf, we require the adjoint scalars Φ_1 and Φ_2 to be diagonal. (If the off-diagonal elements are non-zero, we reach a generic point in the moduli space, not the leaf in the middle of the Hasse diagram Figure 4.15b.)

This reduces F-term equations (4.17) to (4.14) and the FI parameters are identified as $\zeta_{41} = \zeta_1,\ \zeta_{23} = \zeta_2,\ \zeta_{34} = \zeta_{12},\ \zeta_{12} = \zeta_{12}$. This also indicated that the FI parameters of the two decorated nodes should be identical, verifying that the two $\mathbb{P}^1$s are connected when moving around the singular locus of the base leaf, as illustrated in Figure 4.17.

From D_4 to B_3, G_2. Consider the various examples of the affine D_4 quiver with decorations, as given in Figure 4.18. There are four different cases: (a) two decorations, (b) three decorations, (c) four decorations, (d) two decorations of one type and two decorations of another type.

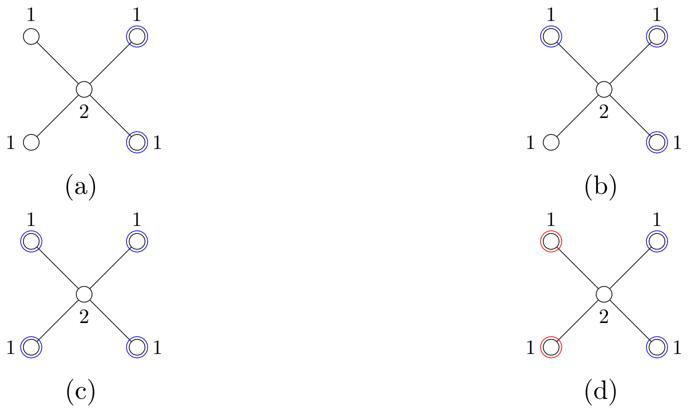

Figure 4.18: Affine D_4 under (a): Two decorated nodes. (b): Three decorated nodes. (c): Four decorated nodes. (d): Two nodes under one decoration and two two nodes under another.

The $3d$ $\mathcal{N} = 2$ decomposition of hypermultiplets of D_4 quiver is shown in Figure 4.19, and the non-trivial Higgs branch operators are given in in Table 4.5.

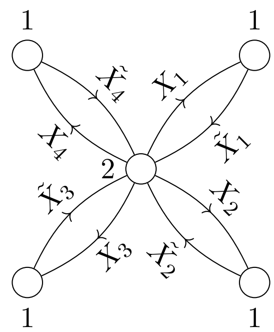

Figure 4.19: $3d$ $\mathcal{N} = 2$ decomposition of hypermultiplets of D_4 quiver.

Generators	Chiral Polynomials	Degree
w	$X_3^a \tilde{X}_{3\,b} X_4^b \tilde{X}_{4\,a}$	4
v	$(X_1^a \tilde{X}_{1\,b} - X_2^a \tilde{X}_{2\,b}) X_3^b \tilde{X}_{3\,a}$	4
u	$(X_1^a \tilde{X}_{1\,c} - X_2^a \tilde{X}_{2\,c}) X_3^c \tilde{X}_{3\,b} X_4^b \tilde{X}_{4\,a}$	6
	Relations (F-term)	
	$X_1^a \tilde{X}_{1\,a} = X_2^a \tilde{X}_{2\,a} = X_3^a \tilde{X}_{3\,a} = X_4^a \tilde{X}_{4\,a} = 0$	2
	$X_1^a \tilde{X}_{1\,b} + X_2^a \tilde{X}_{2\,b} + X_3^a \tilde{X}_{3\,b} + X_4^a \tilde{X}_{4\,b} = 0$	2
Relations(GIO)		
$u^2 + v^2 w = w^3$		12

Table 4.6: Chiral ring operators of the affine D_4 quiver.

For case (a), these two decorated U(1)s are exchanged by an S_2 - the scalars change as:

$$X_1 \longleftrightarrow X_2, \;\; \tilde{X}_1 \longleftrightarrow \tilde{X}_2. \tag{4.19}$$

The induced action on the GIOs is $v \to -v, \;\; u \to -u$, which gives a ring isomorphism. Adding a further set of decorations on the undecorated U(1)s generates the same S_2 action; hence, there is an identification of the quivers in Figure 4.18a and Figure 4.18d. The Namikawa Weyl group is $\mathcal{W}_{B_3}$. The slice is called C_3 following the notation of [6], which will become clearer following the discussion of the symplectic dual of this slice.

The identification between Figure 4.18a and Figure 4.18d also implies the identification between Figure 4.18b and Figure 4.18c. It is easy to check that Figure 4.18b and Figure 4.18c have the same S_3 monodromy map; the Namikawa Weyl group is $\mathcal{W}_{G_2}$ and the slice is G_2.

A union of 2. A simple case containing a union of slices appears in the Higgs branch Hasse diagram in Figure 4.20. On the next-to-minimal leaf, there are two A_1 sub-quivers that contribute two A_1 components of the transverse slice. The two decorated U(1)s are exchanged under the action of $\mathcal{W}_{\mathrm{U}(2)} \cong S_2$, the Weyl group of the gauge group U(2). Since this S_2 Weyl action belongs to the automorphism of the gauge transformation, these two components should not be connected to two different Higgsing phases/leaves, but form a union and are connected to a single phase/leaf.
In general, the union and monodromy maps can appear at the same time. Examples of this are given in section 4.4.

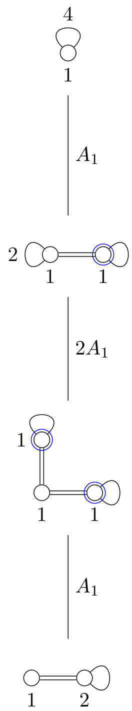

Figure 4.20: The Higgs branch of this quiver is the 2nd symmetric product of A_1.

4.4 Examples from Nilpotent Cones

Nilpotent cones (nilcones) are a distinguished class of symplectic singularities that underpin much of the progress made in recent years concerning the moduli spaces of vacua of gauge theories with eight supercharges. Although generic Hasse diagrams can be constructed straightforwardly using minimal degenerations, nilpotent cones are one of the few examples wherein the Higgs branch of a gauge theory can be checked against a known Hasse diagram – in this sense, graduating the nilpotent dōjō provides a non-trivial test of any subtraction algorithm.[12]

The Higgs branch subtraction algorithm presented in this paper identifies several gauge theories whose Higgs branches are Słodowy intersections inside nilcones of simple Lie algebras. Such theories are identified both by their Hasse diagrams and Hilbert series. Of course, Hasse diagrams are not unique to a moduli space, and thus explicit Hilbert series computations are required, alongside calculations involving the localisation formula [124, 142–145], to verify the identity of the moduli spaces presented in the following section.

Some quivers presented in this section contain hypermultiplets in the adjoint representation of a unitary gauge group – each such hypermultiplet contributes an extra degree 1 generator of the Higgs branch and hence gives a free factor $\mathbb{H}$ to the Higgs branch. In the analysis of this section, such extra factors are ignored.

A further interesting property of nilcones concerns the action of *Lusztig-Spaltenstein du-*

[12]Reciprocally, most recent additions to the combinatoric toolbox for quiver gauge theories have their origin in nilcones.

ality [146–149], which acts as an involution and appears to relate the Higgs and Coulomb branches of theories when both lie in the same nilcone.

In the following, a quiver will be denoted by $\mathcal{Q}$ with either an equation number or figure number in the subscript. The Higgs branch of a quiver will be denoted with $\mathcal{H}$ and its Coulomb branch by $\mathcal{C}$.

4.4.1 Examples of Słodowy Intersections in G_2, F_4, and E_8 Nilcones

The following one-parameter family of quivers $\mathcal{Q}_{4.20}$ contains several examples of theories whose moduli spaces of vacua appear in the nilcones of exceptional algebras.

They equally arise as magnetic quivers corresponding to intermediate leaves in the phase diagram of n M5 branes probing an A_1 Klein singularity with either an M9 brane or a non-trivial boundary condition on one side.

This one-parameter family of quivers is also the $3d$ mirror quiver for the $4d$ $\mathcal{N} = 2$ class $\mathcal{S}$ theory [150, 151] specified by algebra A_{n-1} on a torus with one puncture labelled by partition $(n-2, 1^2)$.

The following examples consider the cases $n = 3, 4, 5$, as these cases are the only ones where the Higgs branch and the Coulomb branch (by Lusztig-Spaltenstein duality [6]) are slices in a nilcone. The moduli spaces of vacua for the cases $n = 3, 4, 5$ are slices in the G_2, F_4, and E_8 nilcones respectively. In fact, any nilcone with a Lusztig canonical quotient S_n, $n = 3, 4, 5$ associated to a leaf will contain both the Higgs and Coulomb branches of (4.20) for $n = 3, 4, 5$ respectively.

$\mathcal{Q}_{4.20} =$ 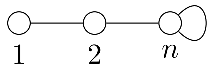 . (4.20)

Note that the following examples will make use of Coulomb branch quiver subtraction [23–25] to compute Hasse diagrams for the Coulomb branches of various unitary quivers.

G_2 Example. First consider this theory at $n = 3$,

$\mathcal{Q}_{4.21} =$ 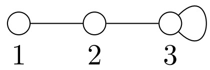 . (4.21)

The Coulomb branch of $\mathcal{Q}_{4.21}$ is well known to be $\overline{sub.reg.G_2}$ [152, 153]. The Hasse diagram for this moduli space is given in Figure 4.21, which may be computed with quiver subtraction [23] or with the fusion and fission algorithm [24, 25].

Lusztig-Spaltenstein duality [6], which acts on the special pieces of Figure 4.21, suggests that the Higgs branch is the Słodowy slice to the minimal nilpotent orbit of G_2, i.e. $\mathcal{S}^{G_2}_{\mathcal{N},A_1}$. Using the Higgs branch subtraction algorithm established in Section 4.3, the Hasse diagram of $\mathcal{H}(\mathcal{Q}_{4.21})$ is computed to be Figure 4.22a, consistent with the Hasse diagram

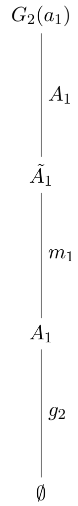

Figure 4.21: The Hasse diagram of $\overline{sub.reg.G_2}$ in the G_2 nilcone with each orbit specified by its Bala-Carter label. This is the same Hasse diagram for the Coulomb branch of $\mathcal{Q}_{4.21}$.

of $\mathcal{S}^{G_2}_{\mathcal{N},A_1}$[6] given in Figure 4.22b. The top slice is identified as G_2 since this corresponds to the subtraction of an affine D_4 quiver with three decorated U(1), as given in Table 4.2. Additionally, the Namikawa-Weyl group for the Higgs branch is identified as $\mathcal{W}_{G_2} = \mathrm{Dih}_6$ of order 12 using the prescription in Section 4.3.3. The Higgs branch Hilbert series of $\mathcal{Q}_{4.21}$ is computed to be

$$\mathrm{HS}[\mathcal{H}(\mathcal{Q}_{4.21})] = \mathrm{PE}\left[[2]_{\mathrm{SU}(2)}t^2 + [3]_{\mathrm{SU}(2)}t^3 - t^{12}\right] = \mathrm{HS}\left[\mathcal{S}^{G_2}_{\mathcal{N},A_1}\right] \tag{4.22}$$

where the label $[n]_G$ specifies the character of the representation given by the Dynkin label. This confirms that the Higgs branch $\mathcal{H}(\mathcal{Q}_{4.21}) = \mathcal{S}^{G_2}_{\mathcal{N},A_1}$.

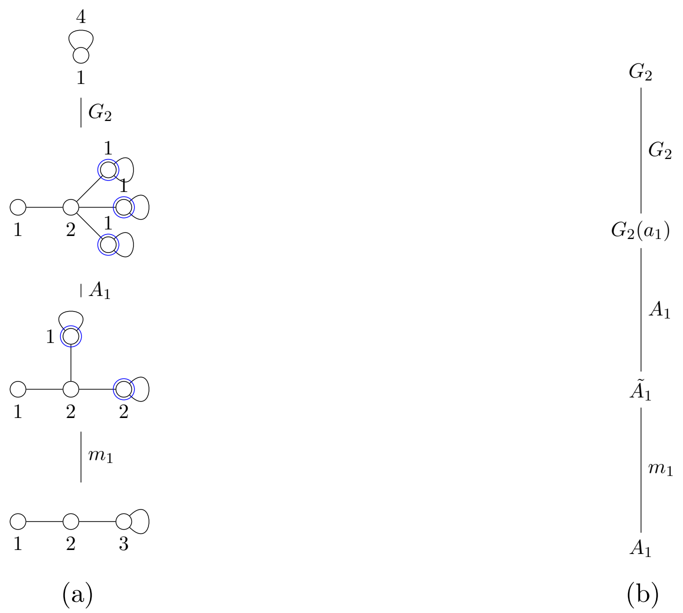

Figure 4.22: (a): The Higgs branch Hasse diagram of $\mathcal{Q}_{4.21}$. (b): The Hasse diagram for the Słodowy slice $\mathcal{S}^{G_2}_{\mathcal{N},A_1}$ in the G_2 nilcone to the minimal orbit with orbits labelled by their Bala-Carter labels. This is the same Hasse diagram as in Figure 4.22a.

F_4 **Example.** Next consider $\mathcal{Q}_{4.20}$ at $n = 4$

$$\mathcal{Q}_{4.23} = \tag{4.23}$$

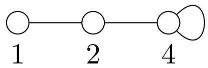

The Hasse diagram for the Higgs branch is shown in Figure 4.23a, which matches the Hasse diagram of the Słodowy intersection, $\mathcal{S}^{F_4}_{F_4(a_2),A_2+\tilde{A}_1}$, in the nilcone of F_4 [6] explicitly shown in Figure 4.23b. From the Higgs branch Hasse diagram, the Namikawa-Weyl group for the Higgs branch is identified as $\mathbb{Z}_2 \times \mathbb{Z}_2$. Note that the quiver corresponding to $F_4(a_3)$ admits two different subtractions as given in Table 4.2. One possibility is the subtraction of an affine D_4 with four decorated U(1) nodes, this gives rise to the G_2 slice. The other possibility is the subtraction of affine D_4 with three decorated U(1) with $\binom{4}{3} = 4$ different subtractions, giving rise to the $4G_2$ slice.

This identification of $\mathcal{H}\left(\mathcal{Q}_{4.23}\right) = \mathcal{S}^{F_4}_{F_4(a_2),A_2+\tilde{A}_1}$ is also confirmed by the refined Hilbert series, where for brevity only the unrefined series is presented. The result matches with the calculation from localization for Słodowy intersections [144].

$$\begin{aligned} \mathrm{HS}\left[\mathcal{H}(\mathcal{Q}_{4.23})\right] &= \frac{1 + 2t^4 + 2t^5 + 3t^6 + 3t^8 + 4t^9 + 6t^{10} + 4t^{11} + 3t^{12} + 3t^{14} + 2t^{15} + 2t^{16} + t^{20}}{(1-t^2)^3(1-t^3)^4(1-t^4)^3} \\ &= \mathrm{HS}\left[\mathcal{S}^{F_4}_{F_4(a_2),A_2+\tilde{A}_1}\right] . \end{aligned} \tag{4.24}$$

By Lusztig-Spaltenstein duality, the Coulomb branch of $\mathcal{Q}_{4.23}$ also appears in the F_4 nilcone. To compute the Lusztig-Spaltenstein dual we note that $F_4(a_2)$ is a special orbit, hence there is no problem in computing its dual which is the special orbit $A_1 + \tilde{A}_1$. On the other hand, the $A_2 + \tilde{A}_1$ orbit is the lowest non special orbit in an S_4 special piece which is self dual. Hence the dual is the special orbit $F_4(a_3)$. Calculation of the refined Hilbert series for the Coulomb branch verifies that the Coulomb branch of $\mathcal{Q}_{4.23}$ is the Słodowy intersection $\mathcal{S}^{F_4}_{F_4(a_3),A_1+\tilde{A}_1}$. For brevity, only the unrefined Hilbert series is given below.

$$\begin{aligned} \mathrm{HS}\left[\mathcal{C}(\mathcal{Q}_{4.23})\right] &= \frac{\begin{pmatrix} 1 + t^2 + 4t^3 + 5t^4 + 6t^5 + 12t^6 + 14t^7 + 19t^8 + 20t^9 + 20t^{10} \\ + 20t^{11} + 19t^{12} + 14t^{13} + 12t^{14} + 6t^{15} + 5t^{16} + 4t^{17} + t^{18} + t^{20} \end{pmatrix}}{(1-t^2)^5(1-t^3)^6(1-t^4)} \\ &= \mathrm{HS}\left[\mathcal{S}^{F_4}_{F_4(a_3),A_1+\tilde{A}_1}\right] . \end{aligned} \tag{4.25}$$

The Hasse diagram for $\mathcal{S}^{F_4}_{F_4(a_3),A_1+\tilde{A}_1}$ is given in Figure 4.24 which matches the Hasse diagram for $\mathcal{C}\left(\mathcal{Q}_{4.23}\right)$.

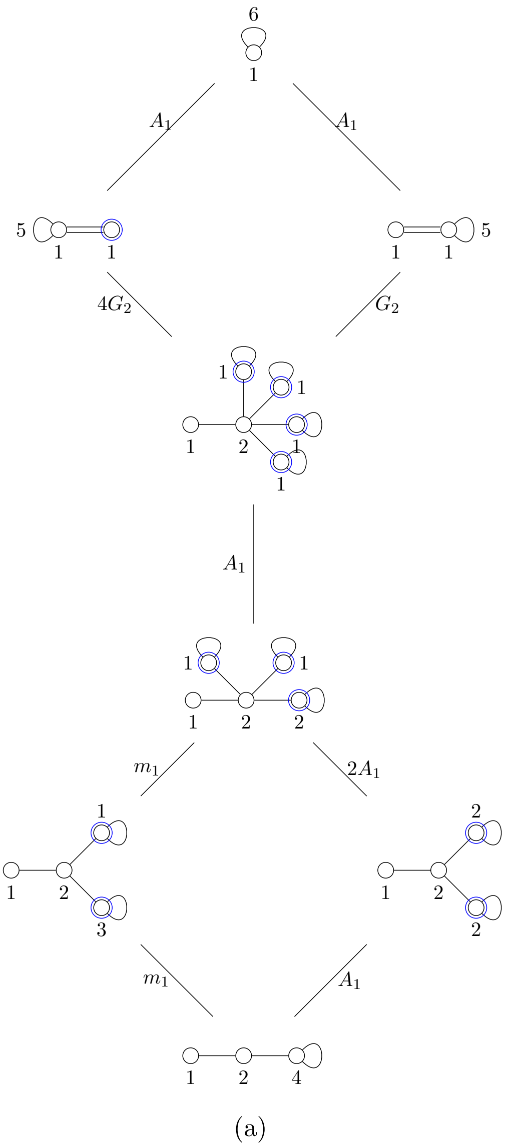

Figure 4.23: (a): The Higgs branch Hasse diagram for the quiver $\mathcal{Q}_{4.23}$. (b): The Hasse diagram for the Słodowy intersection $\mathcal{S}^{F_4}_{F_4(a_2),A_2+\tilde{A}_1}$ in the F_4 nilcone with orbits labelled by their Bala-Carter labels. This is the same Hasse diagram as Figure 4.23a.

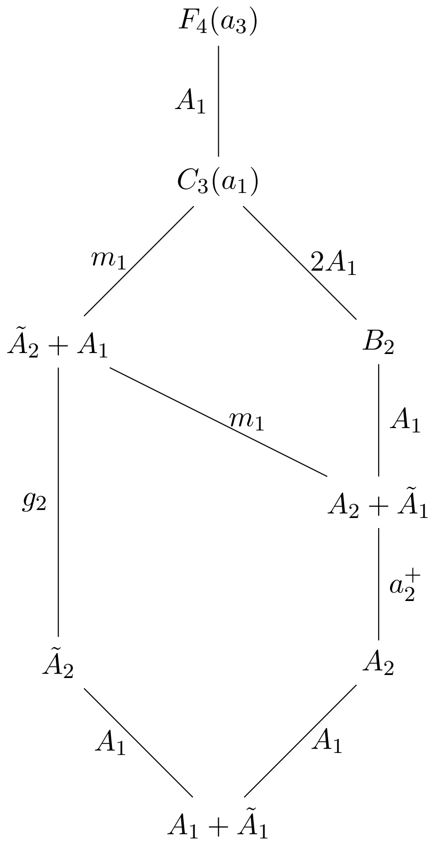

Figure 4.24: The Hasse diagram for $\mathcal{S}^{F_4}_{F_4(a_3),A_1+\tilde{A}_1}$ in the F_4 nilcone with orbits labelled by their Bala-Carter labels. This Hasse diagram is the same as for the Coulomb branch of $Q_{4.23}$.

E_8 **Example.** Finally consider $\mathcal{Q}_{4.20}$ at $n = 5$

$\mathcal{Q}_{4.26} =$ 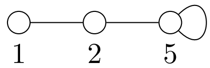 . (4.26)

The Hasse diagram for the Higgs branch is given in Figure 4.25a, which matches the Hasse diagram for the Słodowy intersection $\mathcal{S}^{E_8}_{D_5+A_2,A_4+A_3}$ in the E_8 nilcone [6], explicitly shown in Figure 4.25b. Note that the quiver corresponding to the leaf with Bala-Carter label $E_8(a_7)$ admits two possible subtractions as given in Table 4.2. The first possible subtraction is of an affine D_4 quiver with four decorated U(1) nodes, there are $\binom{5}{4} = 5$ ways of subtracting it and so gives rise to the $5G_2$ slice. The other possibility is to subtract an affine D_4 quiver with three decorated U(1) nodes, this time there are $\binom{5}{3} = 10$ ways of subtracting it and gives rise to the $10G_2$ slice. The Higgs branch Hasse diagram also allows the identification of the Higgs branch Namikawa-Weyl group as $\mathbb{Z}_2 \times \mathbb{Z}_2$.

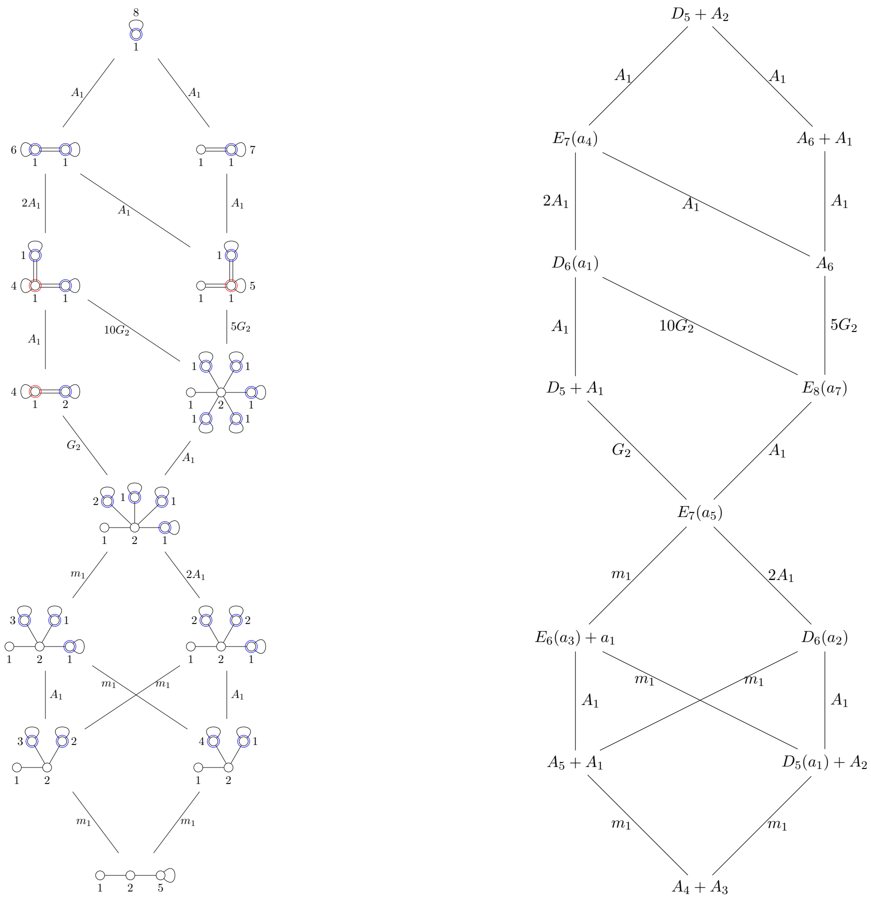

(a) (b)

Figure 4.25: (a): The Higgs branch Hasse diagram of $\mathcal{Q}_{4.26}$. (b): The Słodowy intersection $\mathcal{S}^{E_8}_{D_5+A_2,A_4+A_3}$ in the E_8 nilcone with orbits specified by their Bala-Carter labels. This is the same Hasse diagram as in Figure 4.25a.

It is computationally challenging to confirm that the Hilbert series of the Słodowy slice

$\mathcal{S}^{E_8}_{D_5+A_2,A_4+A_3}$ matches that of $\mathcal{H}\left(\mathcal{Q}_{4.26}\right)$ which is

$$\mathrm{HS}\left[\mathcal{H}\left(\mathcal{Q}_{4.26}\right)\right]=\frac{\left(\begin{array}{l}1+t^4+5t^5+6t^6+6t^7+7t^8+9t^9+21t^{10}+30t^{11}+39t^{12}+39t^{13}+37t^{14}+45t^{15}+\\ 53t^{16}+65t^{17}+65t^{18}+53t^{19}+45t^{20}+37t^{21}+39t^{22}+39t^{23}+30t^{24}+21t^{25}+9t^{26}+\\ 7t^{27}+6t^{28}+6t^{29}+5t^{30}+t^{31}+t^{35}\end{array}\right)}{(1-t^2)^3(1-t^3)^4(1-t^4)^4(1-t^5)^3}. \tag{4.27}$$

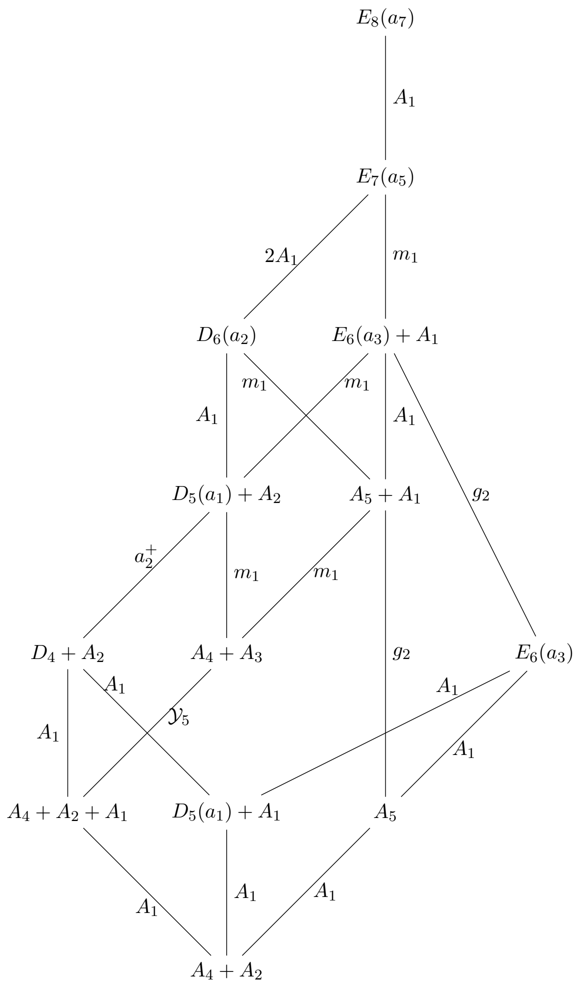

Figure 4.26: The Hasse diagram for $\mathcal{S}^{E_8}_{E_8(a_7),A_4+A_2}$ in the E_8 nilcone with orbits specified by their Bala-Carter labels. This is the same Hasse diagram as for the Coulomb branch of $\mathcal{Q}_{4.26}$. The slice $\mathcal{Y}_5$ was introduced in [6] (where it was called χ) and further studied in [7, 8].

Lusztig-Spaltenstein duality suggests that the Coulomb branch is also in the E_8 nilcone, specifically being the Słodowy intersection $\mathcal{S}^{E_8}_{E_8(a_7),A_4+A_2}$. The Hasse diagram for $\mathcal{S}^{E_8}_{E_8(a_7),A_4+A_2}$ is given in Figure 4.26 and matches the Hasse diagram of the Coulomb branch of $\mathcal{Q}_{4.26}$.

Once again it is computationally challenging to confirm that the Hilbert series of the

Słodowy intersection $\mathcal{S}^{E_8}_{E_8(a_7),A_4+A_2}$ is the same as for $\mathcal{C}\left(\mathcal{Q}_{4.26}\right)$ which is

$$\mathrm{HS}\left[\mathcal{C}\left(\mathcal{Q}_{4.26}\right)\right] = \frac{\begin{pmatrix} 1+t^2+11t^4+20t^6+65t^8+109t^{10}+221t^{12}+285t^{14}+401t^{16}+394t^{18} \\ +401t^{20}+285t^{22}+221t^{24}+109t^{26}+65t^{28}+20t^{30}+11t^{32}+t^{34}+t^{36} \end{pmatrix}}{(1-t^2)^5(1-t^4)^7(1-t^6)^2}. \tag{4.28}$$

4.4.2 A Second F_4 Example.

Now consider the quiver $\mathcal{Q}_{4.29}$ which is similar to $\mathcal{Q}_{4.23}$.

$\mathcal{Q}_{4.29} =$ 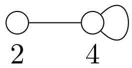 . (4.29)

The Coulomb branch of $\mathcal{Q}_{4.29}$ is known to be d_4/S_4 [97, 117] but is also equivalently $\mathcal{S}^{F_4}_{F_4(a_3),A_2}$ [1]. The Hasse diagram for $\mathcal{S}^{F_4}_{F_4(a_3),A_2}$ is drawn in Figure 4.27 [103], which matches the Hasse diagram of $\mathcal{C}\left(\mathcal{Q}_{4.29}\right)$.

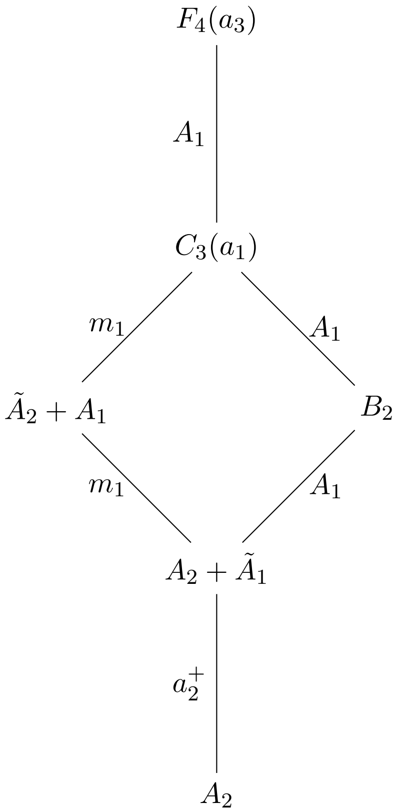

Figure 4.27: The Hasse diagram for $\mathcal{S}^{F_4}_{F_4(a_3),A_2}$ in the F_4 nilcone with orbits specified by their Bala-Carter labels. This Hasse diagram is the same as for the Coulomb branch of $\mathcal{Q}_{4.29}$.

Lusztig-Spaltenstein duality suggests that the Higgs branch is again a slice in the F_4 nilcone. The Hasse diagram for the Higgs branch is computed using the rules introduced in this paper in Figure 4.28a, which matches the Hasse diagram for $\mathcal{S}^{F_4}_{B_3,A_2+\tilde{A}_1}$ explicitly given in Figure 4.28b. The Higgs branch Hilbert series is computed as

$$\mathrm{HS}[\mathcal{H}(\mathcal{Q}_{4.29})] = (1+t^4+t^{10}+t^{14}-[3]_{\mathrm{SU}(2)}t^7)\mathrm{PE}\left[[2]_{\mathrm{SU}(2)}t^2 + [3]_{\mathrm{SU}(2)}t^3 + [4]_{\mathrm{SU}(2)}t^4 - t^4 - t^{12}\right], \tag{4.30}$$

which is not a complete intersection, but does confirm that $\mathcal{H}(\mathcal{Q}_{4.29}) = \mathcal{S}^{F_4}_{B_3,A_2+\tilde{A}_1}$. The Namikawa-Weyl group for the Higgs branch is the Weyl group of G_2, $\mathcal{W}_{G_2} = \mathrm{Dih}_6$ of order 12.

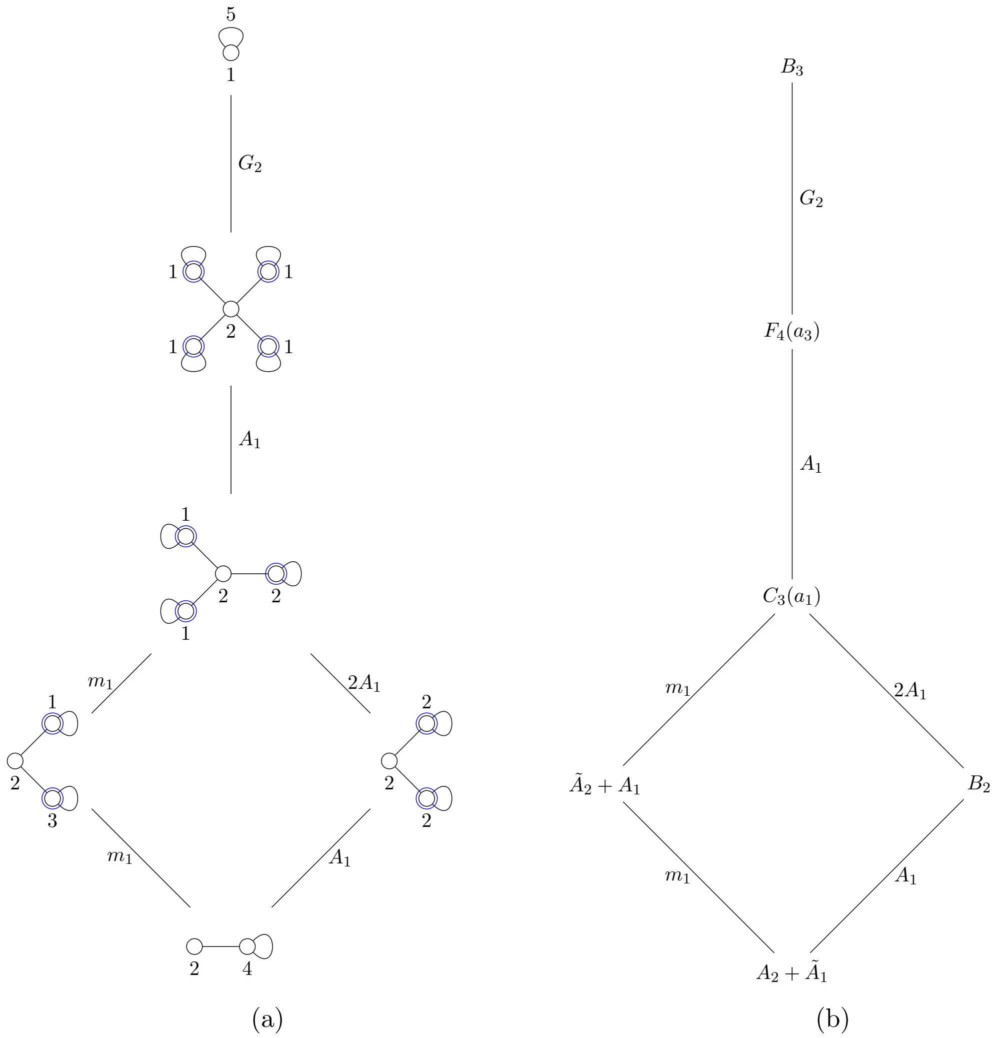

Figure 4.28: (a): The Higgs branch Hasse diagram of $\mathcal{Q}_{4.29}$. (b): The Słodowy intersection $\mathcal{S}^{F_4}_{B_3,A_2+\tilde{A}_1}$ in the F_4 nilcone with orbits specified by their Bala-Carter labels. This is the same Hasse diagram as in Figure 4.28a.

Comment. Note that the quiver $\mathcal{Q}_{4.29}$ is a subquiver of $\mathcal{Q}_{4.23}$ - its Higgs and Coulomb branch Hasse diagrams are contained in those of $\mathcal{Q}_{4.23}$. In Figure 4.29, the Hasse diagram for the F_4 nilcone is given with the Higgs branch Hasse diagrams of $\mathcal{Q}_{4.23}$ and $\mathcal{Q}_{4.29}$ outlined in blue and orange respectively. The Coulomb branch Hasse diagrams for these quivers are outlined in red and green respectively.

Below, the quivers $\mathcal{Q}_{4.37}$ and $\mathcal{Q}_{4.40}$ obey the same relationship. The Higgs branch Hasse diagram of $\mathcal{Q}_{4.40}$ can be embedded into $\mathcal{Q}_{4.37}$ explicitly, as apparent from Figure 4.37 and

Figure 4.35.

In general, if a undecorated quiver $\mathcal{Q}_1$ is a subquiver of another undecorated quiver $\mathcal{Q}_2$, then the Higgs branch of $\mathcal{Q}_1$ is a leaf of the Higgs branch of $\mathcal{Q}_2$, and the Coulomb branch of $\mathcal{Q}_1$ is a slice of the Coulomb branch of $\mathcal{Q}_2$.

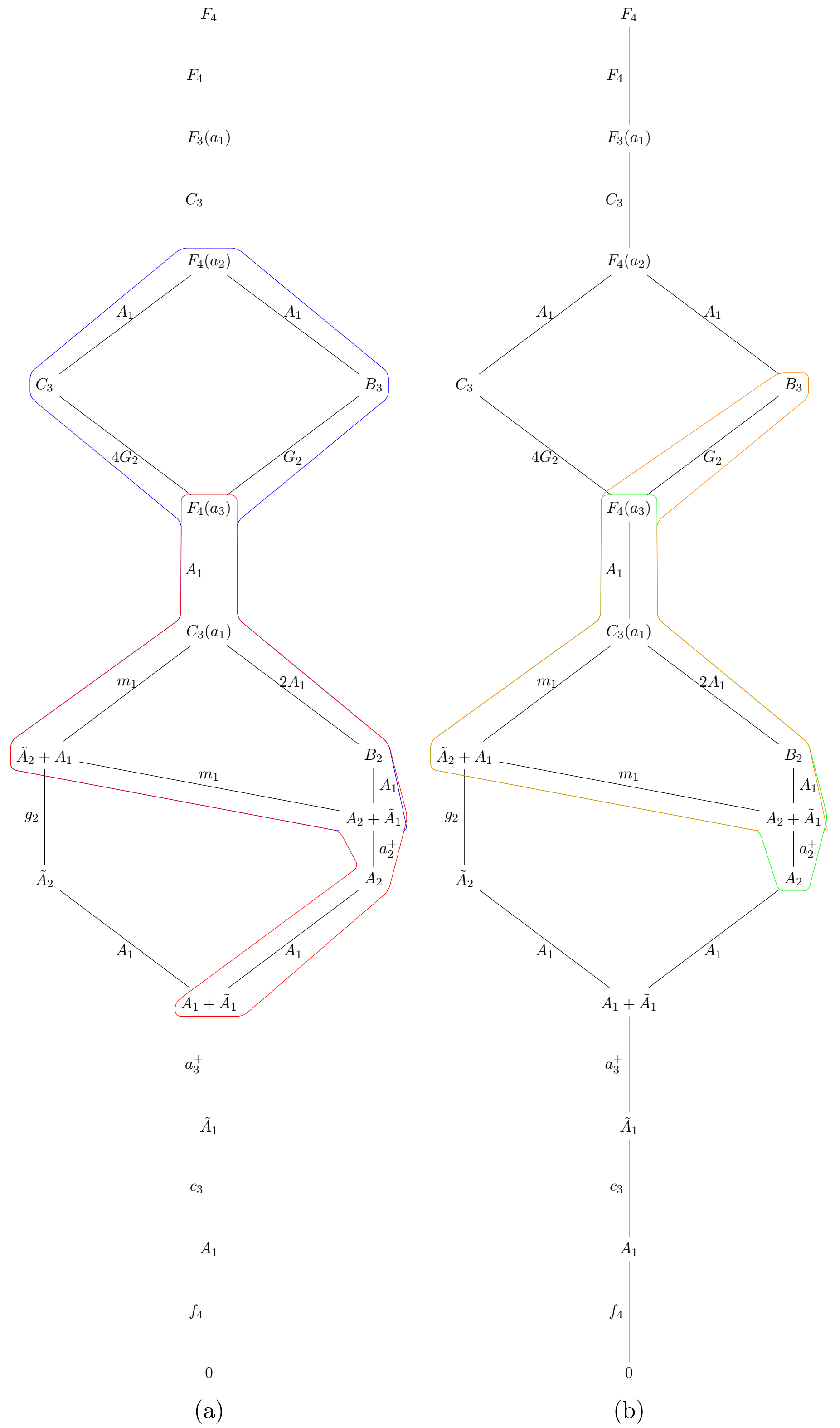

Figure 4.29: (4.29a) The Hasse diagram of the F_4 nilcone where blue is the intersection $\mathcal{S}^{F_4}_{F_4(a_2),A_2+\tilde{A}_1} = \mathcal{H}\left(\mathcal{Q}_{4.23}\right)$ and red is the intersection $\mathcal{S}^{F_4}_{F_4(a_3),A_1+\tilde{A}_1} = \mathcal{C}\left(\mathcal{Q}_{4.23}\right)$. (4.29b) The Hasse diagram of the F_4 nilcone where orange is the intersection $\mathcal{S}^{F_4}_{B_3,A_2+\tilde{A}_1} = \mathcal{H}\left(\mathcal{Q}_{4.29}\right)$ and green is the intersection $\mathcal{S}^{F_4}_{F_4(a_3),A_2} = \mathcal{C}\left(\mathcal{Q}_{4.29}\right)$.

4.4.3 Example: C_3

Now consider the following quiver

$\mathcal{Q}_{4.31} =$ 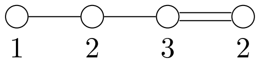 . (4.31)

The Coulomb branch of $\mathcal{Q}_{4.31}$ is $\overline{\mathcal{O}}^{B_3}_{(3^2,1)}$ [27, 117] which is a nilpotent orbit of height 4. This makes $\mathcal{Q}_{4.31}$ a rare example of a unitary quiver whose Coulomb branch is a height 4 nilpotent orbit for an algebra other than A_k. The Hasse diagram of $\overline{\mathcal{O}}^{B_3}_{(3^2,1)}$ is shown in Figure 4.30 which matches the Hasse diagram of $\mathcal{C}\left(\mathcal{Q}_{4.31}\right)$.

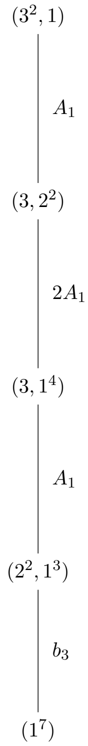

Figure 4.30: The Hasse diagram for $\overline{\mathcal{O}}^{B_3}_{(3^2,1)}$ in the B_3 nilcone with orbits labelled by partitions of 7. This Hasse diagram is the same as the Hasse diagram for the Coulomb branch of $\mathcal{Q}_{4.31}$.

Lusztig-Spaltenstein duality suggests that the Higgs branch is the Słodowy intersection $\mathcal{S}^{C_3}_{\mathcal{N},(2^3)}$. The Hasse diagram for the Higgs branch is given in Figure 4.31a, which is consistent with the Hasse diagram of $\mathcal{S}^{C_3}_{\mathcal{N},(2^3)}$ given in Figure 4.31b. The computation of the Higgs branch Hilbert series proceeds as

$$\mathrm{HS}[\mathcal{H}(\mathcal{Q}_{4.31})] = \mathrm{PE}\left[[2]_{\mathrm{SU}(2)}t^2 + [4]_{\mathrm{SU}(2)}t^4 - t^8 - t^{12}\right] = \mathrm{HS}\left[\mathcal{S}^{C_3}_{\mathcal{N},(2^3)}\right], \tag{4.32}$$

which confirms that $\mathcal{H}(\mathcal{Q}_{4.31}) = \mathcal{S}^{C_3}_{\mathcal{N},(2^3)}$. The Higgs branch Namikawa-Weyl group is $\mathcal{W}_{C_3} = \mathbb{Z}_2^3 \rtimes S_3$.

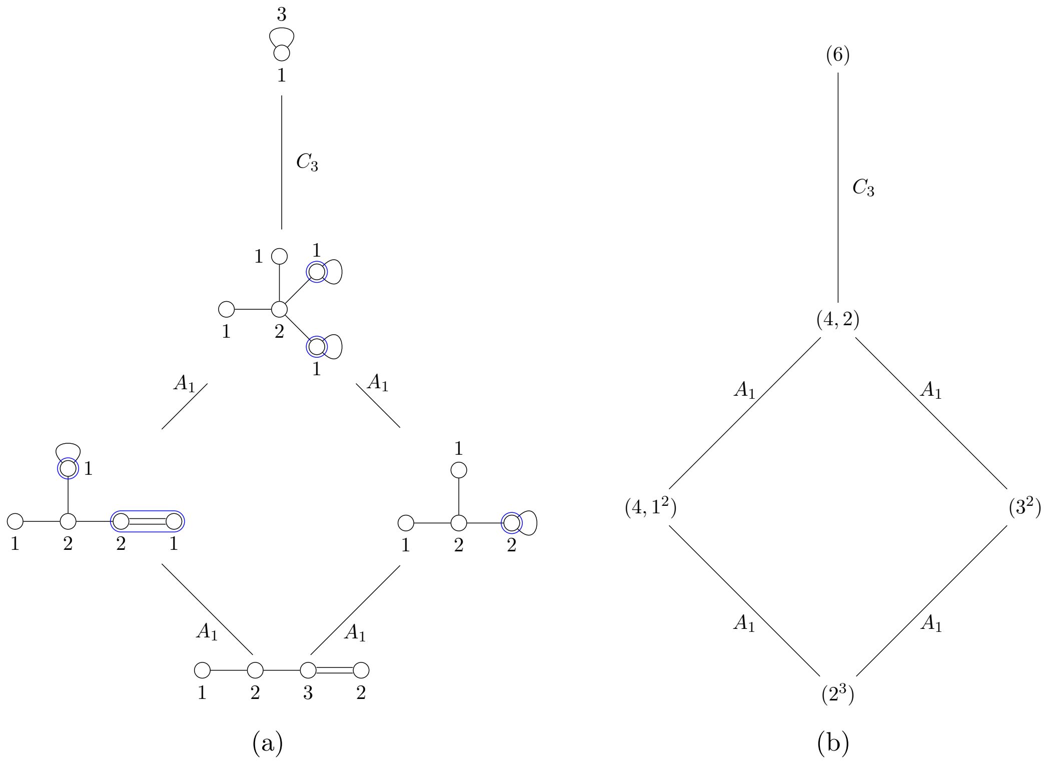

Figure 4.31: (a): The Higgs branch Hasse diagram of $\mathcal{Q}_{4.31}$. (b): The Słodowy intersection $\mathcal{S}^{C_3}_{\mathcal{N},(2^3)}$ in the C_3 nilcone with orbits specified by partitions of 6. This is the same Hasse diagram as in Figure 4.31a.

4.4.4 Example: E_6

Consider now the theory given by $\mathcal{Q}_{4.33}$.

$\mathcal{Q}_{4.33} =$ 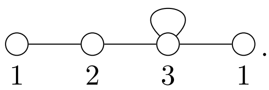 . (4.33)

The Hasse diagram for the Higgs branch of $\mathcal{Q}_{4.33}$ is shown in Figure 4.32a, which matches the Słodowy intersection $\mathcal{S}^{E_6}_{D_5(a_1),2A_2+A_1}$ in the E_6 nilcone shown in Figure 4.32b. The Higgs branch Namikawa-Weyl group is S_3. The unrefined Higgs branch Hilbert series is given below for brevity, however the refined Hilbert series is verified to match that of $\mathcal{S}^{E_6}_{D_5(a_1),2A_2+A_1}$.

$$\mathrm{HS}\left[\mathcal{H}(\mathcal{Q}_{4.33})\right] = \frac{\begin{pmatrix} 1+2t^3+t^4+4t^5+7t^6+4t^7+8t^8+10t^9+6t^{10} \\ +10t^{11}+8t^{12}+4t^{13}+7t^{14}+4t^{15}+t^{16}+2t^{17}+t^{20} \end{pmatrix}}{(1-t^2)^3(1-t^3)^4(1-t^4)^3} \tag{4.34}$$

$$= \mathrm{HS}\left[\mathcal{S}^{E_6}_{D_5(a_1),2A_2+A_1}\right]. \tag{4.35}$$

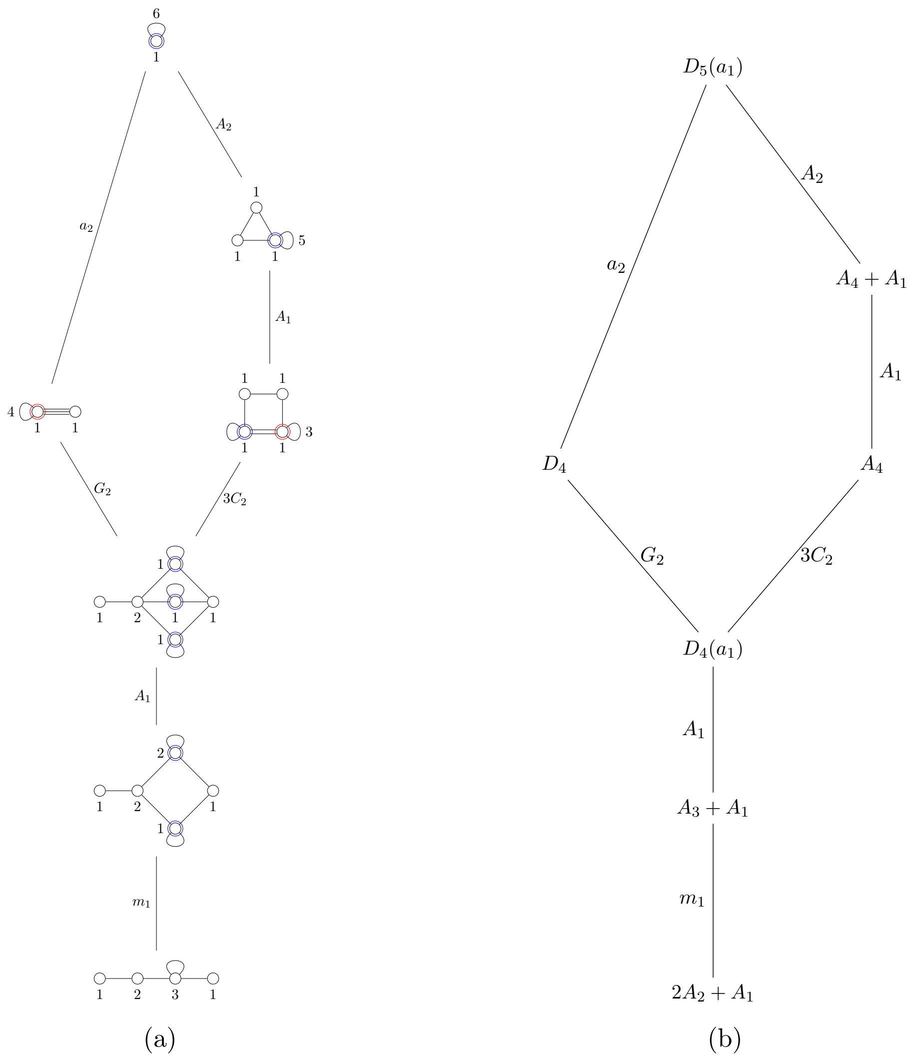

Figure 4.32: (a): The Higgs branch Hasse diagram of $\mathcal{Q}_{4.33}$. (b): The Hasse diagram of $\mathcal{S}^{E_6}_{D_5(a_1),2A_2+A_1}$ in the E_6 nilcone with orbits specified by their Bala-Carter labels. This is the same Hasse diagram as in Figure 4.32a.

The Coulomb branch of $\mathcal{Q}_{4.33}$ is found to be $\mathcal{S}^{E_6}_{D_4(a_1),A_2+A_1}$ via a calculation of its refined Hilbert series. Again, only the unrefined series is presented here for brevity.

$$\mathrm{HS}\left[\mathcal{C}(\mathcal{Q}_{4.33})\right] = \frac{(1-t)\begin{pmatrix}1+t+4t^2+7t^3+17t^4+26t^5+46t^6+62t^7+89t^8+105t^9+125t^{10}+124t^{11}\\ +125t^{12}+105t^{13}+89t^{14}+62t^{15}+46t^{16}+26t^{17}+17t^{18}+7t^{19}+4t^{20}\\ +t^{21}+t^{22}\end{pmatrix}}{(1-t^2)^6(1-t^3)^5(1-t^4)^2} \tag{4.36}$$

This is as expected from Lusztig-Spaltenstein duality.

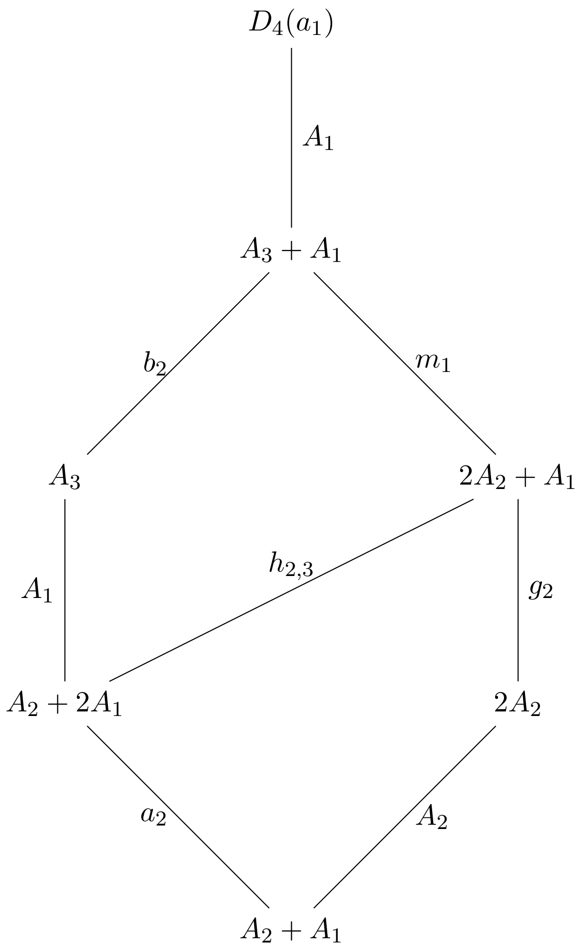

Figure 4.33: The Hasse diagram for $\mathcal{S}^{E_6}_{D_4(a_1),A_2+A_1}$ in the E_6 nilcone with orbits specified by their Bala-Carter labels. This is the same Hasse diagram as for the Coulomb branch of $\mathcal{Q}_{4.33}$. More information regarding the slice $h_{2,3}$, which is called τ in [6], can be found in [9].

4.4.5 Example: E_7

Consider the theory given by $\mathcal{Q}_{4.37}$.

$$\mathcal{Q}_{4.37} = \underset{1}{\circ} - \underset{2}{\circ} - \underset{4}{\circ} = \underset{3}{\circ} \, . \tag{4.37}$$

The Coulomb branch of $Q_{4.37}$ is computed to be the Słodowy intersection $\mathcal{S}^{E_7}_{A_3+A_2+A_1,A_2+2A_1}$ [27, 117]. The Hasse diagram for $\mathcal{S}^{E_7}_{A_3+A_2+A_1,A_2+2A_1}$ is given in Figure 4.34 and matches the Hasse diagram for $\mathcal{C}\left(Q_{4.37}\right)$.

As predicted by Lusztig-Spaltenstein duality, the Higgs branch is the Słodowy intersection $\mathcal{S}^{E_7}_{E_7(a_4),A_4+A_2}$ in the E_7 nilcone. The Hasse diagram for the Higgs branch is shown in Figure 4.35a, which matches $\mathcal{S}^{E_7}_{E_7(a_4),A_4+A_2}$, as can be seen in Figure 4.35b. The Higgs branch Namikawa-Weyl group is $\mathbb{Z}_2 \times \mathbb{Z}_2 \times \mathbb{Z}_2$. The identification of the moduli space is

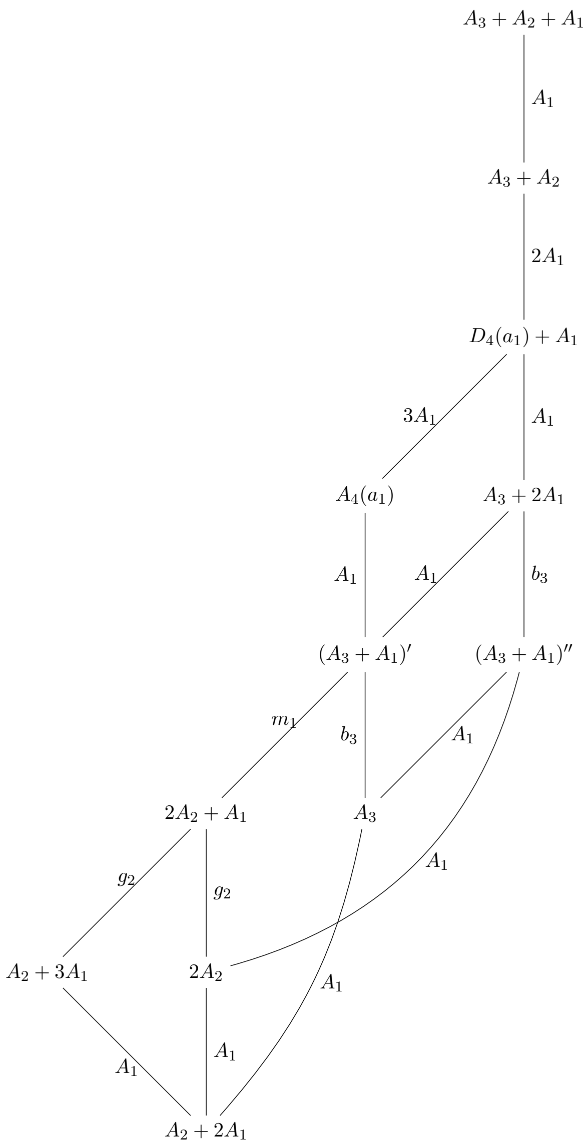

Figure 4.34: The Hasse diagram of $\mathcal{S}^{E_7}_{A_3+A_2+A_1,A_2+2A_1}$ in the E_7 nilcone with orbits specified by their Bala-Carter labels. This is the same Hasse diagram as for the Coulomb branch of $\mathcal{Q}_{4.37}$.

verified via the refined Higgs branch Hilbert series, presented in its unrefined form below.

$$\mathrm{HS}\left[\mathcal{H}(\mathcal{Q}_{4.37})\right] = \frac{\begin{pmatrix} 1 + 2t^4 + 6t^6 + 8t^8 + 12t^{10} + 23t^{12} + 27t^{14} + 25t^{16} \\ + 27t^{18} + 23t^{20} + 12t^{22} + 8t^{24} + 6t^{26} + 2t^{28} + t^{32} \end{pmatrix}}{(1-t^2)^3(1-t^4)^3(1-t^6)^4} \tag{4.38}$$

$$= \mathrm{HS}\left[\mathcal{S}^{E_7}_{E_7(a_4),A_4+A_2}\right]. \tag{4.39}$$

The quivers for the slice between A_5' and $E_7(a_4)$, and for the slice between $D_5(a_1) + A_1$ and $E_7(a_4)$ have the same Hasse diagram, although their moduli spaces are not identical since they have different Hilbert series, calculated from localizaztion. This provides an example of two different spaces with the same Hasse diagram. There are also pairs of quivers without decoration that they share the same Hasse diagram but the Higgs branch

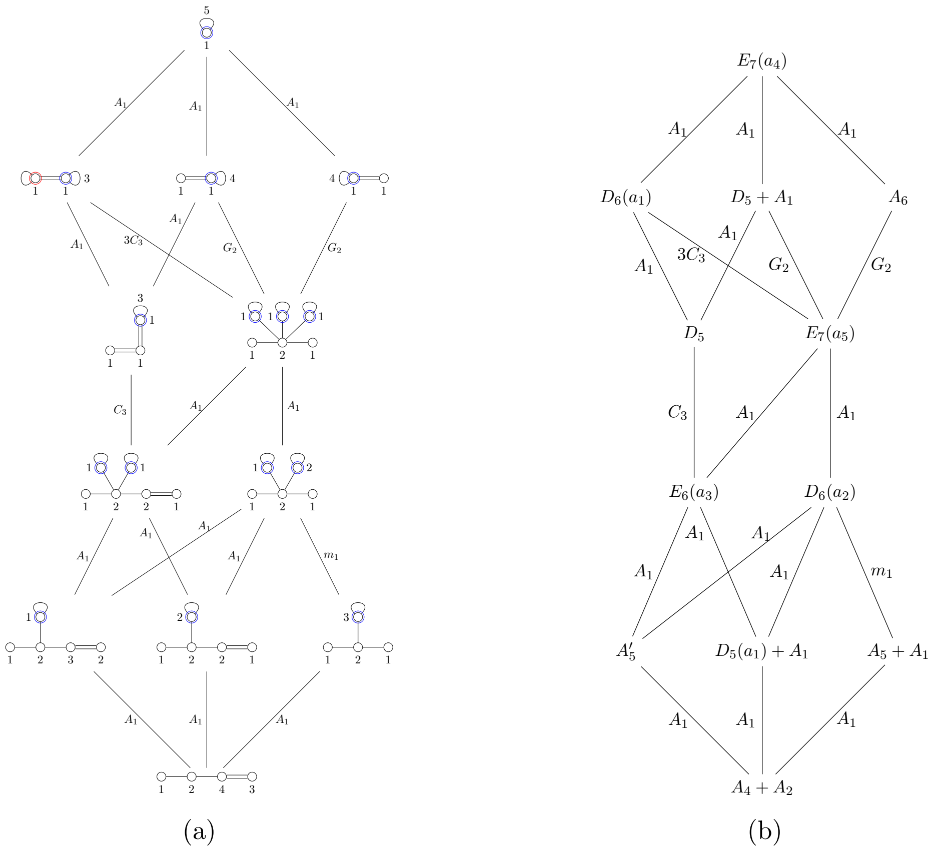

Figure 4.35: (a): The Higgs branch Hasse diagram of $\mathcal{Q}_{4.37}$. (b): The Hasse diagram of $\mathcal{S}^{E_7}_{E_7(a_4),A_4+A_2}$ in the E_7 nilcone with orbits specified by their Bala-Carter labels. This is the same Hasse diagram as Figure 4.35a.

are different [94].

Example: E_7 Again Now consider the following theory:

$$\mathcal{Q}_{4.40} = \quad \text{(quiver)} \quad . \tag{4.40}$$

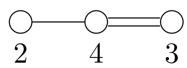

The Coulomb branch Hilbert series of $\mathcal{Q}_{4.40}$ identifies the moduli space as $\mathcal{C}(\mathcal{Q}_{4.40}) = \mathcal{S}^{E_7}_{A_3+A_2+A_1,A_2+3A_1}$ [27]. The Hasse diagram of $\mathcal{S}^{E_7}_{A_3+A_2+A_1,A_2+3A_1}$ is given in Figure 4.36 and matches the Hasse diagram for $\mathcal{C}(\mathcal{Q}_{4.40})$.

The Higgs branch Hasse diagram of $\mathcal{Q}_{4.40}$ is computed as Figure 4.37a. This Hasse diagram matches that of $\mathcal{S}^{E_7}_{A_6,A_4+A_2}$ shown explicitly in Figure 4.37b. The Namikawa-Weyl group of the Higgs branch is identified as $\mathcal{W}_{G_2} = \mathrm{Dih}_6$ of order 12. The unrefined Higgs branch Hilbert series is given below, which (when refined) agrees with that for $\mathcal{S}^{E_7}_{A_6,A_4+A_2}$.

$$\mathrm{HS}\left[\mathcal{H}(\mathcal{Q}_{4.40}\right] = \frac{(1-t^{12})\begin{pmatrix} 1+3t^2+6t^4+13t^6+24t^8+29t^{10}+29t^{12}+29t^{14}+24t^{16}+13t^{18} \\ +6t^{20}+3t^{22}+t^{24} \end{pmatrix}}{(1-t^4)^5(1-t^6)^4}. \tag{4.41}$$

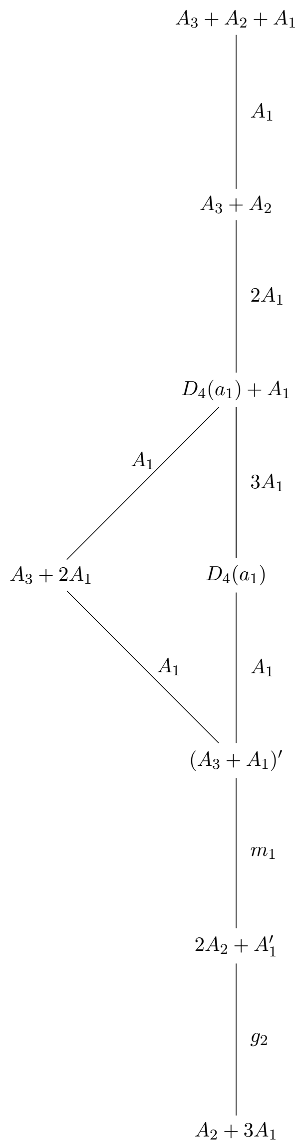

Figure 4.36: The Hasse diagram of $\mathcal{S}^{E_7}_{A_3+A_2+A_1, A_2+3A_1}$ in the E_7 nilcone with orbits specified by their Bala-Carter labels. This is the same Hasse diagram as for the Coulomb branch of $\mathcal{Q}_{4.40}$.

4.4.6 A Family of Quivers with Multiple Adjoint Loops

The one-parameter family of theories labelled by the number of adjoint hypermultiplet loops g given in $\mathcal{Q}_{4.42}$ also arise in the nilcones of simple Lie algebras.

$$\mathcal{Q}_{4.42} = \underset{1}{\bigcirc} \!-\!\!-\!\!-\! \underset{2}{\bigcirc}\!\!\bigcirc\, g \tag{4.42}$$

The Higgs branch Hasse diagram for $\mathcal{Q}_{4.42}$ is shown in Figure 4.38. The Namikawa Weyl group for the Higgs branch is $\mathbb{Z}_2$ in all cases. It is currently not known how to compute the Coulomb branch Hasse diagram for quivers with multiple loops.

Nevertheless, Hilbert series computations may still be performed to identify the moduli spaces of vacua. The identification may be supported additionally with the use of the

Lusztig-Spaltenstein duality for slices in classical and exceptional nilcones, as has been extensively used in the previous examples. In particular slices in $\mathrm{Sp}(k)$ nilcones are Spaltenstein dual to slices in $\mathrm{SO}(2k+1)$ nilcones.

However, some slices in the nilcones of $\mathrm{Sp}(k)$ algebras enjoy a more exotic duality to other slices in the same $\mathrm{Sp}(k)$ nilcone, under the metaplectic Lusztig-Spaltenstein duality [154–156]. This type of duality also has a realisation in string theory from Type IIB brane systems with two $\tilde{O}^+$ orientifold planes [31].

Sp to SO duality. In particular, for $g \geq 2$ the Higgs branch is a Słodowy slice in the C_{g+1} nilcone

$$\mathcal{H}\left(\mathcal{Q}_{4.42}\right) = \mathrm{Norm}\left[\mathcal{S}^{C_{g+1}}_{(3^2,1^{2g-4}),(2,1^{2g})}\right] \tag{4.43}$$

where 'Norm' denotes the normalisation of the singularity.

In fact, for $g \geq 4$ the nilpotent orbit closure $\overline{\mathcal{O}}^{C_{g+1}}_{(3^2,1^{2g-4})}$ is non-normal [10] as is the Słodowy intersection from this orbit to the $\overline{\mathcal{O}}^{C_{g+1}}_{(2,1^{2g})}$.It is convenient to convert the Hilbert series for these one parameter family of moduli spaces to a Highest Weight Generating function (HWG) [157] which is given as

$$\mathrm{HWG}\left[\mathcal{S}^{C_{g+1}}_{(3^2,1^{2g-4}),(2,1^{2g})}\right] = \begin{cases} \mathrm{PE}[\mu_1^2t^2 + \mu_1t^3 + \mu_2^2t^4 + \mu_2t^4 + \mu_1\mu_2t^5 - \mu_1^2\mu_2^2t^{10}] & g=2 \\ \mathrm{PE}[\mu_1^2t^2 + \mu_1t^3 + \mu_3t^3 + \mu_2^2t^4 + \mu_2t^4 + \mu_1\mu_2t^5 - \mu_1^2\mu_2^2t^{10}] & g=3 \\ (1 + \mu_1\mu_2t^5 + \mu_1\mu_3t^6 + \mu_2\mu_3t^7 + \mu_1\mu_2\mu_3t^8 - \mu_1\mu_2\mu_3t^{10}) & \\ \times\, \mathrm{PE}[\mu_1^2t^2 + \mu_1t^3 + \mu_2^2t^4 + \mu_3^2t^6 + \mu_2t^4] & g \geq 4 \end{cases}, \tag{4.44}$$

for the Słodowy intersection and also for its normalisation

$$\mathrm{HWG}\left[\mathrm{Norm}\left[\mathcal{S}^{C_{g+1}}_{(3^2,1^{2g-4}),(2,1^{2g})}\right]\right] = \begin{cases} \mathrm{PE}[\mu_1^2t^2 + \mu_1t^3 + \mu_2^2t^4 + \mu_2t^4 + \mu_1\mu_2t^5 - \mu_1^2\mu_2^2t^{10}], & g=2. \\ \mathrm{PE}[\mu_1^2t^2 + \mu_1t^3 + \mu_3t^3 + \mu_2^2t^4 + \mu_2t^4 + \mu_1\mu_2t^5 - \mu_1^2\mu_2^2t^{10}], & g \geq 3. \end{cases} \tag{4.45}$$

The μ_i are highest weight fugacities for $\mathrm{Sp}(g)$.

Lusztig-Spaltenstein duality predicts that the Coulomb branch is a slice in B_{g+1}. Indeed, $\mathcal{C}\left(\mathcal{Q}_{4.42}\right) = \mathcal{S}^{B_{g+1}}_{(2g+1,1^2),(2g-1,2^2)}$. The HWG is

$$\mathrm{HWG}\left[\mathcal{S}^{B_{g+1}}_{(2g+1,1^2),(2g-1,2^2)}\right] = \mathrm{PE}[\mu^2t^2 + t^4 + \mu t^{2g-1} + \mu t^{2g+1} - \mu^2t^{4g+2}], \quad g \geq 2, \tag{4.46}$$

where μ is a highest weight fugacity for $\mathrm{SU}(2) \simeq \mathrm{Sp}(1)$.

Note the collapse of the partitions for the transposition for the duality. The above results were computed for up to $g = 5$.

Sp to Sp duality. The same moduli spaces may be thought of in a different way which brings to light a metaplectic Lusztig-Spaltenstein duality between the Coulomb and Higgs branches. The Coulomb branch of $\mathcal{Q}_{4.42}$ may also be identified as the following slice in the nilcone of C_g [113],

$$\mathcal{C}\left(\mathcal{Q}_{4.42}\right) = \mathcal{S}^{C_g}_{(2g),(2g-2,1^2)}. \tag{4.47}$$

The Higgs branch may be also be identified as the double cover of the following nilpotent orbit closure in the nilcone of C_g,

$$\mathcal{H}\left(\mathcal{Q}_{4.42}\right)/S_2 = \overline{\mathcal{O}}^{C_g}_{(4,1^{2g-4})}. \tag{4.48}$$

This duality agrees with the metaplectic Lusztig-Spaltenstein duality defined in [156]. The double cover relation can be checked by comparing the volumes of the moduli spaces through the Hilbert series,

$$\mathsf{Vol}\left[\mathcal{H}\left(\mathcal{Q}_{4.42}\right)\right]/\mathsf{Vol}\left[\overline{\mathcal{O}}^{C_g}_{(4,1^{2g-4})}\right] = 2, \tag{4.49}$$

with explicit examples for $g = 2, 3, 4$ shown in Table 4.7.

The HWG for $\overline{\mathcal{O}}^{C_g}_{(4,1^{2g-4})}$ is

$$\mathrm{HWG}\left[\overline{\mathcal{O}}^{C_g}_{(4,1^{2g-4})}\right] = \begin{cases} \mathrm{PE}\left[\mu_1^2t^2 + \mu_2^2t^4 + \mu_1^2t^6 + \mu_2t^4 + \mu_1^2\mu_2t^8 - \mu_1^4\mu_2^2t^{16}\right] & g=2 \\ \left(1 + \mu_1\mu_3t^6 + \mu_1^2\mu_2t^8 + \mu_1\mu_2\mu_3t^8\right)\mathrm{PE}\left[\mu_1^2t^2 + \mu_2^2t^4 + \mu_2t^4 + \mu_1^2t^6 + \mu_3^2t^6\right] & g\geq 3 \end{cases}. \tag{4.50}$$

The S_2 action may be seen at the level of the HWG by the following assignment of S_2 irreps to the terms in the HWG of $\mathcal{H}\left(\mathcal{Q}_{4.42}\right)$ then performing a group average [97],

$$\mathrm{HWG}\left[\mathcal{H}\left(\mathcal{Q}_{4.42}\right)/S_2\right] = \begin{cases} \mathrm{PE}[\mu_1^2t^2 + \epsilon\mu_1t^3 + \mu_2^2t^4 + \mu_2t^4 + \epsilon\mu_1\mu_2t^5 - \mu_1^2\mu_2^2t^{10}], & g=2. \\ \mathrm{PE}[\mu_1^2t^2 + \epsilon\mu_1t^3 + \epsilon\mu_3t^3 + \mu_2^2t^4 + \mu_2t^4 + \epsilon\mu_1\mu_2t^5 - \mu_1^2\mu_2^2t^{10}], & g\geq 3, \end{cases} \tag{4.51}$$

where ϵ denotes the signed representation of S_2 and the trivial representation is not explicitly written.

Quiver/Label	HS	Volume
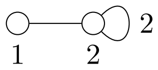	$\frac{(1+t^2)(1+t^2+4t^3+t^4+t^6)}{(1-t^2)^8}$	$\frac{1}{16}$
$\overline{\mathcal{O}}^{C_2}_{(4)}$	$\frac{(1+t^2)(1+t^2+t^4+t^6)}{(1-t^2)^8}$	$\frac{1}{32}$
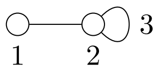	$\frac{(1+t^2)(1+6t^2+20t^3+21t^4+36t^5+56t^6+36t^7+21t^8+20t^9+6t^{10}+t^{12})}{(1-t^2)^{14}}$	$\frac{7}{256}$
$\overline{\mathcal{O}}^{C_3}_{(4,1^2)}$	$\frac{(1+t^2)(1+6t^2+21t^4+56t^6+21t^8+6t^{10}+t^{12})}{(1-t^2)^{14}}$	$\frac{7}{512}$
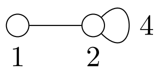	$\frac{(1+t^2)(1+15t^2+56t^3+120t^4+336t^5+680t^6+960t^7+1296t^8+1520t^9+\cdots+t^{18})}{(1-t^2)^{20}}$	$\frac{33}{2048}$
$\overline{\mathcal{O}}^{C_4}_{(4,1^4)}$	$\frac{(1+t^2)(1+15t^2+120t^4+680t^6+1296t^8+1296t^{10}+680t^{12}+120t^{14}+15t^{16}+t^{18})}{(1-t^2)^{20}}$	$\frac{33}{4096}$

Table 4.7: The Hilbert series and volume of the Higgs branch of $\mathcal{Q}_{4.42}$ and the corresponding orbit closure for $g = 2, 3, 4$. The Hilbert series of the orbit closures are firstly computed in [10]. The $\cdots$ denotes a palindromic series.

Note that in this family, the Coulomb branch and Higgs branch have a different number of leaves.

4.4.7 Example: E_8 with Multiloops

The final example arising as a slice in a nilcone is that of $\mathcal{Q}_{4.52}$.

$\mathcal{Q}_{4.52} =$ 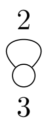 (4.52)

As first shown in [1], the Coulomb branch of $\mathcal{Q}_{4.52}$ is a_2/S_4. The Coulomb branch Hilbert series is computed as

$$\mathrm{HS}\left[\mathcal{C}\left(\mathcal{Q}_{4.52}\right)\right] = \frac{1+2t^6+2t^8+t^{14}}{(1-t^4)^3(1-t^6)}. \tag{4.53}$$

This moduli space is particularly interesting as it has been shown in [103] that a_2/S_4 appears as a slice in the nilcone of E_8, specifically as $\mathcal{S}^{E_8}_{E_8(a_6),E_8(b_6)}$. The Hasse diagram for this slice is given in Figure 4.39. It is currently not possible to make a comparison with the Coulomb branch Hasse diagram of $\mathcal{Q}_{4.52}$ since it is not known how to compute the Coulomb branch Hasse diagram for quivers with multiple adjoint hypermultiplet loops.

Since the Coulomb branch of $\mathcal{Q}_{4.52}$ appears as a slice in E_8 one should expect that the Higgs branch is related to the Spaltenstein dual slice in the nilcone of E_8 up to some factor of $\mathbb{Z}_2$, which may be acting as a quotient or as a cover on this slice. This factor of $\mathbb{Z}_2$ arises due to $\mathcal{Q}_{4.52}$ having two adjoint hypermultiplet loops, which is the same as seen for $\mathcal{Q}_{4.42}$ studied in Section 4.4.6.

In the example at hand, the Higgs branch is the double cover of the Słodowy intersection $\mathcal{S}^{E_8}_{D_4(a_1)+A_2,2A_2+2A_1}$, verified via the refined Hilbert series. For brevity, only the unrefined Hilbert series are presented

$$\mathrm{HS}\left[\mathcal{H}\left(\mathcal{Q}_{4.52}\right)\right] = \frac{\begin{pmatrix} 1+t^2+13t^3+20t^4+29t^5+96t^6+160t^7+188t^8+304t^9+420t^{10}+388t^{11} \\ +388t^{12}+420t^{13}+304t^{14}+188t^{15}+160t^{16}+96t^{17}+29t^{18} \\ +20t^{19}+13t^{20}+t^{21}+t^{23} \end{pmatrix}}{(1-t^2)^9(1-t^3)^7} \tag{4.54}$$

$$\mathrm{HS}\left[\mathcal{S}^{E_8}_{E_8(a_6),E_8(b_6)}\right] = \frac{\begin{pmatrix} 1+5t^2+13t^3+25t^4+61t^5+131t^6+229t^7+413t^8+655t^9+973t^{10} \\ +1381t^{11}+1785t^{12}+2157t^{13}+2490t^{14}+2641t^{15}+2641t^{16}+2490t^{17} \\ +2157t^{18}+1785t^{19}+1381t^{20}+973t^{21}+655t^{22}+413t^{23}+229t^{24}+131t^{25}+ \\ 61t^{26}+25t^{27}+13t^{28}+5t^{29}+t^{31} \end{pmatrix}}{(1-t^2)^5(1-t^3)^7(1-t^4)^4}, \tag{4.55}$$

from which it is clear to see that

$$\frac{\mathsf{Vol}\left[\mathcal{H}\left(\mathcal{Q}_{4.52}\right)\right]}{\mathsf{Vol}\left[\mathcal{S}^{E_8}_{E_8(a_6),E_8(b_6)}\right]} = \lim_{t\to 1} \frac{\mathrm{HS}\left[\mathcal{H}\left(\mathcal{Q}_{4.52}\right)\right]}{\mathrm{HS}\left[\mathcal{S}^{E_8}_{E_8(a_6),E_8(b_6)}\right]} = 2, \tag{4.56}$$

indicating that $\mathcal{H}\left(\mathcal{Q}_{4.52}\right)$ is the double cover of $\mathcal{S}^{E_8}_{D_4(a_1)+A_2,2A_2+2A_1}$.

The Higgs branch Hasse diagram is computed as Figure 4.40a. As predicted by Lusztig-Spaltenstein duality, the Coulomb branch is the Słodowy intersection $\mathcal{S}^{E_8}_{E_8(a_6),E_8(b_6)}$, with corresponding Hasse diagram given in Figure 4.40b. The Higgs branch Namikawa-Weyl group is trivial as there is no codimension 1 slice. The top slice of Figure 4.40a is $a_3 = d_3$ and under a $\mathbb{Z}_2$ quotient this top slice breaks into two, A_1 then b_2 as seen in Figure 4.40b. This phenomenon has been observed in the study of $6d$ $\mathcal{N} = (1,0)$ Higgs branches using magnetic quivers, in particular those theories that have an F-theory description involving the collapse of a (-2)-curve [54, 55, 58, 89, 90].

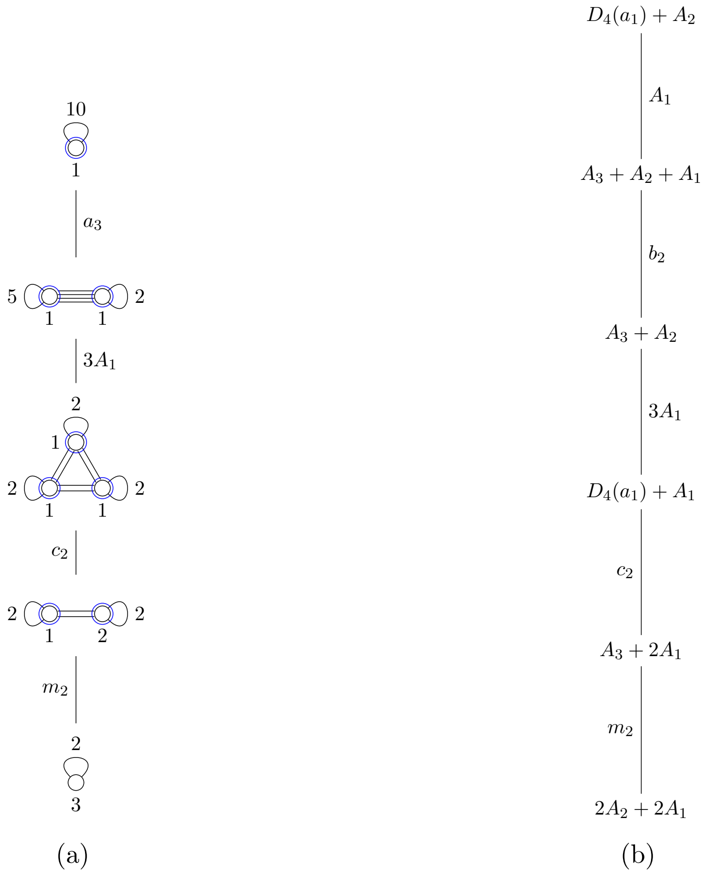

Figure 4.40: (a): Higgs branch Hasse diagram of (4.52), which equals the double cover of $\mathcal{S}^{E_8}_{D_4(a_1)+A_2,2A_2+2A_1}$. (b): Hasse diagram of $\mathcal{S}^{E_8}_{D_4(a_1)+A_2,2A_2+2A_1}$ with orbits specified by their Bala-Carter labels.

Quiver	Coulomb Branch	Higgs Branch	Checked with HS?
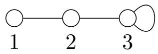	$\overline{sub.reg.G_2}$	$\mathcal{S}^{G_2}_{\mathcal{N},A_1}$	✓
	$\mathcal{S}^{F_4}_{F_4(a_3),\tilde{A}_2}$	$\mathcal{S}^{F_4}_{B_2,\tilde{A}_2+A_1}$	✓
	$\mathcal{S}^{E_6}_{D_4(a_1),2A_2}$	$\mathcal{S}^{E_6}_{D_4,2A_2+A_1}$	✓
	$\mathcal{S}^{E_7}_{D_4(a_1),A_2+3A_1}$	$\mathcal{S}^{E_7}_{A_6,A_5+A_1}$	✓
	$\mathcal{S}^{E_7}_{D_4(a_1),2A_2}$	$\mathcal{S}^{E_7}_{D_5+A_1,A_5+A_1}$	✓
	$\mathcal{S}^{E_7}_{E_7(a_5),A_5''}$	$\mathcal{S}^{E_7}_{D_4,2A_2+A_1}$	✓
	$\mathcal{S}^{E_8}_{E_8(b_5),E_6}$	$\mathcal{S}^{E_8}_{D_4,2A_2+A_1}$	
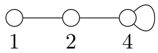	$\mathcal{S}^{F_4}_{F_4(a_3),A_1+\tilde{A}_1}$	$\mathcal{S}^{F_4}_{F_4(a_2),A_2+\tilde{A}_1}$	✓
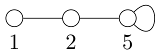	$\mathcal{S}^{E_8}_{E_8(a_7),A_4+A_2}$	$\mathcal{S}^{E_8}_{D_5+A_2,A_4+A_3}$	
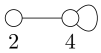	$\mathcal{S}^{F_4}_{F_4(a_3),A_2}$	$\mathcal{S}^{F_4}_{B_3,A_2+\tilde{A}_1}$	✓
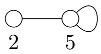	$\mathcal{S}^{E_8}_{E_8(a_7),A_4+A_2+A_1}$	$\mathcal{S}^{E_8}_{A_6+A_1,A_4+A_3}$	
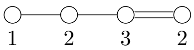	$\overline{\mathcal{O}}^{B_3}_{(3^2,1)}$	$\mathcal{S}^{C_3}_{\mathcal{N},(2^3)}$	✓
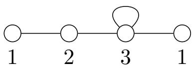	$\mathcal{S}^{E_6}_{D_4(a_1),A_2+A_1}$	$\mathcal{S}^{E_6}_{D_5(a_1),2A_2+A_1}$	✓
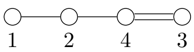	$\mathcal{S}^{E_7}_{A_3+A_2+A_1,A_2+2A_1}$	$\mathcal{S}^{E_7}_{E_7(a_4),A_4+A_2}$	✓
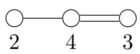	$\mathcal{S}^{E_7}_{A_3+A_2+A_1,A_2+3A_1}$	$\mathcal{S}^{E_7}_{A_6,A_4+A_2}$	✓
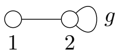	Norm $\left[\mathcal{S}^{C_{g+1}}_{(3^2,1^{2g-4}),(2,1^{2g})}\right]$	$\mathcal{S}^{B_{g+1}}_{(2g+1,1^2),(2g-1,2^2)}$	✓
	$\mathcal{S}^{C_g}_{(2g),(2g-2,1^2)}$	S_2 cover of $\overline{\mathcal{O}}^{C_g}_{(4,1^{2g-4})}$	✓
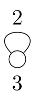	$\mathcal{S}^{E_8}_{E_8(a_6),E_8(b_6)}$	S_2 cover of $\mathcal{S}^{E_8}_{D_4(a_1)+A_2,2A_2+2A_1}$	✓

Table 4.8: Summary of unitary quivers studied here whose moduli spaces of vacua are slices in nilcones. The slices in E_8 remains unchecked due to the computational complexity of the Hilbert series.

4.5 Outlook

The algorithm presented in this work successfully determines the Higgs branch Hasse diagram for a wide variety of unitary 3d $\mathcal{N} = 4$ quiver gauge theories, and the techniques admit extensions to various families of more exotic quivers. For instance, it would be interesting to augment the algorithm in this paper such that it includes non-simply-laced unitary theories, alongside developing a similar algorithm for orthosymplectic quivers. Given the successes of the Coulomb and Higgs branch subtraction algorithms used to determine the moduli space for theories with 8 supercharges, it may be time to turn to theories with less supersymmetry where the moduli spaces of vacua are less constrained and much more difficult to study. Other extensions include a subtraction algorithm for the Higgs branch of a theory with non-general values of FI deformations.

A slightly different point of view may consider the implications of the monodromies present in this work to theories in six-dimensions; for instance, it would be interesting to consider whether such global data can be seen from F-theory constructions and whether there is a similar global structure around the tensor branch.

Slightly more in keeping with the focus of this paper, it would be interesting to sharpen current understanding of the effect of changing $\mathrm{U}(n)$ gauge nodes to $\mathrm{SU}(n)$ on the Higgs branch. Previous work on this matter includes [44], wherein the $\mathrm{SU}(n)$ nodes open up a d_k transition.

The question of whether a slice can be defined globally also remains unsettled. As already mentioned, a neighbourhood of any point in a given symplectic singularity decomposes as a product of a neighbourhood of the leaf through the point and a neighbourhood of the origin of the slice. In some cases the slice is not just defined in a neighbourhood, but as a subset of the whole symplectic singularity. Słodowy intersections and slices in affine Grassmanians are such examples. Globally a slice within the Słodowy intersections can be defined as the intersection of a transverse slice and an orbit. In the case of affine Grassmanian slices, a slice in the Hasse diagram is defined again as the intersection of some (infinite dimensional) transverse space and some orbit. These are two examples where a slice can be globally defined. It thus remains a question as to the conditions under which such a global definition is available for an arbitrary symplectic singularity.

The decoration on Higgs and Coulomb branch can be used to generalise the notion of “special" and “non-special" to the symplectic singularity outside of nilcone and predict the symplectic duality of the slices. This will be discussed in the future papers.

Further, the field theory description of the decorated quiver remains unexplored.

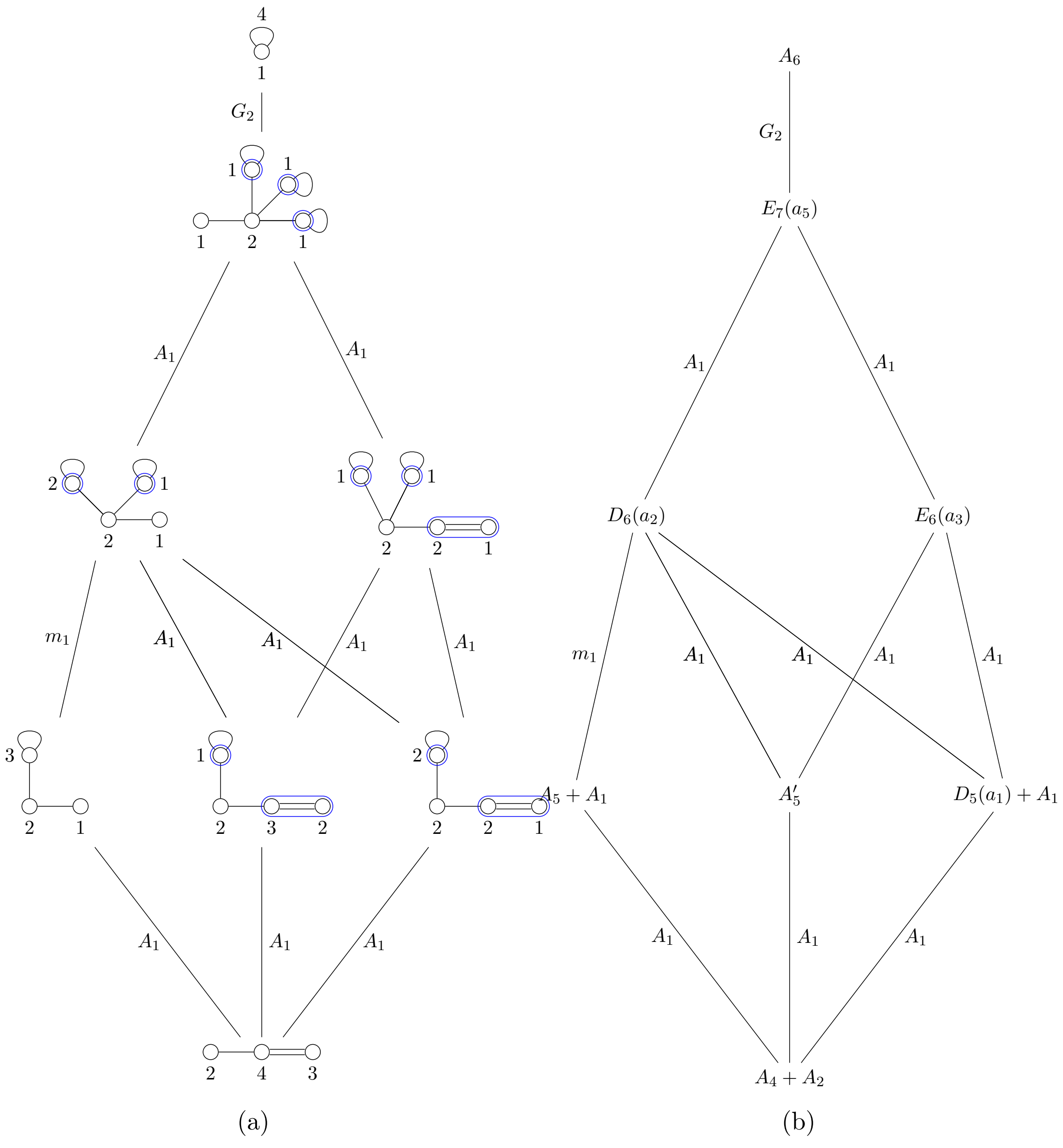

Figure 4.37: (a): The Higgs branch Hasse diagram of $\mathcal{Q}_{4.40}$. (b): The Hasse diagram of $\mathcal{S}^{E_7}_{A_6,A_4+A_2}$ in the E_7 nilcone with orbits specified by their Bala-Carter labels. This is the same Hasse diagram as in Figure 4.37a.

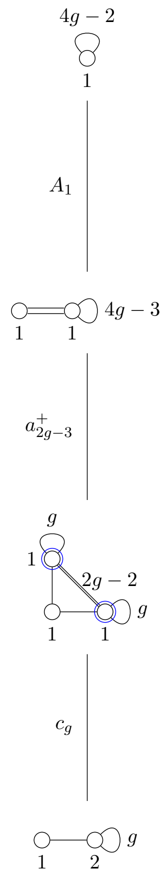

Figure 4.38: The Higgs branch Hasse diagram of the one-parameter family of quivers $\mathcal{Q}_{4.42}$.

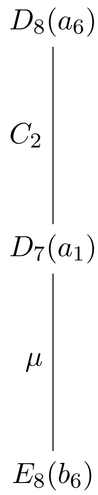

Figure 4.39: The Hasse diagram of $\mathcal{S}^{E_8}_{E_8(a_6),E_8(b_6)}$ in the E_8 nilcone with orbits specified by their Bala-Carter labels. Where μ is a non-normal slice with normalisation A_3 as explained in [1, 6].

Chapter 5

Conclusions and outlook

Although the conclusions and outlook are included in separate chapters, here they are summarized, and some other outlook directions are also briefly discussed here.

The realm of moduli spaces of vacua is large, and this work only focused on a relatively small part of it. The main results of this thesis have two parts.

On one hand, actions on two quivers furnish orbifold relations between their Coulomb branches. The operation is realized by diagrammatic techniques of merging several U(1) gauge nodes into a single gauge node, and of turning simply laced edges into multiiple laced edges. In computation, two tools are utilized: the generalized Molien sum of the monopole formula, and the Abelianization process. All the operations combines nicely to explain why the orbifolding operation on the Coulomb branch can be realized by the diagramatic operation on quivers.

On the other hand, the quiver subtraction on the Higgs branch provides a bottom to up derivation of the Hasse diagram of the Higgs branch. The minimal transitions, global structure of monodromies, and the Namikawa Weyl group can be read off from the subtraction process. All minimal Higgsing patterns are summarized into three rules.

There are still a lot of interesting questions that remain to be solved following the two works. Firstly, it used to be challenging to study the stratification of Coulomb branch of quivers with g adjoint loops since it needs to deal with complicated symmetric products. But now the work sheds some light on the problem since the Abelianization procedure provides a way to directly write down the relations between the chiral ring generators. It is also interesting to come up with a criteria of what quivers are orbifolds of flat spaces. This is interesting because many moduli spaces end up being orbifolds of flat spaces by reflection groups. Secondly, it remains a big problem to define the Higgs branches of non-simply laced quivers and study their stratification. It is also worth mentioning the question of stratification for the moduli space of theories with less supersymmetry. The difficulty is F-flat spaces are not always a complete intersection, i.e. F-term equations can have syzygies and not necessarily transform in the adjoint representation, which is different from the case of 8 supercharges. The physical explanation of the monodromy on the Higgs branch remains to be explored. Whether the slice can be defined in a global sense is also a difficult question to answer.

With all the tools introduced in the thesis, there are also further questions to be answered. Analytic structures in the refined Hilbert series related with different Higgsing patterns are interesting to analyze. It is previously understood that when the flavor symmetry is broken by vev, the Hilbert series is given by a residue calculation. But it is also possible that after Higgsing the flavor symmetry doesn't change, and in this case there is a pole in Hilbert series of order higher than 1. This happens when a vev is assigned to a GIO with R charge higher than 2. This structure also sheds light on a recipe for calculating Hilbert series for decorated quivers. It is also expected that whenever non-flavor Higgsing is happening, different leaves in the Coulomb branches are dual to the same slice in the Higgs branch, and vice versa. There are also other interesting future directions to work on. For example, a quiver subtraction algorithm for O/Sp quivers can be worked out in a similar way by analyzing the Higgsing patterns.

Another interesting question is the (compactified) moduli space of instantons on ALE spaces. The quivers for those moduli spaces are affine Dynkin quivers with framing on it, and can be realized by brane construction and T-duality. Those spaces are recently termed as double affine Grassmanians in literature. But it remains a question how to understand the local transitions from the 4d gauge theory point of view. The case for $\mathbb{C}^2$ are studied in previous work, where the local singularities correspond to small instanton transitions and colliding two small instantons. But for (blow-ups of) singular 4d spacetime, it is expected that when moving instantons onto the spacetime singularity, the corresponding local transition in the moduli space should be the same type as the spacetime singularity. However by applying the subtraction algorithm, it's found that there are local transitions that cannot be explained in those ways. From the 3d gauge theory viewpoint, as in the affine Grassmanian case, a generating Hilbert series for the infinite-dimensional slice is also expected. But as different from the quivers for affine Grassmanians, non-flavor Higgsing can happen for double affine Grassmanians.

With all those tools on magnetic quivers and 3d mirror symmetry, a physically interesting question is to study the moduli space geometry of 6d $\mathcal{N} = (1, 0)$ SCFT's. The classification of 6d SCFT's is based on F-theory, combining the elliptic fibred CY3 and anomaly conditions, in a way to represent the theory like a quiver. Many of 6d $\mathcal{N} = (1, 0)$ theories have a brane realization and thus a magnetic quiver. So previously mentioned techniques can be used to study their moduli space. But it's unnatural to expect any theory has a magnetic quiver description. So although their moduli spaces are also symplectic singularities, new techniques should be developed to study them due to the lack of a magnetic quiver.

It's also exciting to study generalized symmetries related to a quiver gauge theory, and their relation to moduli spaces. An example is the minimal orbit a_n which is the Coulomb branch of the affine A_n quiver. A $\mathbb{Z}_{n+1}$ symmetry can be gauged to get a $\mathbb{Z}_{n+1}$ 1-form symmetry. This changes the Coulomb branch to $a_n/\mathbb{Z}_{n+1}$ where the action is free, thus resulting in an isolated singularity. It remains to be explored whether the generalized symmetries can be seen directly from the moduli spaces or stacks.

Chapter 6

Appendices

6.1 Monopole formula

The Coulomb branch chiral ring operators are monopole operators dressed by complex scalars in the vector multiplet. The Hilbert series counts those dressed monopole operators, graded by their conformal dimension. A bare monopole operator is labelled by its magnetic charge $m \in \mathrm{Hom}(\mathrm{U}(1), G) = \Lambda_\omega^{G^\vee}$, which is the coweight lattice of the gauge group G. For gauge group G and hypermultiplet representation $\mathcal{R}$, the conformal dimension is given by [22, 82–84]

$$\Delta(m) = -\sum_{\alpha \in \Phi^+} |\langle \alpha, m \rangle| + \frac{1}{4} \sum_{\omega_i \in \mathcal{R}} |\langle \omega_i, m \rangle|. \tag{6.1}$$

The set of positive roots α of the algebra $\mathfrak{g}$ are denoted by Φ^+, and the ω_i are the weights for the matter representation $\mathcal{R}$ for the hypermultiplets. If the representation $\mathcal{R}$ is polarizable, $\mathcal{R} = \mathcal{N} \oplus \bar{\mathcal{N}}$, then the conformal dimension simplifies to

$$\Delta(m) = -\sum_{\alpha \in \Phi^+} |\langle \alpha, m \rangle| + \frac{1}{2} \sum_{\omega_i \in \mathcal{N}} |\langle \omega_i, m \rangle|. \tag{6.2}$$

Then the refined Hilbert series is given by:

$$\mathrm{HS}(z, t) = \sum_{m \in \Lambda_\omega^{G^\vee} / \mathcal{W}_G} z^{J(m)} t^{2\Delta(m)} P_G[G_m](t)\,. \tag{6.3}$$

Here t is a fugacity for R-charge, and z is a fugacity for counting topological quantum numbers $J(m)$. There is a dressing factor, $P_G[G_m](t)$, accounting for the dressing of the monopole operators by the complex scalar in the vector multiplet, and it depends on the residual gauge group G_m that is unbroken by the magnetic charges. The dressing factor is counting Casimir invariants of the unbroken gauge group G_m.

Weyl chamber and dressing factor. Here detailed explanation of the role of Weyl chamber and the dressing factor $P_G[G_m](t)$ is given, since this is where the S_n is acting in the monopole formula.

The principal Weyl chamber for $\mathrm{U}(n)$ in $\mathcal{Q}_{3.3b}$ can be taken as $\{m_1 \geq \cdots \geq m_n\}$ in $\mathbb{R}^n$. This is S_n quotient on $\mathbb{R}^n$, the principal Weyl chamber for $\mathrm{U}(1)^n$ in $\mathcal{Q}_{3.3a}$. The magnetic lattice that is summed over is the intersection of principal Weyl chamber with $\mathbb{Z}^n$.

The principal Weyl chamber is viewed as a polyhedral cone, as in [19, 158]. One can decompose the principal Weyl chamber σ into a union of loci,

$$\sigma = \bigcup_i \sigma_i \tag{6.4}$$

The summation over magnetic lattice in (6.3) is a summation over all the loci $\sigma_i \cap \mathbb{Z}^n$. Each locus is fixed by a subgroup of the Weyl group $\mathcal{W}_G$ and gives a pattern of breaking of the gauge group.

For a given magnetic charge m, the unbroken gauge group G_m is a subgroup of G which commute with the magnetic charges m. The whole Weyl group of G is also broken to the Weyl group of G_m, denoted by $\mathcal{W}_m$. The Weyl group of G_m, $\mathcal{W}_m$, is just the subgroup of $\mathcal{W}_G$ that fixes the locus σ_i that m lives in.

The complex scalars of the unbroken gauge group G_m combines into Casimirs, giving the ring $\mathbb{C}[\mathfrak{g}_m]^{G_m} = \mathbb{C}[\mathfrak{h}_m]^{\mathcal{W}_m}$, whose Hilbert series gives the dressing factor and the calculation is explained in next appendix. This $\mathcal{W}_m$ action on the $\mathbb{C}[\mathfrak{h}_m]$ justifies the action on the dressing factor that were used in the main context.

Notice that the dressing factors $P_G[G_m](t)$ have the same order of pole at $t = 1$. The residue at $t = 1$ is related by a factor of $1/|\mathcal{W}_m|$, since it only counts $\mathcal{W}_m$ invariant polynomials. It immediately follows that the volumes of the Coulomb branches of quivers $\mathcal{Q}_{3.3b}$ and $\mathcal{Q}_{3.3a}$ are related by an $|S_n|$ quotient, as a consistentency check of (3.5).

6.2 Molien sum

The Molien sum is used to compute the Hilbert series of an orbifold V/Γ, where V is a n-dim module of discrete group Γ, i.e. a n-dim complex vector space with Γ acting on with certain representation:

$$\mathrm{HS} = \frac{1}{|\Gamma|} \sum_{\gamma \in \Gamma} \frac{1}{\det(1 - \gamma \cdot t)}. \tag{6.5}$$

To explain this formula, recall the orthogonality of characters, i.e. the sum of characters of any non-trivial irrep of Γ is zero:

$$\frac{1}{|\Gamma|} \sum_{\gamma \in \Gamma} \chi(\gamma) = \begin{cases} 1 & \text{if } \gamma \text{ in trivial irrep} \\ 0 & \text{if } \gamma \text{ in non-trivial irrep} \end{cases} \tag{6.6}$$

For any $\gamma \in \Gamma$, there exists a basis $(x_1, \ldots, x_n)$ of V that diagonalises γ, such that $\gamma = \mathrm{diag}(\gamma_1, \ldots, \gamma_n)$ under this basis. The Molien sum is independent of basis. The basis of the space of polynomials $\prod_{d=0}^{\infty} Sym^d(V)$ can be encoded into a formal series:

$$\frac{1}{(1-x_1)\cdots(1-x_n)} \tag{6.7}$$

The element γ acts on this series as:

$$\frac{1}{(1-x_1)\cdots(1-x_n)} \quad \xrightarrow{\gamma} \quad \frac{1}{(1-\gamma_1 x_1)\cdots(1-\gamma_n x_n)}. \tag{6.8}$$

If x_i is set to $x_i = t$, the coefficient of t^d is the character of γ on $Sym^d(V)$:

$$\frac{1}{(1-\gamma_1 t)\cdots(1-\gamma_n t)} = \sum_{d=0}^{\infty} \chi_d(\gamma) t^d. \tag{6.9}$$

Now the sum over the group Γ is performed, only the trivial rep will remain and each copy of trivial rep will contribute one to the coefficients. One can see from Molien sum, the result is exactly the Hilbert series:

$$\begin{aligned}
\frac{1}{|\Gamma|}\sum_{\gamma\in\Gamma}\frac{1}{\det(1-\gamma\cdot t)} &= \frac{1}{|\Gamma|}\sum_{\gamma\in\Gamma}\frac{1}{(1-\gamma_1 t)\dots(1-\gamma_n t)} \\
&= \frac{1}{|\Gamma|}\sum_{\gamma\in\Gamma}\sum_{d=0}^{\infty}\chi_d(\gamma)t^d \\
&= \sum_{d=0}^{\infty}\dim\left((Sym^d(V))^{\Gamma}\right)t^d \\
&= \mathrm{HS}.
\end{aligned} \tag{6.10}$$

The Molien sum can be generalised for any variety with Γ acting on it:

$$\begin{aligned}
\mathrm{HS} &= \frac{1}{|\Gamma|}\sum_{\gamma\in\Gamma}\mathrm{HS}_0^{\gamma} \\
&= \frac{1}{|\Gamma|}\sum_{\gamma\in\Gamma}\sum_{d=0}^{\infty}\chi_d(\gamma)t^d,
\end{aligned} \tag{6.11}$$

where HS_0^{γ} is the Hilbert series of the original variety refined with respect to the action of $\gamma \in \Gamma$ and $\chi_d(\gamma)$ is the character of γ in the vector space spanned by polynomials of degree d. See [97] for more examples. The key of Molien sum is using the orthogonality property of characters to throw away any terms transforming non-trivially under Γ, so that the remaining terms are invariant under the action of Γ. Note that the Molien sum is representation dependent. The same logic can be extend to continuous group, for example, the Weyl integral for Lie groups.

6.3 Outer S_4 action on a_2

In this section the S_4 action on the ring of a_2 following [103] is discussed. The ring can be expressed as a 3×3 complex matrix $M \in \mathrm{SL}(3,\mathbb{C})$ with conditions traceless and the rank no greater than 1: $\mathbb{C}[M^i_j]/\langle \mathrm{Tr}(M) = 0,\ \mathrm{rk}(M) \leq 1\rangle$, with $i, j = 1, 2, 3$. We can also use an alternative choice of coordinates by set $M^i_j = x_i y_j$: $\mathbb{C}[x_i y_j]/\langle x_1y_1 + x_2y_2 + x_3y_3 = 0\rangle$, with $i, j = 1, 2, 3$. This set of coordinates automatically impose the condition of $\mathrm{rk}(M) \leq 1$. In the matrix form:

$$\begin{pmatrix} x_1y_1 & x_1y_2 & x_1y_3 \\ x_2y_1 & x_2y_2 & x_2y_3 \\ x_3y_1 & x_3y_2 & x_3y_3 \end{pmatrix}. \tag{6.12}$$

The action of $S_4 = \mathbb{Z}_2^2 \rtimes S_3$ are generated by the action of S_3 together with the action of $\mathrm{Klein}_4 = \mathbb{Z}_2^2$. Start with the action of Klein_4, which is a subgroup of $\mathrm{SL}(3,\mathbb{C})$:

$$(x_1, y_1) \to (-x_1, -y_1),\ (x_2, y_2) \to (-x_2, -y_2),\ (x_3, y_3) \to (-x_3, -y_3). \tag{6.13}$$

It is easy to see that there are only two independent $\mathbb{Z}_2$ actions on the ring of a_2, for example, the $(x_1, y_1) \to (-x_1, -y_1)$ together with $(x_2, y_2) \to (-x_2, -y_2)$ can be composed to $(x_3, y_3) \to (-x_3, -y_3)$. The fundamental invariants under this action (after eliminating with the relation) are $x_i y_i$ and $x_i^2 y_j^2$ where $i \neq j$. We have the induced relations by requiring the following matrix has rank no greater than 1 (any 2×2 sub-matrix has zero determinant):

$$\begin{pmatrix} x_1^2y_1^2 & x_1^2y_2^2 & x_1^2y_3^2 \\ x_2^2y_1^2 & x_2^2y_2^2 & x_2^2y_3^2 \\ x_3^2y_1^2 & x_3^2y_2^2 & x_3^2y_3^2 \end{pmatrix}. \tag{6.14}$$

Now let us look at the S_3 action, which is not a subgroup of $\mathrm{SL}(3,\mathbb{C})$. Here the invariants under Klein_4 are labelled as $\alpha_i = x_{i+1}y_{i+1} - x_{i-1}y_{i-1}$, $\beta_i = x_i^2 y_{i-1}^2$ and $\gamma_i = x_{i-1}^2 y_i^2$. The action of S_3 is:

$$\alpha_i \to \alpha_{\sigma(i)},\ \beta_i \to \beta_{\sigma(i)},\ \gamma_i \to \gamma_{\sigma(i)}. \tag{6.15}$$

Combine these two actions (6.13) and (6.15), there is the action of S_4 on a_2. We call it outer S_4 since it is not a subgroup of $\mathrm{SL}(3,\mathbb{C})$ but belongs to its outer-automorphism. One can examine it and find consistency with the action in Section 3.5.4.

6.4 Higgs Branch Subtraction Cheat Sheet

It merits repeating that the local rules, introduced in Section 4.2, gives partial information regarding the slice associated to a given subtraction. This is of course a result of a monodromy and is a global effect. In section 4.3.3, the question of monodromy (which on the quiver is drawn as a decoration) was addressed at length, alongside a prescription for applying decorations to quivers on the Higgs branch Hasse diagram.

The steps below give a quick summary of the the Higgs branch subtraction algorithm.

Generic examples may contain further complexities (the likes of which are described in the main text) and hence this cheat sheet is only intended to indicate the standard approach.

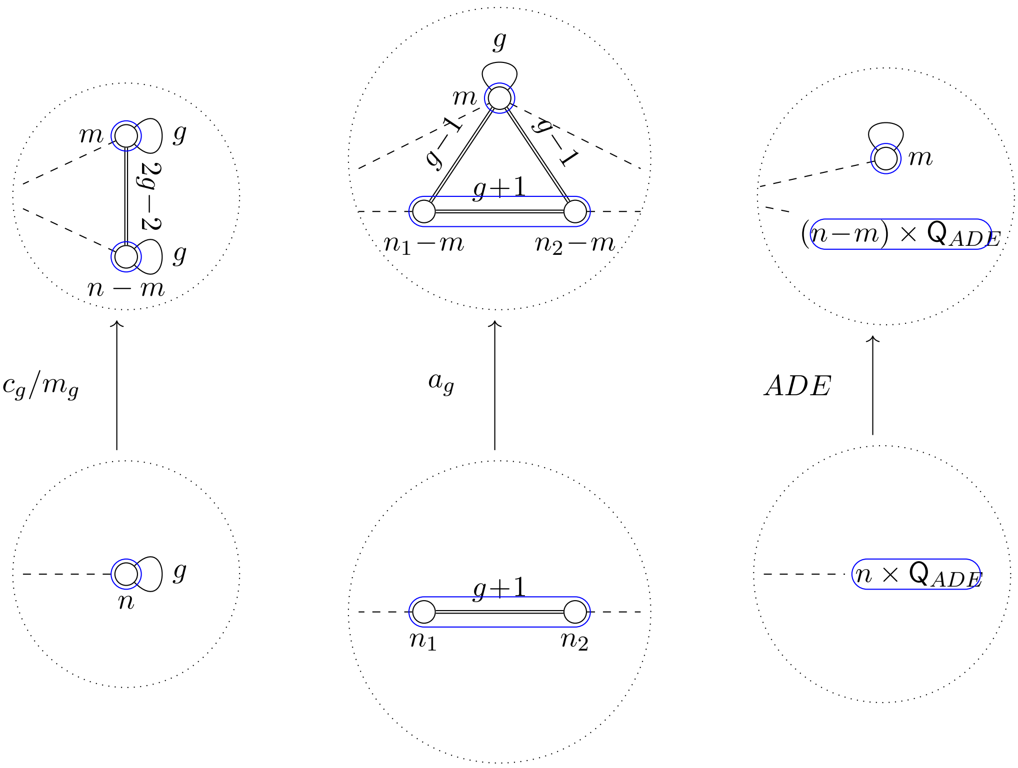

Figure 6.1: A reproduction of Figure 4.11. Recall that the decorations on the bottom row of quivers, although formally trivial, are applied before the subtraction step such that the subtraction products "inherit" the decoration from the initial nodes.

1. Scan the quiver for a sub-quiver that admits a Higgsing via Rules 1, 2 or 3. If such a sub-quiver exists, and is not already entirely decorated, apply a decoration.
2. Using Figure 6.1, apply the appropriate rule to the decorated sub-quiver, whose subtraction products will inherit the decoration as shown.

The process described above is the most consistent way to think about the Higgs branch subtraction process. Of course, given the identification of Figure 4.10, the decorations on the bottom row of Figure 6.1 can strictly be omitted — their inclusion serves only as a reminder that decorations are considered to be "inherited" under subtraction.

6.5 One Example to Rule Them All

The example in Figure 6.2 uses all the features of the subtraction algorithm introduced in this paper, including Rules 1, 2, and 3, multiple loops, decoration of nodes, merging of decorations, unions of cones, and non-trivial monodromy. The example is included to indicate the level of complexity that often arises in the course of Higgs branch quiver subtraction. The following will go through the transitions step-by-step. Note that since the algorithm proceeds from the bottom up, 'the nth row' counts from the bottom.

- In the first step, either the U(3) node or the U(2) node can be split using Rule 1, giving m_1 and c_1 transitions respectively. The associated monodromies are tracked via the introduction of red and blue decorations.

- For the quiver with blue decoration in the second row, the only transition that is permitted is to break the node of rank 3 into two nodes of ranks 1 and 2 under Rule 1. Since the node of rank 3 is initially undecorated, a red decoration is introduced on the products, as seen in the third row.

- The quiver with a red decoration on the second row sees two transitions. The c_1 transition simply comes from splitting the decorated node of rank 2 into two nodes of rank 1 under Rule 1. Since the node undergoing the splitting is initially decorated, no new decoration is imposed. The A_1 transition arises from the subtraction of a subdiagram of affine A_1 under Rule 2 or Rule 3.

- The third row contains three quivers. The quiver with green decoration admits only one transition, which under Rule 1 splits the node of rank 2 into two nodes of rank 1 (inheriting both the decoration and loops). The quiver in the middle of the third row similarly admits a transition under Rule 1, splitting the node of rank 2 into two nodes of rank 1. In this case, since the node of rank 2 is initially undecorated, a new decoration is picked up. The quiver in the third row with both red and blue decorations has two possible transitions, the first of which (under Rule 1) has the same result as the transition just mentioned. The other possible transition uses Rule 3 and the blue and red decorations merge to form a green decoration.

- The leftmost quiver in the fourth row has six possible subtractions of an affine A_1 quiver with one node decorated red and the other blue under Rule 3. This multiplicity is reflected in the slice $6A_1$. The rightmost quiver in the fourth row has two transitions, the first of which (giving a slice c_1) comes from the application of Rule 2 to the node of rank 2. The other transition results from applying Rule 3 to affine A_1 sub-quiver spanned by the nodes with blue and green decorations.

- The fifth row contains two quivers, the leftmost of which sees three Rule 3 transitions. The rightmost quiver undergoes a transition under Rule 1 to split the node of rank 2 into two nodes of rank 1, each inheriting the original red decoration.

- The sixth row contains three quivers, the leftmost of which sees the Rule 3 transitions $2A_1$ and a_3^+. The former arises with multiplicity 2 since the two green nodes are decorated under the same decoration, while the latter is a subtraction of the affine A_3 quiver with loops defined by the green decorated nodes. The central quiver has three Rule 3 transitions, with the a_3 slice arising from an affine A_3 subtraction along the two rank 1 nodes with four bifundamental hypers between them. The rightmost quiver has only one a_3 transition of multiplicity 2, arising from an affine A_3 subtraction on each of the two decorated nodes.

- The seventh row contains two quivers, each of which see a single a_5 transition under Rule 3.

- The eighth row contains a single quiver which sees one a_3 transition under Rule 3 on account of the four hypermultiplets in the bifundamental representation of the two rank 1 gauge nodes.

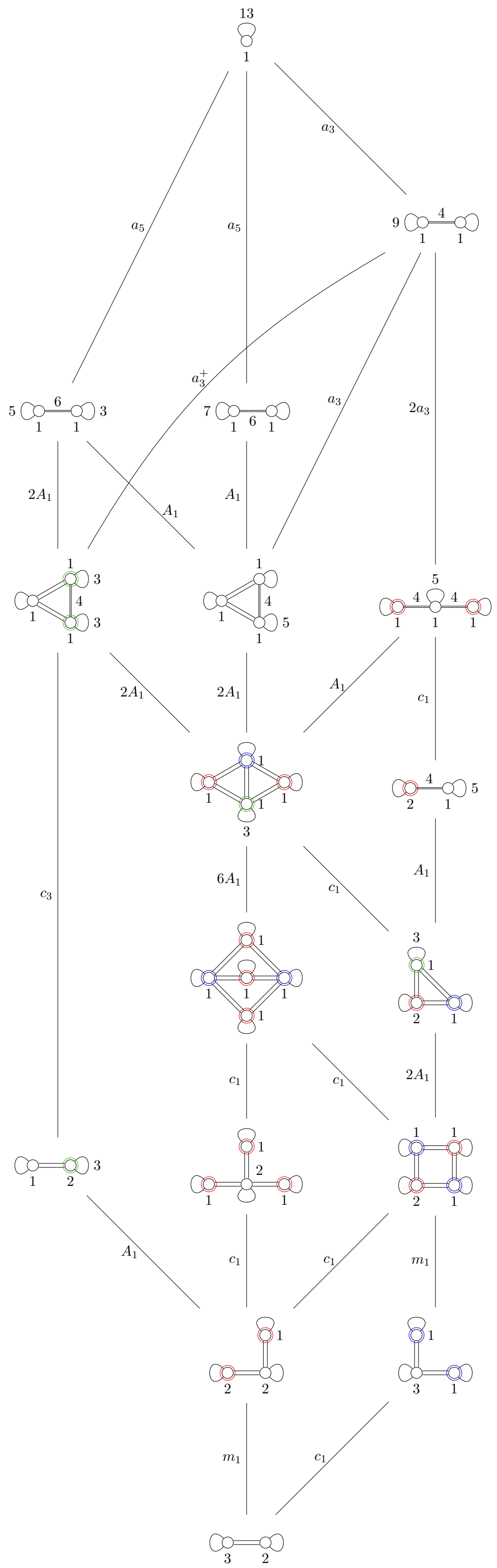

Figure 6.2: The red decoration comes from the U(3) node with a loop, the blue decoration comes from the U(2) node with a loop, the green decoration comes from the 2 copies of Q_{A_1} subquiver, or equivalently, it can be thought of as the result of merging the red and blue decorations. a_3^+ is a_3 with an S_2 monodromy, coming from the two identically decorated nodes.

6.6 The Non-normal Varieties m_g

The non-normal variety m_1 of quaternionic dimension 1 is the simplest example of a non-normal variety that is both symplectic and holomorphic [159]. The simplest definition of m_1 starts with the ring of functions of $\mathbb{C}^2$ with the two generators removed. The Hilbert series and Highest Weight Generating function describe this process

$$\mathrm{HS}(m_1) = \frac{1}{(1-at)(1-t/a)} - (a+1/a)t \ , \tag{6.16}$$

$$\mathrm{HWG}(m_1) = \frac{1}{1-\mu t} - \mu t = \sum_{1\neq n\in\mathbb{Z}_{\geq 0}} (\mu t)^n = \mathrm{PE}[\mu^2t^2 + \mu^3t^3 - \mu^6t^6] \ , \tag{6.17}$$

with a and μ the fugacity and highest weight fugacity respectively of the Sp(1) symmetry acting on m_1 .

The ring of functions of m_1 can now be specified, using coordinates x and y of $\mathbb{C}^2$ as:

$$\mathcal{R}_{m_1} = \mathbb{C}[x^2, xy, y^2, x^3, x^2y, xy^2, y^3], \tag{6.18}$$

with $m_1 = \mathrm{Spec}\ \mathcal{R}_{m_1}$.

The variety m_1 appears as the fixed locus of $S_k \times S_{n-k}$ in $\mathbb{C}^{2n}/S_n$ when $k \neq n-k$. To see this, take the coordinates of $\mathbb{C}^{2n}$ as $(x_1, y_1, \cdots, x_n, y_n)$ and remove the free $\mathbb{C}^2$ by setting $\sum_i x_i = \sum_i y_i = 0$. The invariant subspace fixed by the action of $S_k \times S_{n-k}$ is (up to conjugation),

$$V = (\underbrace{-(n-k)x, -(n-k)y, \cdots, -(n-k)x, -(n-k)y}_{k}, \underbrace{kx, ky, \cdots, kx, ky}_{n-k}). \tag{6.19}$$

The invariant local functions on V under S_n give the ring of functions of m_1 i.e, $V/S_n = m_1$.

The above construction of m_1 may be generalised easily to any dimension. Namely taking the ring of functions of $\mathbb{C}^l$, $l \in \mathbb{N}^+$ and removing the l generators. However, the holomorphic-symplectic property of the variety is preserved if only if l is even.

The construction of the g quaternionic-dimensional non-normal variety m_g proceeds by taking $l = 2g$, $g \in \mathbb{N}^+$. This is, once again, easily seen through the Hilbert series and Highest Weight Generating function

$$\mathrm{HS}(m_g) = \mathrm{PE}\left[[1,0,\cdots,0]_{\mathrm{Sp}(g)}t\right] - [1,0,\cdots,0]_{\mathrm{Sp}(g)}t \ , \tag{6.20}$$

$$\mathrm{HWG}(m_g) = \mathrm{PE}[\mu_1^2t^2 + \mu_1^3t^3 - \mu_1^6t^6] \ , \tag{6.21}$$

where the Dynkin label $[1,0,\cdots,0]_{\mathrm{Sp}(g)}$ is shorthand for the character of the fundamental representation of Sp(g) and μ_1 the highest weight fugacity for Sp(g).

The coordinate ring is specified as:

$$\mathcal{R}_{m_g} = \mathbb{C}[x_1, \ldots, x_g, y_1, \ldots, y_g] \backslash \{x_1, \ldots, x_g, y_1, \ldots, y_g\}. \tag{6.22}$$

Similarly as in (6.18), the ring (6.22) is generated by generators at degree 2 and 3. There are $g(2g+1)$ generators at degree 2 and $\frac{2g(g+1)(2g+1)}{3}$ generators at degree 3.

Bibliography

[1] A. Hanany, G. Kumaran, C. Li, D. Liu and M. Sperling, *Actions on the quiver: discrete quotients on the Coulomb branch*, *JHEP* **05** (2024) 318, [2311.02773].

[2] S. Bennett, A. Hanany, G. Kumaran, C. Li, D. Liu and M. Sperling, *Quiver subtraction on the Higgs branch*, *Nucl. Phys. B* **1016** (2025) 116917, [2409.16356].

[3] J. F. Grimminger, W. Harding and N. Mekareeya, *Generalised-edged quivers and global forms*, *JHEP* **03** (2025) 021, [2410.16353].

[4] J. de Boer, K. Hori, H. Ooguri, Y. Oz and Z. Yin, *Mirror symmetry in three-dimensional gauge theories, and d-brane moduli spaces*, *Nuclear Physics B* **493** (may, 1997) 148–176.

[5] S. Cremonesi, G. Ferlito, A. Hanany and N. Mekareeya, *Coulomb branch and the moduli space of instantons*, *Journal of High Energy Physics* **2014** (Dec., 2014) .

[6] B. Fu, D. Juteau, P. Levy and E. Sommers, *Generic singularities of nilpotent orbit closures*, *arXiv e-prints* (Feb., 2015) arXiv:1502.05770, [1502.05770].

[7] G. Bellamy, C. Bonnafé, B. Fu, D. Juteau, P. Levy and E. Sommers, *A new family of isolated symplectic singularities with trivial local fundamental group*, 2021.

[8] A. Bourget and J. F. Grimminger, *Fibrations and Hasse diagrams for 6d SCFTs*, *JHEP* **12** (2022) 159, [2209.15016].

[9] A. Bourget, J. F. Grimminger, A. Hanany, M. Sperling and Z. Zhong, *Branes, quivers, and the affine grassmannian*, 2021.

[10] A. Hanany and R. Kalveks, *Quiver Theories for Moduli Spaces of Classical Group Nilpotent Orbits*, *JHEP* **06** (2016) 130, [1601.04020].

[11] A. Hanany, G. Kumaran, C. Li, D. Liu and M. Sperling, *Actions on the quiver – Discrete quotients on the Coulomb branch*, 2311.02773.

[12] S. R. Coleman and J. Mandula, *All Possible Symmetries of the S Matrix*, *Phys. Rev.* **159** (1967) 1251–1256.

[13] R. Haag, J. T. Lopuszanski and M. Sohnius, *All Possible Generators of Supersymmetries of the s Matrix*, *Nucl. Phys. B* **88** (1975) 257.

[14] E. Witten, *Constraints on Supersymmetry Breaking*, *Nucl. Phys. B* **202** (1982) 253.

[15] V. Pestun et al., *Localization techniques in quantum field theories*, *J. Phys. A* **50** (2017) 440301, [1608.02952].

[16] N. Seiberg, *Naturalness versus supersymmetric nonrenormalization theorems*, *Phys. Lett. B* **318** (1993) 469–475, [hep-ph/9309335].

[17] N. Seiberg and E. Witten, *Electric - magnetic duality, monopole condensation, and confinement in N=2 supersymmetric Yang-Mills theory*, *Nucl. Phys. B* **426** (1994) 19–52, [hep-th/9407087].

[18] N. Seiberg and E. Witten, *Monopoles, duality and chiral symmetry breaking in N=2 supersymmetric QCD*, *Nucl. Phys. B* **431** (1994) 484–550, [hep-th/9408099].

[19] A. Hanany and M. Sperling, *Algebraic properties of the monopole formula*, *JHEP* **02** (2017) 023, [1611.07030].

[20] M. R. Douglas and G. W. Moore, *D-branes, quivers, and ALE instantons*, hep-th/9603167.

[21] A. Hanany and E. Witten, *Type IIB superstrings, BPS monopoles, and three-dimensional gauge dynamics*, *Nucl. Phys. B* **492** (1997) 152–190, [hep-th/9611230].

[22] D. Gaiotto and E. Witten, *S-Duality of Boundary Conditions In N=4 Super Yang-Mills Theory*, *Adv. Theor. Math. Phys.* **13** (2009) 721–896, [0807.3720].

[23] S. Cabrera and A. Hanany, *Quiver Subtractions*, *JHEP* **09** (2018) 008, [1803.11205].

[24] A. Bourget, M. Sperling and Z. Zhong, *Decay and Fission of Magnetic Quivers*, 2312.05304.

[25] A. Bourget, M. Sperling and Z. Zhong, *Higgs branch RG-flows via Decay and Fission*, 2401.08757.

[26] A. Hanany, R. Kalveks and G. Kumaran, *Quotient Quiver Subtraction*, 2308.05853.

[27] A. Hanany, R. Kalveks and G. Kumaran, *Quiver Polymerisation*, 2406.11561.

[28] K. A. Intriligator and N. Seiberg, *Mirror symmetry in three-dimensional gauge theories*, *Phys. Lett. B* **387** (1996) 513–519, [hep-th/9607207].

[29] G. Chalmers and A. Hanany, *Three-dimensional gauge theories and monopoles*, *Nucl. Phys. B* **489** (1997) 223–244, [hep-th/9608105].

[30] A. Hanany and A. Zaffaroni, *Monopoles in string theory*, *JHEP* **12** (1999) 014, [hep-th/9911113].

[31] A. Hanany and J. Troost, *Orientifold planes, affine algebras and magnetic monopoles*, *JHEP* **08** (2001) 021, [hep-th/0107153].

[32] S. Cremonesi, A. Hanany and A. Zaffaroni, *Monopole operators and Hilbert series of Coulomb branches of* 3*d* $\mathcal{N} = 4$ *gauge theories*, *JHEP* **01** (2014) 005, [1309.2657].

[33] M. Bullimore, T. Dimofte and D. Gaiotto, *The Coulomb Branch of 3d* $\mathcal{N} = 4$ *Theories*, *Commun. Math. Phys.* **354** (2017) 671–751, [1503.04817].

[34] M. Bullimore, T. Dimofte, D. Gaiotto and J. Hilburn, *Boundaries, Mirror Symmetry, and Symplectic Duality in 3d* $\mathcal{N} = 4$ *Gauge Theory*, *JHEP* **10** (2016) 108, [1603.08382].

[35] M. Bullimore, T. Dimofte, D. Gaiotto, J. Hilburn and H.-C. Kim, *Vortices and Vermas*, *Adv. Theor. Math. Phys.* **22** (2018) 803–917, [1609.04406].

[36] T. Dimofte, N. Garner, M. Geracie and J. Hilburn, *Mirror symmetry and line operators*, *JHEP* **02** (2020) 075, [1908.00013].

[37] B. Assel and J. Gomis, *Mirror Symmetry And Loop Operators*, *JHEP* **11** (2015) 055, [1506.01718].

[38] A. Braverman, M. Finkelberg and H. Nakajima, *Coulomb branches of* 3*d* $\mathcal{N} = 4$ *quiver gauge theories and slices in the affine Grassmannian*, *Adv. Theor. Math. Phys.* **23** (2019) 75–166, [1604.03625].

[39] H. Nakajima, *Towards a mathematical definition of Coulomb branches of* 3*-dimensional* $\mathcal{N} = 4$ *gauge theories, I*, *Adv. Theor. Math. Phys.* **20** (2016) 595–669, [1503.03676].

[40] A. Braverman, M. Finkelberg and H. Nakajima, *Towards a mathematical definition of Coulomb branches of* 3*-dimensional* $\mathcal{N} = 4$ *gauge theories, II*, *Adv. Theor. Math. Phys.* **22** (2018) 1071–1147, [1601.03586].

[41] O. Aharony, S. S. Razamat, N. Seiberg and B. Willett, *3d dualities from 4d dualities*, *JHEP* **07** (2013) 149, [1305.3924].

[42] M. Akhond, G. Arias-Tamargo, F. Carta, J. F. Grimminger and A. Hanany, *On brane systems with* O^+ *planes — 5d and 6d SCFTs*, *JHEP* **03** (2025) 137, [2411.02491].

[43] A. Bourget, J. F. Grimminger, A. Hanany, R. Kalveks, M. Sperling and Z. Zhong, *A tale of N cones*, *JHEP* **09** (2023) 073, [2303.16939].

[44] A. Bourget, J. F. Grimminger, A. Hanany, R. Kalveks and Z. Zhong, *Higgs branches of U/SU quivers via brane locking*, *JHEP* **08** (2022) 061, [2111.04745].

[45] A. Bourget, S. Cabrera, J. F. Grimminger, A. Hanany and Z. Zhong, *Brane Webs and Magnetic Quivers for SQCD*, *JHEP* **03** (2020) 176, [1909.00667].

[46] A. Bourget, J. F. Grimminger, A. Hanany, M. Sperling and Z. Zhong, *Magnetic Quivers from Brane Webs with O5 Planes*, *JHEP* **07** (2020) 204, [2004.04082].

[47] A. Hanany and E. V. d. Driessche, *Higgs branch of 5d $\mathcal{N} = 1$ symplectic gauge theories and dressed instanton operators*, 2507.08669.

[48] S. Bennett, A. Hanany and G. Kumaran, *Orthosymplectic Quotient Quiver Subtraction II: Framed Quivers*, 2503.19954.

[49] J. F. Grimminger, A. Hanany and D. Liu, *3d Mirrors and Phase Diagrams of Abelian Gauge Theories*, 2503.08791.

[50] S. Bennett and A. Hanany, O/SO *Gauge Groups, BC Quivers and O3 Planes*, 2503.05443.

[51] S. Cremonesi, G. Ferlito, A. Hanany and N. Mekareeya, *Instanton Operators and the Higgs Branch at Infinite Coupling*, *JHEP* **04** (2017) 042, [1505.06302].

[52] G. Ferlito, A. Hanany, N. Mekareeya and G. Zafrir, *3d Coulomb branch and 5d Higgs branch at infinite coupling*, *JHEP* **07** (2018) 061, [1712.06604].

[53] S. Cabrera, A. Hanany and F. Yagi, *Tropical Geometry and Five Dimensional Higgs Branches at Infinite Coupling*, *JHEP* **01** (2019) 068, [1810.01379].

[54] S. Cabrera, A. Hanany and M. Sperling, *Magnetic quivers, Higgs branches, and 6d N=(1,0) theories*, *JHEP* **06** (2019) 071, [1904.12293].

[55] S. Cabrera, A. Hanany and M. Sperling, *Magnetic quivers, Higgs branches, and 6d $\mathcal{N}$ = (1, 0) theories — orthogonal and symplectic gauge groups*, *JHEP* **02** (2020) 184, [1912.02773].

[56] A. Bourget, J. F. Grimminger, A. Hanany, M. Sperling, G. Zafrir and Z. Zhong, *Magnetic quivers for rank 1 theories*, *JHEP* **09** (2020) 189, [2006.16994].

[57] A. Bourget, S. Giacomelli, J. F. Grimminger, A. Hanany, M. Sperling and Z. Zhong, *S-fold magnetic quivers*, *JHEP* **02** (2021) 054, [2010.05889].

[58] A. Hanany and M. Sperling, *Magnetic quivers and negatively charged branes*, *JHEP* **11** (2022) 010, [2208.07270].

[59] W. Nahm, *Supersymmetries and Their Representations*, *Nucl. Phys. B* **135** (1978) 149.

[60] C. Cordova, T. T. Dumitrescu and K. Intriligator, *Multiplets of Superconformal Symmetry in Diverse Dimensions*, *JHEP* **03** (2019) 163, [1612.00809].

[61] N. Seiberg, *Five-dimensional SUSY field theories, nontrivial fixed points and string dynamics*, *Phys. Lett. B* **388** (1996) 753–760, [hep-th/9608111].

[62] A. Hanany and A. Zaffaroni, *Branes and six-dimensional supersymmetric theories*, *Nucl. Phys. B* **529** (1998) 180–206, [hep-th/9712145].

[63] P. Jefferson, S. Katz, H.-C. Kim and C. Vafa, *On Geometric Classification of 5d SCFTs*, *JHEP* **04** (2018) 103, [1801.04036].

[64] J. J. Heckman and T. Rudelius, *Top Down Approach to 6D SCFTs*, *J. Phys. A* **52** (2019) 093001, [1805.06467].

[65] O. Aharony, A. Hanany and B. Kol, *Webs of (p,q) five-branes, five-dimensional field theories and grid diagrams*, *JHEP* **01** (1998) 002, [hep-th/9710116].

[66] N. J. Hitchin, A. Karlhede, U. Lindstrom and M. Rocek, *Hyperkahler Metrics and Supersymmetry*, *Commun. Math. Phys.* **108** (1987) 535.

[67] A. Beauville, *Symplectic singularities*, *Invent. Math.* **139** (2000) 541–549, [math/9903070].

[68] A. Bourget, S. Cabrera, J. F. Grimminger, A. Hanany, M. Sperling, A. Zajac et al., *The higgs mechanism — hasse diagrams for symplectic singularities*, *Journal of High Energy Physics* **2020** (Jan., 2020) .

[69] T. Braden, A. Licata, N. Proudfoot and B. Webster, *Quantizations of conical symplectic resolutions II: category $\mathcal{O}$ and symplectic duality*, *Asterisque* **384** (2016) 75–179, [1407.0964].

[70] J. Kamnitzer, *Symplectic resolutions, symplectic duality, and Coulomb branches*, *Bull. London Math. Soc.* **54** (2024) 1515–1551, [2202.03913].

[71] S. Benvenuti, B. Feng, A. Hanany and Y.-H. He, *Counting BPS Operators in Gauge Theories: Quivers, Syzygies and Plethystics*, *JHEP* **11** (2007) 050, [hep-th/0608050].

[72] J. Wess and J. Bagger, *SUPERSYMMETRY AND SUPERGRAVITY: NOTES FROM LECTURES GIVEN AT PRINCETON UNIVERSITY. PART 2.* 6, 1982.

[73] P. C. Argyres, *Introduction to Supersymmetry.* 1996.

[74] D. Tong, *Supersymmetric Field Theory.* 2022.

[75] O. Aharony, A. Hanany, K. A. Intriligator, N. Seiberg and M. J. Strassler, *Aspects of N=2 supersymmetric gauge theories in three-dimensions*, *Nucl. Phys. B* **499** (1997) 67–99, [hep-th/9703110].

[76] J. de Boer, K. Hori and Y. Oz, *Dynamics of N=2 supersymmetric gauge theories in three-dimensions*, *Nucl. Phys. B* **500** (1997) 163–191, [hep-th/9703100].

[77] N. Seiberg and E. Witten, *Gauge dynamics and compactification to three-dimensions*, in *Conference on the Mathematical Beauty of Physics (In Memory of C. Itzykson)*, pp. 333–366, 6, 1996. hep-th/9607163.

[78] V. Borokhov, A. Kapustin and X.-k. Wu, *Topological disorder operators in three-dimensional conformal field theory*, *JHEP* **11** (2002) 049, [hep-th/0206054].

[79] N. Seiberg, *IR dynamics on branes and space-time geometry*, *Phys. Lett. B* **384** (1996) 81–85, [hep-th/9606017].

[80] N. Seiberg, *Exact results on the space of vacua of four-dimensional SUSY gauge theories*, *Phys. Rev. D* **49** (1994) 6857–6863, [hep-th/9402044].

[81] W. Lerche, C. Vafa and N. P. Warner, *Chiral Rings in N=2 Superconformal Theories*, *Nucl. Phys. B* **324** (1989) 427–474.

[82] V. Borokhov, A. Kapustin and X.-k. Wu, *Monopole operators and mirror symmetry in three-dimensions*, *JHEP* **12** (2002) 044, [hep-th/0207074].

[83] M. K. Benna, I. R. Klebanov and T. Klose, *Charges of Monopole Operators in Chern-Simons Yang-Mills Theory*, *JHEP* **01** (2010) 110, [0906.3008].

[84] D. Bashkirov and A. Kapustin, *Supersymmetry enhancement by monopole operators*, *JHEP* **05** (2011) 015, [1007.4861].

[85] B. Feng, A. Hanany and Y.-H. He, *Counting gauge invariants: The Plethystic program*, *JHEP* **03** (2007) 090, [hep-th/0701063].

[86] H. Kraft and C. Procesi, *On the geometry of conjugacy classes in classical groups*, *Commentarii Mathematici Helvetici* **57** (1982) 539–602.

[87] H. Kraft and C. Procesi, *Minimal singularities in gln*, *Invent. math* **62** (1981) 503–515.

[88] D. Kaledin, *Symplectic singularities from the poisson point of view*, *arXiv preprint math/0310186* (2003) .

[89] A. Hanany and G. Zafrir, *Discrete Gauging in Six Dimensions*, *JHEP* **07** (2018) 168, [1804.08857].

[90] A. Hanany and M. Sperling, *Discrete quotients of 3-dimensional $\mathcal{N} = 4$ Coulomb branches via the cycle index*, *JHEP* **08** (2018) 157, [1807.02784].

[91] A. Hanany and A. Zajac, *Discrete Gauging in Coulomb branches of Three Dimensional $\mathcal{N} = 4$ Supersymmetric Gauge Theories*, *JHEP* **08** (2018) 158, [1807.03221].

[92] D. Kaledin, *Symplectic singularities from the Poisson point of view*, *arXiv Mathematics e-prints* (Oct., 2003) math/0310186, [math/0310186].

[93] A. Bourget, S. Cabrera, J. F. Grimminger, A. Hanany, M. Sperling, A. Zajac et al., *The Higgs mechanism — Hasse diagrams for symplectic singularities*, *JHEP* **01** (2020) 157, [1908.04245].

[94] J. F. Grimminger and A. Hanany, *Hasse diagrams for 3d $\mathcal{N} = 4$ quiver gauge theories — Inversion and the full moduli space*, *JHEP* **09** (2020) 159, [2004.01675].

[95] S. Cabrera and A. Hanany, *Branes and the Kraft-Procesi Transition*, *JHEP* **11** (2016) 175, [1609.07798].

[96] S. Cabrera and A. Hanany, *Branes and the Kraft-Procesi transition: classical case*, *JHEP* **04** (2018) 127, [1711.02378].

[97] A. Bourget, A. Hanany and D. Miketa, *Quiver origami: discrete gauging and folding*, *JHEP* **01** (2021) 086, [2005.05273].

[98] A. Bourget, J. F. Grimminger, A. Hanany, R. Kalveks, M. Sperling and Z. Zhong, *Folding orthosymplectic quivers*, *JHEP* **12** (2021) 070, [2107.00754].

[99] R. Brylinski and B. Kostant, *Nilpotent orbits, normality, and Hamiltonian group actions*, *arXiv Mathematics e-prints* (Mar., 1992) math/9204227, [math/9204227].

[100] S. Cremonesi, G. Ferlito, A. Hanany and N. Mekareeya, *Coulomb Branch and The Moduli Space of Instantons*, *JHEP* **12** (2014) 103, [1408.6835].

[101] A. Hanany and A. Zajac, *Ungauging Schemes and Coulomb Branches of Non-simply Laced Quiver Theories*, *JHEP* **09** (2020) 193, [2002.05716].

[102] S. Nawata, M. Sperling, H. E. Wang and Z. Zhong, *3d $\mathcal{N} = 4$ mirror symmetry with 1-form symmetry*, *SciPost Phys.* **15** (2023) 033, [2301.02409].

[103] B. Fu, D. Juteau, P. Levy and E. Sommers, *Local geometry of special pieces of nilpotent orbits*, *arXiv e-prints* (Aug., 2023) arXiv:2308.07398, [2308.07398].

[104] D. Xie, *General Argyres-Douglas Theory*, *JHEP* **01** (2013) 100, [1204.2270].

[105] S. Giacomelli, N. Mekareeya and M. Sacchi, *New aspects of Argyres–Douglas theories and their dimensional reduction*, *JHEP* **03** (2021) 242, [2012.12852].

[106] S. Cecotti, A. Neitzke and C. Vafa, *R-Twisting and 4d/2d Correspondences*, 1006.3435.

[107] N. Mekareeya and M. Sacchi, *Mixed anomalies, two-groups, non-invertible symmetries, and 3d superconformal indices*, *JHEP* **01** (2023) 115, [2210.02466].

[108] C. Teleman, *The rôle of Coulomb branches in 2D gauge theory*, *J. Eur. Math. Soc.* **23** (2021) 3497–3520, [1801.10124].

[109] M. Lehn, Y. Namikawa and C. Sorger, *Slodowy slices and universal poisson deformations*, *Compositio Mathematica* **148** (nov, 2011) 121–144.

[110] R. Yamagishi, *Four-dimensional conical symplectic hypersurfaces*, *Journal of Algebra* **560** (oct, 2020) 538–573.

[111] A. Hanany, "Hypersurface symplectic singularities." https://indico.ipmu.jp/event/314/contributions/5047/attachments/3229/4135/AmihayHanany.pdf, 2020.

[112] A. Hanany and N. Mekareeya, *Tri-vertices and SU(2)'s*, *JHEP* **02** (2011) 069, [1012.2119].

[113] M. Finkelberg and E. Goncharov, *Coulomb branch of a multiloop quiver gauge theory*, *Functional Analysis and Its Applications* **53** (2019) 241–249, [1903.05822].

[114] S. Cecotti, M. Del Zotto and S. Giacomelli, *More on the N=2 superconformal systems of type $D_p(G)$*, *JHEP* **04** (2013) 153, [1303.3149].

[115] L. Bhardwaj, M. Bullimore, A. E. V. Ferrari and S. Schafer-Nameki, *Generalized Symmetries and Anomalies of 3d N=4 SCFTs*, 2301.02249.

[116] A. Bourget, J. F. Grimminger, A. Hanany and Z. Zhong, *The Hasse diagram of the moduli space of instantons*, *JHEP* **08** (2022) 283, [2202.01218].

[117] K. Gledhill and A. Hanany, *Coulomb branch global symmetry and quiver addition*, *JHEP* **12** (2021) 127, [2109.07237].

[118] F. Englert and R. Brout, *Broken Symmetry and the Mass of Gauge Vector Mesons*, *Phys. Rev. Lett.* **13** (1964) 321–323.

[119] P. W. Higgs, *Broken Symmetries and the Masses of Gauge Bosons*, *Phys. Rev. Lett.* **13** (1964) 508–509.

[120] G. S. Guralnik, C. R. Hagen and T. W. B. Kibble, *Global Conservation Laws and Massless Particles*, *Phys. Rev. Lett.* **13** (1964) 585–587.

[121] T. W. B. Kibble, *Symmetry breaking in non-abelian gauge theories*, *Phys. Rev.* **155** (Mar, 1967) 1554–1561.

[122] D. Bashkirov, *Examples of global symmetry enhancement by monopole operators*, 1009.3477.

[123] S. Cremonesi, A. Hanany, N. Mekareeya and A. Zaffaroni, *Coulomb branch Hilbert series and Hall-Littlewood polynomials*, *JHEP* **09** (2014) 178, [1403.0585].

[124] S. Cremonesi, A. Hanany, N. Mekareeya and A. Zaffaroni, *T_ρ^σ (G) theories and their Hilbert series*, *JHEP* **01** (2015) 150, [1410.1548].

[125] D. Kaledin, *Symplectic singularities from the poisson point of view*, .

[126] H. Nakajima, *Instantons on ALE spaces, quiver varieties, and Kac-Moody algebras*, *Duke Math. J.* **76** (1994) 365–416.

[127] H. Nakajima, *Quiver varieties and Kac-Moody algebras*, *Duke Mathematical Journal* **91** (1998) 515 – 560.

[128] W. Crawley-boevey, *Geometry of the Moment Map for Representations of Quivers*, *Compositio Mathematica* **126** (05, 2000) .

[129] W. Crawley-Boevey, *Normality of marsden-weinstein reductions for representations of quivers*, math/0105247.

[130] T. Schedler and G. Bellamy, *Minimal degenerations of quiver varieties, work in progress* .

[131] D. Gaiotto and P. Koroteev, *On Three Dimensional Quiver Gauge Theories and Integrability*, *JHEP* **05** (2013) 126, [1304.0779].

[132] J. Gu, Y. Jiang and M. Sperling, *Rational Q-systems, Higgsing and mirror symmetry*, *SciPost Phys.* **14** (2023) 034, [2208.10047].

[133] H. Hayashi, S.-S. Kim, K. Lee and F. Yagi, *5-brane webs for 5d $\mathcal{N} = 1$ G_2 gauge theories*, *JHEP* **03** (2018) 125, [1801.03916].

[134] H. Hayashi, S.-S. Kim, K. Lee and F. Yagi, *Dualities and 5-brane webs for 5d rank 2 SCFTs*, *JHEP* **12** (2018) 016, [1806.10569].

[135] I. Losev, L. Mason-Brown and D. Matvieievskyi, *Unipotent ideals and harish-chandra bimodules*, 2024.

[136] Y. Namikawa, *Poisson deformations of affine symplectic varieties*, *Duke Mathematical Journal* **156** (Jan., 2011) .

[137] Y. Namikawa, *Poisson deformations of affine symplectic varieties, ii*, *Kyoto Journal of Mathematics* **50** (Jan., 2010) .

[138] B. Assel and S. Cremonesi, *The Infrared Physics of Bad Theories*, *SciPost Phys.* **3** (2017) 024, [1707.03403].

[139] P. Slodowy, *Simple singularities and simple algebraic groups*, 1980.

[140] E. B. V. Arkadij L. Onishchik, *Lie groups and algebraic groups*, 1990. DOI.

[141] Y. Wu, *Namikawa-weyl groups of affinizations of smooth nakajima quiver varieties*, 2023.

[142] A. Gadde, L. Rastelli, S. S. Razamat and W. Yan, *Gauge Theories and Macdonald Polynomials*, *Commun. Math. Phys.* **319** (2013) 147–193, [1110.3740].

[143] A. Hanany and R. Kalveks, *Quiver Theories and Formulae for Nilpotent Orbits of Exceptional Algebras*, *JHEP* **11** (2017) 126, [1709.05818].

[144] S. Cabrera, A. Hanany and R. Kalveks, *Quiver Theories and Formulae for Slodowy Slices of Classical Algebras*, *Nucl. Phys. B* **939** (2019) 308–357, [1807.02521].

[145] A. Hanany and R. Kalveks, *Quiver Theories and Hilbert Series of Classical Slodowy Intersections*, *Nucl. Phys. B* **952** (2020) 114939, [1909.12793].

[146] G. Lusztig, *A class of irreducible representations of a weyl group*, in *Indagationes Mathematicae (Proceedings)*, vol. 82, pp. 323–335, North-Holland, 1979.

[147] G. Lusztig, *A class of irreducible representations of a weyl group. ii*, in *Indagationes Mathematicae (Proceedings)*, vol. 85, pp. 219–226, Elsevier, 1982.

[148] N. Spaltenstein, *Classes unipotentes et sous-groupes de Borel*, vol. 946. Springer, 2006.

[149] D. Juteau, P. Levy and E. Sommers, *Minimal special degenerations and duality*, *arXiv preprint arXiv:2310.00521* (2023) .

[150] D. Gaiotto, *N=2 dualities*, *JHEP* **08** (2012) 034, [0904.2715].

[151] F. Benini, Y. Tachikawa and D. Xie, *Mirrors of 3d Sicilian theories*, *JHEP* **09** (2010) 063, [1007.0992].

[152] D. Gaiotto and S. S. Razamat, *Exceptional Indices*, *JHEP* **05** (2012) 145, [1203.5517].

[153] S. Cremonesi, A. Hanany, N. Mekareeya and A. Zaffaroni, *Coulomb branch Hilbert series and Three Dimensional Sicilian Theories*, *JHEP* **09** (2014) 185, [1403.2384].

[154] C. Moeglin, *Sur la classification des séries discrètes des groupes classiques p-adiques: paramètres de langlands et exhaustivité*, *Journal of the European Mathematical Society* **004** (2002) 143–200.

[155] D. Jiang, B. Liu and G. Savin, *Raising nilpotent orbits in wave-front sets*, *arXiv e-prints* (Dec., 2014) arXiv:1412.8742, [1412.8742].

[156] D. Barbasch, J.-J. Ma, B. Sun and C.-B. Zhu, *On the notion of metaplectic Barbasch-Vogan duality*, *arXiv e-prints* (Oct., 2020) arXiv:2010.16089, [2010.16089].

[157] A. Hanany and R. Kalveks, *Highest Weight Generating Functions for Hilbert Series*, *JHEP* **10** (2014) 152, [1408.4690].

[158] A. Hanany and M. Sperling, *Coulomb branches for rank 2 gauge groups in 3d* $\mathcal{N} = 4$ *gauge theories*, *JHEP* **08** (2016) 016, [1605.00010].

[159] È. B. Vinberg and V. L. Popov, *On a class of quasihomogeneous affine varieties*, *Mathematics of the USSR-Izvestiya* **6** (1972) 743.